HU ISSN 1586–2070

JOURNAL OF COMPUTATIONAL AND APPLIED MECHANICS

A Publication of the University of Miskolc

VOLUME 1, NUMBER 2 (2000)

MISKOLC UNIVERSITY PRESS

HU ISSN 1586–2070

JOURNAL OF COMPUTATIONAL AND APPLIED MECHANICS

A Publication of the University of Miskolc

VOLUME 1, NUMBER 2 (2000)

MISKOLC UNIVERSITY PRESS

EDITORIAL BOARD

LOCAL EDITORIAL COUNCIL

T. CZIBERE, I. KOZÁK, I. PÁCZELT, G. PATKÓ, G. SZEIDL

Journal of Computational and Applied Mechanics, Vol. 1., No. 2., (2000) pp. 103–107

PREFACE

Imre Kozák

This special issue of the Journal of Computational and Applied Mechanics is dedicated by friends, colleagues and former students to Imre Kozák, Professor at the University of Miskolc, on the occasion of his 70^{th} birthday. The range of topics covered by the various contributions reflects the scientific interests of Imre Kozák. The papers are also related, as they cover various problems of engineering mechanics, beginning with issues of continuum mechanics and dealing with some questions of computational mechanics and optimization problems.

Imre Kozák was born in Gór, a small village in Western Hungary, in 1930. After graduating from a grammar school in Szombathely in 1949 he was admitted to the Faculty of Mechanical Engineering of the Technical University of Heavy Industry in Miskolc – today's University of Miskolc. In 1953 he obtained an M.Sc. degree in Mechanical Engineering.

He began his graduate studies at the Department of Mechanics of the same university with the then Department Head István Sályi as his scientific supervisor, in 1953. This work later culminated in a Ph.D. thesis entitled *Small elastic plastic deformations of a thin walled cylindrical shell subjected to internal pressure*. This thesis was the first in which the Prandtl-Reuss equations were applied to bent cylindrical shells. The main difficulty of the problem raised lay in the fact that the solution required large amounts of computations before the advent of computers [1]. He was awarded his Ph.D. degree in 1961 and was appointed Associate Professor at the Department of Mechanics.

In 1967 he took part in the organization of the first Colloquium on Plasticity held in Miskolc in honor of Professor Reuss, who was a well known specialist in this field. This was the first scientific meeting of mechanical nature in Hungary after World War II.

From 1967 to 1970 he was the Prorector responsible for scientific matters.

In 1968 Kozák was appointed Full Professor. Three years later, in 1971 he took over leadership at the Department of Mechanics and held the post of Head of Department till 1993.

Since 1971 the Hungarian Conference on Engineering Mechanics has been organized at the University of Miskolc every four years. He has taken part in the preparations and organization of the conferences on each occasion.

From 1966 to 1969 he greatly contributed in cooperation with Professor Béda (Technical University of Budapest) and Professor Sályi to a new initiative by launching academic programs for mechanical engineers specialized in theoretical and applied mechanics. The students who chose the new program of theoretical and applied mechanics graduated from the university with an M.Sc. degree. He took part in designing

the new curriculum and red lectures, for the first time in the academic programs for mechanical engineers in Hungary, on such subjects as Theory of Shells, Mechanics of Continua, Differential Geometry with Indicial Notations etc. It is worthy of mention that six of his former students are Full Professors today.

In the years 1972 to 1978 he was appointed General Prorector of the University of Miskolc. After office hours he devoted time to updating the materials of the fundamental courses of engineering mechanics (Statics, Strength of Materials, Dynamics, Theory of Vibration).

In 1978 he received the Gold Medal of the Order of Labor.

As regards his research, his aim was to work out a linear shell theory in terms of stresses. Because of the unresolved problems in connection with the compatibility of strain fields – what are the independent, necessary and sufficient conditions the strains should meet in order to be compatible if the displacements are not variables of the governing equations, what is the solution to the Southwell paradox[1], – he had to do some supplementary research.

As regards his results, it is worthy of mention that he modified and supplemented the dual formulation of linear elasticity and the system of dual variational principles by solving the aforementioned Southwell paradox, i.e., by pointing out that only three of the six Saint-Venant compatibility conditions are independent provided that the so-called compatibility boundary conditions are satisfied and showing that the independent compatibility conditions and independent stress functions should be chosen according to the same rule [2,3]. Based on these results he was able to establish a general theory of shells in dual system regarding the stresses as fundamental variables [4]. This work led to the thesis *Theory of thin shells in terms of stresses.* After its defence the Committee of Scientific Qualifications at the Hungarian Academy of Sciences awarded him the degree Doctor of Science in 1981.

From 1980 to 1983 he was again the Prorector responsible for scientific matters.

Between 1983 and 1985 Kozák wrote the textbooks *Continuum Mechanics* [5, 1986 (in Hungarian)] and *Mechanics of Elastic Bodies* [6, 1987 (in Hungarian)] with coauthors. The book *Continuum Mechanics* contains his most important results concerning the investigations he carried out in dual system. The book *Mechanics of Elastic Bodies* contains, among others, the linear theory of shells in indicial notations making use of the curvilinear coordinate system built onto the middle surface of the shell and in primal and dual formulations (in terms of stresses) as well.

In the late 80s Kozák began to deal with the relative motion of continua. By relative motion we mean the motion of a solid body (continuum) with respect to an

[1]It was Southwell (1936, 1938), who first derived the compatibility conditions from the principle of minimum complementary energy as a variational principle. At the same time he pointed out that – utilizing Maxwell's (1870) and Morera's (1892) solutions – only three of the six Saint-Venant compatibility conditions follow from the principle of minimum complementary energy. Since any stress condition can be given in terms of three stress functions chosen appropriately, he arrived at a contradiction because for the displacements to be single-valued all the six Saint-Venant compatibility conditions should be satisfied. This contradiction was named Southwell's paradox after him. After Southwell's papers the following problems remained unresolved. Is it sufficient for the strains to satisfy three Saint-Venant compatibility equations? If yes, which three? If yes, are there further conditions to satisfy?

arbitrary curvilinear coordinate system, which is also in motion and therefore is capable of deformation (one can regard it as if it were a fictitious body). This motion is distinguished from the motion of the solid body (continuum) relative to an arbitrary but fixed curvilinear coordinate system (absolute motion). Within the framework of these investigations he set up the necessary formalism. In headwords: relative and absolute velocity fields, relative and absolute deformations, deformation gradients, strain tensors, volume and surface elements, material time derivatives (for the deformation gradients, volume and surface elements), some questions of the physically objective material time derivatives of the strain tensors, principle of virtual power and work in each configuration with special regard to the case of follower loads. One of his major results was the derivation of some new and known materially objective (invariant under any coordinate transformation) time derivatives with a systematic method.

In 1988 he won the Apáczai Csere János Prize. In 1990 and 1993 he was awarded the medals Pro Unversitate and Pro Urbe of Miskolc.

The graduate education that leads to the degree of Doctor of Philosophy had earlier been controlled formally by the Hungarian Academy of Sciences (Russian system) but was taken over by the Hungarian Universities in 1990. He took part in establishing new curricula for the graduate students at the Faculty of Mechanical Engineering of the University of Miskolc.

A revised and supplemented English edition of the book *Continuum Mechanics* [7] was published in 1995. This edition contains, among others, Kozák's method of deriving materially objective time derivatives.

The textbook *Continuum Mechanics* (in Hungarian) written for graduate students was also published in 1995.

He was elected corresponding member of the Hungarian Academy of Sciences in 1995. He gave his inaugural lecture with the title *Continuum Mechanics and Geometry* at the Seat of the Miskolc Committee of the Hungarian Academy of Sciences in 1996.

In 1996 the City Council of Miskolc awarded Kozák honorary citizenship.

In the 90s he proceeded with his research in continuum mechanics. The results are applicable to investigating geometrically non-linear static stability problems and postcritical equilibrium paths. Some of the results are listed below very briefly:

1. The incremental form of the principle of virtual displacements for follower loads and the derivation of the formulae for the Newton–Raphson iteration procedure that solves the corresponding non-linear problem. When applying a finite element discretization it is reasonable to introduce, in addition to the usual linear and geometric stiffness matrices, the load-correction stiffness matrix which is symmetric if the follower loads have a potential and is asymmetric if the follower loads have no potential.
2. The Newton-Raphson iteration can be initiated not only from an equilibrium configuration under the given load but from an arbitrary non-equilibrium configuration provided that the latter is appropriately chosen, independently of the loads. In this way both fundamental equilibrium paths and bifurcation paths as well as complementary paths and limit points can be investigated. The critical load can be determined by the path following method and the determinant

search algorithm. The equilibrium surfaces due to the geometrical imperfections and the load parameter(s), their stable and unstable regions and the critical loads can be determined numerically [8].

3. It has been shown that linear eigenvalue problems for follower loads cannot be investigated properly if the load correction matrix is left out of consideration.

In 1999 Kozák won, together with his colleague István Páczelt, the Széchenyi Prize which is the highest Scientific Award in Hungary.

Kozák participated actively in the work of a number of scientific associations and societies. Since 1966 he has been a member of the today's Committee of Theoretical and Applied Mechanics of the Hungarian Academy of Sciences – earlier Committee of Theoretical Mechanics (1966-73) and the Committee of Engineering Mechanics (1973-1993). Since 1973 he has also been a member of the Hungarian National Committee of the International Union of Theoretical and Applied Mechanics. From 1984 to 1996 he was a member of the Committee of Scientific Qualifications at the Hungarian Academy of Sciences.

Kozák has been taking part in the work of the Miskolc Committee of the Hungarian Academy of Sciences since it came into existence in 1979. Since its foundation he has been a member of the Expert Committee of Mechanical Engineering. Between 1984-96 he was the Chair of the Club Council. In 1990 he was elected a member of the Committee. From 1993 to 1996 he was the vice chairman of the Committee. In 1996 he was elected Chairman of the Committee.

Kozák has been visited a number of foreign cities (Vienna, Graz, Leoben, Prague, Brno, Bratislava, Kosice, Cracow, Berlin, Magdeburg, Dresden, St. Petersburg, Moscow, Kharkov, Frunze, Detroit, Algir, Oran, Constantine).

He is an excellent lecturer. He has the gift to present very complicated things – relationships, lines of thoughts – in an elegant and simple manner and to make his audience understand what at first seems difficult. Those who have had the privilege to attend his courses will remember these lectures fondly. The fact that the problems of continuum mechanics (and physics in general) can be formulated and solved in two theoretically equivalent systems – namely in a primal and a dual one – played an important role in his lectures on Elasticity and Continuum Mechanics and in the related lecture notes as well.

He has written altogether 17 university textbooks for his students on Statics, Strength of Materials, Dynamics, Elasticity, Plasticity, Theory of Shells etc. These books came out in Hungarian.

Kozák has been the scientific supervisor of 8 Ph.D. theses and a number of M.Sc. theses.

We are honored that in the name of his friends, colleagues and his former students we can greet him on the occasion of his 70^{th} birthday on the first pages of this issue of the Journal.

György Szeidl
Edgár Bertóti

REFERENCES

1. Kozák, I.: *Small elastic-plastic deformation (caused by internal pressure) of a thin walled tube, clamped at one of its ends to a rigid support*, Acta Techn. Hung., **55**(1–2), (1966), 7–26.
2. Kozák, I.: *Notes on the field equations with stresses and on the boundary conditions in the linearized theory of elasticity,* Acta Techn. Hung., **90**(3–4), (1980), 221–225.
3. Kozák, I.: *Determination of compatibility boundary conditions in linear elastostatics with the aid of the principle of minimum complementary energy*, Publ. Techn. Univ. Heavy Industry, Miskolc, Ser.D. Natural Sciences, **34**(2), (1980), 83–98.
4. Kozák, I.: *Construction of an approximate linear shell theory by asymptotic integration of the equations of elasticity in terms of stresses*, Advances in Mechanics, **6**(1-2), (1983), 91–110.
5. Béda, G., Kozák, I. and Verhás, J.: *Continuum Mechanics*, Műszaki Könyvkiadó, Budapest, 1986 (in Hungarian).
6. Béda, G. and Kozák, I.: *Mechanics of Elastic Bodies*, Műszaki Könyvkiadó, Budapest, 1987 (in Hungarian).
7. Béda, G., Kozák, I. and Verhás, J.: *Continuum Mechanics*, Academic Publisher, Budapest, 1995.
8. Kozák, I., Nándori, F. and Szabó, T.: *FE analysis of geometrically nonlinear static problems with follower loads*, Computer Assisted Mechanics and Engineering Sciences, **6**(1/2), (1999), 369–383.

Journal of Computational and Applied Mechanics, Vol. 1., No. 2., (2000), pp. 109–122

ON THE PRINCIPLE OF COMPLEMENTARY VIRTUAL WORK IN THE NON-LINEAR THEORY OF ELASTICITY

Edgár Bertóti
Department of Mechanics, University of Miskolc
3515 Miskolc – Egyetemváros, Hungary
mechber@gold.uni-miskolc.hu

[Received: September 4, 2000]

Abstract. A generalization of the principle of complementary virtual work in the current configuration is proposed by introducing the orthogonal rotation tensor as an independent variable. Applicability of the modified principle to (numerical) analysis of non-linear elasticity problems assumes the existence of an invertible constitutive relation between the Cauchy stress tensor and the left stretch tensor. It is shown that when transforming it into the reference configuration, the generalized principle of complementary virtual work is equivalent to Fraeijs de Veubeke's two-field dual-mixed principle, *provided* an appropriate constitutive equation between the Biot stress tensor and the right stretch tensor is taken into account. The independent equation system of non-linear elasticity in terms of stresses and rotations is derived, both in the current and reference configurations, using six independent first-order stress functions.

Keywords: Principle of complementary virtual work, non-linear elasticity, rotation tensor

1. Introduction

Applicability of the classical principle of complementary virtual work in non-linear elasticity is limited because (i) in the current configuration the Cauchy stress tensor and the displacement gradient tensor appearing in the principle are not work-conjugate stress and strain measures, thus they cannot be related to each other by constitutive equations; (ii) in the reference configuration the principle contains the first Piola-Kirchhoff stress tensor and the displacement gradient tensor which are work conjugate stress and strain measures, the constitutive relations between them, however, cannot be inverted uniquely. Due to the above mentioned restrictions, the principle of complementary virtual work has primarily theoretical importance in the non-linear theory of elasticity and is usually written in the reference configuration, see for example Novozhilov [1], Zubov [2], Lur'e [3], Washizu [4].

The complementary virtual work theorem is closely related to the principle of stationary complementary energy, as the latter can be derived from the former when invertible constitutive equations can be taken into account. The problem of construction complementary variational principles in non-linear elasticity in terms of stresses alone has been investigated by several authors. The key issue is to find appropriate work-conjugate stress and strain measures for which the constitutive equation is uniquely invertible, i.e. the strain tensor can be expressed as a function of the corresponding conjugate stress tensor. If such a work-conjugate stress and strain measure

exists, a complementary strain energy density can be derived from a given strain energy density through a Legendre transformation.

Levinson [5] pointed out that no complementary energy density as a function of the second Piola-Kirchhoff stress tensor alone can be derived. Construction of complementary energy density as a function of the first Piola-Kirchhoff stress tensor as well as the invertibility of the constitutive equations between the first Piola-Kirchhoff stress tensor and the deformation/displacement gradient tensor has been investigated, among others, by Novozhilov [1], Truesdell–Noll [6], Zubov [2], Fraeijs de Veubeke [7], Christoffersen [8], Koiter [9], Dill [10], Ogden [11]. The final conclusion was that it is impossible, in general, to derive a unique complementary strain energy density in terms of the first Piola-Kirchhoff stresses alone, since the inversion of the stress-strain relation between the first Piola-Kirchhoff stress tensor and the deformation/displacement gradient tensor is not unique [11]. It should be noted, however, that for some special cases, when the sign problem appearing in the inversion of the stress-strain relation is determinable by practical considerations, the principle of stationary complementary energy is applicable to solving non-linear elasticity problems [2][9][13].

The right and perhaps the best way to define a complementary variational principle in non-linear elasticity is using the Biot stress tensor and the right stretch tensor as work-conjugate (Lagrangian) stress and strain measures. In this case the stress-strain relations are uniquely invertible and the complementary strain energy density can always be expressed in terms of the Biot stress tensor alone. Recognizing these facts, a complementary energy-based dual-mixed principle in terms of the first Piola-Kirchhoff stress tensor, depending on the Biot stress tensor and the orthogonal rotation tensor, was derived by Fraeijs de Veubeke [7] in the reference configuration. The possible relationship between this two-field principle and a generalized complementary virtual work theorem, which should be independent of the actual constitutive equations, was not investigated in [7], however. Either, no attempt was made to transform the derived complementary energy principle into the current configuration (which is, otherwise, a rather complicated task), or to derive an applicable principle of complementary virtual work in the current configuration, independently of the developments and results presented in [7].

Considering the above mentioned facts and limitations regarding the applicability of the principle of complementary virtual work theorem in non-linear elasticity, this paper deals with a possible generalization of the classical principle by taking both the stress tensor and the orthogonal rotation tensor as independent variables. Section 2 focuses on the generalization of the classical principle in the current configuration. The orthogonal rotation tensor is introduced into the principle by considering the Cauchy stress tensor to be not a priori symmetric. The rotational equilibrium for the Cauchy stresses becomes a variational result. The modified principle is applicable to numerical analysis of non-linear elasticity problems when invertible constitutive relation between the Cauchy stress tensor and the left stretch tensor exists. Independent equation system of nonlinear elasticity in terms of the Cauchy stresses and orthogonal rotations are derived from the generalized principle in the current configuration, using six independent first-order stress functions.

In Section 3, the generalized principle is transformed into the reference configuration. It is pointed out that, provided an appropriate constitutive equation between the symmetrized Biot stress tensor and the right stretch tensor is taken into account, the generalized principle is equivalent to Fraeijs de Veubeke's two-field dual-mixed principle. Independent equation system of non-linear elasticity in terms of the first Piola-Kirchhoff stresses and orthogonal rotations is derived, using six independent first-order stress functions. Differences between the present and a former (incomplete) derivation given in [7] are emphasized.

Notation. Let the initial or reference configuration of an elastic body (at time $t = 0$) be denoted by ${}^0\Omega$ and its deformed or current configuration at time t ($t > 0$) by ${}^t\Omega$. Points in the reference and current configurations will be denoted by $\mathbf{X}$ and $\mathbf{x}$, respectively. It is assumed that ${}^0\Omega$ as well as ${}^t\Omega$ are simply-connected and bounded by the sufficiently smooth boundaries ${}^0\Gamma = {}^0\Gamma_\sigma \cup {}^0\Gamma_u$ $({}^0\Gamma_\sigma \cap {}^0\Gamma_u = 0)$ and ${}^t\Gamma = {}^t\Gamma_\sigma \cup {}^t\Gamma_u$ $({}^t\Gamma_\sigma \cap {}^t\Gamma_u = 0)$ and that these boundary parts with outward unit normals ${}^0\mathbf{n}$ and ${}^t\mathbf{n}$ are separated, according to Figure 1, by the boundary curves ${}^0\ell$ and ${}^t\ell$, respectively. The mass densities at the reference and current configurations are denoted by ${}^0\rho$ and ${}^t\rho$. The elastic body is subjected to body forces of density ${}^t\rho\mathbf{b}$ in ${}^t\Omega$ ($\mathbf{b}$ is the body force density per unit mass), a surface load of density ${}^t\widetilde{\mathbf{p}}$ on ${}^t\Gamma_\sigma$, whereas on the boundary part ${}^t\Gamma_u$, a displacement field denoted by $\widetilde{\mathbf{u}}$ is prescribed.

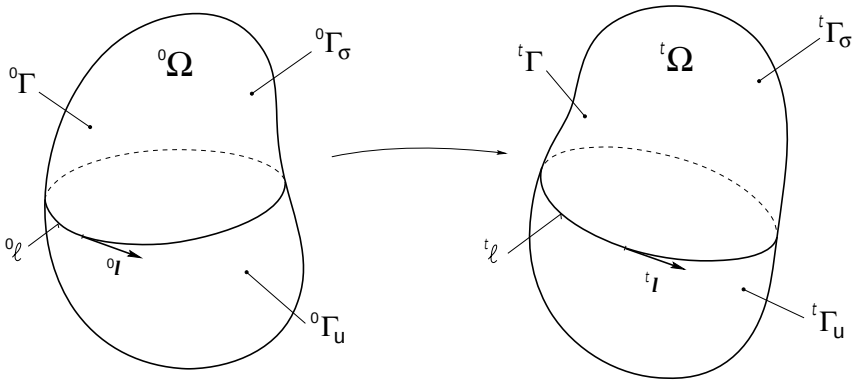

Figure 1. Elastic body: reference and current configuration

Throughout this paper, invariant notation of tensors and tensor operations will be used. Scalar, vectorial, tensorial and inner product of two tensors will be denoted, respectively, by $\cdot$, $\times$, $\otimes$ and $:$. Differential operations *divergence*, *curl* and *gradient* on tensor variables will be denoted by div, curl and grad with respect to the metric of the current configuration and by Div, Curl, and Grad with respect to the metric of the reference configuration. For the divergence, curl and gradient of the arbitrary, differentiable second-order tensor $\mathbf{S}$, definitions of Gurtin [14][15] are employed, i.e.

$$\operatorname{div}\mathbf{S} = \nabla \cdot \mathbf{S}^{\mathsf{T}}, \tag{1.1}$$

$$\operatorname{curl}\mathbf{S} = \nabla \times \mathbf{S}^{\mathsf{T}}, \tag{1.2}$$

$$\operatorname{grad}\mathbf{S} = \nabla \otimes \mathbf{S}^{\mathsf{T}}, \tag{1.3}$$

where a T in the superscript stands for the transpose. It is also convenient to introduce the surface divergence operator div_Γ acting on the surface Γ as

$$\mathrm{div}_\Gamma \mathbf{S} := (\mathbf{n} \times \nabla) \cdot \mathbf{S}^\mathsf{T}, \tag{1.4}$$

where $\mathbf{n}$ is the outward (unit) normal to Γ. This operator involves only tangential derivatives of $\mathbf{S}$ on Γ.

2. The principle of complementary virtual work and its generalization in the current configuration

2.1. The classical principle. The classical complementary virtual work theorem states that if equality

$$\int_{{}^t\Omega} (\mathbf{1} - \mathbf{F}^{-1}) : \delta\boldsymbol{\tau} \, \mathrm{d}\, {}^t\Omega = \int_{{}^t\Gamma_u} \widetilde{\mathbf{u}} \cdot \delta\boldsymbol{\tau} \cdot {}^t\mathbf{n} \, \mathrm{d}\, {}^t\Gamma \tag{2.1}$$

holds in the current configuration for all statically admissible Cauchy stresses $\boldsymbol{\tau}$, i.e. if its variation $\delta\boldsymbol{\tau}$ satisfies the translational equilibrium equations

$$\mathrm{div}\, \delta\boldsymbol{\tau} = \mathbf{0} \qquad \mathbf{x} \in {}^t\Omega \tag{2.2}$$

and the stress boundary conditions

$$\delta\boldsymbol{\tau} \cdot {}^t\mathbf{n} = \mathbf{0} \qquad \mathbf{x} \in {}^t\Gamma_\sigma, \tag{2.3}$$

and the symmetry condition for the Cauchy stress tensor

$$\boldsymbol{\tau} - \boldsymbol{\tau}^\mathsf{T} = \mathbf{0} \qquad \mathbf{x} \in {}^t\Omega \tag{2.4}$$

is also assumed to be a priori satisfied, then the tensor $\mathbf{D} := \mathbf{1} - \mathbf{F}^{-1}$ is the displacement gradient tensor and $\mathbf{F}^{-1}$ is the inverse deformation gradient tensor (the unit tensor is denoted by $\mathbf{1}$). It can also be pointed out that when (2.1) holds, the Riemann-Christoffel curvature tensor of the current metric vanishes, which is a compatibility condition for the metric tensor of the deformed configuration, see Kozák [16].

Applicability of (2.1) is restricted, however, by the fact that the Cauchy stress tensor and the displacement gradient tensor (or the inverse deformation gradient) are not work-conjugate stress and strain measures and, unless the deformation is rotation-free, they cannot be related to each other by constitutive equations. In other words, neither $\mathbf{D}$ nor $\mathbf{F}^{-1}$ can be expressed as a function of $\boldsymbol{\tau}$, which means that the principle of complementary virtual work in its classical form is not suitable for numerical analysis of non-linear elasticity problems. In addition, as the principle gives no information about the rotation of the material points and the principal directions of the strain ellipsoid, the deformed state of the body is indeterminable, in general, using (2.1).

Note that in the linearized theory of elasticity, the infinitesimal rotations can be uniquely determined from the strain tensor and, after taking into account the inverse stress-strain relations, (2.1) is equivalent to Castigliano's variational principle.

2.2. The generalized principle of complementary virtual work in the current configuration. The basic idea in the generalization of the principle of complementary virtual work is to introduce the finite rotations as independent variables into (2.1). This can be accomplished if the Cauchy stress tensor is not considered to be a priori symmetric. Enforcing the rotational equilibrium equations for the Cauchy stresses into the principle is, however, not as straightforward as in the linear case, where the (infinitesimal) rotation tensor is skew-symmetric; it needs the utilization of the fact that for any orthogonal tensor $\mathbf{R}$, the tensor $\delta\mathbf{R}\cdot\mathbf{R}^{\mathsf{T}}$ is skew-symmetric. Then the generalized principle of complementary virtual work can be stated as follows. Let equality

$$\int_{{}^t\Omega} \left[(\mathbf{1}-\mathbf{R}^{\mathsf{T}}\cdot\mathbf{V}^{-1}) : \delta\boldsymbol{\tau} + \boldsymbol{\tau} : (\delta\mathbf{R}\cdot\mathbf{R}^{\mathsf{T}})\right] \mathrm{d}\,{}^t\Omega = \int_{{}^t\Gamma_u} \widetilde{\mathbf{u}}\cdot\delta\boldsymbol{\tau}\cdot\,{}^t\mathbf{n}\,\mathrm{d}\,{}^t\Gamma \tag{2.5}$$

hold for all statically admissible (not a priori symmetric) Cauchy stresses $\delta\boldsymbol{\tau}$ satisfying (2.2) and (2.3), and for all $\delta\mathbf{R}$ obtained from an orthogonal rotation tensor $\mathbf{R}$, where $\mathbf{V}$ is an arbitrary but symmetric tensor. Then the tensor

$$\mathbf{D} := \mathbf{1} - \mathbf{R}^{\mathsf{T}}\cdot\mathbf{V}^{-1} \tag{2.6}$$

is the displacement gradient tensor, $\mathbf{R}^{\mathsf{T}}\cdot\mathbf{V}^{-1}$ is the inverse deformation gradient, and the Cauchy stress tensor $\boldsymbol{\tau}$ is symmetric.

To prove the above statements it should be taken into account that orthogonality of $\mathbf{R}$ implies

$$\delta(\mathbf{R}\cdot\mathbf{R}^{\mathsf{T}}) = \mathbf{0}, \qquad \delta\mathbf{R}\cdot\mathbf{R}^{\mathsf{T}} = -\mathbf{R}\cdot\delta\mathbf{R}^{\mathsf{T}} = -(\delta\mathbf{R}\cdot\mathbf{R}^{\mathsf{T}})^{\mathsf{T}}, \tag{2.7}$$

which means that, as indicated above, the tensor

$$\delta\boldsymbol{\Theta} := \delta\mathbf{R}\cdot\mathbf{R}^{\mathsf{T}} \tag{2.8}$$

appearing in the volume integral of (2.5) is skew-symmetric. Using the above notations, (2.5) can be rewritten in the following brief form:

$$\int_{{}^t\Omega} (\,\mathbf{D} : \delta\boldsymbol{\tau} + \boldsymbol{\tau} : \delta\boldsymbol{\Theta})\,\mathrm{d}\,{}^t\Omega = \int_{{}^t\Gamma_u} \widetilde{\mathbf{u}}\cdot\delta\boldsymbol{\tau}\cdot\,{}^t\mathbf{n}\,\mathrm{d}\,{}^t\Gamma. \tag{2.9}$$

In the course of integral transformations it should be taken into account that

- translational equilibrium (2.2) for the (non-symmetric) Cauchy stresses $\delta\boldsymbol{\tau}$ can be satisfied a priori by introducing a tensor of first-order stress functions $\boldsymbol{\chi}$ as

$$\delta\boldsymbol{\tau} = (\operatorname{curl}\delta\boldsymbol{\chi})^{\mathsf{T}} \qquad \mathbf{x}\in\,{}^t\Omega, \tag{2.10}$$

  where only six out of the nine components of $\delta\boldsymbol{\chi}$ are independent and the other three components can be set to zero;

- the homogeneous stress boundary condition (2.3) for $\delta\boldsymbol{\tau}$ in terms of first-order stress functions takes the form

$$\operatorname{div}_{\Gamma}\delta\boldsymbol{\chi}=\mathbf{0}\qquad \mathbf{x}\in {}^{t}\Gamma_{\sigma}, \tag{2.11}$$

where $\delta\boldsymbol{\chi}$ on ${}^{t}\Gamma_{\sigma}$ can be obtained as the gradient of an arbitrary vector $\mathbf{v}$ defined on ${}^{t}\Gamma_{\sigma}$ as

$$\delta\boldsymbol{\chi}=\operatorname{grad}\mathbf{v}\qquad \mathbf{x}\in {}^{t}\Gamma_{\sigma}, \tag{2.12}$$

provided equation

$$(\delta\boldsymbol{\chi}-\operatorname{grad}\mathbf{v})\cdot {}^{t}\boldsymbol{l}=\mathbf{0}\qquad \mathbf{x}\in {}^{t}\ell \tag{2.13}$$

holds on the common curve ${}^{t}\ell$ of boundary surfaces ${}^{t}\Gamma_{\sigma}$ and ${}^{t}\Gamma_{u}$ with ${}^{t}\boldsymbol{l}$ being the tangent unit vector to ${}^{t}\ell$ [17];

- the arbitrary but skew-symmetric tensor $\delta\boldsymbol{\Theta}$ defined by (2.8) can be written in terms of its vector $\delta\boldsymbol{\theta}$ as

$$\delta\boldsymbol{\Theta}=\mathbf{1}\times\delta\boldsymbol{\theta}, \tag{2.14}$$

where the three components of $\delta\boldsymbol{\theta}$ are also arbitrary.

Applying the Gauss- and Stokes-theorem and taking into account (2.10)-(2.14), (2.9) can be transformed into

$$\int_{{}^{t}\Omega}\left[-(\operatorname{curl}\mathbf{D})^{\mathsf{T}}:\delta\boldsymbol{\chi}+\boldsymbol{\tau}:(\mathbf{1}\times\delta\boldsymbol{\theta})\right]\,\mathrm{d}\,{}^{t}\Omega-\int_{{}^{t}\Gamma_{\sigma}}(\operatorname{div}_{\Gamma}\mathbf{D})\cdot\mathbf{v}\,\mathrm{d}\,{}^{t}\Gamma$$
$$+\int_{{}^{t}\Gamma_{u}}\left[(\mathbf{D}-\operatorname{grad}\widetilde{\mathbf{u}})\times {}^{t}\mathbf{n}\right]:\delta\boldsymbol{\chi}\,\mathrm{d}\,{}^{t}\Gamma-\oint_{{}^{t}\ell}\mathbf{v}\cdot(\mathbf{D}-\operatorname{grad}\widetilde{\mathbf{u}})\cdot {}^{t}\boldsymbol{l}\,\mathrm{d}\,{}^{t}s=0. \tag{2.15}$$

Equation (2.15) holds for all $\delta\boldsymbol{\chi}$, $\delta\boldsymbol{\theta}$ and $\mathbf{v}$, which means that their coefficients should be equal to zero. This condition implies the following independent Euler-Lagrange equations and natural boundary conditions of the generalized principle of complementary virtual work [18]:

the first-order compatibility equations (six independent equations)

$$(\operatorname{curl}\mathbf{D})^{\mathsf{T}}=\mathbf{0}\qquad \mathbf{x}\in {}^{t}\Omega, \tag{2.16}$$

the symmetry of the Cauchy stress tensor (three equations)

$$\boldsymbol{\tau}-\boldsymbol{\tau}^{\mathsf{T}}=\mathbf{0}\qquad \mathbf{x}\in {}^{t}\Omega, \tag{2.17}$$

the first-order compatibility boundary conditions (three equations)

$$\operatorname{div}_{\Gamma}\mathbf{D}=\mathbf{0}\qquad \mathbf{x}\in {}^{t}\Gamma_{\sigma}, \tag{2.18}$$

the strain boundary conditions (six independent equations)

$$(\mathbf{D}-\operatorname{grad}\widetilde{\mathbf{u}})\times {}^{t}\mathbf{n}=\mathbf{0}\qquad \mathbf{x}\in {}^{t}\Gamma_{u}, \tag{2.19}$$

and the continuity condition

$$(\mathbf{D} - \operatorname{grad} \widetilde{\mathbf{u}}) \cdot {}^t\boldsymbol{l} = \mathbf{0} \qquad \mathbf{x} \in {}^t\ell \tag{2.20}$$

on the common curve ${}^t\ell$ of ${}^t\Gamma_u$ and ${}^t\Gamma_\sigma$, where ${}^t\boldsymbol{l}$ is the unit tangent to the curve ${}^t\ell$ (Figure 1). It can be pointed out that condition (2.19) on ${}^t\Gamma_u$ implies compatibility boundary condition $\operatorname{div}_\Gamma \mathbf{D} = \mathbf{0}$ on ${}^t\Gamma_u$ as well. Since compatibility equations (2.16) are satisfied in ${}^t\Omega$ and the compatibility boundary conditions are satisfied on the whole boundary surface ${}^t\Gamma$, tensor $\mathbf{D} = \mathbf{1} - \mathbf{R}^\mathsf{T} \cdot \mathbf{V}^{-1}$ is the displacement gradient tensor, $\mathbf{R}^\mathsf{T} \cdot \mathbf{V}^{-1}$ is the inverse deformation gradient tensor and, following from the polar decomposition theorem, $\mathbf{R}$ and $\mathbf{V}$ are the rotation tensor and the left stretch tensor, respectively.

The independent equation system of non-linear elasticity in terms of the Cauchy stress tensor $\boldsymbol{\tau}$ and the orthogonal rotation tensor $\mathbf{R}$ consists of the translational equilibrium equations $\operatorname{div} \boldsymbol{\tau} + {}^t\rho\mathbf{b} = \mathbf{0}$, rotational equilibrium equations (2.17) and compatibility equations (2.16) as field equations, as well as stress boundary conditions $\boldsymbol{\tau} \cdot {}^t\mathbf{n} = {}^t\widetilde{\mathbf{p}}$, compatibility boundary conditions (2.18), and the boundary conditions for the strain tensor, (2.19) and (2.20). This equation system or, equivalently, the generalized principle of complementary virtual work with functional (2.5) can be used for solving non-linear elasticity problems only in that case, however, when invertible constitutive equation between the Cauchy stress tensor $\boldsymbol{\tau}$ and the left stretch tensor $\mathbf{V}$ exists. Such a constitutive relation for isotropic materials can be given in the form

$$\boldsymbol{\tau}(\mathbf{V}) = a_0\,\mathbf{1} + a_1\,\mathbf{V} + a_{-1}\,\mathbf{V}^{-1}, \tag{2.21}$$

where a_0, a_1 és a_{-1} are functions of the scalar invariants of $\mathbf{V}$ [19][15].

Remark 1. When compatibility equations (2.16), (2.18)-(2.19) hold, $\mathbf{D}$ is the gradient of an arbitrary vector field denoted by $\mathbf{u}$, i.e. $\mathbf{D} = \operatorname{grad} \mathbf{u}$. Assuming that $\mathbf{D}$ is given or obtained using the generalized complementary virtual work theorem, vector field $\mathbf{u}(P)$ at point P of the elastic body can be computed from $\mathbf{D}$ as

$$\mathbf{u}(P) = \mathbf{u}(O) + \int_O^P \mathbf{D} \cdot \mathrm{d}\mathbf{x} = \mathbf{u}(O) + \int_O^P \operatorname{grad} \mathbf{u} \cdot \mathrm{d}\mathbf{x}, \tag{2.22}$$

provided the value $\mathbf{u}(O)$ at an arbitrary point O of the body is known (the integral is path-independent). If $\mathbf{u}(O)$ is the displacement of point $O \in {}^t\Gamma_u$, then $\mathbf{u}(\mathbf{x})$ is the displacement field of the elastic body.

Remark 2. The inner product $\boldsymbol{\tau} : (\delta\mathbf{R} \cdot \mathbf{R}^\mathsf{T})$ in (2.5) can be considered as a Lagrange-multiplier term enforcing the symmetry condition for the Cauchy stress tensor into the principle. If $\boldsymbol{\tau}$ is a priori symmetric, this term disappears from (2.5) and the classical principle of complementary virtual work (2.1) is obtained.

Remark 3. In the dual formulation of the linearized theory of micropolar elasticity, where the use of both second- and first-order stress functions are needed, the correct number of first-order stress functions have been used by Kozák-Szeidl [20].

3. The generalized principle of complementary virtual work in the reference configuration

3.1. Transformations between the current and reference configurations. The generalized principle of complementary virtual work in the reference configuration can be derived from its form (2.5) valid in the current configuration. As a first step, relation between the variations of the Cauchy stress tensor $\delta\boldsymbol{\tau}$ and the first Piola-Kirchhoff stress tensor $\delta\mathbf{T}$ should be taken into account [6]:

$$\delta\boldsymbol{\tau} = J^{-1}\,\delta\mathbf{T}\cdot\mathbf{F}^{\mathsf{T}}, \tag{3.1}$$

where, assuming that (2.5) holds, $\mathbf{F}$ is the deformation gradient tensor and J is the Jacobian of the deformation gradient. Making use of (3.1) as well as the Piola transformation [21], requirements of statically admissibility for $\delta\boldsymbol{\tau}$, (2.2)-(2.3), are equivalent to equilibrium equations

$$\operatorname{Div}\delta\mathbf{T} = \mathbf{0} \qquad \mathbf{X}\in {}^{0}\Omega \tag{3.2}$$

and stress boundary conditions

$$\delta\mathbf{T}\cdot {}^{0}\mathbf{n} = \mathbf{0} \qquad \mathbf{X}\in {}^{0}\Gamma_{\sigma} \tag{3.3}$$

for the first Piola-Kirchhoff stress tensor $\mathbf{T}$. The next step is to transform the integrands of functional (2.5) into the reference configuration by taking into account the relations between the surface and volume elements of the current and reference configurations [6]:

$$\mathrm{d}\,{}^{t}\Omega = J\,\mathrm{d}\,{}^{0}\Omega, \tag{3.4}$$

and

$${}^{t}\mathbf{n}\,\mathrm{d}\,{}^{t}\Gamma = J\,\mathbf{F}^{-\mathsf{T}}\cdot {}^{0}\mathbf{n}\,\mathrm{d}\,{}^{0}\Gamma. \tag{3.5}$$

Then, using (3.1) and (3.4)-(3.5), integrands of (2.5) can be transformed as follows:

$$\mathbf{1}:\delta\boldsymbol{\tau}\,\mathrm{d}\,{}^{t}\Omega = \delta\mathbf{T}:\mathbf{F}\,\mathrm{d}\,{}^{0}\Omega, \tag{3.6}$$

$$(\mathbf{R}^{\mathsf{T}}\cdot\mathbf{V}^{-1}):\delta\boldsymbol{\tau}\,\mathrm{d}\,{}^{t}\Omega = \mathbf{F}^{-1}:(\delta\mathbf{T}\cdot\mathbf{F})\,\mathrm{d}\,{}^{0}\Omega = \delta\mathbf{T}:\mathbf{1}\,\mathrm{d}\,{}^{0}\Omega, \tag{3.7}$$

$$\boldsymbol{\tau}:(\delta\mathbf{R}\cdot\mathbf{R}^{\mathsf{T}})\,\mathrm{d}\,{}^{t}\Omega = (\mathbf{T}\cdot\mathbf{F}^{\mathsf{T}}):(\delta\mathbf{R}\cdot\mathbf{R}^{\mathsf{T}})\,\mathrm{d}\,{}^{0}\Omega, \tag{3.8}$$

$$\widetilde{\mathbf{u}}(\mathbf{x})\cdot\delta\boldsymbol{\tau}\cdot {}^{t}\mathbf{n}\,\mathrm{d}\,{}^{t}\Gamma = \widetilde{\mathbf{u}}(\mathbf{X})\cdot\delta\mathbf{T}\cdot {}^{0}\mathbf{n}\,\mathrm{d}\,{}^{0}\Gamma. \tag{3.9}$$

Inserting (3.6)–(3.9) in (2.5), the first form of the generalized principle of complementary virtual work in the reference configuration reads:

$$\int_{{}^{0}\Omega}\left[\delta\mathbf{T}:(\mathbf{F}-\mathbf{1})+(\mathbf{T}\cdot\mathbf{F}^{\mathsf{T}}):(\delta\mathbf{R}\cdot\mathbf{R}^{\mathsf{T}})\right]\mathrm{d}\,{}^{0}\Omega = \int_{{}^{0}\Gamma_{u}}\widetilde{\mathbf{u}}\cdot\delta\mathbf{T}\cdot {}^{0}\mathbf{n}\,\mathrm{d}\,{}^{0}\Gamma. \tag{3.10}$$

If equality (3.10) holds for all statically admissible first Piola-Kirchhoff stresses $\delta\mathbf{T}$ and all rotations $\delta\mathbf{R}$ (obtained from an arbitrary but orthogonal $\mathbf{R}$), then the tensor $\mathbf{H} := \mathbf{F}-\mathbf{1}$ is the displacement gradient tensor in the reference configuration, $\mathbf{F}$ is the deformation gradient and the product tensor $\mathbf{T}\cdot\mathbf{F}^{\mathsf{T}}$ is symmetric. Following from

the relation between the Cauchy stresses and the first Piola-Kirchhoff stresses [22], the latter condition is equivalent to the symmetry of the Cauchy stress tensor $\boldsymbol{\tau}$.

Proof of the above statements can be accomplished in similar steps to those presented in Section 2.2. However, the principle of complementary virtual work in its form (3.10) is still not applicable to the (numerical) solution of general non-linear elasticity problems, as the constitutive relation between the first Piola-Kirchhoff stress tensor and the displacement gradient (or deformation gradient) tensor is not uniquely invertible [9][11].

To obtain the most useful form of the principle of complementary virtual work in the reference configuration, polar decompositions of tensors $\mathbf{F}$ and $\mathbf{T}$ should be taken into account:

$$\mathbf{F} = \mathbf{R} \cdot \mathbf{U}, \qquad \mathbf{T} = \mathbf{R} \cdot \boldsymbol{\sigma}, \tag{3.11}$$

where $\boldsymbol{\sigma}$ is the Biot stress tensor [23][11]. Making use of (3.11), integrands on the left-hand-side of (3.10) can be transformed as follows:

$$\delta\mathbf{T} : \mathbf{F} = \delta\mathbf{T} : (\mathbf{R} \cdot \mathbf{U}) = \delta\boldsymbol{\sigma} : \mathbf{U} + (\delta\mathbf{R}^{\mathsf{T}} \cdot \mathbf{R}) : (\boldsymbol{\sigma} \cdot \mathbf{U}), \tag{3.12}$$

$$(\mathbf{T} \cdot \mathbf{F}^{\mathsf{T}}) : (\delta\mathbf{R} \cdot \mathbf{R}^{\mathsf{T}}) = (\mathbf{R}^{\mathsf{T}} \cdot \delta\mathbf{R}) : (\boldsymbol{\sigma} \cdot \mathbf{U}). \tag{3.13}$$

On inserting (3.12)-(3.13) in (3.10) and considering that in the reference configuration orthogonality of $\mathbf{R}$ implies

$$\delta(\mathbf{R}^{\mathsf{T}} \cdot \mathbf{R}) = \mathbf{0}, \qquad \delta\mathbf{R}^{\mathsf{T}} \cdot \mathbf{R} = -\mathbf{R}^{\mathsf{T}} \cdot \delta\mathbf{R} = -(\delta\mathbf{R}^{\mathsf{T}} \cdot \mathbf{R})^{\mathsf{T}}, \tag{3.14}$$

by which

$$(\mathbf{R}^{\mathsf{T}} \cdot \delta\mathbf{R}) : (\boldsymbol{\sigma} \cdot \mathbf{U}) + (\delta\mathbf{R}^{\mathsf{T}} \cdot \mathbf{R}) : (\boldsymbol{\sigma} \cdot \mathbf{U}) = 0, \tag{3.15}$$

the final form of the generalized principle of complementary virtual work in the reference configuration is obtained:

$$\int_{{}^0\Omega} (\, \delta\boldsymbol{\sigma} : \mathbf{U} - \delta\mathbf{T} : \mathbf{1} \,) \, \mathrm{d}\, {}^0\Omega = \int_{{}^0\Gamma_u} \widetilde{\mathbf{u}} \cdot \delta\mathbf{T} \cdot {}^0\mathbf{n} \, \mathrm{d}\, {}^0\Gamma. \tag{3.16}$$

If equality (3.16) holds (independently of the above derivation) for all statically admissible first Piola-Kirchhoff stresses $\delta\mathbf{T}$ and all rotations $\delta\mathbf{R}$ together with relation $\delta\boldsymbol{\sigma} = \delta(\mathbf{R}^{\mathsf{T}} \cdot \mathbf{T})$, where $\mathbf{U}$ is a symmetric tensor, then $\mathbf{H} := \mathbf{R} \cdot \mathbf{U} - \mathbf{1}$ is the displacement gradient tensor, $\mathbf{F} := \mathbf{R} \cdot \mathbf{U}$ is the deformation gradient, and the co-rotated Kirchhoff stress tensor $\mathbf{K} := \boldsymbol{\sigma} \cdot \mathbf{U}$ is symmetric, which implies the symmetry of the Kirchhoff- and Cauchy stress tensor as well. The proof of the above statements is given in Section 3.2 Note that due to the symmetry of $\mathbf{U}$, (3.16) depends on the symmetric part of the Biot stress tensor, $\boldsymbol{\sigma}_s = (\boldsymbol{\sigma} + \boldsymbol{\sigma}^{\mathsf{T}})/2 = (\mathbf{R}^{\mathsf{T}} \cdot \mathbf{T} + \mathbf{T}^{\mathsf{T}} \cdot \mathbf{R})/2$, which is sometimes referred to as Jaumann stress tensor [8][9].

Remark 4. The generalized principle of complementary virtual work is independent of the actual constitutive equations. Since $\mathbf{U}$ and $\boldsymbol{\sigma}_s$ are objective stress and strain measures, single-valued, invertible constitutive relation exists between them. Assuming hyperelastic materials, it can be given in the form

$$\mathbf{U}(\boldsymbol{\sigma}_s) = \frac{\partial W_c(\boldsymbol{\sigma}_s)}{\partial \boldsymbol{\sigma}_s}, \tag{3.17}$$

where $W_c(\boldsymbol{\sigma}_s)$ is the complementary strain energy density. Using (3.17), inner product $\delta\boldsymbol{\sigma} : \mathbf{U}$ on the left-hand-side of (3.16) can be written as

$$\delta\boldsymbol{\sigma} : \mathbf{U} = \delta\boldsymbol{\sigma}_s : \mathbf{U} = \delta\boldsymbol{\sigma}_s : \frac{\partial W_c(\boldsymbol{\sigma}_s)}{\partial\boldsymbol{\sigma}_s} = \delta W_c(\boldsymbol{\sigma}_s). \tag{3.18}$$

On inserting (3.18) in (3.16), we obtain the zero-valued first variation of Fraeijs de Veubeke's dual-mixed variational principle in terms of the first Piola-Kirchhoff stress tensor and the orthogonal rotation tensor [7]:

$$\delta\mathcal{F}(\delta\mathbf{T}, \delta\mathbf{R}) = \int_{{}^0\Omega} [\delta W_c(\boldsymbol{\sigma}_s) - \delta\mathbf{T} : \mathbf{1}] \, \mathrm{d}\,{}^0\Omega - \int_{{}^0\Gamma_u} \widetilde{\mathbf{u}} \cdot \delta\mathbf{T} \cdot {}^0\mathbf{n} : \mathrm{d}\,{}^0\Gamma = 0. \tag{3.19}$$

This result indicates that the generalized principle of complementary virtual work in the reference configuration is equivalent to the two-field dual-mixed principle of Fraeijs de Veubeke, provided constitutive equations of type (3.17) are being taken into account. □

3.2. Independent equation system of non-linear elasticity in the reference configuration. The independent equation system of non-linear elasticity in terms of the first Piola-Kirchhoff stress tensor $\mathbf{T}$ and the orthogonal rotation tensor $\mathbf{R}$ can be derived from (3.16) by taking into account subsidiary conditions of statically admissibility, (3.2) and (3.3), for $\delta\mathbf{T}$, the orthogonality condition for $\mathbf{R}$, as well as the symmetry condition for $\mathbf{U}$. In the course of integral transformations it should be taken into account that [18]

- following from (3.11), variation of the Biot stress tensor can be expressed by variations of $\mathbf{T}$ and $\mathbf{R}$ as

$$\delta\boldsymbol{\sigma} = \delta\mathbf{R}^{\mathsf{T}} \cdot \mathbf{T} + \delta\mathbf{T}^{\mathsf{T}} \cdot \mathbf{R}, \tag{3.20}$$

- equilibrated $\delta\mathbf{T}$ satisfying (3.2) can be obtained from an arbitrary tensor of first-order stress functions $\boldsymbol{\Psi}$ as

$$\delta\mathbf{T} = (\mathrm{Curl}\,\delta\boldsymbol{\Psi})^{\mathsf{T}}, \tag{3.21}$$

  where only six out of the nine components of $\delta\boldsymbol{\Psi}$ are independent and the other three components can be set to zero;

- orthogonality of $\mathbf{R}$ and (3.14) implies that tensor

$$\delta\boldsymbol{\phi} := \mathbf{R}^{\mathsf{T}} \cdot \delta\mathbf{R}, \tag{3.22}$$

  is skew-symmetric, from which first variation of the rotation tensor can be expressed as

$$\delta\mathbf{R} = \mathbf{R} \cdot \delta\boldsymbol{\phi}; \tag{3.23}$$

- the homogeneous stress boundary condition (3.3) for $\delta\mathbf{T}$ in terms of first-order stress functions takes the form

$$\mathrm{Div}_\Gamma \, \delta\boldsymbol{\Psi} = \mathbf{0} \qquad \mathbf{X} \in {}^0\Gamma_\sigma, \tag{3.24}$$

where $\delta\boldsymbol{\Psi}$ on ${}^0\Gamma_\sigma$ can be obtained as the gradient of an arbitrary vector $\mathbf{w}$ defined on ${}^0\Gamma_\sigma$ as

$$\delta\boldsymbol{\Psi} = \operatorname{Grad}\mathbf{w} \qquad \mathbf{X} \in {}^0\Gamma_\sigma, \tag{3.25}$$

provided equation

$$(\delta\boldsymbol{\Psi} - \operatorname{Grad}\mathbf{w}) \cdot {}^0\boldsymbol{l} = \mathbf{0} \qquad \mathbf{X} \in {}^0\ell \tag{3.26}$$

holds on the common curve ${}^0\ell$ of boundary surfaces ${}^0\Gamma_\sigma$ and ${}^0\Gamma_u$ with ${}^0\boldsymbol{l}$ being the tangent unit vector to ${}^0\ell$;

- the arbitrary but skew-symmetric tensor $\delta\boldsymbol{\phi}$ defined by (3.22) can be written in terms of its vector $\delta\boldsymbol{\varphi}$ as

$$\delta\boldsymbol{\phi} = \mathbf{1} \times \delta\boldsymbol{\varphi}, \tag{3.27}$$

where the three components of $\delta\boldsymbol{\varphi}$ are also arbitrary.

Introducing the notation

$$\mathbf{H} := \mathbf{R} \cdot \mathbf{U} - \mathbf{1} \tag{3.28}$$

and applying the Gauss- and Stokes-theorem and taking into account (3.20)–(3.27), (3.16) can be transformed into

$$\begin{aligned}&\int_{{}^0\Omega} \left[-(\operatorname{Curl}\mathbf{H})^{\mathsf{T}} : \delta\boldsymbol{\Psi} - (\boldsymbol{\sigma}\cdot\mathbf{U}) : (\mathbf{1}\times\delta\boldsymbol{\varphi})\right] \mathrm{d}\,{}^0\Omega - \int_{{}^0\Gamma_\sigma} (\operatorname{Div}_\Gamma \mathbf{H})\cdot\mathbf{w}\,\mathrm{d}\,{}^0\Gamma \\ &+ \int_{{}^0\Gamma_u} \left[\,(\mathbf{H} - \operatorname{Grad}\widetilde{\mathbf{u}}) \times {}^0\mathbf{n}\,\right] : \delta\boldsymbol{\Psi}\,\mathrm{d}\,{}^0\Gamma - \oint_{{}^0\ell} \mathbf{w}\cdot(\mathbf{H} - \operatorname{Grad}\widetilde{\mathbf{u}})\cdot{}^0\boldsymbol{l}\,\mathrm{d}\,{}^0s = 0.\end{aligned} \tag{3.29}$$

Equality (3.29) holds for all $\delta\boldsymbol{\Psi}$, $\delta\boldsymbol{\varphi}$ and $\mathbf{w}$, which means that their coefficients should be equal to zero. The independent Euler-Lagrange equations and natural boundary conditions of the generalized principle of complementary virtual work in the reference configuration are [18]:

the first-order compatibility equations for $\mathbf{H}$ (six independent equations):

$$(\operatorname{Curl}\mathbf{H})^{\mathsf{T}} = \mathbf{0} \qquad \mathbf{X} \in {}^0\Omega, \tag{3.30}$$

the symmetry condition for the co-rotated Kirchhoff stress tensor $\mathbf{K} = \boldsymbol{\sigma}\cdot\mathbf{U}$ (three equations):

$$\boldsymbol{\sigma}\cdot\mathbf{U} = \mathbf{U}\cdot\boldsymbol{\sigma}^{\mathsf{T}} \qquad \mathbf{X} \in {}^0\Omega, \tag{3.31}$$

the first-order compatibility boundary conditions (three equations):

$$\operatorname{Div}_\Gamma \mathbf{H} = \mathbf{0} \qquad \mathbf{X} \in {}^0\Gamma_\sigma, \tag{3.32}$$

the strain boundary conditions (six independent equations):

$$(\mathbf{H} - \operatorname{Grad}\widetilde{\mathbf{u}}) \times {}^0\mathbf{n} = \mathbf{0} \qquad \mathbf{X} \in {}^0\Gamma_u, \tag{3.33}$$

and the continuity condition

$$(\mathbf{H} - \operatorname{Grad} \widetilde{\mathbf{u}}) \cdot {}^0\boldsymbol{l} = \mathbf{0} \qquad \mathbf{X} \in {}^0\ell \tag{3.34}$$

on the common curve ${}^0\ell$ of surface parts ${}^0\Gamma_u$ és ${}^0\Gamma_\sigma$, where ${}^0\boldsymbol{l}$ is the unit tangent to the curve ${}^0\ell$ (Figure 1). Condition (3.33) implies compatibility boundary condition $\operatorname{Div}_\Gamma \mathbf{H} = \mathbf{0}$ on ${}^0\Gamma_u$, i.e. compatibility boundary conditions are satisfied on the whole surface ${}^0\Gamma$. This fact, together with compatibility equations (3.30) means that tensor field $\mathbf{H}$, defined by (3.28), is the displacement gradient in the reference configuration and $\mathbf{R}\cdot\mathbf{U} = \mathbf{H}+\mathbf{1}$ is the deformation gradient. With the above derivation, statements in Section 3.1 regarding the complementary virtual work theorem in the reference configuration have been proven.

The independent equation system of non-linear elasticity in terms of the first Piola-Kirchhoff stress tensor $\mathbf{T}$ and the orthogonal rotation tensor $\mathbf{R}$ consists of the translational equilibrium equations $\operatorname{Div}\mathbf{T} + {}^0\rho\mathbf{b} = \mathbf{0}$, compatibility equations (3.30) and, taking into account relation $\boldsymbol{\sigma} = \mathbf{R}^{\mathsf{T}}\cdot\mathbf{T}$, symmetry condition (3.31) as field equations, as well as stress boundary conditions $\mathbf{T}\cdot {}^0\mathbf{n} = {}^0\widetilde{\mathbf{p}}$, compatibility boundary conditions (3.32), and boundary conditions for the displacement gradient tensor, (3.33) and (3.34). This equation system or, equivalently, the generalized principle of complementary virtual work with functional (3.16) should, of course, be used together with constitutive equations of type (3.17) when solving non-linear elasticity problems.

In connection with the above derived equation system it should be noted that a derivation has already been given by Fraeijs de Veubeke [7]. However, his derivation is incomplete in the following sense: (i) The nine compatibility equation of [7] is not independent, because all the nine components of the first-order stress function tensor were used (instead of six) in the derivation. (ii) Stress boundary condition (3.24) have been taken into account by the use of a Lagrange-multiplier which was a priori assumed (incorrectly) to be the displacement field on the boundary part ${}^0\Gamma_\sigma$. Due to this assumption, compatibility boundary conditions (3.32) and strain boundary conditions (3.33) did not appear in the equation system of [7] (instead of (3.32), an identity was obtained), and, furthermore, no fitting condition for the Lagrange multiplier and the prescribed displacement field $\widetilde{\mathbf{u}}$ on the curve ${}^0\ell$ was obtained (a condition which would be equivalent to (3.34)).

Remark 5. In geometrically non-linear elasticity problems, instead of $\mathbf{U}$ the use of the Jaumann strain tensor $\boldsymbol{\varepsilon} = \mathbf{U} - \mathbf{1}$ is more practical (due to the linear constitutive relations between the Biot stresses and Jaumann strains in that case). Then, taking into account that from (3.20) we have

$$\delta\boldsymbol{\sigma} : \mathbf{1} = \delta\mathbf{R} : \mathbf{T} + \delta\mathbf{T} : \mathbf{R}, \tag{3.35}$$

the generalized principle of complementary virtual work can be transformed into the following form:

$$\int_{{}^0\Omega} [\, \delta\boldsymbol{\sigma} : \boldsymbol{\varepsilon} + \delta\mathbf{T} : (\mathbf{R} - \mathbf{1}) + \delta\mathbf{R} : \mathbf{T}\,]\, \mathrm{d}\,{}^0\Omega = \int_{{}^0\Gamma_u} \widetilde{\mathbf{u}} \cdot \delta\mathbf{T} \cdot {}^0\mathbf{n} : \mathrm{d}\,{}^0\Gamma. \tag{3.36}$$

Incremental form of this principle and its consistent linearization can be found in [18]. □

4. Concluding remarks

Despite the fact that stress-based methods and numerical models are usually more involved, both theoretically and numerically, than displacement-based methods and models, stress-based formulations receive an emerging interest in computational mechanics. The practical importance of such models and methods in the numerical analysis and solution of linear and non-linear elasticity problems can probably be traced back to the numerical difficulties and convergence problems encountered in the application of the classical displacement-based finite element methods to parameter dependent or constraint problems of elasticity (and plasticity).

Theoretical developments presented in this paper has been motivated by the limited applicability of the stress-based principle of complementary virtual work in non-linear elasticity. A modification of the classical principle is proposed by introducing the orthogonal rotation tensor into the principle. In the current configuration this is done by incorporating the rotational equilibrium for the Cauchy stress tensor into the principle. Applicability of the generalized principle requires, however, the existence of an invertible constitutive relation between the Cauchy stress tensor and the left stretch tensor. From the numerical point of view, it is more useful to transform the principle into the reference configuration, where, provided that constitutive equations between the Biot stress and right stretch tensors are being taken into consideration, the principle is equivalent to the two-field, complementary energy-based variational principle of Fraeijs de Veubeke.

Acknowledgement. The work reported herein was supported in part by the Hungarian Scientific Research Fund under Grant No. OTKA T026292 and by a János Bolyai Research Fellowship of the Hungarian Academy of Sciences as well as by the German Alexander von Humboldt Foundation.

REFERENCES

[1] Novozhilov, V.V.: *Theory of Elasticity*, Pergamon Press, Oxford, 1961.

[2] Zubov, L.M.: *The stationary principle of complementary work in nonlinear theory of elasticity*, Prikl. Mat. Mekh. **34** (1970) 241-245.

[3] Lur'e, A.I.: *Theory of Elasticity*, Nauka, Moscow, 1975.

[4] Washizu, K.: *Complementary variational principles in elasticity and plasticity*, Conference on Duality and Complementarity of Deformable Solids, Jablonna, Poland, Lecture Notes, pp. 7–93, 1977.

[5] Levinson M.: *The complementary energy theorem in finite elasticity*, J. Appl. Mech. **32** (1965) 826-828.

[6] Truesdell, C. and Noll, W.: *The Non-Linear Field Theories*, In Handbuch der Physik, Band III/3, Springer-Verlag, Berlin, 1965.

[7] Fraeijs de Veubeke, B.M.: *A new variational principle for finite elastic displacements*, International Journal for Engineering Sciences **10**, 745-763.

[8] Christoffersen, J.: *On Zubov's principle of stationary complementary energy and a*

related principle, Report 44, Danish Center for Applied Mathematics and Mechanics, 1973.

[9] Koiter, W.T.: *On the complementary energy theorem in non-linear elasticity theory*, Report WTHD No. 72, Department of Mechanical Engineering, Delft University of technology, The Nederlands, June 1975, 37 p.

[10] Dill, E.H.: *The complementary energy principle in nonlinear elasticity*, Letters in Applied Engineering Sciences **5** (1977) 95–106.

[11] Ogden, R.W.: *Inequalities associated with the inversion of elastic stress-deformation relations and their implication*, Math. Proc. Camb. Phil. Soc. **81** (1977) 313-324.

[12] Koiter, W.T.: *On the principle of stationary complementary energy in the nonlinear theory of elasticity*, SIAM J. Appl. Math. **25** (1973) 424-434.

[13] Mikkola, M.J.: *Complementary energy theorem in geometrically non-linear structural problems*, Int. J. Non-Linear Mechanics **24** (1989) 499-508.

[14] Gurtin, M.E.: *The linear theory of elasticity*, In Handbuch der Physik, Band VIa/2, Springer-Verlag, Berlin, 1972, pp. 1-295.

[15] Gurtin, M.E.: *An Introduction to Continuum Mechanics*, Academic Press, New York, 1981.

[16] Kozák, I.: *Principle of complementary virtual work and the Riemann-Christoffel curvature tensor as compatibility condition*, J. Comp. Appl. Mech. **1** (2000) 71–79.

[17] Bertóti, E.: *Indeterminacy of first order stress functions and the stress- and rotation-based formulation of linear elasticity*, Comput. Mech. **14** (1994) 249-265.

[18] Bertóti, E.: *Dual-mixed variational methods in non-linear elasticity. Theory and analysis*, Habilitation thesis, Department of Mechanics, University of Miskolc, Miskolc, 2000 (in Hungarian).

[19] Malvern, L.E.: *Introduction to the Mechanics of a Continuous Medium*, Prentice-Hall, Englewood Cliffs, 1969.

[20] Kozák, I. and Szeidl, G.: *The field equations and the boundary conditions with force stresses and couple stresses in the linearized theory of micropolar elastostatics*, Acta. Techn. Hung. **91**(1–2) (1980) 57–80.

[21] Marsden, J.E. and Hughes, T.J.R.: *Mathematical Foundations of Elasticity*, Prentice-Hall, Englewood Cliffs, 1983.

[22] Béda, G., Kozák, I. and Verhás J.: *Continuum Mechanics*, Akadémiai Kiadó, Budapest, 1995.

[23] Biot, M.A.: *The Mechanics of Incremental Deformations*, John Wiley & Sons, Inc., New York, 1965.

Journal of Computational and Applied Mechanics, Vol. 1., No. 2., (2000), pp. 123–128

A CONSEQUENCE OF THE GENERALIZED CLAPEYRON'S THEOREM

Gyula Béda
Department of Applied Mechanics, Budapest University of Technology and Economics
Műegyetem rkp. 5, 1111 BUDAPEST, Hungary
beda@mm.bme.hu

[Received: June 1, 2000]

Abstract. The investigation of the third order wave necessitates the knowledge of the dynamic compatibility equation. This equation rises from the first equation of motion in case of the acceleration wave. Now it requires the time derivative of the first equation of motion. The material time derivative is not simple in the current configuration. Using the generalized Clapeyron's theorem we obtain an equation of motion of stress-rate. The dynamic compatibility equation can be calculated from it. Many authors have dealt with this question when the body is in equilibrium [8, 9, 10]. The third order wave can be investigated by using the compatibility equations (dynamic, kinematic and constitutive). The generalized acoustic tensor is another important result of these investigations.

Keywords: generalized Clapeyron theorem, equation of motion of stress-rate, acoustic tensor of third order wave

1. Introduction

In its original form, Clapeyron's theorem concerns the transition between two states of equilibrium. If the displacement field u_i takes us from one equilibrium state into the other then the work of the internal forces $t^{ij}u_{i;j}$ is equal to the work done by the body forces q^i and the trections $t^{ij}n_j\big|_A$ acting on the boundary surface A, that is,

$$\int_V t^{ij}u_{i;j}\ \mathrm{d}V = \int_V q^i u_i \mathrm{d}V + \int_A u_i t^{ij} n_j \mathrm{d}A, \tag{1.1}$$

where t^{ij} is the stress tensor, $u_{i;j}$ is the covariant derivative of the displacement vector u_i with respect to the j-th coordinate, n_j is the outward unit normal and V is the part of the geometric space which contains the body B and which is bounded by a closed surface A. Here and in the sequel indicial notations are employed. Accordingly, a Latin index has the range 1,2 and 3; summation over repeated indices is implied and the covariant derivative is denoted by an index preceded by a semicolon. The strain tensor is denoted by e_{ij}.

For moving continua the theory should be modified as follows: the velocity field v_i should be used instead of u_i and, with regard to D'Alembert's principle, q^i is to be replaced by the generalized body force $b^i \equiv q^i - \rho\dot{v}^i$. Let the mass density and the acceleration be denoted by ρ and $\dot{v}^i$, respectively. Obviously, to keep the original meaning of Clapeyron's theorem, the volume and surface integrals should be integrated with respect to time t. This generalization of Clapeyron's theorem remains

valid even for finite displacements, if the proper changes are carried out [1]. The generalized Clapeyron's theorem can be formulated as

$$\int_{t_0}^{t_1}\int_V \left(\dot{t}^{ij} - t^{iq}v^j_{;q} + t^{ij}v^p_{;p}\right) u_{i;j}\mathrm{d}V\mathrm{d}t = \int_{t_0}^{t_1}\int_V \left(\dot{b}^i + b^i v^p_{;p}\right) u_i \mathrm{d}V dt + \\ + \int_{t_0}^{t_1}\int_V \left(\dot{t}^{ij} - t^{iq}v^j_{;q} + t^{ij}v^p_{;p}\right) u_i n_j \mathrm{d}A_j\mathrm{d}t\ , \tag{1.2}$$

where overdot denotes the material time derivative and $\mathrm{d}A_j \equiv n_j \mathrm{d}A$. If $t^{ij}{}_{;j} + b^i = 0$ then the equation of motion is satisfied [1].

2. Equation of motion for the stress-rate

Equation (1.2) is valid for all kinematically (geometrically) admissible displacement fields, thus it holds also for the virtual field u_i^* [11]. By keeping in mind that remark, the last surface integral of the left-hand side of (1.2) can be transformed into volume integral

$$\int_{t_0}^{t_1}\int_V \left[\left(\dot{t}^{ij} - t^{iq}v^j_{;q} + t^{ij}v^p_{;p}\right)_{;j} u_i + \left(\dot{t}^{ij} - t^{iq}v^j_{;q} + t^{ij}v^p_{;p}\right) u_{i;j}\right] \mathrm{d}V\mathrm{d}t\,. \tag{2.1}$$

By substituting (2.1) into (1.2) and performing some rearrangements we have

$$\int_{t_0}^{t_1}\int_V \left[\left(\dot{t}^{ij} - t^{iq}v^j_{;q} + t^{ij}v^p_{;p}\right)_{;j} + \dot{b}^i + b^i v^p_{;p}\right] u_i^* \mathrm{d}V\mathrm{d}t = 0$$

where the virtual displacement u_i^* is written for u_i. This equation is satisfied for any u_i^* if

$$\left(\dot{t}^{ij} - t^{iq}v^j_{;q} + t^{ij}v^p_{;p}\right)_{;j} + \dot{b}^i + b^i v^p_{;p} = 0\,. \tag{2.2}$$

Substituting $b^i \equiv q^i - \rho\dot{v}^i$ and introducing the Lie derivative of the stress tensor $L_v\left(t^{ij}\right) = \dot{t}^{ij} - t^{ip}v^j_{;p} - t^{pj}v^i_{;p}$ as a stress-rate and making use of the continuity equation, the equation of motion (2.2) for the Lie derivative of the stresses assumes the form

$$\left[L_v\left(t^{ij}\right)\right]_{;j} + \left(t^{pj}v^i_{;p} + t^{ij}v^p_{;p}\right)_{;j} + \dot{q}^i + q^i v^p_{;p} = \rho\ddot{v}^i\ . \tag{2.3}$$

This equation is referred to as the equation of motion for the stress-rate [8,9,10,12].

3. The third order wave

When the basic quantities v^k, t^{kl}, e_{kl} and their first derivatives are all continuous, but the second derivatives have a jump when crossing the surface $\varphi\left(x^k, t\right) = 0$, we

speak about third order waves [2]. Let us denote the jump of some quantity $v^k_{;p}$ by $\langle v^k_{;p}\rangle$. When the velocity gradient is $v^k_{;p}$ and we consider a wave of order three then $\langle v^k_{;p}\rangle = 0$ but $\langle v^k_{;qp}\rangle \neq 0$. Thus in (2.3) $\langle L_v\left(t^{kp}\right)\rangle = 0$ but $\langle L_v\left(t^{kp}_{;p}\right)\rangle \neq 0$.

Consequently, the dynamic condition a third order wave should meet is of the form

$$L_v\left(t^{k\ell}_{;\ell}\right) + t^{pq}\langle v^k_{;qp}\rangle + t^{k\ell}\left\langle v^p_{;p\ell}\right\rangle = \rho\langle \ddot{v}^k\rangle\ . \tag{3.1}$$

Let the kinematic equation [4, 5] be

$$\left(L_v e_{ij}\right)^{\cdot} = \ddot{e}_{ij} + \left(e_{kj}v^k_{;i} + e_{ik}v^k_{;j}\right) \tag{3.2}$$

where e_{kj} is the Euler strain tensor. If the Lie derivative of the velocity field is Ł$_v$, the expression $L_v \equiv$Ł$_v + \partial/\partial t$ in (3.2) is a generalization [3]. As is well known, $L_v\left(e_{ij}\right) = v_{ij}$, thus the kinematic compatibility condition for the third order wave is

$$\langle \ddot{v}_{ij}\rangle = \langle \ddot{e}_{ij}\rangle + e_{kj}\langle \dot{v}^k_{;i}\rangle + e_{ik}\langle \dot{v}^k_{;j}\rangle\,. \tag{3.3}$$

It can easily be shown that $\dot{v}^k_{;i} \neq \left(v^k_{;i}\right)^{\cdot}$, but $\langle \dot{v}^k_{;i}\rangle = \left\langle \left(v^k_{;i}\right)^{\cdot}\right\rangle$ and this property is the same for the second derivatives of all other functions.

Let the constitutive equation be [14]

$$f_\alpha\left(L_v\left(t^{ij}\right), Q^{ij}, L_v\left(e_{ij}\right), q_{ij}, t^{ij}, e_{ij}\right) = 0, \qquad (\alpha = 1, 2, ..., 6) \tag{3.4}$$

where $Q^{ij} = B^{ijm}_{\ \ pq}t^{pq}_{\ ;m}$ and $q_{ij} = b_{ij}^{\ pq\ell}e_{pq;\ell}$, if $B^{ijm}_{\ \ pq}$ and $b_{ij}^{\ pq\ell}$ are appropriate tensors transforming tensors $t^{pq}_{\ ;m}$ and $e_{pq;\ell}$ into second order ones.

The constitutive compatibility conditions can be obtained from the material derivative of (3.4)

$$\frac{\partial f_\alpha}{\partial L_v\left(t^{ij}\right)}\left\langle L_v\left(t^{ij}\right)^{\cdot}\right\rangle + \frac{\partial f_\alpha}{\partial Q^{ij}}B^{ijm}_{\ \ pq}\langle \dot{t}^{pq}_{\ ;m}\rangle + \frac{\partial f_\alpha}{\partial L_v\left(e_{ij}\right)}\langle L_v\left(e_{ij}\right)^{\cdot}\rangle + \frac{\partial f_\alpha}{\partial q_{ij}}b_{ij}^{\ pq\ell}\langle \dot{e}_{pq;\ell}\rangle = 0, \qquad (\alpha = 1, 2, ..., 6)$$

or introducing the notations $S^{rs}_{\ \ ij}, R^{rs}_{\ \ ij}, T^{rsij}$ and U^{rsij} for the coefficients

$$S^{rs}_{\ \ ij} \equiv \frac{\partial f_\alpha}{\partial L_v\left(t^{ij}\right)}, R^{rs}_{\ \ ij} \equiv \frac{\partial f_\alpha}{\partial Q^{ij}}, T^{rsij} \equiv \frac{\partial f_\alpha}{\partial L_v\left(e_{ij}\right)}, U^{rsij} \equiv \frac{\partial f_\alpha}{\partial q_{ij}}$$

the constitutitve compatibility condition is

$$S^{rs}_{\ \ ij}\left\langle L_v\left(t^{ij}\right)^{\cdot}\right\rangle + R^{rs}_{\ \ ij}B^{ijm}_{\ \ pq}\langle \dot{t}^{pq}_{\ ;m}\rangle + T^{rsij}\langle L_v\left(e_{ij}\right)^{\cdot}\rangle + U^{rsij}b_{ij}^{\ pq\ell}\langle \dot{e}_{pq;\ell}\rangle = 0\,. \tag{3.5}$$

In the following we use Cartesian coordinates. Let the jumps in the second derivatives of the stress and strain tensors and that of the velocity field, each on the surface $\varphi\left(x^k, t\right) = 0$, are denoted by γ^{ij}, α_{ij} and λ^k. Further denote n_k the unit normal vector

of the wavefront and C and c denote the wave propagation velocity with respect to the material and to the reference frame:

$$n_k \equiv \frac{\dfrac{\partial\varphi}{\partial x^k}}{\sqrt{g^{pq}\dfrac{\partial\varphi}{\partial x^p}\dfrac{\partial\varphi}{\partial x^q}}}, \qquad C = c - v^k n_k,$$

With these notations one can conclude that equations (3.1), (3.3) and (3.5) imply [2 , 4]:

$$\gamma^{k\ell} n_\ell = -\rho C \lambda^k \tag{3.6}$$

$$\alpha_{ij} = \frac{1}{2C}\left[n_i\left(2e_{kj} - g_{kj}\right) + n_j\left(2e_{ik} - g_{ik}\right)\right]\lambda^k \tag{3.7}$$

$$\begin{aligned} S^{rs}_{\ ij}\left(C\gamma^{ij} + t^{iq}n_q\lambda^j + t^{qj}n_q\lambda^i - t^{ij}n_\ell\lambda^\ell\right) - R^{rs}_{\ \ ij}B^{ijm}_{\ \ \ pq}n_m\gamma^{pq} + \\ + T^{rsij}\left[C\alpha_{ij} - \lambda^k\left(e_{ik}n_j + e_{kj}n_i\right)\right] - U^{rsij}b_{ij}^{\ \ pq\ell}n_\ell\alpha_{pq} = 0 \end{aligned} \tag{3.8}$$

Making use of equations (3.6) and (3.7) we get from (3.8) that

$$\begin{aligned} \Big\{2\rho S^{rs}_{\ \ k\ell}C^3 - 2\rho\bar{R}^{rs}_{\ \ k\ell}C^2 + \\ \Big[T^{rsij}\left(g_{kj}n_i + g_{ik}n_j\right) - 2S^{rs}_{\ \ ij}\left(t^{iq}g^j_{\ k} + t^{qj}g^i_{\ k} - t^{ij}g^q_{\ k}\right)n_q\Big]n_\ell C + \\ \bar{U}^{rsij}\left[n_i\left(2a_{kj} - g_{kj}\right) + n_j\left(2a_{ik} - g_{ik}\right)\right]n_\ell\Big\}\gamma^{k\ell} = 0, \end{aligned} \tag{3.9}$$

where $g^j_{\ k}$ denotes Kronecker's symbol. Since $\gamma^{k\ell}$ is different from zero, the determinant of its coefficient matrix must vanish [13], that is,

$$\det\{\} = 0.$$

This is the equation of propagation for the third order wave. Clearly this equation is an algebraic equation of order 18 for the propagation velocity C. Observe that the notations $\bar{R}^{rs}_{\ \ k\ell} \equiv R^{rs}_{\ \ pq}B^{pqm}_{\ \ \ \ k\ell}n_m$ and $\bar{U}^{rsij} \equiv U^{rspq}b_{pq}^{\ \ ijm}n_m$ are used in the matrix $\{\}$. These notations can also be employed in equation (3.8). The matrix $\{\}$ can be considered as the characteristic matrix of a generalization of the acoustic tensor.

Equation (3.8) can also be written in a form consisting of λ^k when $S^{rs}_{\ \ ij}$ takes some of the values 0, $S^r_i g^s_j$, $g^r_i g^s_j$ and $\bar{R}^{rs}_{\ \ ij}$ one of 0, $\bar{R}^r_i g^s_j$, $\bar{R}^{rs}_{\ \ i}n_j$ and we multiply the equations by n_s. (In the case of a solid body S and $\bar{R}$ are probably impossible to be zero at the same time).

In the 9 cases under consideration, the equation for λ^k is

$$\left(E^r_k C^3 + F^r_k C^2 + G^r_k C + H^r_k\right)\lambda^k = 0\,. \tag{3.10}$$

In the second case $E^r_k = g^r_k$ in (3.10).

The wave propagation equation is

$$\det\left(E_k^r C^3 + F_k^r C^2 + G_k^r C + H_k^r\right)\lambda^k = 0\,. \tag{3.11}$$

This is a 9-th order equation for the propagation velocity .

By using [6] the matrix of acoustic tensor in case of (3.10) can be obtained. Let us denote the coefficients of C in the form of 3x3 matrices by $\mathbf{E}, \mathbf{F}, \mathbf{G}, \mathbf{H}$. By introducing the inverse and unit matrices $\mathbf{E}^{-1}$, $\mathbf{I}$ the acoustic tensor is

$$\begin{bmatrix} \mathbf{0} & \mathbf{I} & \mathbf{0} \\ \mathbf{0} & \mathbf{0} & \mathbf{I} \\ -\mathbf{E}^{-1}\cdot\mathbf{H} & -\mathbf{E}^{-1}\cdot\mathbf{G} & -\mathbf{E}^{-1}\cdot\mathbf{F} \end{bmatrix}. \tag{3.12}$$

Comparing the expression (3.1) of [4] and expression (3.9) of this paper we find that these are the same in the case of acceleration wave [4] and in the present one.

The most general acoustic tensor can be obtained from (3.9) when the coefficients have been denoted in the form of 6x6 matrices $\mathbf{E}, \mathbf{F}, \mathbf{G}, \mathbf{H}$. The shape of acoustic tensor is identical to (3.12) [7]. Matrix (3.12) is a 9x9 matrix while this generalized matrix is a 18x18 one.

4. Concluding remarks

Our starting point was the generalized Clapeyron's equation, which, by using continuity equation, resulted in the first Cauchy equation of motion and the equation of motion for stress-rate. In such a way we obtain a more general equation for stress-rate which enables us to write the compatibility equations for the third order wave. These two sets of equations are the main result of this paper. As an application these equations lead to an acoustic tensor, which is identical to the acoustic tensor obtained by acceleration waves, because we used quasilinear integrable second order constitutive equations. This computation justifies that we could similarly get an acoustic tensor in case of a general second order constitutive equation.

REFERENCES

1. Béda, G.: *Generalization of Clapeyron's theorem of solids*, Periodica Polytechnica Ser. Mech. Eng., **44**(1), (2000), 5-7.
2. Eringen, A. C. and Suhubi, E. S.: *Elastodynamics*, Academic Press, New York and London, 1974.
3. Marsden, J. E. and Hughes, T. J. R.: *Mathematical Foundations of Elasticity*, Prentice-Hall, Englewood Cliffs, N.Y., 1983.
4. Béda, G.: *The possible fundamental equations of the constitutive equations of solids*, Newsletter TU Budapest, 10(3), (1992), 5-11.
5. Béda, G.: *The possible fundamental equations of continuum mechanics*, Periodica Polytechnica Ser. Mech. Eng. **35**(1-2), (1991), 15-22.

6. Bishop, R.E.D., Gladwell, G. M. L. and Michaelson, S.: *The Matrix Analysis of Vibration*, Cambridge University Press, 1965.
7. Béda, G.: *Constitutive Equations of Moving Plastic Bodies*, DSc. thesis, Budapest 1982 (in Hungarian).
8. Hill, R.: *Some basic principles in the mechanics of solids without a natural time.* Journal of the Mechanics and Physics of Solids, **7**, (1959), 209-225.
9. Thompson, E.G. and Szu-Wei Yu: *A flow formulation for rate equilibrium equations*, Int. J. for Numerical Methods in Engineering, **30**, (1990), 1619-1632.
10. Dubey R. N.: *Variation method for nonconservative problems,* Trans. ASME Journal of Applied Mechanics, **37(1)**, (1970), 133-136.
11. Béda, G., Kozák I. and Verhás J.: *Continuum mechanics*, Akadémiai Kiadó, Budapest, 1995.
12. Béda, G.: *The principle of virtual work on continuous media*, Newsletter TU of Budapest, 10(1), (1992), 5-9.
13. Béda G. and Béda P.: *A study on constitutive relations of copper using the existence of acceleration waves and dynamical systems*, Proc. of Estonian Academy of Sci. Engin. **5**, (1999), 101-111.
14. Béda, P. and Béda, G.: *Gradient constitutive equation for finite deformation by using acceleration waves and dynamical systems*, Proceedings of ICES2K, Tech. Science Press, 2000 (in press).

Journal of Computational and Applied Mechanics, Vol. 1., No. 2., (2000), pp. 129–135

A NUMERICAL MODEL FOR HOT ROLLING OF ALUMINUM STRIPS

Béla Csonka
Weslin Hungary Autóipari Rt.
Felsőtelep 1., 2840 OROSZLÁNY, Hungary
Bela.Csonka@weslin.com

[Received: April 28, 2000]

Abstract. In this paper, a p version finite element based numerical model is presented for the 3D steady-state analysis of the deformation and velocity field of aluminum strips during hot flat rolling. The material behavior is described by the Levi-Mises type constitutive equation considering no volume change. The assumed roll-strip interaction depends on the relative velocity between the strip and the roll (hydrodynamic lubrication). MATLAB mathematical software was applied for the implementation of the numerical algorithm.

Keywords: flat rolling, p version finite element, Levi-Mises constitutive equation

1. Introduction

The large-scale manufacturing of steel and aluminum rolled products has grown to enormous proportions and ranks as one of the largest industrial segments in modern industry. The major proportion of this market is flat rolled product and represents significant investment which needs to be efficiently operated and regularly upgraded to take advantage of the new technical inventions.

A wide spread form of upgrading in recent years has been the introduction of advanced automation systems with model-based setup and control functions. The design, application and maintenance of these systems have led to significant improvements in mill performance and product quality. The development of model-based systems requires a deep understanding of the physical phenomena involved.

Considering the market requirements for flat rolled aluminum products an increasing demand can be observed for tight dimension tolerance, especially for thickness distribution along the strip length and profile (thickness distribution along the strip width). The strip profile is determined essentially during the hot rolling operation.

Important pieces of information can be predicted by the developed models, such as separation force, separation force distribution in the roll gap, required torque, power, forward and backward slips. These can be utilized for developing and optimizing pass schedules and providing set up data to the mills renting powerful process tools to satisfy the requirement of product developments.

The first 1D numerical model valid both for hot and cold rolling was developed in the form of a non-linear first order differential equation, the so called Kármán equation. Several expressions for the calculation of the separation force were derived

from the approximation of the solution of this differential equation. Due to the basic assumptions this model is incapable of an analysis through the thickness and along the width of the strip. It was applied mainly for modeling cold rolling. Significant efforts were made to improve the reliability of the model predictions, such as shear compensation, roll deformation and yield stress adaptation.

2D models were developed for the study of the plane deformation in the middle section plane of the strip perpendicular to the axis of the work rolls. This approach does not allow us to investigate the lateral spread, the separation force distribution and the velocity field variation along the work roll. Compared with the improved 1D model the yield stress compensation for the shear stress component is not required and the Mises type yielding criteria may be incorporated.

Another family of 2D models was derived in the middle plane of the rolled strip (defined by the traveling direction and the width of the strip). All the properties, parameters and variables are considered in average sense through the thickness requiring the yield stress compensation. These models are able to predict the lateral spread and provide certain information about the along the work roll force distribution and velocity field variation.

The problems and difficulties mentioned above initiated the development of a finite element based 3D numerical model for the calculation of velocity and deformation fields for aluminum strip during hot rolling.

2. Basic equations

The reference system (x, y, z) is defined by the traveling direction, the width and the thickness of the strip. The velocity at a given point P of the strip is given by

$$\mathbf{v}(x, y, z) = v_x(x, y, z)\,\mathbf{e}_x + v_y(x, y, z)\,\mathbf{e}_y + v_z(x, y, z)\,\mathbf{e}_z, \tag{2.1}$$

where $\mathbf{e}_x, \mathbf{e}_y$ and $\mathbf{e}_z$ are the unit vectors in the reference system.

With the velocity field $\mathbf{v}$,

$$\dot{\varepsilon} = \frac{1}{2}(\mathbf{v} \circ \nabla + \nabla \circ \mathbf{v}) \tag{2.2}$$

is the strain rate tensor. According to the Levy-Mises assumption [2] the equation that relates the strain rate to the stresses for hot aluminum rolling is

$$\dot{\varepsilon}_d = \lambda \sigma_d \tag{2.3}$$

and

$$\dot{\varepsilon}_I = 0 \tag{2.4}$$

where $\dot{\varepsilon}_d$ and σ_d are the deviatoric parts of the strain rate and stress tensors, $\dot{\varepsilon}_I$ is the first scalar invariant of the strain rate tensor and λ is given by

$$\lambda = \sqrt{3}\frac{\dot{\varepsilon}_e}{\sigma_e} \tag{2.5}$$

in which $\dot{\varepsilon}_e$ is the effective strain rate

$$\dot{\varepsilon}_e = \sqrt{\dot{\varepsilon} \cdot\cdot \dot{\varepsilon}/2}\,. \tag{2.6}$$

Here double dots stand for the energy product of two tensors. Based on the hot twisting test the effective stress can be given in the following form

$$\sigma_e = \frac{1}{\alpha}\,\mathrm{ash}\left[\left(\frac{\dot{\varepsilon}_e e^{\frac{Q}{RT}}}{A}\right)^{\frac{1}{N}}\right] \tag{2.7}$$

where α, A, N and Q are constants determined from the tests, R is the universal gas constant and T is the absolute temperature.

Table of parameters for the yield stress model				
Alloy code	A	α	N	Q
1050	$3.8 \cdot 10^{11}$	0.0462	3.84	156700
3003	$8.0 \cdot 10^{11}$	0.0311	4.48	167600
545	$1.7 \cdot 10^{10}$	0.0551	2.74	165400

Making use of the notations

$$\overline{\sigma}^T = [\sigma_x,\ \sigma_y,\ \sigma_z,\ \tau_{xy},\ \tau_{xz},\ \tau_{yz}] \qquad \overline{\varepsilon}^T = [\dot{\varepsilon}_x,\ \dot{\varepsilon}_y,\ \dot{\varepsilon}_z,\ \dot{\gamma}_{xy},\ \dot{\gamma}_{xz},\ \dot{\gamma}_{yz}] \tag{2.8}$$

$$\mathbf{C}_0 = \langle\ 2,\quad 2,\quad 2,\quad 1,\quad 1,\quad 1\ \rangle \qquad \mathbf{m}^T = [\ 1,\quad 1,\quad 1,\quad 0,\quad 0,\quad 0,\ ] \tag{2.9}$$

equation (2.3) can be cast into the form

$$\overline{\sigma} = \frac{1}{\lambda}(\mathbf{C}_0 - \frac{2}{3}\mathbf{m} \circ \mathbf{m}^T)\overline{\varepsilon} + \mathbf{m}\overline{\sigma}_h = \frac{1}{\lambda}\mathbf{C}\overline{\varepsilon} + \mathbf{m}\overline{\sigma}_h \tag{2.10}$$

where $\mathbf{C} = \mathbf{C}_0 - 2\mathbf{m} \circ \mathbf{m}^T/3$ and $\overline{\sigma}_h$ is the hydrostatic pressure. The principle of virtual power with an additional penalty term representing the volume change is of the form

$$\int_V \delta\overline{\varepsilon}^T \frac{1}{\lambda}\mathbf{C}\,\overline{\varepsilon}\,\mathrm{d}V + \int_V \delta\overline{\varepsilon}^T \mathbf{m}\overline{\sigma}_h\,\mathrm{d}V + \beta\int_V \delta\overline{\varepsilon}^T \frac{1}{\lambda}\mathbf{m} \circ \mathbf{m}^T\overline{\varepsilon}\mathrm{d}V = \delta W \tag{2.11}$$

where β is a penalty parameter for the numerical calculations in the range of $10^4 - 10^6$ and δW is the power of the external forces. In addition, the weak form of the incompressibility condition can be formulated as

$$\int_V \delta\overline{\sigma}_h \mathbf{m}^T\overline{\varepsilon}\mathrm{d}V = 0\,. \tag{2.12}$$

3. Finite element model

3.1. Finite element approximation. In a given finite element the approximation of the velocity field is calculated using the matrix of shape functions $\mathbf{N}(\xi, \eta, \varsigma)$ regarding the order of the shape functions (p) [3] (for the calculations presented in this

paper $p = 4$ and $p = 5$ elements were applied) and the vector of coefficients $\overline{\mathbf{q}}$ such as

$$\mathbf{v} = \mathbf{N}(\xi, \eta, \varsigma)\,\overline{\mathbf{q}} \tag{3.1}$$

similarly, the hydrostatic pressure can be approximated by linear shape functions as

$$\overline{\sigma}_h = \mathbf{P}(\xi, \eta, \varsigma)\,\overline{\mathbf{p}}$$

where ξ, η and ς are the local coordinates of the element.

It follows from (2.2) by making use of the representation (3.1) that $\overline{\varepsilon}$can be expressed as

$$\overline{\varepsilon} = \mathbf{B}(\xi, \eta, \varsigma)\,\overline{\mathbf{q}} \tag{3.2}$$

where $\mathbf{B}(\xi, \eta, \varsigma)$ is the matrix of the modified shape functions. Substituting this expression into the variational equations (2.11) and (2.12) we have

$$\delta\overline{\mathbf{q}}^T \underbrace{\int_V \frac{1}{\lambda}\mathbf{B}^T\mathbf{C}_0\mathbf{B}J\,\mathrm{d}V}_{\mathbf{K}}\mathbf{q} + \delta\overline{\mathbf{q}}^T \underbrace{\beta\int_V \mathbf{B}^T\left(\mathbf{m}\circ\mathbf{m}^T\right)\mathbf{B}J\,\mathrm{d}V}_{\widetilde{\mathbf{K}}}\overline{\mathbf{q}} + \delta\overline{\mathbf{q}}^T \underbrace{\int_V \mathbf{B}^T\mathbf{m}\mathbf{P}J\,\mathrm{d}V}_{\mathbf{G}}\overline{\mathbf{p}} = \delta W \tag{3.3}$$

and

$$\delta\overline{\mathbf{p}}^T \underbrace{\int_V \mathbf{P}^T\mathbf{m}^T\mathbf{B}J\,\mathrm{d}V}_{\mathbf{G}^T}\overline{\mathbf{q}} = 0 \tag{3.4}$$

where J is the Jacobian of the element considered.

3.2. Boundary conditions. The work roll circumferential velocity $\mathbf{v}_r = v_r\mathbf{t}$ is given in the local coordinate system formed by the tangent of the roll $\mathbf{t}$, the width direction $\mathbf{e}_y$ and the normal vector of the roll surface $\mathbf{n}$. All the nodal point values of the roll-strip contact region are transformed into this local system. In the bite the velocity of the roll surface and the strip surface points slightly differ from each other. On the entry side the velocity of the roll point is higher (backward slip) and in the exit zone the strip point has a higher velocity (forward slip). The strip-roll interaction along the bite length depends on the relative velocity difference between the strip and the roll (hydrodynamic lubrication model). The traction at a point of the bite is given in the form

$$\mathbf{f}^* = \kappa(\mathbf{v}_r - \mathbf{v}) = \kappa\mathbf{v}_r - \langle\kappa, \kappa, 0\rangle\,\mathbf{v} = \kappa\mathbf{v}_r - \mathbf{C}^*\mathbf{v} \tag{3.5}$$

where κ is the hydrodynamic coefficient. The power of the external forces is approximated as

$$\delta W = \delta\overline{\mathbf{q}}^T\int_A \kappa\mathbf{N}^T\mathbf{v}_r J^*\mathrm{d}A - \delta\overline{\mathbf{q}}^T\int_A \mathbf{N}^T\mathbf{C}^*\mathbf{N}J^*\mathrm{d}A\overline{\mathbf{q}} = \delta\overline{\mathbf{q}}^T\left(\overline{\mathbf{f}} - \mathbf{K}^*\overline{\mathbf{q}}\right) \tag{3.6}$$

in which $\overline{\mathbf{f}}$ is the load vector of the element, J^* is the Jacobian of the surface element and $\mathbf{K}^*$ is an additional term which should be added to $\mathbf{K}$ in (3.3).

The normal velocity of the contact points is zero.

3.3. Iterative algorithm. From the variational equations (3.3), (3.6) and (3.4) by assembling the corresponding matrices $\left(\mathbf{K} \to \mathbf{K}^{\Sigma}, \widetilde{\mathbf{K}} \to \widetilde{\mathbf{K}}^{\Sigma} \text{ and } \mathbf{G} \to \mathbf{G}^{\Sigma}\right)$ and introducing the global coefficient vector $\mathbf{q}$, the vector of global pressure coefficients $\mathbf{p}$ and the global generalized load vector $\mathbf{f}$, we obtain the equations

$$\left(\mathbf{K}^{\Sigma} + \widetilde{\mathbf{K}}^{\Sigma}\right)\mathbf{q} + \mathbf{G}\mathbf{p} = \mathbf{f} \tag{3.7}$$

and

$$\mathbf{G}^{\Sigma T}\mathbf{q} = 0\,. \tag{3.8}$$

which can be solved by applying an iterative approach [4] which fulfills a termination criteria $|\mathbf{q}_{n+1} - \mathbf{q}_n| \,/\, |\mathbf{q}_n| < \tau$ (for our numerical calculations $\tau = 10^{-3}$). The integrals are evaluated by using a Gauss type numerical quadrature of order $p+1$ where p is the order of the shape functions that approximate the velocity field.

In the $(n+1)$-th step the global velocity and pressure coefficient vectors $(\mathbf{q}_n, \mathbf{p}_n)$ are determined and

$$\mathbf{p}_{n+1} = \mathbf{p}_n + \rho\mathbf{r}_n \tag{3.9}$$

where $\rho = \lambda_{\min}$ is a factor to improve convergence. The residual of (3.8) is calculated by

$$\mathbf{r}_n = \mathbf{G}^{\Sigma T}\mathbf{q}_n\,. \tag{3.10}$$

Utilizing equations (3.2) and (2.5)-(2.7) we can determine λ at the integration points. If we substitute these values into the expression of $\mathbf{K}$ then, according to the first term of (2.11), the following equation is obtained for $\mathbf{q}_{n+1}$:

$$\left(\mathbf{K}_n^{\Sigma} + \widetilde{\mathbf{K}}^{\Sigma}\right)\mathbf{q}_{n+1} = \mathbf{f} - \mathbf{G}\mathbf{p}_{n+1}\,. \tag{3.11}$$

4. Results

Computational results are compared with hot rolling data of aluminum strips on a four high single stand reversing hot mill. The applied finite element mesh can be seen in Figure 1. With regard to the symmetry conditions – the planes xy and xz are that of symmetry – only one quarter of the strip was considered in our computations. A summary of the measured parameters and the computed values for a 1320 mm wide 1050 alloy strip rolled at 1 m/s speed using 800 mm diameter rolls is given in the table below:

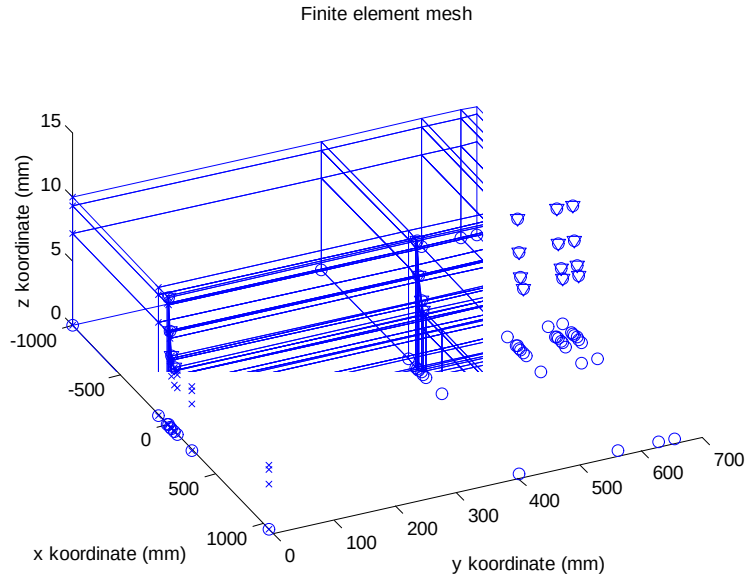
Finite element mesh
z koordinate (mm)
15
10
5
0
-1000
-500
0
500
1000
x koordinate (mm)
0
100
200
300
400
500
600
700
y koordinate (mm)

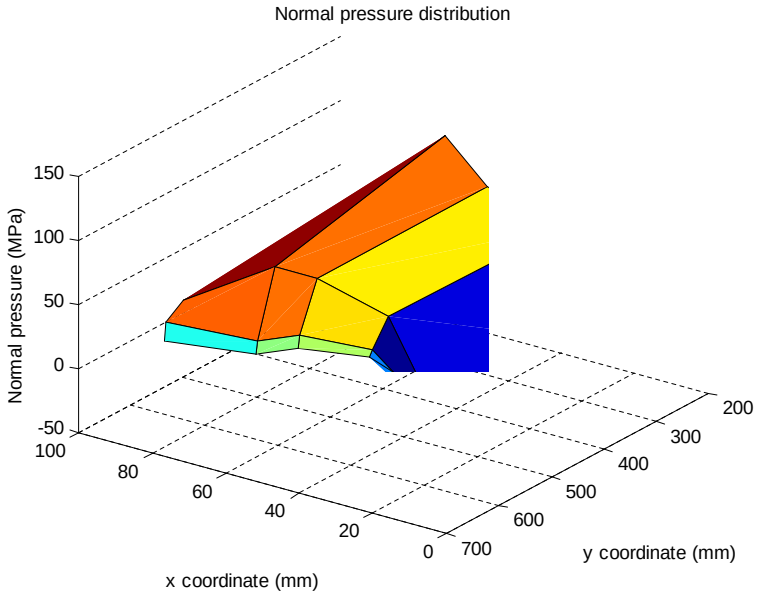
Normal pressure distribution
Normal pressure (MPa)
150
100
50
0
-50
100
80
60
40
20
0
x coordinate (mm)
200
300
400
500
600
700
y coordinate (mm)

Comparison between predicted and measured separation forces				
Temp. $[C^0]$	Entry thick. [mm]	Exit thick. [mm]	Predicted force [kN]	Measured force [kN]
280	16	8	11359	10050
325	16	8	9766	9621
370	16	8	8048	8447
325	16	10	6160	6366

The typical gap pressure distribution indicated in Figure 2 is comparable with the prediction of other types of models (for example: Kármán model) and measurements.

5. Conclusion

A new, effective 3D numerical model has been developed for the steady-state investigation of hot rolling of aluminum strips first time applying p version finite element successfully for the approximation of the velocity field and for the computation of the deformation rates. Hydrodynamic lubrication was assumed for the connection between the strip and the roll. By the development of this model all shortcomings of the 1D and 2D model discussed in the introduction have been eliminated.

The model allows us to predict the separation force, forward and backward slip and the required power/torque for the deformation. Those pieces of information can be utilized for developing, modifying and optimizing pass schedules.

Based on the comparisons of the calculated and measured separation force values it can be concluded that the model predictions are close to the real values and the differences are less than 12%. Based on the practical experiences the differences of the measured and predicted values are within the measurement error range and the predictions are suitable for practical applications.

The MATLAB software was applied for the implementation of the numerical calculations. The built-in spare matrix feature was utilized successfully to reduce the memory requirement of the computations. The graphical output provides a powerful tool for visualizing the computational results.

REFERENCES

1. Kozák I.: Continuum Mechanics, Miskolc University Press, Miskolc, 1995. (in Hungarian)
2. Béda, G., Kozák, I. and Verhás, J.: *Continuum Mechanics*, Mûszaki Könyvkiadó, Budapest, 1994.
3. Páczelt I.: *Linear Plane, Plate and Shell Elements of the Finite Element Method*, Miskolc University Press, Miskolc, 1994. (in Hungarian)
4. Páczelt I.: *Fundamentals of the Finite Element Method*, Manuscript, University of Miskolc, Miskolc, 1993. (in Hungarian)

Journal of Computational and Applied Mechanics, Vol. 1., No. 2., (2000), pp. 137–147

INSTABILITY DUE TO INTERNAL DAMPING OF SYMMETRICAL ROTOR-BEARING SYSTEMS

László Forrai
Department of Mechanics, University of Miskolc
3515 Miskolc – Egyetemváros, Hungary
mechfl@gold.uni-miskolc.hu

[Received: April 30, 2000]

Abstract. This paper deals with the stability analysis of self-excited bending vibrations of linear symmetrical rotor-bearing systems with internal damping using the finite element method. The rotor system consists of uniform circular Rayleigh shafts with both internal viscous and hysteretic damping, symmetric rigid disks, and discrete isotropic damped bearings. The effect of rotatory inertia and gyroscopic moment are also included in the mathematical model. By combining the sensitivity analysis and the eigenvalue problem of the rotor dynamics equations presented in complex form, it is proved theoretically that the whirling motion of the rotor system becomes unstable at all speeds beyond the threshold speed of instability. Furthermore, it is found that the rotor stability is improved by increasing the damping provided by the bearings, whereas increasing internal hysteretic damping will result in a reduction in the threshold speed of instability. It is also shown that the corresponding whirling speed of the rotor is always higher than the first forward bending critical speed. Numerical examples are given to confirm the validity of the theoretical results.

Keywords: rotating machinery, stability, hysteretic damping, sensitivity analysis, threshold speed, finite elements

1. Introduction

Many authors have discussed the stability problems of rotors with internal damping [1-10]. The author of this paper investigated the stability of symmetric rotor-bearing systems using the finite element method in the work [13], in which only the viscous internal damping was incorporated into the mathematical model of the rotor system.

This paper generalizes the main results of the work [13] for similar symmetric rotor systems by using a more realistic model of internal damping, where both internal viscous and hysteretic damping are included into the finite element model of the rotor. By using the sensitivity analysis and the matrix representation of the rotor dynamics equations in complex form to evaulate stability, it is also proved theoretically that the whirling motion of the rotor-bearing system becomes unstable at all speeds above the threshold speed of instability. It is also shown that the rotor stability is improved by increasing the viscous damping provided by the isotropic bearings, whereas increasing internal hysteretic damping always destabilizes the rotor system. Furthermore, it is also found that corresponding whirling speed (frequency) is higher than the first forward bending critical speed.

Numerical examples are given to show the validity of the theoretical results of the

present work. The threshold speed and the whirling speed of the rotor model are calculated using a computer program written in real form, which utilizes a standard QR-algorithm and an iterative technique developed by the author [10].

2. Equations of motion in complex form

2.1. Preliminaries and notations. For completeness and to make the paper self-explanatory, in what follows we repeat the main steps necessary for both the modelling and the stability investigation of the rotor system. In this section, the equations of motion for a rigid disk, finite shaft element with both internal viscous and hysteretic damping, isotropic damped bearing, and the complete rotor system are written in complex form by making use of a recent note by Nelson [11] and the paper by Zorzi and Nelson [8]. Note that the equation of motion for the shaft element in complex form [11] does not contain internal damping, whereas the effects of both viscous and hysteretic internal damping are included into the finite element model in the work by Zorzi and Nelson [8].

Consider a symmetric rotor system as shown in Figure 1. The rotor system consists of symmetrical rigid disks with negligible thicknesses, uniform circular Rayleigh shafts with viscous internal damping, and n isotropic damped bearings with stiffnesses k_i and damping coefficients $c_i\,(i = 1, 2, ..., n)$. The rotor is balanced, and rotates at a constant speed $\Omega(\Omega > 0)$. The reference system $Oxyz$ is fixed in space with the horizontal x-axis coinciding with the undeformed rotor centerline. The external damping, axial load and gravity are neglected.

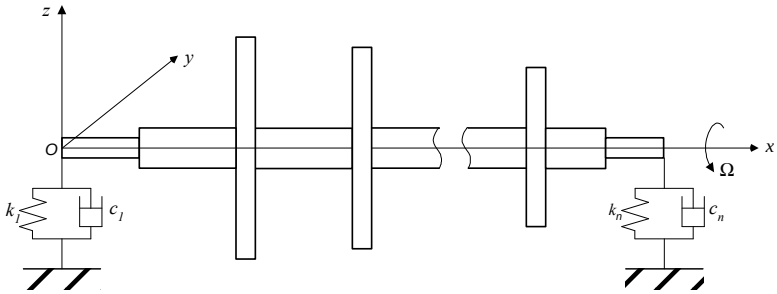

Figure 1. Symmetric rotor in isotropic damped bearings

Any node i of the rotor system has four degrees of freedom: two translations (v_i, w_i) in the (y, z) directions, and two rotations $(\varphi_{yi}, \varphi_{zi})$ about the (y, z) axes, respectively. The complex displacement vector of the ith node is defined by complex coordinates [11] as

$$\mathbf{p}_i = \begin{bmatrix} r_i \\ \varphi_i \end{bmatrix} = \begin{bmatrix} v_i + iw_i \\ \varphi_{yi} + i\varphi_{zi} \end{bmatrix}, \qquad i = \sqrt{-1}\,. \tag{2.1}$$

The component equations and the system equation in complex form may be written as presented below.

2.2. Rigid disk. The equation of motion for a rigid disk in complex form is given

by

$$\left(\mathbf{M}_t^d + \mathbf{M}_r^d\right)\ddot{\mathbf{p}}^d - \Omega\mathbf{G}^d\dot{\mathbf{p}}^d = \mathbf{F}^d\,, \tag{2.2}$$

where $\mathbf{p}^d$ is the complex displacement vector corresponding to the four degrees of freedom $\left(v^d, w^d, \varphi_y^d, \varphi_z^d\right)$ of the node at which the disk is attached. The translational and rotational mass matrices $\left(\mathbf{M}_t^d, \mathbf{M}_r^d\right)$, and the gyroscopic matrix $\mathbf{G}^d$ are defined as

$$\mathbf{M}_t^d = \begin{bmatrix} m^d & 0 \\ 0 & 0 \end{bmatrix}, \tag{2.3}$$

$$\mathbf{M}_r^d = \begin{bmatrix} 0 & 0 \\ 0 & J_D \end{bmatrix}, \tag{2.4}$$

$$\mathbf{G}^d = \begin{bmatrix} 0 & 0 \\ 0 & iJ_P \end{bmatrix}, \tag{2.5}$$

where m^d , J_D and J_P are the mass, the diametral and polar moments of inertia of the disk, respectively.

2.3 Finite shaft element. By making use of the Lagrangian equations of motion for the damped finite element presented in real form in the work by Zorzi and Nelson [8], the equations of motion for the finite rotating shaft element with both hysteretic and viscous forms of internal damping can be rewritten in complex form as

$$\left(\mathbf{M}_t^e + \mathbf{M}_r^e\right)\ddot{\mathbf{p}}^e + \left(\eta_V\mathbf{K}_b^e - \Omega\mathbf{G}^e\right)\dot{\mathbf{p}}^e + \left[\frac{1+\eta_H}{\sqrt{1+\eta_H^2}}\mathbf{K}_b^e + \left(\eta_V\Omega + \frac{\eta_H}{\sqrt{1+\eta_H^2}}\right)\mathbf{K}_c^e\right]\mathbf{p}^e = \mathbf{F}^e\,, \tag{2.6}$$

where

$$\mathbf{p}^e = \begin{bmatrix} \mathbf{p}_i \\ \mathbf{p}_j \end{bmatrix} \tag{2.7}$$

is the $(4x1)$ complex nodal displacement vector of the shaft element with nodes i and j, η_V is the internal viscous damping coefficient, η_H is the hysteretic damping loss factor,

$$\mathbf{K}_c^e = -i\mathbf{K}_b^e \tag{2.8}$$

is the complex circulation matrix of the shaft element.

The translational and rotational mass matrices $(\mathbf{M}_t^e, \mathbf{M}_r^e)$, the gyroscopic matrix $\mathbf{G}^e$, and the bending stiffness matrix $\mathbf{K}_b^e$ of the shaft element are defined as

$$\mathbf{M}_t^e = \frac{\mu l}{420}\begin{bmatrix} 156 & & Hermitian & \\ i22l & 4l^2 & & \\ 54 & -i13l & 156 & \\ -i13l & -3l^2 & -i22l & 4l^2 \end{bmatrix}, \tag{2.9}$$

$$\mathbf{M}_r^e = \frac{\mu r^2}{120l}\begin{bmatrix} 36 & & Hermitian & \\ i3l & 4l^2 & & \\ -36 & -i3l & 36 & \\ i3l & -l^2 & -i3l & 4l^2 \end{bmatrix}, \tag{2.10}$$

$$\mathbf{G}^e = i2\mathbf{M}_r^e\,, \tag{2.11}$$

$$\mathbf{K}_b^e = \frac{EI}{l^3}\begin{bmatrix} 12 & & Hermitian & \\ i6l & 4l^2 & & \\ -12 & i6l & 12 & \\ i6l & 2l^2 & -i6l & 4l^2 \end{bmatrix}, \tag{2.12}$$

where μ is the mass per unit length, l is the length of shaft element, r is the element radius, EI is the bending rigidity of the shaft element. Since, in practice, $\eta_H^2 \ll 1$, we may write equation (2.6) in an approximate form as

$$(\mathbf{M}_t^e + \mathbf{M}_r^e)\,\ddot{\mathbf{p}}^e + (\eta_V \mathbf{K}_b^e - \Omega\mathbf{G}^e)\,\dot{\mathbf{p}}^e + [(1+\eta_H)\mathbf{K}_b^e + (\eta_V\Omega + \eta_H)\mathbf{K}_c^e]\mathbf{p}^e = \mathbf{F}^e\,. \tag{2.13}$$

Note that the above equation is an extended form of equation (2.6) presented in the work [13].

2.4. Linear isotropic damped bearings. The linear isotropic damped bearings can be modeled by the equation:

$$\mathbf{C}^b\dot{\mathbf{p}}^b + \mathbf{K}^b\mathbf{p}^b = \mathbf{F}^b\,, \tag{2.14}$$

where $\mathbf{p}^b$ is the complex displacement vector at the bearing location (node), $\mathbf{F}^b$ is the complex bearing force vector. The damping and stiffness matrices $\left(\mathbf{C}^b, \mathbf{K}^b\right)$ of the isotropic bearings are defined as

$$\mathbf{C}^b = \begin{bmatrix} c^b & 0 \\ 0 & 0 \end{bmatrix} \quad , \qquad \mathbf{K}^b = \begin{bmatrix} k^b & 0 \\ 0 & 0 \end{bmatrix}\,, \tag{2.15}$$

where c^b and k^b are the direct damping and stiffness coefficients for the translational displacements, respectively.

2.5. System equations. The equations of motion of the complete rotor-bearing system can be obtained by assembling all component equations of the form equations (2.2), (2.13) and (2.14). The resulting equation is of the form

$$\mathbf{M}\ddot{\mathbf{p}} + (\eta_V\mathbf{K}_b + \mathbf{C} - \Omega\mathbf{G})\dot{\mathbf{p}} + [1 + \eta_H - i(\eta_V\Omega + \eta_H)]\mathbf{K}_b + \mathbf{K}]\mathbf{p} = 0\,, \tag{2.16}$$

where

$$\mathbf{p}^T = \left[\mathbf{p}_1^T\mathbf{p}_2^T ... \mathbf{p}_N^T\right] \tag{2.17}$$

is the $(2\,Nx1)$ complex nodal displacement vector of the rotor system (N equals the number of nodes), the letter "T" denotes the transpose.

2.6. Positive definite matrices. Since kinetic energy and strain energy cannot be negative, the system matrices $(\mathbf{M}, \mathbf{K}_b)$ are positive definite Hermitian matrices [9]. Thus the following relations hold:

$$\bar{\mathbf{p}}^T\mathbf{M}\mathbf{p} > 0\ , \qquad \bar{\mathbf{p}}^T\mathbf{K}_b\mathbf{p} > 0\ , \qquad (\mathbf{p} \neq 0)\ , \tag{2.18}$$

where the bar denotes the complex conjugate operator.

Note that the system gyroscopic matrix $\mathbf{G}$ is not Hermitian, however, by using the definitions of the component gyroscopic matrices presented by equations (2.5) and (2.11) it, can be expressed as

$$\mathbf{G} = i\mathbf{M}_g\ , \tag{2.19}$$

where

$$\bar{\mathbf{p}}^T\mathbf{M}_g\mathbf{p} > 0, \quad (\mathbf{p} \neq 0)\ . \tag{2.20}$$

Evidently $\mathbf{C}$ and $\mathbf{K}$ are positive definite diagonal matrices, the nonzero elements of which are the damping coefficients and the stiffnesses of the isotropic bearings, respectively.

3. Stability analysis

3.1. Stability threshold speed determination On seeking a solution to equation (2.16) of the form

$$\mathbf{p} = \mathbf{P}e^{\lambda t}\ , \tag{3.1}$$

we obtain the eigenvalue problem

$$\{\lambda^2\mathbf{M} + \lambda\left(\eta_V\mathbf{K}_b + \mathbf{C} - \Omega\mathbf{G}\right) + [1 + \eta_H - i(\eta_V\Omega + \eta_H)]\mathbf{K}_b + \mathbf{K}\}\mathbf{P} = 0 \tag{3.2}$$

with $4N$ eigenvalues λ_j and the corresponding eigenvectors $\mathbf{P}_j$ $(j = 1, 2, ..., 4N)$. The eigenvalues λ are of the form

$$\lambda = \alpha + i\omega\ , \tag{3.3}$$

where α is the damping coefficient or decay rate, ω is the damped natural frequency or whirl speed.

For later use, the eigenvalue problem will be given in a modified form. To this end, we premultiply equation (3.2) by the complex conjugate eigenvector $\bar{\mathbf{P}}^T$. Then we obtain the following scalar equation:

$$\bar{\mathbf{P}}^T\{\lambda^2\mathbf{M} + \lambda(\eta_V\mathbf{K}_b + \mathbf{C} - \Omega\mathbf{G}) + [1 + \eta_H - i(\eta_V\Omega + \eta_H)]\mathbf{K}_b + \mathbf{K}\}\mathbf{P} = 0\ , \tag{3.4}$$

which can be rewritten as

$$m\lambda^2 + (\eta k_b + c - ig\Omega)\lambda + \left[1 + \eta_H - i(\eta_V\Omega + \eta_H)\right]k_b + k = 0\ , \tag{3.5}$$

where the scalars m, k_b, c, g and k_B are in all positive real quantities [9] defined by

$$\bar{\mathbf{P}}^T\mathbf{M}\mathbf{P} = m > 0 \,, \tag{3.6}$$
$$\bar{\mathbf{P}}^T\mathbf{K}_b\mathbf{P} = k_b > 0 \,, \tag{3.7}$$
$$\bar{\mathbf{P}}^T\mathbf{C}\mathbf{P} = c > 0 \,, \tag{3.8}$$
$$\bar{\mathbf{P}}^T\mathbf{G}\mathbf{P} = ig(g > 0) \,, \tag{3.9}$$
$$\bar{\mathbf{P}}^T\mathbf{K}\mathbf{P} = k > 0 \,. \tag{3.10}$$

Note that the inequalities (3.6) - (3.10) hold on account of the positive definite matrices of the rotor system (see Section 2.5.).

Instability occurs if one of the eigenvalues has a positive real part. Thus, the problem of determining the limit of stability of the rotor system is reduced to finding the shaft speed Ω_s (threshold speed of instability), at which the greatest real part of all eigenvalues λ_j equals zero. The corresponding imaginary part ω_s is the *whirling speed*.

For the possible limit ω , the substitution of the eigenvalue of the form

$$\lambda = i\omega \tag{3.11}$$

into equation (3.5) yields

$$-m\omega^2 + g\omega\Omega + (1+\eta_H)k_b + k + i\left[\omega(\eta_V k_b + c) - (\eta_V\Omega + \eta_H)k_b\right] = 0 \,. \tag{3.12}$$

After seperating equation (3.12) into real and imaginary parts, we obtain

$$-m\omega^2 + g\omega\Omega + (1+\eta_H)k_b + k = 0 \,, \tag{3.13}$$
$$\omega(\eta_V k_b + c) = (\eta_V\Omega + \eta_H)k_b \,. \tag{3.14}$$

It is clear from equation (3.14) and inequalities (3.7) and (3.8) that

$$\Omega = \omega\left(1 + \frac{c}{\eta_V k_b}\right) - \frac{\eta_H}{\eta_V} > 0(\omega > 0) \,. \tag{3.15}$$

Thus the particular undamped whirl mode induced at the stability threshold speed is forward ($\omega > 0$) and asynchronous ($\Omega \neq \omega$) It is noteworthy that all backward precessional modes of the rotor are stable for any rotational speed.

Now we shall prove that the rotor loses its stability at all speeds above the possible stability limit. Here, we apply the eigenvalue sensitivity analysis. Let us suppose that the shaft speed Ω is an independent parameter, and differentiate equation (3.5) with respect to Ω :

$$\lambda'(2m\lambda + \eta_V k_b + c - ig\Omega) - ig\lambda - i\eta_V k_b + m'\lambda^2 +$$
$$+(\eta_V k_b' + c' - ig'\Omega)\lambda + [1 + \eta_H - i(\eta_V\Omega + \eta_H)]k_b' + k' = 0 \,. \tag{3.16}$$

where primes denote differentiation with respect to Ω . The quantity $\lambda' = \partial\lambda/\partial\Omega$ is referred to as an eigenvalue sensitivity coefficient [12], which can be written, with the aid of equation (3.3), in the form:

$$\frac{\partial\lambda}{\partial\Omega} = \frac{\partial\alpha}{\partial\Omega} + i\frac{\partial\omega}{\partial\Omega} \,. \tag{3.17}$$

To calculate $\partial\lambda/\partial\Omega$ from equation (3.16) at the possible limit Ω , we substitute again equation (3.11) into equation (3.16):

$$\frac{\partial\lambda}{\partial\Omega}[\eta k_b + c + i(2m\omega - g\Omega)] + g\omega - i\eta k_b + (\underline{-m'\omega^2 + g'\omega\Omega + (1+\eta_H)k_b' + k'}) \\ \underline{+i[\omega(\eta_V k_b' + c') - (\eta_V\Omega + \eta_V)k_b']} = 0. \quad . \tag{3.18}$$

Since the eigenvalue derivative $\partial\lambda/\partial\Omega$ represents the unique solution of equation (3.18) at the possible limit of stability, and hence its value is not influenced by any normalization criterion for the eigenvector $\mathbf{P}$, therefore the underlined terms will vanish:

$$-m\acute{\omega}^2 + \omega\Omega g' + (1+\eta_H)k_b' + k' = 0, \tag{3.19}$$

$$\omega(\eta_V k_b' + c') = (\eta_V\Omega + \eta_V)k_b' \, . \tag{3.20}$$

We then obtain the following expression for the damping sensitivity coefficient $\partial\alpha/\partial\Omega$

$$\frac{\partial\alpha}{\partial\Omega} = \frac{A}{(\eta_V k_b + c)^2 + (2m\omega - g\Omega)^2} \, , \tag{3.21}$$

where

$$A = [\eta_V(2m\omega - g\Omega) - g(\eta_V\Omega + \eta_H)]k_b \, . \tag{3.22}$$

Now let us show that A is positive. To this end we substitute (3.15) into equation (3.22):

$$A = k_b\eta_V\{2\omega\left[m - g\left(1 + \frac{c}{\eta_V k_b}\right)\right] + g\frac{\eta_H}{\eta_V}\} \, . \tag{3.23}$$

The bracketed term in equation (3.23) is positive:

$$m - g\left(1 + \frac{c}{\eta_V k_b}\right) > 0 \, , \tag{3.24}$$

since in this case equation (3.13) has only one positive root ω . The latter statement comes from the following equivalent form of equation (3.13):

$$\omega^2\left[m - g\left(1 + \frac{c}{\eta_V k_b}\right)\right] + \omega g\frac{\eta_H}{\eta_V} - [(1+\eta_H)k_b + k]\} = 0 \, . \tag{3.25}$$

We have thus proved that the damping sensitivity coefficient $\partial\alpha/\partial\Omega$ is positive at any possible limit of stability. Thus, the lowest value of the above stability limits for the particular forward whirl modes is considered as the *threshold speed of instability* of the rotor-bearing system. Consequently, the whirling motion of the rotor becomes unstable at all speeds above the threshold speed of instability.

3.2. Effect of bearing damping on rotor stability Now we shall prove that an increase in the bearing damping coefficients results in an increase in the threshold speed of instability, thus the rotor stability will be improved.

Let us consider the bearing damping coefficient $c_i (i = 1, 2, ..., n)$ of the i-th isotropic damped bearing as an independent parameter, and differentiate equations (3.13) and

(3.14) with respect to c_i :

$$\omega'(g\Omega - 2m\omega) + \omega g\Omega' + \underline{(-m'\omega^2 + \omega\Omega g' + (1+\eta_H)k_b' + k')} = 0 \ , \tag{3.26}$$

$$\omega'(\eta_V k_b + c) - \eta_V k_b \Omega' + \underline{\omega(\eta_V k_b' + \tilde{c}) - (\eta_V\Omega + \eta_H)k_b'} = -\omega c^* \ , \tag{3.27}$$

where primes denote differentiation with respect to c_i ,

$$\tilde{c} = \frac{\partial \bar{\mathbf{P}}^T}{\partial c_i}\mathbf{C}\mathbf{P} + \bar{\mathbf{P}}^T\mathbf{C}\frac{\partial \mathbf{P}}{\partial c_i} \ , \tag{3.28}$$

and

$$c^* = \bar{\mathbf{P}}^T\frac{\partial \mathbf{C}}{\partial c_i}\mathbf{P} > 0 \ . \tag{3.29}$$

By using the same reasoning that we have applied in connection with equation (3.18), it is clear that the underlined terms in equations (3.26) and (3.27) will vanish at the threshold speed Ω . The whirling speed sensitivity coefficient ω' and the threshold speed sensitivity coefficient Ω' can now be obtained from the above two equations as

$$\frac{d\omega}{dc_i} = \frac{gc^*\omega^2}{A} \ , \tag{3.30}$$

$$\frac{d\Omega}{dc_i} = \frac{\omega(2m\omega - g\Omega)c^*}{A} \ . \tag{3.31}$$

By using equations (3.22) and (3.29) as well as the inequality (3.9), it is easy to see that the above sensitivity coefficients are positive. Thus, the addition of bearing damping improves the rotor stability. It is also clear that the whirling speed is always greater than the first forward bending critical speed of the rotor system. The latter statement follows from the fact that the threshold speed of symmetrical rotors with viscous internal damping, supported by undamped isotropic bearing coincides with the first forward critical speed [9]. It can further be concluded from equation (3.30) that when the gyroscopic moments of the rotor are neglected ($g = 0$), then the whirling speed remains constant (the first critical speed of the rotor) regardless of the magnitude of the bearing damping coefficients.

3.3. Influence of internal hysteretic damping on rotor stability We shall now prove that internal hysteretic damping is always a destabilizing influence on rotor systems. Let us assume that η_H is an independent system parameter. By differentiatiating equations (3.13) and (3.14) with respect to η_H, we get

$$\omega'(-2m\omega + g\Omega) + \omega g\Omega' \underline{-m'\omega^2 + g'\omega\Omega + (1+\eta_H)k_b' + k'} = -k_b \ , \tag{3.32}$$

$$\omega'(\eta_V k_b + c) - \eta_V k_b\Omega' + \underline{\omega(\eta_V k_b' + c') - (\eta_V\Omega + \eta_H)k_b'} = k_b \ , \tag{3.33}$$

where prime denotes differentiation with respect to η_H . Since the underlined expressions vanish at the stability threshold, the whirling speed sensitivity coefficient ω' and threshold speed sensitivity coefficient Ω' are determined by

$$\frac{d\omega}{d\eta_H} = \frac{k_b\eta_V - g\omega}{A}k_b \ , \qquad \frac{d\Omega}{d\eta_H} = \frac{-(2m\omega - g\Omega) + (\eta_V k_b + c)}{A}k_b \ . \tag{3.34}$$

By using inequalities (3.6) - (3.10), and equations (3.13) and (3.14), simple reasoning will show that the whirling speed sensitivity coefficient is positive, whereas the threshold speed sensitivity coefficient becomes negative at the stability threshold speed. As can be seen, the introduction of internal hysteretic damping η_H causes a reduction in the threshold speed of instability, thus hysteretic damping has always a destabilizing influence on rotor systems. It is noteworthy that the corresponding whirling frequency will be raised. From equation (3.30) and the work by the author [9] it clearly follows that the latter is always higher than the first forward bending critical speed.

4. Numerical examples

4.1. To demonstrate the validity of the above theoretical results, two numerical examples are provided. In both examples, the simply supported uniform shaft studied by Zorzi [8] is considered. The rotor model consists of a 10.16 cm diameter and 127 cm long steel shaft supported by two identical isotropic damped bearings at both ends. The stiffnesses of the bearings are: $k_1 = 1.75 \times 10^{11} N/mT$. The material properties of shaft are: Young's modulus $E = 2.06 \times 10^{11} N/m^2$, and density $\rho = 7800\, kg/m^3$. The rotor is modeled as an assembly of four finite elements of equal length. In the calculations, the damping coefficients c_1 of the bearings and the hysteretic damping loss factor η_H for the shaft are considered to be parameters.

4.2. As a first example, we shall examine the influence of the damping coefficient c_1 on the rotor stability for $\eta_V = 0.0002\, s$.and $\eta_H = 0.0002$. Table 1 shows the numerical

Table 1. Effect of bearing damping (c_1) on rotor stability

bearing damping	threshold speed	whirling speed
(Ns/m)	(rad/s)	(rad/s)
0	520.410	521.412
100	543.115	521.417
200	565.835	521.430
300	588.563	521.450
400	611.315	521.478
500	634.083	521.513

values of the threshold speeds Ω_s and the whirling speeds ω_s of the rotor for different values of c_1. The first forward critical speed of the rotor was found to be $\Omega_{F1} = 521.392\, rad/s$.

As can be seen from Table 1, the introduction of bearing damping will raise the threshold speed of instability, thus the stability of the rotor system will be improved. It should be noted that increasing the bearing damping may cause only small increases in the whirling speeds, which are greater than the first forward bending critical speed of the rotor. Clearly the numerical results of Table 1 are in quite good agreement with the theoretical results obtained in Section 3.2.

4.3. As a second example, we consider the influence of the hysteretic damping loss

factor η_H on the rotor stability for $c_1 = 500\,Ns/m$ and $\eta_V = 0.0002$. Table 2 presents the calculated values of the threshold speeds and whirling speeds for different values

Table 2. Effect of hysteretic damping (η_H) on rotor stability

hysteretic loss factor	threshold speed (rad/s)	whirling speed (rad/s)
0.0002	634.083	521.513
0.0003	633.622	521.523
0.0004	633.152	521.533
0.0005	632.691	521.544

of η_H . The numerical results show clearly that the stability of the rotor is reduced by increasing internal hysteretic damping. For example, for the hysteretic damping loss factor of $\eta_H = 0.0002$ the rotor becomes unstable at the threshold speed $\Omega_s = 634.083\,rad/s$. By increasing the hysteretic loss factor to $\eta_H = 0.0003$, the stability threshold speed of instability of the rotor will be reduced to $\Omega_s = 633.622\,rad/s$. It should be noted that increasing hysteretic damping causes only small increases in the whirling speed ω_s. Evidently the numerical results summarized in Table 2 are in good agreement with the theoretical results presented in Section 3.3.

5. Summary and conclusions

In this paper a finite element stability analysis of self-excited bending vibrations of symmetric rotors with both internal viscous and hysteretic damping, supported by isotropic damped bearings has been presented. By combining the sensitivity method and the eigenvalue problem of the rotor dynamics equations in complex form, it is proved theoretically that the whirling motion of the rotor becomes unstable at all speeds above the stability threshold speed. Furthermore, the rotor stability is improved by increasing the damping provided by the bearings, whereas internal hysteretic damping destabilizes the whirling motion of the rotor. It is also shown that the corresponding whirling speed of the rotor system is higher than the first forward bending critical speed. Numerical examples are provided to confirm the validity of the above theoretical results.

Acknowledgement. This research has been partially supported by the National Fund for Scientific Research of Hungary (OTKA) under grant T 030096.

REFERENCES

1. Kimball, A. L.: *Internal friction theory of shaft whirling*, General Electric Review, **27**, (1924), 244-251.
2. Newkirk, B.L.: *Shaft Whipping*, General Electric Review, 27 (1924), 169-178.
3. Smith, D.M.: *The motion of a rotor carried by a flexible shaft in flexible bearings*, Proceedings of the Royal Society of London, Series A, 142 (1933), 92-118.

4. Dimentberg, F.M.: *Flexural Vibrations of Rotating Shafts*, Butterworths, London 1961.
5. Ehrich, F.F.: *Shaft whirl induced by rotor internal damping*, ASME Journal of Applied Mechanics 31, (1964), 279-282.
6. Tondl, A.: *Some Problems of Rotor Dynamics*, Publishing House of the Czechoslovak Academy of Sciences, Prague 1965.
7. Gunter, E.J. and Trumpler, P.R.: *The influence of internal friction on the stability of high speed rotors with anisotropic supports*, ASME Journal of Engineering for Industry 91 (1969), 1105-1113.
8. Zorzi, E.S. and Nelson, H.D.: *Finite element simulation of rotor-bearing systems with internal damping*, ASME Journal of Engineering for Power 99 (1977) 71-76.
9. Forrai, L.: *Stability analysis of symmetrical rotor-bearing systems with internal damping using finite element method*, Presented at the International Gas Turbine and Aeroengine Congress and Exhibition, Birmingham, UK (1996), ASME Paper No. 96-GT-407.
10. Forrai, L.: *Stability of rotor-bearing systems with internal damping using finite elements*, Proc. 9th World Congress on the Theory of Machines and Mechanisms, Milano, Italy (1995), 1204-1208.
11. Nelson, H.D.: *Rotor dynamics equations in complex form*, ASME Journal of Vibration, Acoustics, Stress and Reliability in Design 107, (1985), 460-461.
12. Rajan, M., Nelson, H. D. and Chen, W. J.: *Parameter sensitivity in the dynamics of rotor-bearing systems*, Journal of Vibration, Acoustics, Stress, and Reliability in Design, **108**, (1986), 197-206.
13. Forrai, L.: *A finite element model for stability analysis of symmetrical rotor systems with internal damping*, Journal of Computational and Applied Mechanics, **1**(1), (2000), 37-47.

Journal of Computational and Applied Mechanics, Vol. 1., No. 2., (2000), pp. 149–166

OPTIMIZATION OF WELDED STRUCTURES FOR COST

Károly Jármai
Department of Materials Handling and Logistics, University of Miskolc
3515 Miskolc – Egyetemváros, Hungary
altjar@gold.uni-miskolc.hu

[Received: June 15, 2000]

Abstract. Weight or mass minimization is a usual way of finding optima of structures. Due to the high cost of welding, weight and cost optima can be quite different. We have worked out a cost calculation for welded steel structures, considering not only the material, but preparation, cutting, edge grinding, welding, cleaning, painting costs as well. We have used the backtrack combinatorial discrete optimization method for many years. We made weight minimization. For cost minimization we had to modify the algorithm in order to be able to handle cost function. This paper describes this modification. We show two examples for cost minimization: the first example is cost optimization of welded box beams with longitudinal stiffeners. First we show the economics of using stiffeners in the example. The second example is the effect of post-welding treatments on the optimum fatigue design of welded I-beams. We show how cost saving can be achieved by introducing additional treatment.

Keywords: Structural optimization, cost calculation, welded structures, backtrack method, post-welding treatment

1. Introduction

Welding is a relatively expensive production technology, therefore it is important to decrease the cost of welded structures. Designers select a suitable structural version by comparison of several candidate structural solutions, but only optimized versions can be realistically compared to each other. Thus, the structural optimization is a basis not only for achieving savings in weight and cost, but also to help designers to select the most suitable structural version.

Box beams are widely used in load-carrying structures because of their large bending and torsional stiffness. The minimum cross-sectional-area design of a simple welded box beam shows that, in order to decrease this area, the web plate slenderness should be increased. This can be achieved using longitudinal stiffeners placed in 1/5 distance of web height. Although these stiffeners increase the weight and cost, significant savings can be achieved using them. To show these savings the minimum weight and cost design should be worked out.

Fatigue fracture is one of the most dangerous phenomena for welded structures. Welding causes residual stresses and sharp stress concentrations around the weld, which are responsible for significant decrease of fatigue strength. Butt welds with partial penetration, toes and roots of fillet welds are points where fatigue cracks initiate and propagate.

2. The cost function

We have developed a cost function for welded structures using the COSTCOMP database [1,2]. This cost function contains nonlinear expressions for unknowns. The cross-sectional area minimization can be solved analytically, but for the minimum cost design, a computerized mathematical constrained function minimization method should be used, since the cost function is nonlinear.

In the cost function the material and fabrication costs are included

$$K = K_m + K_f = k_m \rho V + k_f \sum_i T_i \,, \tag{2.1}$$

where ρ is the material density, V is the volume of the structure, k_m and k_f are the corresponding cost factors, T_i are the fabrication times. (2.1) can be written in the form of

$$\frac{K}{k_m} = \rho V + \frac{k_f}{k_m} \sum_i T_i \,. \tag{2.2}$$

We use the following cost factors: $k_m = 0.5 \div 1$ \$/kg, $k_{f\,\max} = 60$ \$/h $= 1$ \$/min, thus the ratio of k_m/k_f can be varied in a wide range of $0 \div 2$ kg/min. $k_m/k_f = 0$ means that K/k_m is a weight (mass) function, $k_m/k_f = 2$ kg/min can be used for developed countries.

The fabrication times can be calculated as follows:

$$\sum_i T_i = T_1 + T_2 + T_3 + T_4 \,. \tag{2.3}$$

Time for preparation, assembly and tacking is

$$T_1 = C_1 \Theta_d \sqrt{\kappa \rho V} \,, \tag{2.4}$$

where $C_1 = 1$ min/kg$^{0.5}$, Θ_d is a difficulty factor expressing the complexity of a structure (planar or spatial, consisting of plates or tubes etc.), κ is the number of elements to be assembled.

Time for welding is

$$T_2 = \sum C_{2i} a_{wi}^n L_{wi} \,, \tag{2.5}$$

where $C_{2i} a_{wi}^n$ is given for different welding technologies and weld shapes according to COSTCOMP software [1] and [2], a_w is the weld size, L_w is the weld length.

The additional time for electrode changing, deslagging and chipping can be calculated as

$$T_3 = 0.3 T_2 \,. \tag{2.6}$$

The final form of the cost function contains T_1, T_2, T_3 and T_4 for post-welding treatment, or some other times for cutting, edge grinding, surface preparation, flattening, painting, etc.

It can be seen that this function contains nonlinear members of the unknown structural dimensions, therefore an advanced backtrack method should be used for the minimization.

3. The advanced backtrack method

The backtrack discrete programming method is suitable for problems with few unknowns, but till now, we have used it only for linear objective functions.

For nonlinear objective functions we have worked out a new advanced version. The backtrack method is a combinatorial programming technique, which solves nonlinear constrained function minimisation problems by a systematic search procedure. The advantage of the technique is that it uses only discrete variables, so the solution is usable. The general description of backtrack can be found in the works by Walker [3] and Golomb & Baumert [4]. Farkas & Jármai [5] applied this method to welded I-girder design.

The general formulation of a single-criterion nonlinear programming problem is the following:

minimize

$$f(x), \quad x_1, x_2, ..., x_N \tag{3.1}$$

subject to

$$g_j(x) \leq 0, \quad j = 1, 2, ..., P \tag{3.2}$$

$$h_i(x) = 0, \quad i = P+1, ..., P+M\,. \tag{3.3}$$

Here $f(x)$ is a multivariable nonlinear function, $g_j(x)$ and $h_i(x)$ are nonlinear inequality and equality constraints. The equality constraints should be transformed to inequality ones for the program to handle them:

$$h_i(x) <_{\mid} \epsilon_{\mid}\,, \quad i = P+1, ..., P+M \tag{3.4}$$

ϵ is a given small number.

The algorithm is suitable for finding optimum for problems with monotonically increasing or decreasing objective functions. Thus, the optimum solution can be found by increasing or decreasing the variables. Originally the procedure can find the minimum of the problem. If we are looking for maximum, we should introduce $-f(x)$. The search is time-consuming, because the procedure makes a detailed search.

To find the optimum for a single variable, many single variable search techniques are available. An efficient and suitable search method is the interval halving procedure. We assume that the objective function is monotonously decreasing if the variables are decreasing. At the line search, when only one variable is changing, the aim is to find the minimum feasible value of the variable, starting from the maximum value. All values of variables are calculated by the halving procedure, except the last variable, which is calculated from the objective function.

The starting point, i.e. the maximum value, should satisfy the constraints. When the investigation shows that the minimum value satisfies the constraints, then the

solution is found. If not, the region is divided into two subregions with the middle value. If the constraints are satisfied with the middle value, then the upper region is feasible, all points there satisfy the constraints. In this case we should investigate the lower region, to find the border between the feasible and unfeasible regions.

In the backtrack method the variables are in a vector form $x = \{x_i\}^T$, $(i = 1, ..., n)$ for which the objective function $f(x)$ will be a minimum and which will also satisfy the design constraints $g(x) \geq 0$, $(j = 1, ..., P)$. For the variables, series of discrete values are given in an increasing order. In special cases the series may be determined by $x_{k,\min}, x_{k,\max}$ and by the constant steps Δx between them.

First a partial search is carried out for each variable and if all variations have been investigated, a backtrack is made and a new partial search is performed on the previous variable. If this variable is the first one: no variations have to be investigated (a number of backtracks have been made), then the process stops. The main phases of the calculation are as follows.

1. With a set of constant values of $x_{i,t}(i = 2, ..., n)$, the minimum $x_{i,m}$ value satisfying the design constraints is searched for. The interval halving method can be employed. This method can be employed if the constraints and the objective function are monotonous from the sense of variables.
2. As in the case of the first phase, the halving process is now used with constant values, and the minimum value, satisfying the design constraints is then determined.
3. The least value is calculated from the equation relating to the objective function $f(x)$ where f is the value of the cost function calculated by inserting the maximum x-values.

Regarding the value, three cases may occur as follows.

(3a) We decrease the variables step by step till the constraints are satisfied or till the minimum values are reached. If all variations of the x_n value have been investigated, then the program jumps to the previous variable x_{n-1} and decreases it step by step till x satisfies the constraints or till minimum values are reached.

(3b) If $x_{n,m} < x_{n,1}$, we backtrack to x_{n-1} .

(3c) If $x_{n,m}$ does not satisfy the constraints, we backtrack to $x_{n-1,m}$. If the constraints are satisfied, we continue the calculation according to (3a).

The number of all possible variations is $\prod_{i=1}^{n} t_i$ where t_i is the number of discrete sizes for one variable. However, the method investigates only a relatively small number of these. Since the efficiency of the method depends on many factors (number of unknowns, series of discrete values, position of the optimum values in the series, complexity of the cost function and/or that of the design constraints), it is difficult to predict the run time. The main disadvantage of the method is that the run time increases exponentially if we increase the number of unknowns.

The original version of backtrack was modified by rebuilding the algorithm so that it is independent from the number of variables, since in the original algorithm all variable values are calculated by the halving procedure, except the last one. Another development is that the Van Wijngaarden-Dekker-Brent method (Brent [6]) was built into the algorithm to calculate the last variable value from the cost function. In case of mass minimization this calculation is relatively easy, because of the linearity,

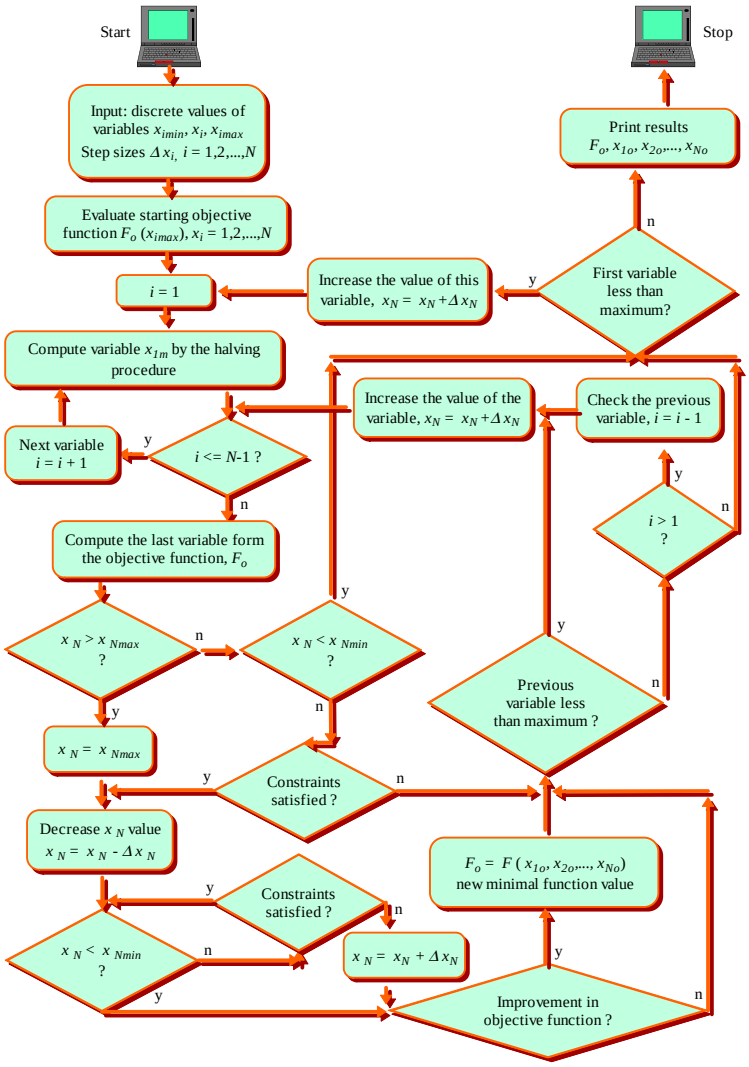

Figure 1. The flowchart of the backtract method

but introducing a nonlinear cost function the analytical solution in most cases is impossible. This method combines root bracketing, bisection and inverse quadratic interpolation to converge from the neighbourhood of a zero crossing. While the false position and secant methods assume approximately linear behaviour between two prior root estimates, inverse quadratic interpolation uses three prior points to fit an inverse quadratic function. This method combines the sureness of bisection with the speed of a high-order method when appropriate. This calculation is built into the computer code with subroutines. The flowchart of the backtrack method is shown in Figure 1.

4. Minimum cross-sectional-area for box beams with stiffeners

In this section we deal with the design of minimum cross-sectional-area for bending of box beams with longitudinal stiffeners. As can be seen from Figure 2 the cross-sectional area to be minimized is

$$A = 2ht_w + 2bt_f + 2t_s(b_1 + b_2)\,, \tag{4.1}$$

The stress constraint can be expressed as

$$\sigma_{\max} = \frac{M_{\max}}{W_x} \le f_y\,, \tag{4.2}$$

where $M_{\max}$ is the maximum bending moment, W_x is the section modulus, f_y is the yield stress. In the moment of inertia the effect of stiffeners is neglected, thus

$$I_x \simeq \frac{h^3 t_w}{6} + 2bt_f \left(\frac{h}{2}\right)^2 . \tag{4.3}$$

The stress constraint (4.2) can be written in the following form

$$W_x \simeq \frac{I_x}{\frac{h}{2}} = \frac{h^2 t_w}{3} + bt_f h \ge W_o = \frac{M_{\max}}{f_y}\,. \tag{4.4}$$

From (4.1) we obtain

$$bt_f = \frac{A}{2} - ht_w - A_S\,. \tag{4.5}$$

Substituting (4.5) into (4.4) we get

$$W_x = \frac{Ah}{2} - \frac{2h^2 t_w}{3} - A_S h \ge W_0\,. \tag{4.6}$$

In addition it follows from (4.6) that

$$A \ge \frac{2W_0}{h} + \frac{4h^2 t_w}{3} + 2A_S\,. \tag{4.7}$$

According to Eurocode 3 [7] the local buckling constraint for the compression flange can be expressed as

$$\frac{b}{t_f} \le \frac{1}{\delta} = 42\varepsilon \qquad \text{and} \qquad \varepsilon = \sqrt{\frac{235}{f_y}}\,. \tag{4.8}$$

The local buckling constraint for the upper part of the webs is

$$\frac{0.2h}{t_w} \le \frac{42\varepsilon}{0.67 + 0.33\psi}\,. \tag{4.9}$$

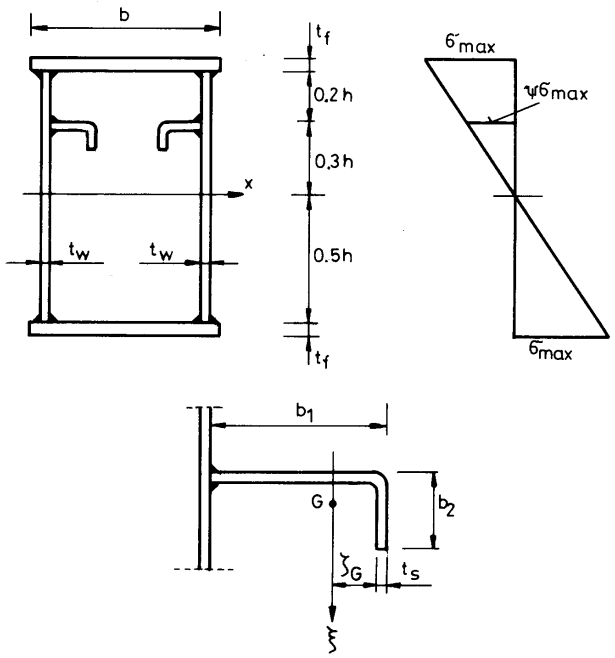

Figure 2. Stiffened box beam and the detail of a stiffener

If $\psi = 0.6$ we get

$$h/t_w \leq 242\varepsilon = 1/\beta\,. \tag{4.10}$$

For the lower part of the webs $\psi = -5/3 = -1.667$ and

$$0.8h/t_w \leq 62\varepsilon(1-\psi)\sqrt{-\psi} \tag{4.11}$$

or

$$h/t_w \leq 267\varepsilon \tag{4.12}$$

thus, the limiting slenderness defined by (4.10) is governing.

The local buckling constraints for the cold-formed stiffeners according to DASt Richtlinie 0l6 [8] are

$$b_1/t_s \leq 1.33\sqrt{E/f_y} \tag{4.13}$$

and

$$b_2/t_s \leq 0.43\sqrt{E/f_y} \tag{4.14}$$

or in other form

$$b_1/t_s \le 30\varepsilon = \delta_1 \qquad \text{and} \qquad b_2/t_s \le 12.5\varepsilon = \delta_2 \,. \tag{4.15}$$

According to API design rules [9] the overall buckling constraints for compressed stiffeners are of the form

$$I_\xi \ge 4at_w^3 \qquad \text{and} \qquad C_s = \frac{1}{12}\left(\delta_1^3 + \frac{3\delta_1^2\delta_2^2}{\delta_1+\delta_2}\right) \,, \tag{4.16}$$

where a is the distance of diaphragms. With

$$b_1 = \delta_1 t_S \qquad \text{and} \qquad b_2 = \delta_2 t_S \tag{4.17}$$

the centre of gravity for a stiffener (Figure 2) is

$$\xi_G = \frac{t_S\delta_1^2}{2(\delta_1+\delta_2)} \tag{4.18}$$

and the moment of inertia is given by

$$I_\xi = C_S t_S^4 \,. \tag{4.19}$$

Expressing a in terms of h

$$a = C_a h \tag{4.20}$$

and using (4.19), from (4.16) one obtains (4.21)

$$t_S = 4\sqrt{\frac{4C_a\beta^4}{C_S}} \,. \tag{4.21}$$

Consequently relation (4.7) can be written as

$$A = 2W_0/h + 4\beta h^2/3 + 2h^2 C_A \,, \tag{4.22}$$

$$C_A = (\delta_1+\delta_2)\sqrt{4C_a\beta^3/C_S} \,. \tag{4.23}$$

The condition $dA/dh = 0$ gives the optimum beam height

$$h_{opt} = \sqrt[3]{\frac{W_0}{4\beta/3 + 2C_A}} \,. \tag{4.24}$$

Without longitudinal stiffeners we obtain

$$h_{opt} = \sqrt[3]{\frac{3W_0}{4\beta_0}} \tag{4.25}$$

where

$$\frac{1}{\beta_0} = 124\varepsilon \tag{4.26}$$

as was already shown in the book [10] by Farkas. Expressing h_{opt} from (4.24), or from (4.25) and substituting it into (4.22) we get

$$A_{\min} = \sqrt[3]{18W_0^2(2\beta + 3C_A)}\,. \tag{4.27}$$

If there are no stiffeners

$$A_{0.\,\min} = \sqrt[3]{36\beta_0 W_0^2}\,. \tag{4.28}$$

Comparison of beams with and without stiffeners: taking $f_y = 235$ MPa, we calculate with the following values: $1/\beta = 242$, $1/\beta_o = 124$, $\delta_1 = 30$, $\delta_2 = 12.5$, $C_s = 3077.2$, in (4.22) taking $C_a = 1.5$ we get $C_A = 1/2006$.

With (4.24) and (4.25) we obtain

$$h_{opt} = 5.36\sqrt[3]{W_0} \tag{4.29}$$

and

$$h_{0.opt} = 4.53\sqrt[3]{W_0}\,, \tag{4.30}$$

respectively, i.e., a beam with longitudinal stiffeners has 15% higher webs than without stiffeners.

According to (4.27)

$$A_{\min} = 0.5601\sqrt[3]{W_0} \tag{4.31}$$

and with (4.28)

$$A_{0.\,\min} = 0.6622\sqrt[3]{W_0}\,, \tag{4.32}$$

i.e., a beam with stiffeners has 18% smaller weight than without stiffeners.

5. Minimum cost design of longitudinally stiffened box beams

A simply supported beam of span length $L = 20$ m is subjected to uniformly distributed factored normal load of intensity $p = 73.5$ N/mm. It is assumed that the beam is constructed with 11 transverse diaphragms of uniform distance $a = 2$ m to stabilize the stiffeners against flexural buckling and to avoid distortions of the rectangular box shape. The longitudinal stiffeners are interrupted and welded to diaphragms.

The volume of the structure is

$$V = AL + 11bht_D/4 + 2A_SL \tag{5.1}$$

where

$$A = 2ht_W + 2bt_f \ . \tag{5.2}$$

The thickness of diaphragms is $t_D = 0.7t_W$, but rounded to 4, 5 or 6 mm.

The cross-sectional area of a stiffener is

$$A_S = (b_1 + b_2)t_S \tag{5.3}$$

in which b_1 and b_2 can be calculated according to the equations $(4.17)_{1,2}$.

The number of structural elements to be assembled is $\kappa = 4 + 11 + 20 = 35$. The difficulty factor is taken to be $\Theta_d = 3$.

The following welding times are considered.

For longitudinal fillet welds of size $a_w = 0.5t_w$, SAW (submerged arc welding), $a_w = 0 \div 15$ mm

$$T_{21} = 0.2349L(0.5t_w)2\text{x}10^{-3} \ \ (L \text{ in mm}) \ . \tag{5.4}$$

For transverse fillet welds of constant size $a_w = 4$ mm connecting the diaphragms to the box section, SMAW (shielded metal arc welding)

$$T_{22} = 0.788911(b + 2h)42\text{x}10^{-3} \ \ (b \text{ and } h \text{ in mm}) \ . \tag{5.5}$$

For the two longitudinal fillet welds of size $a_w = 4$ mm connecting the stiffeners to the webs GMAW-C (gas metal arc welding with CO_2)

$$T_{23} = 0.3394\text{x}2L\text{x}42x10^{-3} \ \ (L \text{ in mm}) \tag{5.6}$$

For transverse fillet welds of size $a_w = 4$ mm connecting the stiffeners to the diaphragms, SMAW

$$T_{24} = 0.7889(42.5t_S\varepsilon)4^2x20x10^{-3} \ \ (t_S \text{ in mm}) \ . \tag{5.7}$$

6. Design constraints

Stress constraint due to bending

$$\frac{M}{W_x} = \frac{pL^2}{8W_x} \leq f_y \tag{6.1}$$

where the first moment and the moment of inertia for the cross secrion are

$$W_x = \frac{2I_x}{h + t_f} \qquad \text{and} \qquad I_x = \frac{h^3 t_w}{6} + \frac{bt_f(h + t_f)^2}{2} \ . \tag{6.2}$$

Note that the moment of inertia of stiffeners is neglected.

The local buckling constraints for box beam webs and flange are given by equations (4.17). The constraint on flexural buckling of stiffener parts with buckling length of

$a = 2000$ mm is given by equation (4.16). Using equations (4.17) and (4.19) the moment of inertia of a stiffener can be calculated as

$$I_\xi = 3077\varepsilon^3 t_S^4 \tag{6.3}$$

The unknowns in the optimization are as follows: h, b, t_w, t_f, t_S.

7. Optimization and results

The optimization of the box beam is performed by the Hillclimb and backtrack methods. In the case of longitudinally stiffened box beam the cost function (2.2) should be minimized considering the constraints (4.2, 4.8, 4.10, 6.1). In the case of box beams without stiffeners the following modifications should be used: $t_S = 0$ and $T_{23} = T_{24} = 0$. The results are given in Tables 1 and 2.

Table 1. Optimum dimensions in mm of the box beam without longitudinal stiffeners obtained by the Hillclimb method

k_f/k_m	h	t_W	b	t_f	K/k_m (kg)
0	1100	9	540	20	6580
1	900	8	740	20	9249
2	910	8	730	20	11474

It can be seen that the results obtained by the Hillclimb and backtrack methods are nearly the same, so the new version of backtrack is suitable for nonlinear objective functions. The comparison of results obtained for unstiffened and stiffened box beams shows cost savings of 18-21%, so the application of longitudinal stiffeners is economical.

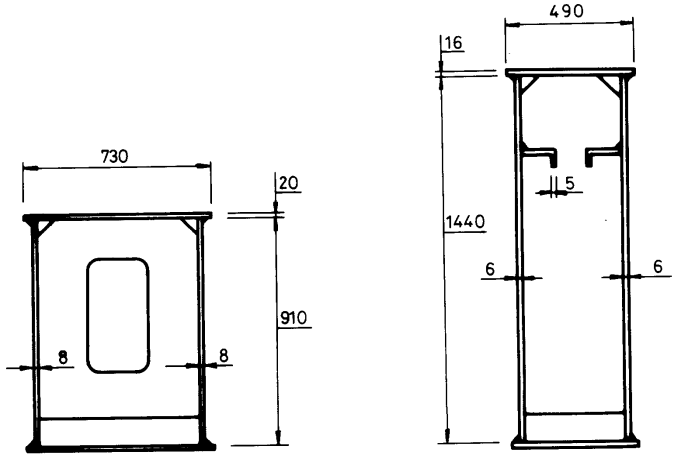

Figure 3. Optimum sizes of box beams without and with longitudinal stiffeners, for $k_f/k_m = 2$

Figure 3 shows the optimized box beams without and with longitudinal stiffeners. It can be seen that the beam with stiffeners is higher and narrower.

Table 2. Optimum dimensions in mm of the box beam with longitudinal stiffeners obtained by the Hillclimb and backtrack method

Method	k_f/k_m	h	t_W	b	t_f	t_S	K/k_m (kg)
	0	1450	6	440	18	5	5610
Hillclimb	1	1450	6	490	16	5	7588
	2	1440	6	500	16	5	9619
	0	1450	6	490	16	5	5591
Backtrack	1	1440	6	470	17	5	7608
	2	1440	6	490	16	5	9585

8. Post-welding treatments and optimum fatigue design of welded I-beams

In order to eliminate or decrease the danger of fatigue fracture several methods have been investigated. Post-welding treatments (PWT-s) such as toe grinding, TIG-dressing, hammer peening and ultrasonic impact treatment (UIT) are the most efficient methods. These methods have been tested and a lot of experimental results show their effectiveness and reliability.

For designers it is important to know the measure of saving in structural weight and cost, which can be achieved by using these treatments. Optimum design is suitable for this task, since the additional cost of PWT can be included in the cost function and the improved fatigue stress range can be considered in the fatigue strength constraint. Thus, our aim is to illustrate this saving by means of a simple numerical example of a welded I-beam.

In this case the transverse fillet welds used for vertical stiffeners decrease the fatigue stress range, thus the effect of PWT can be illustrated minimizing the cost function, which contains also the additional cost of PWT and the increased fatigue stress range can be included in the fatigue stress constraint. Note that Farkas [11] has treated this problem in a recent article for a welded box beam using only a few experimental data given by Woodley [12].

Table 3. Some improvement data according to [13]

	Stress range (MPa) at $2\text{x}10^6$	Improvement % at $2\text{x}10^6$
As welded	86	–
UIT	190	121
TIG dressing	132	53
TIG+UIT	202	135

Haagensen et al [13] have summarized the results of investigations relating to the measure of improvement in a table, from which we cite some basic data in Table 3. Note that the data are obtained for high strength steel of yield stress 780 MPa.

A wide overview of results is given by Braid et al [14]. This article gives a hammer-peening speed of 25 mm/s and uses 6 passes, i.e., 6x1000/(25x60) = 4 min/m.

Maddox et al [15] have given the improvement citing the UK standard fatigue classes stating that the fatigue limit for weld toe burr grinding or hammer peening equals the UK class C at $2x10^6$ cycles. According to BS 5400 Part 10 (1980) [16] for transverse fillet welds in as welded state the fatigue limit is given by Class F of 40 MPa at 10^7 cycles, and for Class C of 78 MPa. Calculation for $2x10^6$ cycles gives 68 and 123 MPa, respectively, thus, the improvement is 123/78 = 1.8 (80%).

Lobanov and Garf [17] have treated the effect of UIT in connections of tubular structures.

According to Gregor [18] TIG-dressing results in 40% improvement. Woodley [12] gives also 40% improvement for toe burr grinding and the necessary time for grinding 60 min/m.

According to Janosch et al [19] the ultrasonic peening of fillet welded T-joints results in a fatigue stress range at $2x10^6$ cycles of 290 MPa, which is 70-80% improvement compared to the as-welded value of 168 MPa. For a treatment of 3 passes 15 min/m specific time has been necessary.

Huther et al [20] worked out a summary of improvement methods and results using data of 51 references. For fillet welded T- or cruciform joints the following final design fatigue stress ranges at $2x10^6$ cycles can be used: for TIG dressing 124 MPa (70% improvement as compared to EC3 data); for hammer peening 209 MPa (190% improvement). These data are valid for steels of yield stress less than 400 MPa.

For our purpose those publications are suitable in which data are given not only for the measure of improvement (α), but also for the time required for treatment (T_0). These data are summarized in Table 4.

Table 4. Measure of improvement and specific treatment time for various treatments according to the published data

Method	Reference	T_0 (min/m)	Improvement %	α	Remark
Grinding	[12]	60	40	1.4	
TIG dressing	[21]	18	40	1.4	70-100%
Hammer peening	[14]	4	100	2.0	175-190%
UIT	[19]	15	70	1.7	

It should be mentioned that we want to calculate with the minimum value of improvement. A value larger than 100% cannot be realized in our numerical example.

9. Minimum cost design of a welded I-beam considering the improved fatigue stress range and the additional PWT cost

In the investigated numerical example transverse vertical stiffeners are welded to a welded I-beam with double fillet welds. PWT is used only in the middle of the span,

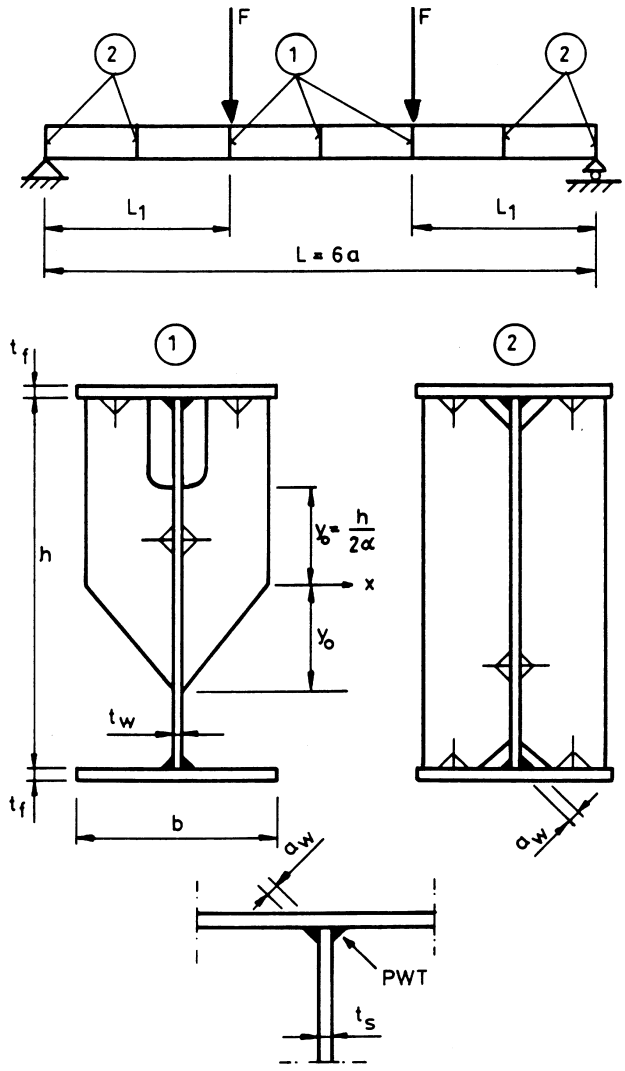

Figure 4. Welded I-beam with vertical stiffeners. Double fillet welds with (1) and without (2) PWT

since near the supports the bending stresses are small. The tension part of stiffeners in the middle of span is not welded to the lower flange and to the lower part of the web. Thus, PWT is needed only for welds connecting the stiffeners to the upper flange (Figure 4). For this reason two types of stiffeners are used as it can be seen in Figure 4.

The beam is loaded by a pair of forces fluctuating in the range of $0 \div F_{\max}$, so the bending stress range is calculated from $F_{\max}$.

Time for PWT is

$$T_4 = T_0 L_t \tag{9.1}$$

where T_0 is the specific time (min/mm) and L_t is the treated weld length (mm).

The final form of the cost function is as described in [22]

$$\frac{K}{k_m} = \rho V + \frac{k_f}{k_m}\left(\Theta_d\sqrt{\kappa\rho V} + 1.3\sum C_{2i}a_{wi}^n L_{wi} + T_0 L_t\right) . \tag{9.2}$$

10. Design constraints

The constraint on fatigue stress range can be formulated as

$$\frac{F_{\max}L_1}{W_x} \leq \frac{\alpha\Delta\sigma_C}{\gamma_{Mf}} \tag{10.1}$$

where

$$W_x = \frac{I_x}{\frac{h}{2}+\frac{t_f}{2}}; I_x = \frac{h^3 t_w}{12} + 2bt_f\left(\frac{h}{2}+\frac{t_f}{2}\right)^2 . \tag{10.2}$$

According to Eurocode 3 (EC3) the fatigue stress range for as welded structure is $\Delta\sigma_C = 80$ MPa, the fatigue safety factor is $\gamma_{Mf} = 1.25$.

The quotient α expresses the measure of improvement

$$\alpha = \frac{\Delta\sigma_{Cimproved}}{\Delta\sigma_{Caswelded}} . \tag{10.3}$$

The constraint on local buckling of the web according to EC3 is

$$\frac{h}{t_w} \leq 69\varepsilon; \qquad \varepsilon = \sqrt{\frac{235}{\alpha\Delta\sigma_C/\gamma_{Mf}}} \tag{10.4}$$

Note that we calculate in the denominator of ε with the maximum compressive stress instead of yield stress [23].

The constraint on local buckling of the compression flange is

$$b/t_f \leq 28\varepsilon . \tag{10.5}$$

11. Numerical example

Data: $F_{\max} = 138$ kN, $L = 12$ m, $L_1 = 4$ m, $\Delta\sigma_C/\gamma_{Mf} = 80/1.25 = 64$ MPa, $\varepsilon = 1.916/\sqrt{\alpha}$; $\Theta_d = 3$. The number of stiffeners is 2x7 = 14, thus $\kappa = 3 + 14 = 17$.

The volume of the structure is

$$V = (ht_w + 2bt_f)L + 4bht_S + 1.5bht_S\left(1+\frac{1}{\alpha}\right) \tag{11.1}$$

in which $t_s = 6$ mm.

The second member expresses the volume of stiffeners without PWT, the third member gives the volume of stiffeners with PWT.

For longitudinal GMAW-C (gas metal arc welding with CO_2) fillet welds of size 4 mm we calculate with

$$C_2 a_w^n L_w = 0.3394\text{x}10^{-3}\text{x}42\text{x}4L = 260 \text{ mm}\,, \tag{11.2}$$

for transverse SMAW (shielded metal arc welding) fillet welds the following formula holds

$$C_2 a_w^n L_w = 0.7889\text{x}10^{-3}\text{x}4^2 \left[6\left(b + \frac{2h}{\alpha}\right) + 16\,(b+h)\right]\,. \tag{11.3}$$

For the constrained minimization of the nonlinear cost function the Rosenbrock Hill-climb mathematical programming method is used complemented with an additional search for optimum rounded discrete values of unknowns. The results of computation, i.e. the unknown dimensions h, t_w, b and t_f as well as the minimum costs for different values of k_f/k_m and α are given in Table 5.

Table 5. Optimum rounded dimensions in mm and K/k_m (kg) values for different k_f/k_m ratios for various PWT-s. $k_f/k_m = 0$ means the minimum weight design without effect of PWT

PWT	k_f/k_m (kg/min)	h	t_w	b	t_f	K/k_m (kg)
as	0	1300	10	320	14	2191
welded	1	1230	10	310	16	3802
	2	1230	10	310	16	5399
Grinding	1	940	9	340	15	3343
	2	890	8	300	19	4704
TIG	1	1000	9	330	14	3235
dressing	2	1110	10	310	12	4770
Hammer	1	820	9	310	13	2762
peening	2	820	9	310	13	3999
UIT	1	970	10	300	12	3021
	2	810	8	300	17	4202

12. Conclusions

In this paper the benefits of using optimization methods for welded structures are presented. The two examples shown illustrate the possibility of cost and mass reduction. In the first example comparisons of the optimized cross-sectional areas and costs of box beams without and with longitudinal stiffeners placed at a distance of 1/5 web height show that the use of stiffeners results in considerable savings. The minimum cross-sectional area design is solved analytically deriving closed formulae for the optimum beam dimensions. The cost function contains material and welding costs, considering also the welds necessary for transverse diaphragms. Since this cost function is nonlinear, a new version of backtrack discrete combinatorial programming

method is developed and used. This version contains a subroutine for the computation of the roots of a nonlinear function (cost function) with one variable. Results obtained by Hillclimb and backtrack methods are nearly the same, so the new version of backtrack is suitable for nonlinear objective functions. The comparison of results obtained for unstiffened and stiffened box beams shows cost savings of 18-21%, so the application of longitudinal stiffeners is economical.

In the second example a welded I-beams with vertical stiffeners was optimized using double fillet welds with and without post-welding treatment. It can be seen, that using various treatment methods one can achieve cost saving even if these treatments are expensive. The example shows that elimination or decreasing the danger of fatigue fracture in welded structures can be connected to cost saving. The following cost savings can be achieved: grinding 14-15 %, TIG dressing 13-17 %, hammer peening 35-38 %, UIT 26-28 %. Thus, the cost savings are significant, and the most efficient method is hammer peening. It can be also seen that PWT methods affect the optimum dimensions.

Acknowledgement. This research was supported by the Hungarian National Research Foundation (project No.: OTKA 22846 and 29326) and the Fund for Higher Education grant 8/2000.

REFERENCES

1. COSTCOMP: *Programm zur Berechnung der Schweisskosten*, Düsseldorf, Deutscher Verlag für Schweisstechnik, 1990.
2. Bodt, H. J. M.: *The global approach to welding costs*, The Hague, The Netherlands Welding Institute, 1990.
3. Walker, R. J.: *An enumerative technique for a class of combinatorical problems,* In Proc. of Symposia in Appl. Math Amer. Math. Soc., Providence, R.I. **10**, (1960), 91-94.
4. Golomb, S. W. and Baumert, L. D.: *Backtrack programming.* J .Assoc. Computing Machinery, **12**, (1965), 516-524.
5. Farkas, J. and Jármai, K.: *Analysis and optimum design of metal structures*, Rotterdam-Brookfield, Balkema, 1997.
6. Brent, R. P.: *Algorithms for minimization without derivatives,* Englewood Cliffs NJ. Prentice Hall, 1973.
7. Eurocode 3. *Design of steel structures. Part 1.1. General rules and rules for buildings*, European Prestandard ENV 1993-1-1.CEN European Committee for Standardisation, Brussels, 1992.
8. DASt Richtlinie 016. *Entwurf, Bemessung und konstruktive Gestaltung von Tragwerken aus dünnwandigen kaltgeformten Bauteilen,* Deutscher Ausschuss für Stahlbau, 1986.
9. Americal Petroleum Institute (API) Bul.2V. *Bulletin on design of flat plate structures.* 1st edition Washington, D.C. 1987.
10. Farkas, J.: *Optimum design of metal structures,* Budapest, Akadémiai Kiadó, Chichester, Ellis Horwood, 1984.
11. Farkas, J.: *Techno-economic considerations in the optimum design of welded structures*, Welding in the World, **29**(9-10), (1991), 295-300.

12. Woodley, C. C.: *Practical applications of weld toe grinding.* In Improving the Fatigue Strength of Welded Joints. The Welding Institute, Abington, Cambridge, UK, (1983), 19-22.

13. Haagensen, P. J., Statnikov, E. S. and Lopez-Martinez, L.: *Introductory fatigue tests on welded joints in high strength steel and aluminium improved by various methods including ultrasonic impact treatment* (UIT), IIW-Doc. XIII-1748-98, 1998.

14. Braid, J. E. M., Bell, R. Militaru, D. V.: *Fatigue life of as-welded, repaired, and hammer-peened joints in high-strength structural steel*, Welding in the World, **39**(5), (1997), 248-261.

15. Maddox, S. J., Manteghi, S. et al.: *The application of fatigue life improvement techniques to steel welds.* IIW Comm.XIII Workshop on Improvement Methods, Hamburg, 1998.

16. BS 5400: Part 10: *Steel, concrete and composite bridges. Code of practice for fatigue.* British Standard Institution, 1980.

17. Lobanov, L. M. and Garf, E. F.: *Estimation of life of metal tubular structure connections at ultrasonic peening treatment of welded joint zone*, Journal of Constructional Steel Research, **46**(1-3), (1998), Paper No. 353.

18. Gregor, V.: *The effect of surface preparation by TIG remelting on fatigue life*, Zváracské Správy Welding News, **39**, (1989), 60-65.

19. Janosch, J. J., Koneczny, H. et al.: *Improvement of fatigue strength in welded joints (in HSS and aluminium alloys) by ultrasonic hammer peening*, Welding in the World, **37**(2), (1996), 72-83.

20. Huther, I., Lieurade, H. P. et al.: *Analysis of results on improved welded joints*, Welding in the World, **37**(5), (1996), 242-266.

21. Horn, A. A., Huther, I. and Lieurade, H. P.: *Fatigue behaviour of T-joints improved by TIG dressing*, Welding in the World, **41**(4), (1998), 273-280.

22. Jármai, K. and Farkas, J.: *Cost calculation and optimization of welded steel structures*, Journal of Constructional Steel Research, **50**, (1999), 115-135.

23. Farkas, J. and Jármai, K.: *Fatigue constraints in the optimum design of welded structures.* Int.Conf. Fatigue of Welded Components and Structures. Senlis (France) Eds. Lieurade, H.P. and Rabbe, P. Les Editions de Physique, Les Ulis, France, (1996), 49-56.

Journal of Computational and Applied Mechanics, Vol. 1., No. 2., (2000), pp. 167–178

VIBRATIONS OF CIRCULAR ARCHES SUBJECTED TO HYDROSTATIC FOLLOWER LOADS – COMPUTATIONS BY THE USE OF GREEN FUNCTIONS

Katalin Kelemen
Department of Mechanics, University of Miskolc
3515 Miskolc – Egyetemváros, Hungary
mechgab1@gold.uni-miskolc.hu

[Received: April 30, 2000]

Abstract. Using the Green function matrix, self adjoint eigenvalue problems governed by degenerate systems of differential equations and homogeneous linear boundary conditions can be replaced – like the case of scalar equations – by an eigenvalue problem for a system of Fredholm integral equations with the Green function matrix as a kernel. We have determined the Green function matrix for simply supported and fixed circular arches provided that the arch is also subjected to a hydrostatic follower load. In the knowledge of the Green function matrix, the self adjoint eigenvalue problem giving the natural frequencies of the vibrations as a function of the follower load can be replaced by an eigenvalue problem described by a system of Fredholm integral equations. The latter is reduced to an algebraic eigenvalue problem and the first eigenvalues are computed by applying the QZ algorithm. The results computed show how the load affects the first natural frequencies of the arches.

Keywords: Circular arch, natural frequencies, stability, hydrostatic follower load, Green function matrix, eigenvalue problem

1. Introduction

There is a classical definition for the Green function of ordinary linear inhomogeneous differential equations associated with homogeneous boundary conditions [1]. The definition has been generalized – see paper [2] for details – for a degenerate system of linear differential equations by keeping up the structure of the definition given in [1]. It is also well known that in the knowledge of the corresponding Green function eigenvalue problems for the differential equation can be replaced by an eigenvalue problem for a Fredholm integral equation with the Green function as a kernel. The latter can effectively be solved by various algorithms – see [3] for details.

There are a lot of works on eigenvalue problems associated with the free vibration and stability of circular arches. Without trying to achieve completeness we should mention the book by Federhoffer [5], and the papers [6,7]. For further references the reader is referred to the papers mentioned. To the author's knowledge the issue how the load affects the vibration of the arch has not been investigated yet. With regard to this fact the main objectives of the present paper are as follows:

– to determine the Green function matrices for simply supported and fixed circular arches subjected to a constant hydrostatic follower load;
– to reduce the eigenvalue problem giving the natural frequencies of the free

vibrations as a function of the hydrostatic follower load to an eigenvalue problem for a system of Fredholm integral equations with the Green function matrix as a kernel and

– to compute and analyse the first natural frequencies as functions of the follower load.

The paper is organized into four sections. Section 2 is devoted to some preliminaries with an emphasis on the definition of the Green function matrix. Section 3 presents the governing equations for the two problems and gives the corresponding Green functions. Section 4 is a brief summary of the solution algorithm and some solutions can also be found there. The last section is a summary of the results.

2. The Green function matrix

Consider the degenerate system of differential equations

$$\mathbf{K}(\mathbf{y}) = \sum_{\nu=0}^{n} \overset{\nu}{\mathbf{P}}(x)\mathbf{y}^{(\nu)}(x) =$$

$$= \begin{bmatrix} 0 & 0 \\ 0 & \overset{n}{\mathbf{P}}_{22} \end{bmatrix} \begin{bmatrix} \mathbf{y}_1 \\ \mathbf{y}_2 \end{bmatrix}^{(n)} + \cdots + \begin{bmatrix} 0 & 0 \\ 0 & \overset{k+1}{\mathbf{P}}_{22} \end{bmatrix} \begin{bmatrix} \mathbf{y}_1 \\ \mathbf{y}_2 \end{bmatrix}^{(k+1)} +$$

$$+ \begin{bmatrix} \overset{k}{\mathbf{P}}_{11} & \overset{k}{\mathbf{P}}_{12} \\ 0 & \overset{k}{\mathbf{P}}_{22} \end{bmatrix} \begin{bmatrix} \mathbf{y}_1 \\ \mathbf{y}_2 \end{bmatrix}^{(k)} + \cdots + \begin{bmatrix} \overset{s}{\mathbf{P}}_{11} & \overset{s}{\mathbf{P}}_{12} \\ \overset{s}{\mathbf{P}}_{21} & \overset{s}{\mathbf{P}}_{22} \end{bmatrix} \begin{bmatrix} \mathbf{y}_1 \\ \mathbf{y}_2 \end{bmatrix}^{(s)} +$$

$$+ \cdots + \begin{bmatrix} \overset{0}{\mathbf{P}}_{11} & \overset{0}{\mathbf{P}}_{12} \\ \overset{0}{\mathbf{P}}_{21} & \overset{0}{\mathbf{P}}_{22} \end{bmatrix} \begin{bmatrix} \mathbf{y}_1 \\ \mathbf{y}_2 \end{bmatrix} = \begin{bmatrix} \mathbf{r}_1 \\ \mathbf{r}_2 \end{bmatrix} \tag{2.1}$$

where $n > k > s > 0$, l is the number of unknown functions (the size of $\mathbf{y}$), j is the size of $\mathbf{y}_2$ and the matrices $\overset{\nu}{\mathbf{P}}$ and $\mathbf{r}^T = [\, \mathbf{r}_1^T \,|\, \mathbf{r}_2^T \,]$ are continuous for $x \in [a, b]$; $a < b$. The matrices $\overset{n}{\mathbf{P}}_{22}$ and $\overset{k}{\mathbf{P}}_{11}$ are assumed to be invertible if $x \in [a, b]$.

The system of ODEs (2.1) is associated with linear homogeneous boundary conditions

$$\mathbf{U}_\mu(\mathbf{y}) = \sum_{\nu=0}^{n-1} \left[\mathbf{A}_{\nu\mu}\mathbf{y}^{(\nu)}(a) + \mathbf{B}_{\nu\mu}\mathbf{y}^{(\nu)}(b) \right] =$$

$$= \sum_{\nu=0}^{n-1} \left\{ \begin{bmatrix} \overset{11}{\mathbf{A}}_{\nu\mu} & \overset{12}{\mathbf{A}}_{\nu\mu} \\ \overset{21}{\mathbf{A}}_{\nu\mu} & \overset{22}{\mathbf{A}}_{\nu\mu} \end{bmatrix} \begin{bmatrix} \mathbf{y}_1(a) \\ \mathbf{y}_2(a) \end{bmatrix}^{(\nu)} + + \begin{bmatrix} \overset{11}{\mathbf{B}}_{\nu\mu} & \overset{12}{\mathbf{B}}_{\nu\mu} \\ \overset{21}{\mathbf{B}}_{\nu\mu} & \overset{22}{\mathbf{B}}_{\nu\mu} \end{bmatrix} \begin{bmatrix} \mathbf{y}_1(b) \\ \mathbf{y}_2(b) \end{bmatrix}^{(\nu)} \right\} = \begin{bmatrix} 0 \\ 0 \end{bmatrix} \tag{2.2}$$

where $\mu = 1, \ldots, n$; and for $\nu \leq k$ the constant matrices $\mathbf{A}_{\nu\mu}$ and $\mathbf{B}_{\nu\mu}$ fulfill the conditions

$$\overset{11}{\mathbf{A}}_{\nu\mu} = \overset{21}{\mathbf{A}}_{\nu\mu} = \overset{11}{\mathbf{B}}_{\nu\mu} = \overset{21}{\mathbf{B}}_{\nu\mu} = 0.$$

Solution to the boundary value problem (2.1),(2.2) is sought in the form

$$\mathbf{y}(x) = \int_a^b \mathbf{G}(x,\xi)\mathbf{r}(\xi)d\xi \tag{2.3}$$

in which $\mathbf{G}(x,\xi)$ is the Green function matrix [3,4].

If there exists the Green function matrix for the BVP (2.1), (2.2) then the vector (2.3) satisfies the differential equation (2.1) and the boundary conditions (2.2) [3,4].

As regards a proof of existence for the Green function matrix we refer to [4].

Let the system of differential equations read

$$\mathbf{K}[\mathbf{y}] = \lambda\mathbf{y} \tag{2.4}$$

in which $\mathbf{K}[\mathbf{y}]$ is given by (2.1) and λ is the eigenvalue sought. The ODEs (2.4) are associated with the linear homogeneous boundary conditions (2.2). These are assumed to be independent of λ.

Recalling (2.3) the eigenvalue problem (2.4), (2.2) can be replaced by an eigenvalue problem for the system of integral equations

$$\mathbf{y}(x) = \lambda \int_a^b \mathbf{G}(x,\xi)\mathbf{y}(\xi)d\xi. \tag{2.5}$$

On the basis of [3] a procedure for the numerical solution of the above problem (2.5) has been presented in [4].

3. Vibration of circular arches subjected to a hydrostatic follower load

The arch with radius R is symmetric with respect to the plane of its center line. The cross sectional area and the second moment of inertia with respect to the centroidal axis perpendicular to the plane of the arch are denoted by A and I, respectively. The angle coordinate φ changes in the interval $[-\vartheta,\vartheta]$, the central angle $\bar{\vartheta}$ subtended by the arch is equal to 2ϑ. The Young modulus of elasticity is denoted by E.

Vibrations of circular arches subjected to a constant follower load are governed by the differential equation

$$\begin{aligned}\mathbf{K}[\mathbf{y},\varepsilon_0] = &\begin{bmatrix} 0 & 0 \\ 0 & 1 \end{bmatrix}\begin{bmatrix} U \\ W \end{bmatrix}^{(4)} + \begin{bmatrix} -m & 0 \\ 0 & 2-m\varepsilon_0 \end{bmatrix}\begin{bmatrix} U \\ W \end{bmatrix}^{(2)} + \\ &+\begin{bmatrix} 0 & -m \\ m & 0 \end{bmatrix}\begin{bmatrix} U \\ W \end{bmatrix}^{(1)} + \begin{bmatrix} 0 & 0 \\ 0 & M-m\varepsilon_0 \end{bmatrix}\begin{bmatrix} U \\ W \end{bmatrix} = \lambda\begin{bmatrix} U \\ W \end{bmatrix}.\end{aligned} \tag{3.1}$$

Here $(\dots)^{(n)} = d^{(n)}/d\varphi^{(n)}$, U and V are the amplitudes of the tangential and normal displacements,

$$M=\frac{AR^2}{I},\ m = M-1. \tag{3.2}$$

ε_0 is the axial strain on the center line of the circular arch (this value is constant and uniquely determined constant by the current volume of the load). Neglecting the vibrations, i.e., setting λ to 0 we obtain an ODE

$$U^{(6)} + 2U^{(4)} + U^{(2)} - m\varepsilon_0 \left(U^{(4)} + U^{(2)}\right) = 0 \tag{3.3}$$

which – provided that it is associated with appropriate boundary conditions – gives the critical load. Setting ε_0 to 0 we get a system of ODEs for the free vibrations of the arch [4].

It can be proved that the first critical axial strain (for the first buckling mode) [2] is of the form:

$$\varepsilon_{0crit} = -\frac{1}{m}\left[\left(s_i \frac{\pi}{\vartheta}\right)^2 - 1\right] < 0 \tag{3.4}$$

where

$$s_1 = 1 \tag{3.5}$$

for a simply supported arch and

$$s_2 = s_2(\vartheta) \approx$$
$$\approx \begin{cases} 0.03436558207\vartheta^2 - 0.01102140558\vartheta + 1.431758411 & \text{if} \quad \vartheta \in (0; 1.7] \\ 0.1760886555\vartheta^2 - 0.5259986022\vartheta + 1.899253872 & \text{if} \quad \vartheta \in (1.7; 3.14] \end{cases} \tag{3.6}$$

for a fixed arch.

The corresponding hydrostatic follower load can be obtained from the equations

$$p_{crit} = \frac{1}{k_i(m, \vartheta)} \frac{IE}{R^3}\left[\left(s_i \frac{\pi}{\vartheta}\right)^2 - 1\right] \tag{3.7}$$

where

$$k_i = \frac{g_i(\vartheta)}{\vartheta/m + g_i(\vartheta)}$$

and

$$g_1 = \frac{3}{2}\vartheta + \tan\vartheta\left[\frac{\vartheta}{2}\tan\vartheta - \frac{3}{2}\right], \qquad g_2 = \vartheta - \frac{2\sin^2\vartheta}{\vartheta + \sin\vartheta\cos\vartheta}. \tag{3.8}$$

There are no closed form solutions giving the natural frequencies of the free vibration of the arches.

Depending on the supports applied, the system of ODEs (3.1) is associated with the following boundary conditions:

Simple supported arch $[i=1]$:

$$\begin{array}{ll} U(-\vartheta)=0 & U(\vartheta)=0 \\ W(-\vartheta)=0 & W(\vartheta)=0 \\ W^{(2)}(-\vartheta)=0 & W^{(2)}(\vartheta)=0 \end{array} \tag{3.9}$$

Fixed arch $[i=2]$:

$$\begin{array}{ll} U(-\vartheta)=0 & U(\vartheta)=0 \\ W(-\vartheta)=0 & W(\vartheta)=0 \\ W^{(1)}(-\vartheta)=0 & W^{(1)}(\vartheta)=0 \end{array} \tag{3.10}$$

Each of the eigenvalue problems (3.1),(3.9) and (3.1), (3.10) is self adjoint and positive definite if $\varepsilon_0 < 0$. The corresponding Green function matrix assumes the form

$$\underbrace{\mathbf{G}(\varphi,\psi)}_{(2\times 2)} = \sum_{j=1}^{4} \mathbf{Y}_j(\varphi)\left[\mathbf{A}_j(\psi) \pm \mathbf{B}_j(\psi)\right] \tag{3.11}$$

where the sign is {positive}[negative] if $\{\varphi \le \psi\}[\varphi \ge \psi]$ and

$$\begin{array}{ll} \mathbf{Y}_1 = \begin{bmatrix} \cos\varphi & 0 \\ \sin\varphi & 0 \end{bmatrix} & \mathbf{Y}_2 = \begin{bmatrix} -\sin\varphi & 0 \\ \cos\varphi & 0 \end{bmatrix} \\ \mathbf{Y}_3 = \begin{bmatrix} \cos(k\varphi) & (M-m\varepsilon_o)\varphi \\ k\sin(k\varphi) & -m \end{bmatrix} & \mathbf{Y}_4 = \begin{bmatrix} -\sin(k\varphi) & 1 \\ k\cos(k\varphi) & 0 \end{bmatrix} \end{array} \tag{3.12}$$

are solutions of the homogenous $\mathbf{K}[\mathbf{y},\varepsilon_0] = \mathbf{0}$ with

$$k^2 = 1 + \varepsilon_0 - M\varepsilon_0, \tag{3.13}$$

and

$$\mathbf{A}_j = \begin{bmatrix} \overset{j}{A}_{11} & \overset{j}{A}_{12} \\ \overset{j}{A}_{21} & \overset{j}{A}_{22} \end{bmatrix}, \qquad \mathbf{B}_j = \begin{bmatrix} \overset{j}{B}_{11} & \overset{j}{B}_{12} \\ \overset{j}{B}_{21} & \overset{j}{B}_{22} \end{bmatrix} \qquad j = 1,\ldots,4 \tag{3.14}$$

are functions of the angle coordinate ψ. The equation systems giving the unknowns

$$a = \overset{1}{B}_{1i},\ b = \overset{2}{B}_{1i},\ c = \overset{3}{B}_{1i},\ d = \overset{3}{B}_{2i},\ e = \overset{4}{B}_{1i},\ f = \overset{4}{B}_{2i} \qquad i = 1,2$$

can be set up from the second property of the Green function matrix – see the definition in [4]. The functions $\overset{1}{B}_{11}(\psi),\ldots,\overset{4}{B}_{22}(\psi); \psi \in [-\vartheta,\vartheta]$ are independent of the boundary conditions.

The first system of equations ($i = 1$):

$$\begin{bmatrix} \cos\psi & -\sin\psi & \cos(k\psi) & (M-m\varepsilon_o)\psi & -\sin(k\psi) & 1 \\ \sin\psi & \cos\psi & k\sin(k\psi) & -m & k\cos(k\psi) & 0 \\ -\sin\psi & -\cos\psi & -k\sin(k\psi) & M-m\varepsilon_o & -k\cos(k\psi) & 0 \\ \cos\psi & -\sin\psi & k^2\cos(k\psi) & 0 & -k^2\sin(k\psi) & 0 \\ -\sin\psi & -\cos\psi & -k^3\sin(k\psi) & 0 & -k^3\cos(k\psi) & 0 \\ -\cos\psi & \sin\psi & -k^4\cos(k\psi) & 0 & k^4\sin(k\psi) & 0 \end{bmatrix} \begin{bmatrix} a \\ b \\ c \\ d \\ e \\ f \end{bmatrix} = \begin{bmatrix} 0 \\ 0 \\ \frac{1}{2m} \\ 0 \\ 0 \\ 0 \end{bmatrix} \tag{3.15}$$

We have found the following solutions:

$$\left.\begin{array}{ll} a = \overset{1}{B}_{11} = -\dfrac{1}{1-k^2}\dfrac{\sin\psi}{2} & b = \overset{2}{B}_{11} = -\dfrac{1}{1-k^2}\dfrac{\cos\psi}{2} \\ c = \overset{3}{B}_{11} = \dfrac{1}{2}\dfrac{\sin k\psi}{k^3(1-k^2)} & d = \overset{3}{B}_{21} = \dfrac{1}{2mk^2} \\ e = \overset{4}{B}_{11} = \dfrac{\cos k\psi}{2k^3(1-k^2)} & f = \overset{4}{B}_{21} = -\dfrac{1}{2}\left(k^2+m\right)\dfrac{\psi}{mk^2} \end{array}\right\} \tag{3.16}$$

The second system of equations ($i = 2$):

$$\begin{bmatrix} \cos\psi & -\sin\psi & \cos(k\psi) & (M-m\varepsilon_o)\psi & -\sin(k\psi) & 1 \\ \sin\psi & \cos\psi & k\sin(k\psi) & -m & k\cos(k\psi) & 0 \\ -\sin\psi & -\cos\psi & -k\sin(k\psi) & M-m\varepsilon_o & -k\cos(k\psi) & 0 \\ \cos\psi & -\sin\psi & k^2\cos(k\psi) & 0 & -k^2\sin(k\psi) & 0 \\ -\sin\psi & -\cos\psi & -k^3\sin(k\psi) & 0 & -k^3\cos(k\psi) & 0 \\ -\cos\psi & \sin\psi & -k^4\cos(k\psi) & 0 & k^4\sin(k\psi) & 0 \end{bmatrix} \begin{bmatrix} a \\ b \\ c \\ d \\ e \\ f \end{bmatrix} = \begin{bmatrix} 0 \\ 0 \\ 0 \\ 0 \\ 0 \\ -\frac{1}{2} \end{bmatrix} \tag{3.17}$$

We have found the following solutions:

$$\left.\begin{array}{ll} a = \overset{1}{B}_{12} = \dfrac{\cos\psi}{2(1-k^2)} & b = \overset{2}{B}_{12} = -\dfrac{\sin\psi}{2(1-k^2)} \\ c = \overset{3}{B}_{12} = -\dfrac{\cos k\psi}{2k^2(1-k^2)} & d = \overset{3}{B}_{22} = 0 \\ e = \overset{4}{B}_{12} = \dfrac{1}{2k^2(1-k^2)}\sin k\psi & f = \overset{4}{B}_{22} = \dfrac{1}{2k^2} \end{array}\right\} \tag{3.18}$$

Taking into account that the Green function matrix should meet boundary conditions (3.9) (3.10) one can find the functions

$$\overset{1}{A}_{11}(\psi), \ldots, \overset{4}{A}_{22}(\psi); \qquad \psi \in [-\vartheta, \vartheta]$$

as well.

Simply supported arch ($i = 1$):

$$\begin{bmatrix} \cos\vartheta & \sin\vartheta & \cos(k\vartheta) & -(M-m\varepsilon_o)\vartheta & \sin(k\vartheta) & 1 \\ \cos\vartheta & -\sin\vartheta & \cos(k\vartheta) & (M-m\varepsilon_o)\vartheta & -\sin(k\vartheta) & 1 \\ -\sin\vartheta & \cos\vartheta & -k\sin(k\vartheta) & -m & k\cos(k\vartheta) & 0 \\ \sin\vartheta & \cos\vartheta & k\sin(k\vartheta) & -m & k\cos(k\vartheta) & 0 \\ \sin\vartheta & -\cos\vartheta & k^3\sin(k\vartheta) & 0 & -k^3\cos(k\vartheta) & 0 \\ -\sin\vartheta & -\cos\vartheta & -k^3\sin(k\vartheta) & 0 & -k^3\cos(k\vartheta) & 0 \end{bmatrix} \begin{bmatrix} \overset{1}{A}_{1i} \\ \overset{2}{A}_{1i} \\ \overset{3}{A}_{1i} \\ \overset{3}{A}_{2i} \\ \overset{4}{A}_{1i} \\ \overset{4}{A}_{2i} \end{bmatrix} =$$

$$= \begin{bmatrix} -a\cos\vartheta - b\sin\vartheta - c\cos(k\vartheta) + d(M-m\varepsilon_o)\vartheta - e\sin(k\vartheta) - f \\ a\cos\vartheta - b\sin\vartheta + c\cos(k\vartheta) + d(M-m\varepsilon_o)\vartheta - e\sin(k\vartheta) + f \\ a\sin\vartheta - b\cos\vartheta + ck\sin(k\vartheta) + dm - ek\cos(k\vartheta) \\ a\sin\vartheta + b\cos\vartheta + ck\sin(k\vartheta) - dm + ek\cos(k\vartheta) \\ -a\sin\vartheta + b\cos\vartheta - ck^3\sin(k\vartheta) + ek^3\cos(k\vartheta) \\ -a\sin\vartheta - b\cos\vartheta - ck^3\sin(k\vartheta) - ek^3\cos(k\vartheta) \end{bmatrix} \tag{3.19}$$

Solving the equations (3.19) we have

$$\left.\begin{aligned}
\overset{1}{A}_{1i} &= \frac{1}{C}\left[\left(1-k^2\right)b\cos\vartheta + dk^2m\right] \\
\overset{2}{A}_{1i} &= \frac{1}{D}\left\{k\cos k\vartheta\left[-k^2m\cos\vartheta + \vartheta\left(1-k^2\right)(M-m\varepsilon_o)\sin\vartheta\right] - \right. \\
&\quad \left. -m\sin k\vartheta\sin\vartheta\right\}a - \frac{k^3m}{D}\left[c + f\cos k\vartheta\right] \\
\overset{3}{A}_{1i} &= -\frac{1}{k\left(1-k^2\right)\sin k\vartheta}\left[dm - ek\left(1-k^2\right)\cos k\vartheta\right] \\
\overset{3}{A}_{2i} &= \frac{k}{D}\left[a\left(1-k^2\right)\cos k\vartheta + c\left(1-k^2\right)\cos\vartheta + f\left(1-k^2\right)\cos k\vartheta\cos\vartheta\right] \\
\overset{4}{A}_{1i} &= \frac{1}{D}\left\{am + c\left[k\vartheta\left(1-k^2\right)(M-m\varepsilon_o)\sin k\vartheta\cos\vartheta + \right.\right. \\
&\quad \left.\left. +m\left(k^3\sin k\vartheta\sin\vartheta + \cos k\vartheta\cos\vartheta\right)\right] + fm\cos\vartheta\right\} \\
\overset{4}{A}_{2i} &= -\frac{1}{k\left(\sin k\vartheta\right)C}\left\{bk\left(1-k^2\right)\sin k\vartheta + ek\left(1-k^2\right)\sin\vartheta\right\} + \\
&\quad + \frac{1}{k\left(\sin k\vartheta\right)C}d\left[k\vartheta\left(1-k^2\right)(M-m\varepsilon_o)\left(\sin k\vartheta\sin\vartheta\right) - \right. \\
&\quad \left. -m\left(k^3\sin k\vartheta\cos\vartheta - \cos k\vartheta\sin\vartheta\right)\right]
\end{aligned}\right\} \tag{3.20}$$

where

$$\begin{aligned} C &= \left(1-k^2\right)\sin\vartheta \\ D &= \vartheta k\left(1-k^2\right)(M-m\varepsilon_o)\cos k\vartheta\cos\vartheta + mk^3\cos k\vartheta\sin\vartheta - m\sin k\vartheta\cos\vartheta. \end{aligned}$$

Fixed arch ($i = 2$):

$$\begin{bmatrix} \cos\vartheta & \sin\vartheta & \cos(k\vartheta) & -(M-m\varepsilon_o)\vartheta & \sin(k\vartheta) & 1 \\ \cos\vartheta & -\sin\vartheta & \cos(k\vartheta) & (M-m\varepsilon_o)\vartheta & -\sin(k\vartheta) & 1 \\ -\sin\vartheta & \cos\vartheta & -k\sin(k\vartheta) & -m & k\cos(k\vartheta) & 0 \\ \sin\vartheta & \cos\vartheta & k\sin(k\vartheta) & -m & k\cos(k\vartheta) & 0 \\ \cos\vartheta & \sin\vartheta & k^2\cos(k\vartheta) & 0 & k^2\sin(k\vartheta) & 0 \\ \cos\vartheta & -\sin\vartheta & k^2\cos(k\vartheta) & 0 & -k^2\sin(k\vartheta) & 0 \end{bmatrix} \begin{bmatrix} \overset{1}{A}_{1i} \\ \overset{2}{A}_{1i} \\ \overset{3}{A}_{1i} \\ \overset{3}{A}_{2i} \\ \overset{4}{A}_{1i} \\ \overset{4}{A}_{2i} \end{bmatrix} =$$

$$= \begin{bmatrix} -a\cos\vartheta - b\sin\vartheta - c\cos(k\vartheta) + d(M-m\varepsilon_o)\vartheta - e\sin(k\vartheta) - f \\ a\cos\vartheta - b\sin\vartheta + c\cos(k\vartheta) + d(M-m\varepsilon_o)\vartheta - e\sin(k\vartheta) + f \\ a\sin\vartheta - b\cos\vartheta + ck\sin(k\vartheta) + dm - ek\cos(k\vartheta) \\ a\sin\vartheta + b\cos\vartheta + ck\sin(k\vartheta) - dm + ek\cos(k\vartheta) \\ -a\cos\vartheta - b\sin\vartheta - ck^2\cos(k\vartheta) - ek^2\sin(k\vartheta) \\ a\cos\vartheta - b\sin\vartheta + ck^2\cos(k\vartheta) - ek^2\sin(k\vartheta) \end{bmatrix} \tag{3.21}$$

Solving the equation system (3.21) we have:

$$\left.\begin{aligned}
\overset{1}{A}_{1i} &= \frac{1}{D}\left[ek^2 + b\left(k\cos k\vartheta\cos\vartheta + \sin\vartheta\sin k\vartheta\right) - dmk\cos k\vartheta\right] \\
\overset{2}{A}_{1i} &= -\frac{1}{C}a\left[m\left(1-k^2\right)\sin k\vartheta\cos\vartheta - \right. \\
&\quad \left. -\vartheta k\left(M-m\varepsilon_o\right)\left(k\sin\vartheta\sin k\vartheta + \cos k\vartheta\cos\vartheta\right)\right] \\
\overset{3}{A}_{1i} &= -\frac{1}{kD}\left[b + ek\left(k\sin\vartheta\sin k\vartheta + \cos k\vartheta\cos\vartheta\right) - dm\cos\vartheta\right] \\
\overset{3}{A}_{2i} &= -\frac{1}{C}\left[a\left(1-k^2\right)\sin k\vartheta + ck\left(1-k^2\right)\sin\vartheta - \right. \\
&\quad \left. -fk\left(k\sin k\vartheta\cos\vartheta - \cos k\vartheta\sin\vartheta\right)\right] \\
\overset{4}{A}_{1i} &= -\frac{1}{C}c\left[k\vartheta\left(M-m\varepsilon_o\right)\left(k\cos\vartheta\cos k\vartheta + \sin k\vartheta\sin\vartheta\right)\right] - \\
&\quad -\frac{1}{C}\left[a\left(M-m\varepsilon_o\right)\vartheta + cm(1-k^2)\cos k\vartheta\sin\vartheta + mf\sin\vartheta\right] \\
\overset{4}{A}_{2i} &= \frac{1}{D}\left[\tfrac{1}{k}b\left(1-k^2\right)\cos k\vartheta + e\left(1-k^2\right)\cos\vartheta\right] - \\
&\quad -\frac{1}{kD}d\left[k\vartheta\left(M-m\varepsilon_o\right)\left(\sin k\vartheta\cos\vartheta - k\sin\vartheta\cos k\vartheta\right) - \right. \\
&\quad \left. -m\left(1-k^2\right)\cos k\vartheta\cos\vartheta\right]
\end{aligned}\right\} \tag{3.22}$$

where

$$\begin{aligned} C &= m(1-k^2)\left(\sin\vartheta\sin k\vartheta\right)+\vartheta k\left(M-m\varepsilon_o\right)\left(k\sin k\vartheta\cos\vartheta-\sin\vartheta\cos k\vartheta\right) \\ D &= k\cos k\vartheta\sin\vartheta-\sin k\vartheta\cos\vartheta. \end{aligned}$$

In the knowledge of the above functions we can substitute in the formula (3.11) to get the Green function matrix.

The eigenvalues $\lambda=\lambda\left[\varepsilon_0(p)\right]$ and the natural frequencies $\alpha=\alpha\left[\varepsilon_0(p)\right]$ – each as a function of the follower load p – can then be obtained by solving the eigenvalue problem

$$\mathbf{y}(\varphi)=\lambda\int_a^b \mathbf{G}(\varphi,\psi,\varepsilon_0)\mathbf{y}(\psi)d\psi \quad . \tag{3.23}$$

The numerical solution was found by reducing the eigenvalue problem (3.23) to an algebraic eigenvalue problem and solving the latter by the QZ algorithm - see [3,4] for details.

The functions $\lambda_1/\lambda_{1free}=\lambda_1/\lambda_{1free}(\varepsilon_0/\varepsilon_{0crit})$ and $\alpha_1^2/\alpha_{1free}^2=\alpha_1^2/\alpha_{1free}^2\left(p/p_{crit}\right)$ have proved to be linear for the central angles considered. Here λ_1 and α_{1j} are the first eigenvalues and the natural freqencies computed for a value of ε_0 while λ_{1free} and α_{1free} are also the eigenvalue and the corresponding natural freqency for the same circular arch if it is free of loads ($\varepsilon_0=0$).

4. Conclusions

Using the Green function matrix, self adjoint eigenvalue problems, which are governed by a degenerate system of differential equations and homogeneous linear boundary conditions, can be replaced by an eigenvalue problem for a system of Fredholm integral equations with the Green function matrix as kernel.

We have determined the Green function matrix for simply supported and fixed circular arches subjected to hydrostatic and constant follower loads. In the knowledge of the Green function matrix the self adjoint eigenvalue problem giving the natural frequencies of the free vibrations as a function of the hydrostatic follower load has been replaced by an eigenvalue problem described by a system of Fredholm integral equations. The latter is reduced to an algebraic eigenvalue problem and the first eigenvalues as functions of the load are computed by using the QZ algorithm.

The results are shown in Figures 1 and 2.

The variable along the longitudinal axis is the quotient

$$\frac{p}{p_{crit}}=\frac{\varepsilon_0}{\varepsilon_{0crit}} \tag{4.1}$$

where ε_{0crit} and p_{crit} are given by the equation (3.4) and (3.7).

Figures 1 and 2 represent the quotient

$$\frac{\lambda_1}{\lambda_{1free}}=\frac{\alpha_1^2}{\alpha_{1free}^2} \tag{4.2}$$

for simply supported and fixed arches respectively. λ_1 and α_1 are the eigenvalues and the corresponding circular frequencies computed under the assumption that the

Table 1

			Simply supported arch(1)		Fixed arch(2)	
ϑ	m	Symbol	$\varepsilon_0/\varepsilon_{0crit}$	$\lambda_1/\lambda_{1free}$	$\varepsilon_0/\varepsilon_{0crit}$	$\lambda_1/\lambda_{1free}$
0,4	35000	○	0.1153	0.8847	0.2229	0.7821
			0.346	0.654	0.4457	0.562
			0.5767	0.4233	0.6686	0.3392
			0.8074	0.1926	0.8914	0.1133
0,6	60000	+	0.2271	0.7729	0.1206	0.7821
			0.4543	0.5457	0.3619	0.562
			0.6814	0.3185	0.7237	0.3392
			0.9086	0.0913	0.965	0.1133
0,8	120000	◇	0.0008	0.99	0.2057	0.8022
			0.3328	0.667	0.4104	0.6014
			0.6657	0.3339	0.615	0.3969
			0.9985	0.009	0.8197	0.1881
1	240000(1) and 360000(2)	□	0.1082	0.8918	0.1027	0.9056
			0.4329	0.567	0.3068	0.7136
			0.7576	0.2423	0.5102	0.5163
			0.8658	0.1339	0.9183	0.1001

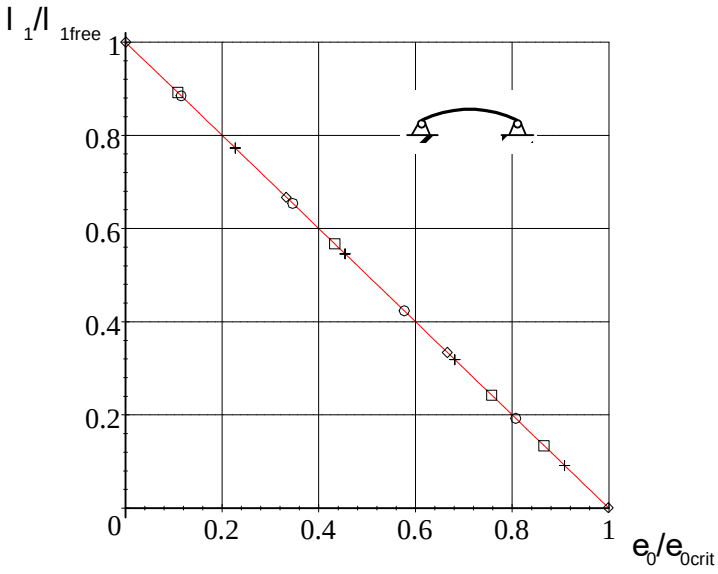

Figure 1.

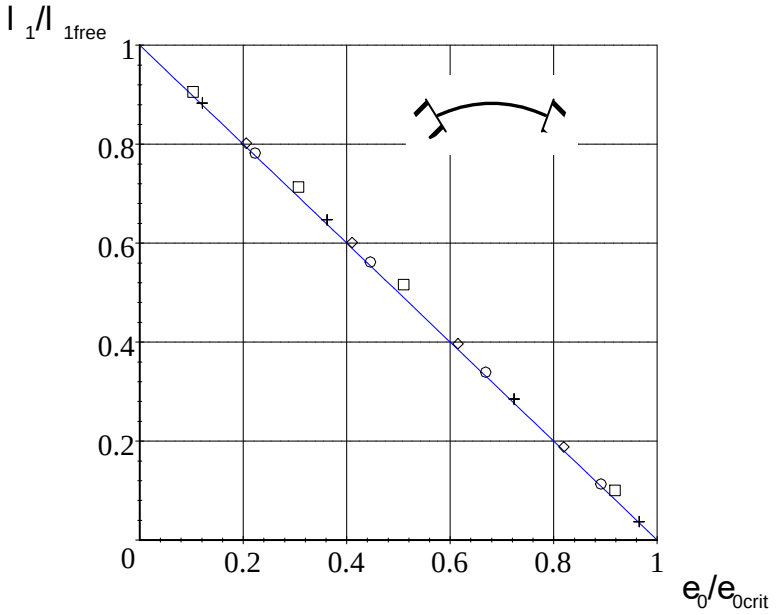

Figure 2.

arch is subjected to a follower load p which produces the axial strain ε_0. λ_{1free} and α_{1free} are also the eigenvalue and corresponding circular frequency for the same but unloaded arches.

Computations were carried out for $m = 20000; 35000; 60000; 120000; 240000; 360000$ provided that $\vartheta \in [0.1; 3]$. Some numerical results are presented in Table 1.

Figures 1 and 2 represent the quotient $\lambda_1/\lambda_{1free}$ as a function of the quotient $\varepsilon_0/\varepsilon_{0crit}$. It is clear from Figures 1 and 2 that

$$\frac{\lambda_1}{\lambda_{1free}} = 1 - \frac{\varepsilon_0}{\varepsilon_{0crit}} \tag{4.3}$$

for both cases, i.e., this result is the same for both support arrangements. We remark that the agreement of (4.3) with the results computed - see Figure 2 - is not as good for the fixed arch as for the simple supported arch. The reason for this is probably the fact that the solution for s_2 (3.8) is also an approximation obtained by the method of least squares [2]. It is also worthy of mention that function (4.3) is independent of m.

Acknowledgement. The support provided by the Hungarian National Research Foundation (project No. T031998) is gratefully acknowledged.

REFERENCES

1. Collatz, L.: *Eigenwertaufgaben mit technischen Anwendungen*, Izdatelstvo Nauka, Moscow, 1968. (in Russian)
2. Szeidl, G.: *Effect of Change in Length on Natural Frequencies and Stability of Circular Arches*, Ph.D. Thesis, Department of Mechanics, University of Miskolc, Hungary, 1975. (in Hungarian)
3. Baker, C. T. H.: *The Numerical Treatment of Integral Equations – Monographs on Numerical Analysis edited by L. Fox and J. Walsh.* Clarendon Press, Oxford, 1977.
4. Szeidl, G., Kelemen, K., and Szeidl, A.: *Natural frequencies of a circular arch - computation by the use of Green functions,* Publ. Univ. of Miskolc, Series D. Natural Sciences, Mathematics, **38**, (1998), 117-132.
5. Federhoffer, K.: *Über den Einfluss der Achsendehnung der Rotationsträgheit und der Schubkraft auf die Frequenzen der Biegungsschwingungen eines Kreisringes.* Sitz-Ber. Akad. Wiss. Austria, Series IIa. Vol. 144., 1935
6. Matsunaga, H.: *Effects of higher order deformations on in-plane vibration and stability of thick circular rings,* Acta Mechanika, **124**, (1997), 47-61.
7. Lin, S. M.: *Exact solutions for extensible circular curved Timoshenko beams with non-homogeneous elastic boundary conditions*, Acta Mechanika, Vol. 130, (1998), 67-79.

Journal of Computational and Applied Mechanics, Vol. 1., No. 2., (2000), pp. 179–189

THE INVERSE OF DIFFERENTIAL OPERATORS AND AN EXTENSION OF TREFFTZ'S METHOD

György Richlik
Research Group of the Dynamics of Machines and Vehicles,
Hungarian Academy of Sciences
richlik@kme.bme.hu

[Received: April 30, 2000]

Abstract. The purpose of the paper is to present an extension of Trefftz's idea. The essential of this method is to obtain lower bounds for eigenfrequencies of the elastic continuous structures. Let us suppose that we have good upper bounds that are sufficient in number and accuracy as well. This paper also contains a discussion of differential operators and their inverses or generalized inverses. A new example presents a technique for making generalized Green matrix.

Keywords: Trefftz's method, inverse of differential operator, Moore Penrose generalized inverse of differential operator

1. Introduction

The estimation of natural frequencies for elastic continuous rod structures is possible in several ways [1, 2]. For certain procedures - we think of the method of Trefftz or the method of orthogonal invariants - the explicit knowledge of the inverse to the ordinary differential operators is needed [3]. These procedures essentially lead to the construction of Green matrices. The present paper has two aims, one is an extension of Trefftz's idea [4] to obtain lower bounds for the eigenfreqencies of elastic continuous structures if we have good upper bounds, the other is to examine some problems related to the inverses of differential operators. Both will be illustrated by examples.

2. Differential operator and the Green matrix

By the interval $[a, b]$ we mean the set of all real numbers t such that $a \leq t \leq b$. Thus $[a, b] = \{t \in \mathbb{R} : a \leq t \leq b \quad a, b \in \mathbb{R}\}$ is a finite closed set, and $\mathbb{R}$ denotes the set of all real numbers. Let $L^2(a, b)$ denote the set of all Lebesgue integrable n-vector functions with real-valued coordinates. If $\mathbf{x}, \mathbf{y} \in L^2(a, b)$ are n-vector functions with the property that $\mathbf{y}^T\mathbf{x}$ is integrable, then

$$\langle \mathbf{x}, \mathbf{y} \rangle = \int_a^b \mathbf{y}(t)^T \mathbf{x}(t)\, \mathrm{d}t \tag{2.1}$$

is the inner product, where $\mathbf{y}(t)^T$ as a row vector is the transpose of the column vector $\mathbf{y}(t)$. Thus $L^2(a, b)$ with the inner product (2.1) is a Hilbert space [5]. (A complete

inner product space is called Hilbert space.) Let $\mathbf{A}_1$ and $\mathbf{A}_0$ denote $n \times n$ matrix functions, $\mathbf{A}_1$ being absolutely continuous and nonsingular, and $\mathbf{A}_0$ being integrable on the interval $[a, b]$. Then

$$\mathcal{A}\mathbf{x} = \mathbf{A}_0(t)\mathbf{x}' + \mathbf{A}_1(t)\mathbf{x} \,. \tag{2.2}$$

is a linear differential operator with the domain $\mathcal{D}_\mathcal{A}$ which is the collection of all absolutely continuous n-dimensional vector functions $\mathbf{x}$. In order to formulate the boundary conditions as well, let ξ be a $2n$-vector made up of the n components of $\mathbf{x}(a)$ followed by the n components of $\mathbf{x}(b)$. Thus

$$\mathcal{D}_\mathcal{A} = \{\mathbf{x} \in L^2(a,b) : \mathcal{A}\mathbf{x} = L^2(a,b) \ \wedge \ \mathbf{M}\xi = \mathbf{0}\}, \tag{2.3}$$

where the boundary conditions are given by the relation $\mathbf{M}\xi = \mathbf{0}$, $\mathbf{M}$ denotes an $r \times 2n$ matrix ($r \leq 2n$) and $\xi \in \mathbb{R}^{2n}$ is composed of the elements of the vectors $\mathbf{x}(a) \in \mathbb{R}^n$, and $\mathbf{x}(b) \in \mathbb{R}^n$. Since the set of solutions of the differential equation $\mathcal{A}\mathbf{x} = \mathbf{0}$ is n-dimensional, $\mathrm{Ker}\mathcal{A}$ is a finite-dimensional vector space. If $\dim\mathrm{Ker}\mathcal{A} = k$, it is known [3, 6], that

$$\max(0, n - r) \leq k \leq \min(n, 2n - r).$$

Now suppose that the operator $\mathcal{A}$ is invertible and its inverse is $\mathcal{A}^{-1}$. Then $\mathcal{A}$ is an injective operator ($k = 0$) and its range is the set $\mathcal{R}_\mathcal{A} = L^2(a,b)$. If $\mathcal{A}$ is invertible then $\mathcal{A}^{-1}$ is an integral operator with the kernel $\mathbf{G}(t,s)$. $\mathbf{G}(t,s)$ is an $n \times n$ matrix and is called Green's matrix. The inversion of $\mathcal{A}$ is given by the formula

$$\mathbf{x}(t) = (\mathcal{A}^{-1}\mathbf{y})(t) = \int_a^b \mathbf{G}(t,s)\mathbf{y}(s)\,\mathrm{d}s \tag{2.4}$$

$\forall \mathbf{y} \in L^2(a,b)$, and (2.4) is equivalent to $\mathcal{A}\mathbf{x} = \mathbf{y}$. Existence, uniqueness and properties of the Green matrix have been proved by several authors [5, 6]. The existence theorem for the Green matrix reads as

Theorem 1 *If the boundary value problem $\mathcal{A}\mathbf{x} = \mathbf{0}$, $\mathbf{M}\xi = \mathbf{0}$ has only a trivial solution, then there is one and only one Green matrix $\mathbf{G}(t,s)$ of the differential operator $\mathcal{A}$ generated by the differential expression (2.2). The matrix $\mathbf{G}(t,s)$ has the following properties:*

- *the elements of $\mathbf{G}(t,s)$ are continuous and have continuous first derivatives in t except at $t = s$; $t, s \in [a,b]$;*
- *as t increases through s, $\mathbf{G}(t,s)$ has a jump discontinuity equal to $\mathbf{A}_0(s)^{-1}$, namely*

$$\mathbf{G}(s+0,s) - \mathbf{G}(s-0,s) = \mathbf{A}_0(s)^{-1}; \tag{2.5}$$

- *as a function of t, $\mathbf{G}(t,s)$ satisfies the boundary value problem $\mathcal{A}\mathbf{G} = \mathbf{0}$, $\mathbf{M}\xi = \mathbf{0}$ for $a \leq t \leq s \leq b$ and $a \leq s \leq t \leq b$.*

If $\mathcal{A}$ is an invertible differential operator and its kernel is the matrix $\mathbf{G}(t,s)$, we find by using (2.4) that

$$(\mathcal{A}\mathbf{x})(t) = \int_a^b (\mathcal{A}\mathbf{G})(t,s)\mathbf{y}(s)\,\mathrm{d}s = \mathbf{y}(t) \,. \tag{2.6}$$

According to [3, 6] and (2.6) we have the following equations:

$$\mathcal{A}\mathbf{G} = \delta_{\mathcal{A}}, \qquad \mathbf{MG} = \mathbf{0}, \tag{2.7}$$

where $\delta_{\mathcal{A}} = \delta\mathbf{E}$, $\mathbf{E}$ is a unit matrix and δ is Dirac's distribution [2]. The elements of the Green matrix can be obtained by integrating the equations (2.7) and the arbitrary functions consequent upon the integration can be determined by using the properties in Theorem 1.

3. An extension of Trefftz's method

Let $\mathcal{A}^{-1}$ be a real symmetric positive semidefinite completely continuous integral operator defined on the interval $[a, b]$ by the equation

$$(\mathcal{A}^{-1}\mathbf{x})(t) = \int_a^b \mathbf{G}(t, s)\mathbf{x}(s)\,\mathrm{d}s,$$

in which $\mathbf{G}(t, s) = \mathbf{G}(s, t)$ is the kernel. Then $\mathcal{A}^{-1}$ is also self-adjoint [6]. According to the Hilbert - Schmidt theorem [3] for $k \in \mathbb{N}$ ($\mathbb{N}$ is the set of all natural numbers)

$$\begin{aligned}(\mathcal{A}^{-1}\mathbf{x})(t) = \int_a^b \mathbf{G}(t, s)\mathbf{x}(s)\,\mathrm{d}s = \int_a^b \mathbf{x}(s)^T\mathbf{G}(t, s)\,\mathrm{d}s = \\ = \sum_k \lambda_k \left(\int_a^b \mathbf{x}(s)^T\mathbf{x}_k(s)\,\mathrm{d}s\right)\mathbf{x}_k(t) = \\ = \int_a^b \mathbf{x}(s)^T \left(\sum_k \lambda_k\mathbf{x}_k(s)\mathbf{x}_k(t)^T\right)\,\mathrm{d}s.\end{aligned}$$

Since the function $\mathbf{x}(t) \in L^2(a, b)$ is arbitrary we can write

$$\mathbf{G}(t, s) = \sum_k \lambda_k\mathbf{x}_k(t)\mathbf{x}_k(s)^T, \tag{3.1}$$

where $\{\mathbf{x}_i\}$ is an orthonormal collection of the eigenvectors for $\mathcal{A}^{-1}$ with associated eigenvalues $\{\lambda_i\}$ and $\mathbf{x}_i \in L^2(a, b)$, $i \in \mathbb{N}$. If $\mathcal{A}^{-1}$ is a positive compact self-adjoint operator, then the eigenvalues λ_i of $\mathcal{A}^{-1}$ are all real and nonnegative. Moreover, we have

$$\int_a^b \operatorname{Spur}\mathbf{G}(t, t)\,\mathrm{d}t = \sum_k \lambda_k \int_a^b \mathbf{x}_k(t)^T\mathbf{x}_k(t)\,\mathrm{d}t = \sum_k \lambda_k. \tag{3.2}$$

For the application of the Trefftz's method let's suppose $\mathcal{A}^{-1}$ being a symmetric positive semidefinite completely continuous integral operator and we have the first k of the lower bounds

$$\mu_1 \geq \mu_2 \geq \cdots \geq \mu_k \tag{3.3}$$

ordered to the first k of the eigenvalues

$$\lambda_1 \geq \lambda_2 \geq \cdots \geq \lambda_k \tag{3.4}$$

of the integral operator. If $j \leq k$ according to Trefftz [4] and (3.2) we get

$$\lambda_j \leq \mu_j + \int_a^b \text{Spur } \mathbf{G}(t,t)\ \mathrm{d}t - \sum_{i=1}^{k} \mu_i := \nu_j, \tag{3.5}$$

which is an estimation for the j^{th} eigenvalue. (3.5) is a new extension of the method of Trefftz. Thus, with the knowledge of the lower bounds (3.3) and the Green matrix $\mathbf{G}(t,s)$ one can use the inequality (3.5) to find upper bounds for the first k eigenvalues from the set of eigenvalues $\{\lambda_i\}$ that belong to the integral operator $\mathcal{A}^{-1}$.

4. Numerical example

Suppose that $\mathcal{A}$ is the differential operator

$$\mathcal{A}\mathbf{x} = \mathbf{A}_0(t)\mathbf{x}' + \mathbf{A}_1(t)\mathbf{x}, \tag{4.1}$$

$$\mathbf{A}_0(t) = \begin{pmatrix} 0 & 0 & 0 & -1 \\ 0 & 0 & -1 & 0 \\ 0 & 1 & 0 & 0 \\ 1 & 0 & 0 & 0 \end{pmatrix}, \qquad \mathbf{x}'(t) = \begin{pmatrix} x_1'(t) \\ x_2'(t) \\ x_3'(t) \\ x_4'(t) \end{pmatrix},$$

$$\mathbf{A}_1(t) = \begin{pmatrix} 0 & 0 & 0 & 0 \\ 0 & 0 & 0 & -1 \\ 0 & 0 & -p^{-1} & 0 \\ 0 & -1 & 0 & 0 \end{pmatrix}, \qquad \mathbf{x}(\mathbf{t}) = \begin{pmatrix} x_1(t) \\ x_2(t) \\ x_3(t) \\ x_4(t) \end{pmatrix},$$

on $L^2(0,1)$, with the domain $\mathcal{D}_\mathcal{A} \subset L^2(0,1)$; and $p(t) > 0$, $\forall t \in [0,1]$. The boundary conditions are

$$x_1(0) = x_2(0) = x_3(1) = x_4(1) = 0.$$

We note that the operator $\mathcal{A}$ is self-adjoint, namely

$$\langle \mathcal{A}\mathbf{x}, \mathbf{y} \rangle = \langle \mathbf{x}, \mathcal{A}\mathbf{y} \rangle, \qquad \forall \mathbf{x}, \mathbf{y} \in L^2(0,1).$$

It should be noted that

$$\begin{aligned} \langle \mathcal{A}\mathbf{x}, \mathbf{y} \rangle \quad = \quad & \int_a^b (x_4 y_1' + x_3 y_2' + x_2 y_3' - x_1 y_4' - x_4 y_2 - p^{-1} x_3 y_3 - x_2 y_4)\, \mathrm{d}t + \\ & + [-x_4 y_1 - x_3 y_2 + x_2 y_3 + x_1 y_4]_0^1. \end{aligned}$$

The integral operator $\mathcal{A}^{-1}$ is self-adjoint as well, and $\mathbf{G}(t,s) = \mathbf{G}(s,t)$. It can be seen easily from [2] and (2.7), that for instance

$$G_{11}(t,s) = H(t-s)\int_s^t \int_s^u \frac{v-s}{p(v)}\,\mathrm{d}s\mathrm{d}u + \int_0^t \int_0^u \frac{s-v}{p(v)}\,\mathrm{d}v\mathrm{d}u \tag{4.2}$$

where H is Heaviside's distribution. Now consider the transverse vibration of a beam [2]. The equation of motion is of the form

$$\frac{\partial^2}{\partial x^2}\left(EI_z\frac{\partial^2 u}{\partial x^2}\right) = -\rho Q\frac{\partial^2 u}{\partial t^2}.$$

where $E = 2.1\cdot 10^7$ [Pa], $\rho = 7.86\cdot 10^3$ [kg/m^3], $Q(x) = \frac{\pi}{4}(-10^{-2}x + 4\cdot 10^{-2})^2$ [m^2], $I_z(x) = \frac{\pi}{64}(-10^{-2}x + 4\cdot 10^{-2})^4$ [m^4], and $x \in [0,1]$ for our example. If we assume that $u(x,t) = v(x)\sin(\alpha t)$ we obtain

$$\frac{\mathrm{d}^2}{\mathrm{d}x^2}\left(EI_z\frac{\mathrm{d}^2 v}{\mathrm{d}x^2}\right) = \alpha^2\rho Q v\ , \tag{4.3}$$

in which α stands for the angular eigenfrequency. By assumption equation (4.3) is associated with the boundary conditions (beam fixed at the left end and free at the right end):

$$v(0) = v'(0) = v''(1) = v'''(1) = 0.$$

By introducing the functions

$$p(x) = EI_z(x), \quad q(x) = \rho Q(x),$$

we can easily see that the 4^{th}-order differential operator in (4.3) can be reduced by elementary transforms to the differential operator (4.1). Now to obtain lower bounds for eigenfrequencies of the beam we can use the inequality (3.5). By introducing the function

$$K(t,s) = \sqrt{q(t)}\sqrt{q(s)}G_{11}(t,s),$$

the inequality (3.5) becomes in our case (on basis of [2])

$$\frac{1}{\alpha_j^2} \le \frac{1}{(\alpha_j^u)^2} + \int_a^b K(t,s)\ \mathrm{d}t - \sum_{i=1}^{k}\frac{1}{(\alpha_i^u)^2} := \frac{1}{(\alpha_j^l)^2}, \qquad j \le k, \tag{4.4}$$

where α_j is the angular eigenfrequency, α_j^l is the lower bound and α_j^u is the upper bound ($j \in \mathbb{N}$). It is also easy to see from (4.3), if the inequality (3.5) is formulated for the squares of the angular eigenfrequencies as the eigenvalues, that the lower and upper designations exchange their roles. The table shows the numerical results of the calculations:

	$j=1$	$j=2$	$j=3$	$j=4$	$j=5$
α_j^u	2.06152	10.8457	28.8438	55.7227	91.5596
α_j^l	2.03926	8.5541	12.5324	13.4998	13.7565

The first line of the table contains upper bounds calculated by the method of interval-matrices. In the second line lower bounds calculated by the aid of the estimation (4.4) can be found. The numerical investigations show that the estimation is good only for the first eigenfrequency and is not satisfactory in the other cases. A little improvement can be achieved by taking more eigenfrequencies into account. The problem is of theoretical importance and our aim was to show a practical application of the inequality (3.5). Obviously, the estimation becomes a useful tool in the case of complicated structures.

5. Appendix. The generalized Green matrix

The aim of this section is to give a summary - on the basis of [6,7,8,9] - for the case when the differential operator $\mathcal{A}$ is noninvertible. If $r \neq n$ or $r = n$ but $k \neq 0$, neither the operator $\mathcal{A}$, nor $\mathcal{A}^*$ is invertible. (The adjoint of $\mathcal{A}$ is denoted by $\mathcal{A}^*$.) There are various ways to define a generalized inverse for $\mathcal{A}$ [6]. In this section we shall use an analogue to the Moore Penrose generalized inverse, often called pseudoinverse [6], for differential operators:

Definition 2 *Let $\mathcal{P}$ and $\mathcal{Q}$ denote the projections whose ranges are $\mathcal{R}_{\mathcal{P}} = Ker\mathcal{A}$ and $\mathcal{R}_{\mathcal{Q}} = Ker\mathcal{A}^*$. Let $\mathcal{E} = \mathcal{I} - \mathcal{P}$ and $\mathcal{F} = \mathcal{I} - \mathcal{Q}$ be two projections where $\mathcal{I}$ is the unit operator. The generalized inverse of $\mathcal{A}$ denoted by $\mathcal{A}^\dagger$, is given by*

$$\mathcal{A}^\dagger = \mathcal{E}\underline{\mathcal{A}}\mathcal{F}, \tag{5.1}$$

where $\underline{\mathcal{A}}$ is such a generalized inverse of $\mathcal{A}$ that if $\mathbf{z} \in \mathcal{R}_{\mathcal{A}}$ and $\mathbf{y} = \underline{\mathcal{A}}\mathbf{z}$, then $\mathbf{y} \in \mathcal{D}_{\mathcal{A}}$ and $\mathcal{A}\mathbf{y} = \mathbf{z}$, and $\mathcal{R}_{\mathcal{A}} \subset \mathcal{D}_{\underline{\mathcal{A}}}$.

$\mathcal{A}^\dagger$ as defined above is unique. The generalized inverse as defined is an integral operator with a uniquely defined kernel, which will be denoted by $\mathbf{G}^\dagger(t,s)$. $\mathbf{G}^\dagger(t,s)$ is referred to as the generalized Green matrix for the operator $\mathcal{A}$. There are several ways of constructing $\mathbf{G}^\dagger(t,s)$, based on the various properties of the generalized inverse. In this paper we shall give two ways for constructing $\mathbf{G}^\dagger(t,s)$. We shall need explicit expressions for the projections $\mathcal{P}$ and $\mathcal{Q}$.

Let $\mathbf{u}_1(t), \cdots, \mathbf{u}_k(t)$ be linearly independent solutions to the equation $\mathcal{A}\mathbf{x} = \mathbf{0}$. This set is a basis for the vector space Ker$\mathcal{A}$ where dimKer$\mathcal{A} = k$. Let $\mathbf{U}(t)$ denote an $n \times n$ matrix with k columns denoted by $\mathbf{u}_1(t), \cdots, \mathbf{u}_k(t)$. Due to the linear independence of the columns $\mathbf{u}_1(t), \cdots, \mathbf{u}_k(t)$, the $k \times k$ matrix

$$\mathbf{W}_{\mathcal{P}} = \int_a^b \mathbf{U}(w)^T \mathbf{U}(w)\, \mathrm{d}w \tag{5.2}$$

is a nonsingular, positive definite symmetric one. Let the kernel $\mathbf{G}_{\mathcal{P}}(t,s)$ be defined by

$$\mathbf{G}_{\mathcal{P}}(t,s) = \mathbf{U}(w)\mathbf{W}_{\mathcal{P}}^{-1}\mathbf{U}(w)^T. \tag{5.3}$$

Clearly, $\mathbf{G}_{\mathcal{P}}(t,s)$ is also an $n \times n$ matrix. The projection $\mathcal{P}$ onto Ker$\mathcal{A}$ is then the integral operator

$$(\mathcal{P}\mathbf{x})(t) = \int_a^b \mathbf{G}_{\mathcal{P}}(t,s)\mathbf{x}(s)\,\mathrm{d}s. \tag{5.4}$$

The operator $\mathcal{P}$ as defined by (5.4) is clearly Hermitian and idempotent. Similarly if Ker$\mathcal{A}^*$ (dimKer$\mathcal{A}^* = k'$) is spanned by the linearly independent set of solutions $\mathbf{v}_1(t), \cdots, \mathbf{v}_{k'}(t)$ to the equation $\mathcal{A}^*\mathbf{x} = \mathbf{0}$, we can form the matrix $\mathbf{V}(t)$ with k' columns

$$\mathbf{W}_{\mathcal{Q}} = \int_a^b \mathbf{V}(w)^T\mathbf{V}(w)\mathrm{d}w, \tag{5.5}$$

and the kernel is

$$\mathbf{G}_{\mathcal{Q}}(t,s) = \mathbf{V}(w)\mathbf{W}_{\mathcal{Q}}^{-1}\mathbf{V}(w)^T. \tag{5.6}$$

The projection $\mathcal{Q}$ onto Ker$\mathcal{A}^*$ is given by

$$(\mathcal{Q}\mathbf{x})(t) = \int_a^b \mathbf{G}_{\mathcal{Q}}(t,s)\mathbf{x}(s)\,\mathrm{d}s. \tag{5.7}$$

Note, that if the vectors $\mathbf{u}$ and the vectors $\mathbf{v}$ are chosen to be orthonormal, then $\mathbf{W}_{\mathcal{P}} = \mathbf{W}_{\mathcal{Q}} = \mathbf{E}$. Now we require a kernel for the operator $\underline{\mathcal{A}}$. Let us solve the differential equation

$$\mathcal{A}\mathbf{x} = \mathbf{z} \qquad \mathbf{z} \in \mathcal{R}_{\mathcal{A}} \tag{5.8}$$

by variation of parameters. The solution to this problem can always be made to satisfy the boundary conditions $\mathbf{M}\xi = \mathbf{0}$ of $\mathcal{A}$. In fact, there will always remain k undetermined constants after integration because an arbitrary element of Ker$\mathcal{A}$ can always be added to the solution. The formula for $\mathbf{x}$ in terms of $\mathbf{z}$ is the integral

$$\mathbf{x}(t) = \int_a^b \underline{\mathbf{G}}(t,s)\mathbf{z}(s)\,\mathrm{d}s \tag{5.9}$$

where $\underline{\mathbf{G}}(t,s)$ can be chosen as simply as possible. As a function of t, $\underline{\mathbf{G}}(t,s)$ will satisfy the boundary conditions for $\mathcal{A}$ and will have, as t increases through s, the same continuity properties as the Green matrix for an invertible operator. Therefore the kernels $\mathbf{G}_{\mathcal{P}}(t,s)$, $\underline{\mathbf{G}}(t,s)$ and $\mathbf{G}_{\mathcal{Q}}(t,s)$ are available.

Theorem 3 *The kernel of $\mathcal{A}^\dagger$, i.e., the generalized Green matrix, assumes the form [6]:*

$$\begin{aligned}\mathbf{G}^\dagger(t,s) \;=\; & \underline{\mathbf{G}}(t,s) - \int_a^b \mathbf{G}_{\mathcal{P}}(t,u)\underline{\mathbf{G}}(u,s)\,du - \int_a^b \underline{\mathbf{G}}(t,v)\mathbf{G}_{\mathcal{Q}}(v,s)\,dv + \\ & + \int_a^b\int_a^b \mathbf{G}_{\mathcal{P}}(t,u)\underline{\mathbf{G}}(u,v)\mathbf{G}_{\mathcal{Q}}(v,s)\,dv\,du.\end{aligned} \tag{5.10}$$

In the noninvertible case a similar calculation is possible as in the invertible case. The kernels $\underline{\mathbf{G}}$ and $\mathbf{G}^\dagger$ have the same discontinuity at $t = s$ as the ordinary Green matrix. When the operator $\mathcal{A}$ is applied to

$$\mathbf{g}(t) = \int_a^b \underline{\mathbf{G}}(t, v)\mathbf{f}(v)\,\mathrm{d}v, \tag{5.11}$$

the result is $\mathbf{f}(t) = (\mathcal{A}\mathbf{g})(t)$, whereas it is $\mathcal{A}\underline{\mathbf{G}} = \mathbf{0}$ for $a \le t < s \le b$ and for $a \le s < t \le b$. Since $\mathcal{A}\mathbf{G}_\mathcal{P} = \mathbf{0}$, we find from (5.10) that

$$\mathcal{A}\mathbf{G}^\dagger = -\mathbf{G}_\mathcal{Q} \quad a \le t < s \le b \quad a \le s < t \le b. \tag{5.12}$$

We can recover $\mathbf{G}^\dagger(t, s)$ by determining the solution of the differential equation (5.12), so as to satisfy, as a function of t, the known properties of $\mathbf{G}^\dagger(t, s)$, namely

1. $\mathbf{G}^\dagger(t, s)$ should have the appropriate discontinuity at $t = s$,
2. $\mathbf{G}^\dagger(t, s)$ should satisfy the boundary conditions $\mathbf{M}\xi = \mathbf{0}$ of the operator $\mathcal{A}$ and
3. $\mathbf{G}^\dagger(t, s)$ should be orthogonal to $\mathrm{Ker}\mathcal{A}$.

It can also be proved that these properties uniquely determine $\mathbf{G}^\dagger(t, s)$.

6. A new example for the generalized Green matrix

As a brief example, consider the differential equation of the simple harmonic motion

$$x'' + \alpha^2 x = 0. \tag{6.1}$$

We obtain a system of first order equations by the elementary transforms

$$\begin{aligned} x_1 + x_2' &= 0, \\ -x_1' + \alpha^2 x_2 &= 0. \end{aligned} \tag{6.2}$$

Now consider the differential operator from (6.2)

$$\mathcal{A}\mathbf{x} = \begin{pmatrix} x_1 + x_2' \\ -x_1' + \alpha^2 x_2 \end{pmatrix}$$

with the boundary conditions $x_1(0) = x_1(\pi)$ and $x_2(0) = x_2(\pi)$. For simplicity we shall assume that $\alpha = 2m$, $m \in \mathbb{N}$. Under these conditions the fundamental matrix $\mathbf{\Phi}(t)$ for the equation $\mathcal{A}\mathbf{x} = \mathbf{0}$ is:

$$\mathbf{\Phi}(t) = \begin{pmatrix} \alpha \sin \alpha t & -\alpha \cos \alpha t \\ \cos \alpha t & \sin \alpha t \end{pmatrix}.$$

The orthonormal base vectors are given by

$$\mathbf{U}(t) = \begin{pmatrix} \mathbf{u}_1(t) & \mathbf{u}_2(t) \end{pmatrix} = \sqrt{\frac{2}{\pi(1 + \alpha^2)}}\mathbf{\Phi}(t).$$

On the basis of (5.6) we have

$$\mathbf{G}_{\mathcal{Q}}(t,s) = \frac{2}{\pi(1+\alpha^2)} \begin{pmatrix} \alpha^2 \cos(\alpha(t-s)) & \alpha \sin(\alpha(t-s)) \\ -\alpha \sin(\alpha(t-s)) & \cos(\alpha(t-s)) \end{pmatrix}.$$

For example one of the solutions of the differential equation $\mathcal{A}\mathbf{G}^{\dagger} = -\mathbf{G}_{\mathcal{Q}}$ is:

$$G_{21}^{\dagger}(t,s) = \begin{cases} C_{11}(s)\cos\alpha t + C_{21}(s)\sin\alpha t - \dfrac{t}{\pi}\cos(\alpha(t-s)) & t < s \\ C_{12}(s)\cos\alpha t + C_{22}(s)\sin\alpha t - \dfrac{t}{\pi}\cos(\alpha(t-s)) & t > s \end{cases}.$$

Since

$$\mathbf{A}_0^{-1} = \begin{pmatrix} 0 & -1 \\ 1 & 0 \end{pmatrix},$$

the elements of the matrix $\mathbf{G}^{\dagger}$ satisfy the discontinuity conditions:

$$\begin{aligned} &G_{11}^{\dagger}(s+0,s) - G_{11}^{\dagger}(s-0,s) = 0, \\ &G_{12}^{\dagger}(s+0,s) - G_{12}^{\dagger}(s-0,s) = -1, \\ &G_{21}^{\dagger}(s+0,s) - G_{21}^{\dagger}(s-0,s) = 1, \\ &G_{22}^{\dagger}(s+0,s) - G_{22}^{\dagger}(s-0,s) = 0. \end{aligned}$$

Hence

$$G_{21}^{\dagger}(t,s) = \begin{cases} C_{11}(s)\cos\alpha t + C_{21}(s)\sin\alpha t - \dfrac{t}{\pi}\cos(\alpha(t-s)) & t < s \\ C_{11}(s)\cos\alpha t + C_{21}(s)\sin\alpha t - (1-\dfrac{t}{\pi})\cos(\alpha(t-s)) & t > s \end{cases}.$$

It can be seen easily that if

$$\mathbf{g}_1(t) = \begin{pmatrix} G_{11}^{\dagger}(t,s) \\ G_{21}^{\dagger}(t,s) \end{pmatrix}, \quad \mathbf{g}_2(t) = \begin{pmatrix} G_{12}^{\dagger}(t,s) \\ G_{22}^{\dagger}(t,s) \end{pmatrix},$$

and

$$\int_0^{\pi} \mathbf{g}_i(t)\mathbf{u}_j(t)\mathrm{d}t = 0 \quad i,j = 1,2,$$

then the elements of the generalized Green's matrix $\mathbf{G}^{\dagger}(t,s)$ are

$$G_{11}^{\dagger}(t,s)=\begin{cases}\gamma_1(s)\cos(\alpha(s-t))+\dfrac{\alpha}{2\pi}(\pi-2(s-t))\sin(\alpha(s-t)) & t<s\\ \gamma_1(s)\cos(\alpha(t-s))+\dfrac{\alpha}{2\pi}(\pi-2(t-s))\sin(\alpha(t-s)) & t>s\end{cases},$$

$$G_{21}^{\dagger}(t,s)=\begin{cases}\gamma_2(s)\sin(\alpha(s-t))-\dfrac{1}{2\pi}(\pi-2(s-t))\cos(\alpha(s-t)) & t<s\\ -\gamma_2(s)\sin(\alpha(t-s))+\dfrac{1}{2\pi}(\pi-2(t-s))\cos(\alpha(t-s)) & t>s\end{cases},$$

$$G_{12}^{\dagger}(t,s)=\begin{cases}-\gamma_2(s)\sin(\alpha(s-t))+\dfrac{1}{2\pi}(\pi-2(s-t))\cos(\alpha(s-t)) & t<s\\ \gamma_2(s)\sin(\alpha(t-s))-\dfrac{1}{2\pi}(\pi-2(t-s))\cos(\alpha(t-s)) & t>s\end{cases},$$

$$G_{22}^{\dagger}(t,s)=\begin{cases}\gamma_3(s)\cos(\alpha(s-t))+\dfrac{1}{2\alpha\pi}(\pi-2(s-t))\sin(\alpha(s-t)) & t<s\\ \gamma_3(s)\cos(\alpha(t-s))+\dfrac{1}{2\alpha\pi}(\pi-2(t-s))\sin(\alpha(t-s)) & t>s\end{cases}$$

where γ_1, γ_2, and γ_3 are constants depending on α^2 [8].

7. Conclusions

The method outlined in Section 3 will produce lower bounds for eigenfrequencies of the elastic continuous structures by using (3.5) if we have good upper bounds calculated by some kind of a simple method. Since the solution of our problem requires the invertation of differential operators we expatiated on the constructions of Green matrices by solving the matrix equation (2.7). In the first part of the Appendix we give a short summary of the results connected to the generalized Green matrix on the basis of [6]. In Section 6 with the help of the example, not published yet, we present a technique for making a generalized Green matrix.

REFERENCES

1. Bosznay A.: *Improvable bracketing of the eigenfrequencies of a space frame structure modelled as continuum,* Doctoral dissertation, Budapest, *(1974), (*in Hungarian)
2. Richlik, G. and Tóth, G.: *Application of Trefftz-Fichera's method for improvable bracketing of the natural angular eigenfrequencies of a beam subject to bending vibration*, Acta Technica Hung., 92(3-4), (1981), 393-404.
3. Richlik, G.: *Bracketing of the eigenfrequencies of ordinary differential operators with the application of Green matrix*, Thesis, ELTE TTK, (1985), (in Hungarian)
4. Trefftz, E.: *Über Fehlerschätzung bei Berechnung von Eigenwerten,* Math. Annalen, Bd. 108., (1933), 595-604.
5. Blies, G. A.: *A boundary value problem for a system of ordinary linear differential equations of the first order*, Trans. Amer. Math. Soc., 28, (1926), 561-584.
6. Loud, W. S.: *Some examples of generalized Green's functions and generalized Green's matrices*, SIAM Review, 12(12), (1970), 194-210.

7. Reid, W. T.: *Generalized Green's matrices for two - point boundary problems*, SIAM J. Appl. Math., 15(4), (1967), 856-870.

8. Richlik, G.: *Construction of the inverse of differential operators with the aid of Green matrix*, Studies, 4^{th} Scientific Session of the Research Group of Technical Mechanics, Hungarian Academy of Sciences, (1986), 248-262.

9. Richlik, G.: *Inverse of ordinary differential operators and their application in the theory of vibration*, Study, 5^{th} Scientific Session of Research Group of Technical Mechanics, Hungarian Academy of Sciences, (1994)

Journal of Computational and Applied Mechanics, Vol. 1., No. 2., (2000), pp. 191–203

KINEMATIC ADMISSIBILITY OF STRAINS FOR SOME MIXED BOUNDARY VALUE PROBLEMS IN THE DUAL SYSTEM OF MICROPOLAR THEORY OF ELASTICITY

György Szeidl
Department of Mechanics, University of Miskolc
3515 Miskolc – Egyetemváros, Hungary
mechszgy@gold.uni-miskolc.hu

[Received: April 11, 2000]

Abstract. Making use of the principle of minimum complementary energy we have clarified what conditions the strains should meet in order to be kinematically admissible for some mixed boundary value problems of micropolar elasticity in a dual formulation. Emphasis is laid on the question as to what form the boundary conditions have since neither the displacements nor the microrotations belong to the set of fundamental variables.

Keywords: Dual system, mixed boundary value problems, micropolar elasticity, strain boundary conditions

1. Introduction

1.1. The necessary and sufficient conditions the strains in the linear theory of micropolar elasticity should meet in order to be kinematically admissible were found by Kozák-Szeidl [1] under the conditions that the boundary surface S of the region V under consideration was divided into two parts S_u and S_t on which tractions (force stresses and couple stresses) and generalized displacements (displacements and microrotations) were imposed.

Similar investigations within the framework of the classical theory have been performed by Kozák [2] who used stress functions of order two when setting up the entire system of variational principles in the dual system of elasticity. The necessary and sufficient conditions of kinematic admissibility for the strains were obtained from the stationary condition of the corresponding functionals.

Bertóti [3] confined himself to the case when the stresses are given in terms of stress functions of order one and under this condition he clarified, among other things, what form the equation system of linear elasticity has including those conditions the strains should meet in order to be kinematically admissible on a simple connected region. Some generalizations of these results are given in [4].

Returning to the micropolar theory, to the author's knowledge the cases when force stresses and microrotations or couple stresses and displacement fields are given on a part of the boundary (tractions are imposed on the other part of the boundary) has not been investigated yet though there are some preliminary results in this respect for the first plane problem – see Szeidl [5] and Iván-Szeidl [6] for details.

1.2. The main objective of the present paper is to clarify the form of the boundary conditions in the dual system if microrotations $\hat{\varphi}^b$ and force stresses $\hat{t}^k$ are imposed on the part $S_{t\varphi}$ of the boundary surface S while tractions (force stresses $\hat{t}^k$ and couple stresses $\hat{\mu}_b$) are prescribed on the other part $S_{t\mu}$ ($S_{t\mu} \cup S_{t\varphi} = S$, $S_{t\mu} \cap S_{t\varphi} = \emptyset$). It is a further aim to derive the unknown boundary conditions if displacements $\hat{u}_l$ and couple stresses $\hat{\mu}_b$ are imposed on $S_{u\mu}$ while tractions (force stresses $\hat{t}^k$ and couple stresses $\hat{\mu}_b$) are given on $S_{t\mu}$ ($S_{t\mu} \cup S_{u\mu} = S$, $S_{t\mu} \cap S_{u\mu} = \emptyset$). By solving the problem posed we shall also clarify all the conditions the strains should meet to be kinematically admissible under the given boundary conditions.

Observe that the problems posed are meaningless in the primal system of micropolar elasticity since the displacement field u_l and the microrotation φ^b (referred to together as displacements) are the configuration variables in this system.

1.3. The paper is organized into six Sections. In Section 2 notations and some preliminary results are presented. Sections 3 and 4 are devoted to the derivation of the missing conditions. Our analysis is based on the principle of minimum complementary energy which, as a variational principle, ensures the fulfillment of all conditions the strains should meet in order to be kinematically admissible. Section 5 is a short summary of the results. The last Section is an Appendix which contains some longer transformations.

2. Notations and preliminaries

2.1. For the sake of simplicity we shall assume that the volume region V occupied by the body under consideration is simple-connected. The boundary surface S is divided into two parts from which the boundary conditions on $S_{t\mu}$ are the same for the two problems considered. The common bounding curve is denoted by g. Figure 1 represents the region V and the parts $S_{t\varphi}$, $S_{t\mu}$ and $S_{u\mu}$, $S_{t\mu}$ for both problems.Indicial notations and two coordinate systems, the (x^1, x^2, x^3) curvilinear and the (ξ^1, ξ^2, ξ^3) curvilinear, defined on the surface S – see [7] for details – are employed throughout this paper. Scalars and tensors, unless otherwise stated, are denoted independently of the coordinate system by the same letter. Distinction is aided by the indication of the arguments x and ξ being used to denote the totality of the corresponding coordinates. Volume integrals and surface integrals are considered, respectively, in the coordinate systems $(x^1x^2x^3)$ and $(\xi^1\xi^2\xi^3)$. Consequently, in the case of integrals, arguments are omitted. In accordance with the general rules of indicial notations summation over repeated indices is implied and subscripts preceded by a semicolon denote covariant differentiation with respect to the corresponding subscripts. Latin and Greek indices range over the integers 1, 2, 3 and 1, 2 respectively. ϵ^{klm} and ϵ_{pqr} stand for the permutation tensors; δ^l_k is the *Kronecker* delta. In the system of coordinates $(x^1x^2x^3)$ $\mathbf{g}_k$ and $\mathbf{g}^l$ are the covariant and contravariant base vectors. The corresponding metric tensors are denoted by g_{kl} and g^{pq}. The equation of the boundary surface is written as $x^k = x^k(\xi^1, \xi^2)$ where the coordinates ξ^1 and ξ^2 are the surface parameters. Let ξ^3 be the distance measured on the outward unit normal $\mathbf{n}$ to the surface. On S $\xi^3 = 0$. [Base vectors] {Metric tensors} on S are denoted by $[\mathbf{a}^k$ and $\mathbf{a}_k]$ $\{a_{kl}$ and $a^{kl}\}$. In the

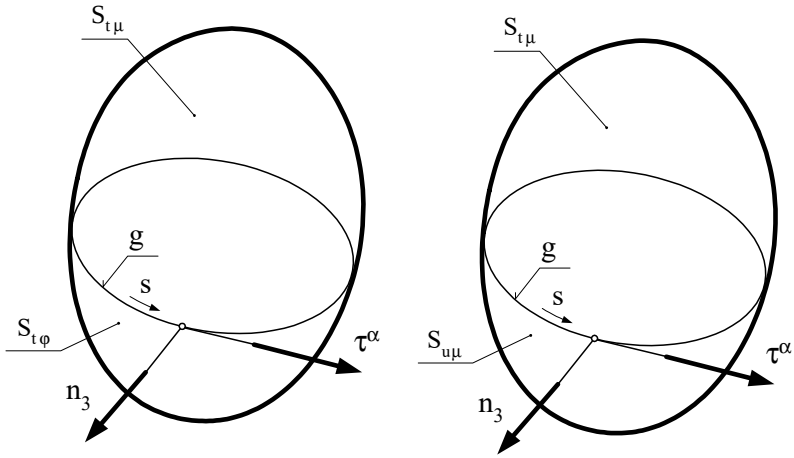

Figure 1.

coordinate system $(\xi^1\xi^2\xi^3)$

$$\mathbf{n} = \mathbf{a}_3 = \mathbf{a}^3\,, \qquad n^3 = 1 \qquad \text{and} \qquad n^\eta = 0\,. \tag{2.1}$$

If $\left|\xi^3\right| / (\min\{|R_1|, |R_2|\}) < 1$ in which R_1 and R_2 are the principal radii of curvature on S then the relationship $x^k = x^k(\xi^1, \xi^2, \xi^3)$ is always one-to-one.

2.2. The components of the asymmetric strain tensor and rotation tensor (together strains), and the force stress tensor and couple stress tensor (together stresses) are denoted by γ_{lk}, $\kappa_a{}^b$ and t^{kl}, $\mu^a{}_b$ respectively. In the primal system of micropolar elasticity the field equations can be given by the displacements u_l, φ^b as configuration variables, the strains γ_{lk}, $\kappa_a{}^b$ as intermediate variables of order one and the stresses t^{kl}, $\mu^a{}_b$ as intermediate variables of order two:

kinematic equations:

$$\gamma_{lk} = u_{l;k} + \varepsilon_{lks}\varphi^s, \qquad \kappa_a{}^b = \varphi^b{}_{;a} \qquad\qquad x \in V \tag{2.2}$$

Hook's law for centrosymmetric body [8]:

$$t^{kl} = \underset{-1}{a}{}^{klpq}\,\gamma_{pq}, \qquad \mu^{ab} = \underset{-1}{c}{}^{klpq}\,\kappa_{pq} \qquad\qquad x \in V \tag{2.3}$$

equilibrium equations:

$$t^{kl}{}_{;k} + b^l = 0, \qquad \mu^a{}_{b;a} + \varepsilon_{bpq}t^{pq} + c_b = 0 \qquad x \in V \tag{2.4}$$

where $\underset{-1}{a}{}^{klpq}$ and $\underset{-1}{c}{}^{klpq}$ are the tensors of elastic coefficients while b^l and c_b are body forces and couples. These equations are associated with the boundary conditions

$$n_3 t^{3l} = \hat{t}^l, \qquad \varphi^a = \hat{\varphi}^a \qquad\qquad \xi \in S_{t\varphi} \tag{2.5a}$$

$$n_3 t^{3l} = \hat{t}^l, \qquad n_3\mu^3{}_b = \hat{\mu}_b \qquad\qquad \xi \in S_{t\mu} \tag{2.5b}$$

for the first problem and with the boundary conditions

$$u_l = \hat{u}_l\,, \qquad n_3\mu^3{}_b = \hat{\mu}_b \qquad \xi \in S_{u\mu} \tag{2.6a}$$

$$n_3 t^{3l} = \hat{t}^l\,, \qquad n_3\mu^3{}_b = \hat{\mu}_b \qquad \xi \in S_{t\mu} \tag{2.6b}$$

for the second one.

2.3. The stresses t^{kl} and $\mu^a{}_b$ are said to be equilibrated {statically admissible} if they satisfy the equilibrium equations (2.4) {and the traction boundary conditions $(2.5a)_1$, (2.5b) or $(2.6a)_2$, (2.6b) }. Let

$$\overset{\circ}{t}{}^{kl} = p^l{}_{;m} g^{mk} \qquad \text{and} \qquad \overset{\circ}{\mu}{}^a{}_b = g^{am}(\varepsilon_{mby} p^y + q_{b;m}) \qquad x \in V \tag{2.7a}$$

where

$$g^{mn} p^l{}_{;mn} = -b^l \qquad \text{and} \qquad g^{mn} q_{b;mn} = -c_b\,. \qquad x \in V \tag{2.7b}$$

Further let $\mathcal{F}_y{}^l$ and $\mathcal{H}_{yb}$ $x \in V$ be stress function tensors. Then the stresses

$$t^{kl} = \varepsilon^{kmy} \mathcal{F}_y{}^l{}_{;m} + \overset{\circ}{t}{}^{kl}, \qquad \mu^a{}_b = \varepsilon^{apy}\left(\mathcal{H}_{yb;p} + \varepsilon_{bps}\mathcal{F}_y{}^s\right) + \overset{\circ}{\mu}{}^a{}_b \qquad x \in V \tag{2.8}$$

are equilibrated and $\overset{\circ}{\mu}{}^a{}_b$, $\overset{\circ}{t}{}^{kl}$ are particular solutions to the equilibrium equations (2.4) [9,10]. We shall assume that the particular solutions are known.

Remark 2.1.: Let $\alpha_{yb}(x)$ and $\beta^y{}_l(x)$ be differentiable otherwise arbitrary tensors on V. Further let ${}_{AB}$ and ${}^L_K$ be the subsets of the index pairs ${}_{yb}$ and ${}^l_y$ for which the differential equations

$$r^L{}_{;K} = \beta^L{}_K(x) \qquad \text{and} \qquad w_{B;A} + \varepsilon_{BAs} r^s = \alpha_{AB}(x) \qquad x \in V \tag{2.9}$$

always have a solution for the vector fields r^l and w_b. It can be shown that the stress function triplets $\mathcal{H}_{AB}$ and $\mathcal{F}_K{}^L$ can be set to zero [1].

Remark 2.2.: The proof of Remark 2.1 [1] is based on the observation that there belong identically zero stresses to the stress functions

$$\mathcal{F}_y{}^l = r^l{}_{;y}(x) \qquad \text{and} \qquad \mathcal{H}_{yb} = w_{b;y}(x) + \varepsilon_{bys} r^s(x)\,. \qquad x \in V \tag{2.10}$$

Remark 2.3.: Let ${}_{XY}$ and ${}^T_S$ be the complementary subsets of the index pairs ${}_{AB}$ and ${}^L_K$. It follows from Remark 2.1 that any stress condition can be given in terms of the stress functions $\mathcal{F}_S{}^T$ and $\mathcal{H}_{AB}$, i.e., by means of six-six stress functions.

Remark 2.4.: For this reason we shall assume that the stress functions and their variations have only six independent components each which are identified by the index pairs ${}_{XY}$ and ${}^T_S$.

2.4. The strains γ_{lk}, $\kappa_a{}^b$ are said to be compatible {kinematically admissible} if the kinematic equations (2.2) have single valued solutions for the displacements u_l, φ^b {and the solutions meet the boundary condition $(2.5a)_2$ or $(2.6a)_2$}.

The incompatibility tensors $\mathcal{Y}^{xy}$ and $\mathcal{D}^{s}{}_{t}$ are defined by the equations

$$\mathcal{Y}^{xy}(x) = \varepsilon^{xpa}\kappa_{a}{}^{y}{}_{;p} \quad \text{and} \quad \mathcal{D}^{s}{}_{t}(x) = \varepsilon^{spk}\left(\gamma_{kt;p} + \varepsilon_{ktb}\kappa_{p}{}^{b}\right) . \qquad x \in V \tag{2.11}$$

It can be seen [1] that the strains γ_{lk}, $\kappa_{a}{}^{b}$ are compatible on a simple connected domain V if the six-six compatibility field equations

$$\mathcal{Y}^{XY}(x) = 0 \qquad \text{and} \qquad \mathcal{D}^{S}_{T}(x) = 0 \qquad x \in V \tag{2.12a}$$

and the compatibility boundary conditions

$$n_3\mathcal{Y}^{3b}(x) = 0 \qquad \text{and} \qquad n_3\mathcal{D}^{3}{}_{t}(x) = 0 \qquad \xi \in S \tag{2.12b}$$

are satisfied [1].

2.5. In the dual system of micropolar elasticity the stress functions $\mathcal{F}_{S}{}^{T}$, $\mathcal{H}_{XY}$ are the configuration variables ($\mathcal{F}_{K}{}^{L}$ and $\mathcal{H}_{AB}$ are set to zero), the stresses t^{kl}, $\mu^{a}{}_{b}$ are the intermediate variables of order one and the strains γ_{lk}, $\kappa_{a}{}^{b}$ are the intermediate variables of order two. The field equations consists of

the dual kinematic equations

$$t^{kl} - \overset{\circ}{t}{}^{kl} = \varepsilon^{kmy}\mathcal{F}_{y;m}{}^{l}, \qquad \mu^{a}{}_{b} - \overset{\circ}{\mu}{}^{a}{}_{b} = \varepsilon^{apy}\left(\mathcal{H}_{yb;p} + \varepsilon_{bps}\mathcal{F}_{y}{}^{s}\right) \qquad x \in V \tag{2.13}$$

Hook's law

$$\gamma_{kl} = a_{klpq}t^{pq}, \qquad \kappa_{ab} = c_{abpq}\mu^{pq} \qquad x \in V \tag{2.14}$$

(a_{klpq} and c_{abpq} are the inverses of $\underset{-1}{a}{}^{klpq}$ and $\underset{-1}{c}{}^{klpq}$)

and the dual equilibrium equations

$$\mathcal{Y}^{XY}(x) = \varepsilon^{Xpa}\kappa_{a}{}^{Y}{}_{;p} = 0 , \qquad \mathcal{D}^{S}_{T}(x) = \varepsilon^{Spk}\left(\gamma_{kT;p} + \varepsilon_{kTb}\kappa_{p}{}^{b}\right) = 0 . \qquad x \in V \tag{2.15}$$

In view of (2.13) it follows from equations (2.5a,b) and (2.6a,b) that the field equations (2.13), (2.14) and (2.15) should be associated with the traction boundary conditions

$$n_3\overset{\circ}{t}{}^{3l} + n_3\varepsilon^{3\mu\eta}\mathcal{F}_{\eta;\mu}{}^{l} = \hat{t}^{l} \qquad \xi \in S \tag{2.16a}$$

$$n_3\overset{\circ}{\mu}{}^{3}{}_{b} + n_3\varepsilon^{3\pi\eta}\left(\mathcal{H}_{\eta b;\pi} + \varepsilon_{b\pi s}\mathcal{F}_{\eta}{}^{s}\right) = \hat{\mu}_{b} \qquad \xi \in S_{t\mu} \tag{2.16b}$$

for the first problem and with the traction boundary conditions

$$n_3\overset{\circ}{t}{}^{3l} + n_3\varepsilon^{3\mu\eta}\mathcal{F}_{\eta;\mu}{}^{l} = \hat{t}^{l} \qquad \xi \in S_{t\mu} \tag{2.17a}$$

$$n_3\overset{\circ}{\mu}{}^{3}{}_{b} + n_3\varepsilon^{3\pi\eta}\left(\mathcal{H}_{\eta b;\pi} + \varepsilon_{b\pi s}\mathcal{F}_{\eta}{}^{s}\right) = \hat{\mu}_{b} \qquad \xi \in S \tag{2.17b}$$

for the second one.

It is obvious that the compatibility boundary conditions (2.12b) should also be fulfilled.

We remind again the reader of the fact that no boundary conditions can be imposed directly on the displacements u_l and φ^b since these variables do not belong to the set of dual variables.

The strains γ_{kl}, κ_{ab} are said to be statically admissible if they are given in terms of statically admissible stresses t^{pq} and μ^{pq} by means of Hook's law (2.14).

3. Kinematic admissibility of strains for the first problem

3.1. The total complementary energy functional for the first problem assumes the form

$$K_I = \frac{1}{2}\int_V \left(t^{kl}\gamma_{kl} + \mu^a{}_b\kappa_a{}^b\right)\,\mathrm{d}V - \int_{S_{t\varphi}} n_3\mu^3{}_b\hat{\varphi}^b\,\mathrm{d}A \tag{3.1}$$

where both the stresses t^{kl}, $\mu^a{}_b$ and the strains γ_{kl}, $\kappa_a{}^b$ are statically admissible.

According to the principle of minimum complementary energy, the first variation of the functional K_I should vanish:

$$\delta K_I = I_1^V + I_1^{S_{t\varphi}} = \int_V \left(\gamma_{kl}\delta t^{kl} + \kappa_a{}^b\delta\mu^a{}_b\right)\,\mathrm{d}V - \int_{S_{t\varphi}} n_3\delta\mu^3{}_b\hat{\varphi}^b\,\mathrm{d}A = 0\,. \tag{3.2}$$

Because the stresses and strains are statically admissible, variations δt^{kl} and $\delta\mu^a{}_b$ of the force and couple stresses can not be arbitrary but should meet the side conditions

$$\delta t^{kl}{}_{;k} = 0\,, \qquad \delta\mu^a{}_{b;a} + \varepsilon_{bkl}\delta t^{kl} = 0 \qquad x \in V \tag{3.3a}$$

and

$$n_3\delta t^{3l} = 0\,, \qquad \xi \in S \tag{3.3b}$$

$$n_3\delta\mu^3{}_b = 0\,. \qquad \xi \in S_{t\mu} \tag{3.3c}$$

In the sequel we shall assume that the variations of the particular solutions $\overset{\circ}{t}{}^{kl}$ and $\overset{\circ}{\mu}{}^a{}_b$ are equal to zero.

It can be proved by direct substitutions that the side conditions (3.3a) are identically fulfilled if the variations of stresses are given in terms of the variations of stress functions as follows:

$$\delta t^{kl} = \varepsilon^{kmy}\delta\mathcal{F}_y{}^l{}_{;m}\,, \qquad x \in V \tag{3.4a}$$

$$\delta\mu^a{}_b = \varepsilon^{apy}\left(\delta\mathcal{H}_{yb;p} + \varepsilon_{bps}\delta\mathcal{F}_y{}^s\right)\,. \qquad x \in V \tag{3.4b}$$

Let r^l and w_b be arbitrary differentiable vector fields on S and $S_{t\mu}$, respectively. Further let the variations of the stress functions on $S_{t\mu}$ and $S_{t\varphi}$ be given in terms of the variations of r^l and w_b as follows:

$$\delta\mathcal{F}_\eta{}^l = \delta r^l{}_{;\eta}\,, \qquad \xi \in S \tag{3.5a}$$

$$\delta\mathcal{H}_{\eta b} = \delta w_{b;\eta} + \varepsilon_{b\pi l}r^l\,. \qquad \xi \in S_{t\mu} \tag{3.5b}$$

If this is the case, side conditions (3.3b) and (3.3c) are also identically satisfied.

3.2. If we utilize that

$$\delta K_I = I_2^V + I_1^{S_{t\varphi}} + I_1^S = I_2^V + I_2^{S_{t\varphi}} + I_3^{S_{t\varphi}} + I_1^{S_{t\mu}} + I_2^{S_{t\mu}} + I_2^S + I_1^G$$

(the details of the manipulations leading to this form are given in Subsection 6.2) and substitute equations (6.5), (6.6) and (6.7) into the above equation then the stationary condition (3.2) yields

$$\begin{aligned}\delta K_I = &\int_V (\mathcal{Y}^{XY}\delta\mathcal{H}_{XY} + \mathcal{D}^S{}_T\delta\mathcal{F}_S{}^T)\,\mathrm{d}V - \int_{S_{t\varphi}} \varepsilon^{3\pi\eta}(\kappa_\pi{}^b - \hat{\varphi}^b{}_{;\pi})\delta\mathcal{H}_{xy}\,\mathrm{d}A\\ &- \int_{S_{t\varphi}} \varepsilon^{3\eta\chi}(\gamma_{\chi l;\eta} - \varepsilon_{\chi lb}\hat{\varphi}^b{}_{;\eta})\delta r^l\,\mathrm{d}A - \int_{S_{t\mu}} \left[n_3\mathcal{Y}^{3b}\delta w_b + n_3\mathcal{D}^3{}_l\delta r^l\right]\,\mathrm{d}A\\ &+ \int_g \tau^\eta(\kappa_\eta{}^b - \hat{\varphi}^b{}_{;\eta})\delta w_b\,\mathrm{d}s = 0\,. \end{aligned} \tag{3.6}$$

With regard to the arbitrariness of the variations $\delta\mathcal{H}_{XY}, \ldots, \delta w_b$ this equation is equivalent to the compatibility field equations (2.15), the strain boundary conditions

$$\kappa_\pi{}^b - \hat{\varphi}^b{}_{;\pi} = 0\,, \qquad \xi \in S_{t\varphi} \tag{3.7}$$

$$\varepsilon^{3\eta\chi}(\gamma_{\chi l;\eta} - \varepsilon_{\chi lb}\hat{\varphi}^b{}_{;\eta}) = 0\,, \qquad \xi \in S_{t\varphi} \tag{3.8}$$

the compatibility boundary conditions (2.12b) on $S_{t\mu}$ and the continuity condition $d\hat{\varphi}^b/ds - \tau^\eta\kappa_\eta{}^b = 0$ on g.

Remark 3.1.: It can be shown with ease that the fulfillment of the strain boundary conditions (3.7) and (3.8) ensures that of the compatibility boundary conditions (2.12b) on $S_{t\varphi}$.

4. Kinematic admissibility of strains for the second problem

4.1. The total complementary energy functional and the corresponding stationary condition are of the form

$$K_{II} = \frac{1}{2}\int_V \left(t^{kl}\gamma_{kl} + \mu^a{}_b\kappa_a{}^b\right)\,\mathrm{d}V - \int_{S_{u\mu}} n_3 t^{3l}\hat{u}_l\,\mathrm{d}A \tag{4.1}$$

and

$$\delta K_{II} = I_1^V + I_1^{Su\mu} = \int_V \left(\gamma_{kl}\delta t^{kl} + \kappa_a{}^b\delta\mu^a{}_b\right)\,\mathrm{d}V - \int_{S_{u\mu}} n_3\delta t^{3l}\hat{u}_l\,\mathrm{d}A = 0\,, \tag{4.2}$$

respectively. In this case the variations δt^{kl} and $\delta\mu^a{}_b$ of the force and couple stresses should meet the side conditions (3.3a) and

$$n_3\delta t^{3l} = 0\,, \qquad n_3\delta\mu^3{}_b = 0\,, \qquad \xi \in S_{t\mu} \tag{4.3a}$$

$$n_3\delta\mu^3{}_b = 0\,. \qquad \xi \in S_{u\mu} \tag{4.3b}$$

Side conditions (3.3a) are again identically fulfilled if the variations of stresses are given in terms of the variations of stress functions in the same form as for the first problem – see equations (3.4a,b) for details.

Let r^l and w_b be arbitrary differentiable vector fields on $S_{t\mu}$, respectively. If the variations of the stress functions on $S_{t\mu}$ are given in terms of the variations of r^l and w_b:

$$\delta\mathcal{F}_\eta{}^l = \delta r^l{}_{;\eta} \qquad \delta\mathcal{H}_{\eta b} = \delta w_{b;\eta} + \varepsilon_{b\pi l} r^l \quad \xi \in S_{t\mu} \tag{4.4}$$

then side conditions (4.3a) are fulfilled. If the variations of the couple stresses are given in terms of the variations of stress functions, then substitution of representation (3.4b) into the side condition (4.3b) yields

$$n_3 \delta\mu^3{}_b = \varepsilon^{3\pi\eta}\left(\delta\mathcal{H}_{\eta b;\pi} + \varepsilon_{b\pi s}\delta\mathcal{F}_\eta{}^s\right) = 0 \quad \xi \in S_{u\mu} \tag{4.5}$$

from which it follows with regard to (6.2,c) that the variations $\delta\mathcal{F}_2{}^2$ and $\delta\mathcal{F}_\beta{}^3$ can not be arbitrary but should meet the conditions

$$\delta\mathcal{F}_2{}^2 = -\delta\mathcal{F}_1{}^1 - \varepsilon^{3\pi\eta}(\delta\mathcal{H}_{\eta 3||\pi} + b^\sigma_\pi \delta\mathcal{H}_{\eta\sigma} - b_{\eta\pi}\delta\mathcal{H}_{33}) \,, \qquad \xi \in S_{tu} \tag{4.6a}$$

$$\delta\mathcal{F}_\rho{}^3 = \varepsilon^{3\pi\eta}\delta\mathcal{H}_{\eta\rho;\pi} = \varepsilon^{3\pi\eta}\left(\delta\mathcal{H}_{\eta\rho||\pi} - b_{\eta\pi}\delta\mathcal{H}_{3\rho} - b_{\rho\pi}\delta\mathcal{H}_{\eta 3}\right) \,. \qquad \xi \in S_{tu} \tag{4.6b}$$

Derivation of the equations that follow from the stationary condition (4.2) requires a lengthy formal transformation which is based on the use of equations (3.4a,b) and (4.4), (4.6a,b) since their fulfillment ensures that of the side conditions on V and S. In addition integrations by parts should be performed by utilizing the Gauss and Stokes theorems. As regards the transformation the details are given in Subsections 6.3 to 6.4. Here we confine ourselves only to gathering the results. Comparison of the stationary condition (4.2) with equations (6.8), (6.9), (6.13) and (6.15) yields

$$\begin{aligned}\delta K_{II} &= I_1^V + I_1^{S_{u\mu}} = I_2^V + I_2^{S_{u\mu}} + I_3^{S_{u\mu}} + I_3^{S_{t\mu}} + I_2^G = \\ &= I_2^V + I_4^{S_{u\mu}} + I_3^{S_{t\mu}} + I_2^G + I_3^G = I_2^V + I_4^{S_{u\mu}} + I_4^{S_{t\mu}} + I_2^G + I_3^G + I_3^G = 0 \,.\end{aligned} \tag{4.7}$$

The final form of stationary condition (4.7) is obtained by substituting (6.4) for I_2^V, (6.14a) for $I_4^{S_{u\mu}}$, (6.16a) for $I_4^{S_{t\mu}}$ and (6.17) for $I_2^G + I_3^G + I_3^G$. After making some rearrangements we have

$$\begin{aligned}\delta K_{II} = &\int_V (\mathcal{Y}^{XY}\delta\mathcal{H}_{XY} + \mathcal{D}^S_T\delta\mathcal{F}_S{}^T)\,\mathrm{d}V + \int_{S_{u\mu}} \varepsilon^{3\pi\eta}(\tilde\varphi^\rho{}_{||\pi} - b^\rho_\pi\tilde\varphi^3 - \kappa_\pi{}^\rho)\delta\mathcal{H}_{\eta\rho}\,\mathrm{d}A + \\ &+ \int_{S_{u\mu}} \left[\varepsilon^{312}\left(\hat u_{1;1} - \gamma_{11}\right)\delta\mathcal{F}_2{}^1 + \varepsilon^{321}\left(\hat u_{2;2} - \gamma_{22}\right)\delta\mathcal{F}_1{}^1\right]\,\mathrm{d}A + \\ &+ \int_{S_{u\mu}} \varepsilon^{3\pi\eta}(\tilde\varphi^3{}_{||\pi} + b_{\rho\pi}\tilde\varphi^\rho - \kappa_\pi{}^3)\delta\mathcal{H}_{\eta 3}\,\mathrm{d}A - \\ &- \int_{S_{u\mu}} \varepsilon^{312}\left[\hat u_{2;1} + \hat u_{1;2} - (\gamma_{12} + \gamma_{21})\right]\delta\mathcal{F}_1{}^1\mathrm{d}A - \int_{S_{t\mu}} \left[n_3\mathcal{Y}^{3b}\delta w_b + n_3\mathcal{D}^3{}_l\delta r^l\right]\,\mathrm{d}A \\ &- \oint_g (\frac{d\tilde\varphi^b}{ds} - \tau^\eta\kappa_\eta{}^b)\delta w_b\,\mathrm{d}s - \oint_g \left[\frac{d\hat u_\lambda}{ds} - \tau^\eta\left(\gamma_{\eta\lambda} + \varepsilon_{\eta\lambda 3}\tilde\varphi^3\right)\right]\delta r^\lambda\,\mathrm{d}s = 0 \,.\end{aligned} \tag{4.8}$$

Since the variations $\delta\mathcal{H}_{XY}, \ldots, \delta r^{\lambda}$ in the stationary condition $\delta K_{II} = 0$ are arbitrary we obtain

– the compatibility field equations

(2.12a);

– the strain boundary conditions

$$\tilde{\varphi}^{\rho}{}_{||\pi} - b^{\rho}_{\pi}\tilde{\varphi}^{3} - \kappa_{\pi}{}^{\rho} = 0\,, \qquad \xi \in S_{u\mu} \tag{4.9a}$$

$$\tilde{\varphi}^{3}{}_{||\pi} + b_{\rho\pi}\tilde{\varphi}^{\rho} - \kappa_{\pi}{}^{3} = 0\,, \qquad \xi \in S_{u\mu} \tag{4.9b}$$

and

$$\hat{u}_{1;1} - \gamma_{11} = 0\,, \qquad \hat{u}_{2;2} - \gamma_{22} = 0\,, \qquad \xi \in S_{u\mu} \tag{4.10a}$$

$$\hat{u}_{2;1} + \hat{u}_{1;2} - (\gamma_{12} + \gamma_{21}) = 0\,; \qquad \xi \in S_{u\mu} \tag{4.10b}$$

– the compatibility boundary conditions

(2.12b)

on $S_{t\mu}$

and

the continuity conditions

$$\frac{d\tilde{\varphi}^{b}}{ds} - \tau^{\eta}\kappa_{\eta}{}^{b} = 0\,, \qquad \frac{d\tilde{u}_{\lambda}}{ds} - \tau^{\eta}\left(\gamma_{\eta\lambda} + \varepsilon_{\eta\lambda 3}\tilde{\varphi}^{3}\right)\,. \qquad \xi \in g \tag{4.11}$$

REMARK 4.1.: It can be shown by performing lengthy paper and pencil calculations, which require some attention, that the fulfillment of the strain boundary conditions (4.9a,b) and (4.10a,b) ensures that of the compatibility boundary conditions (2.12b) on $S_{u\mu}$.

5. Concluding remarks

5.1. We have clarified what boundary conditions the strains of the micropolar theory should meet in order to be kinematically admissible if

– microrotations and force stresses

or

– displacements and couple stresses

are imposed on a part of the boundary surface. The corresponding boundary conditions – like those found by Kozák-Szeidl in 1981 [2], - are referred to as strain boundary conditions. We draw the reader's attention to the fact that the fulfillment of the strain boundary conditions ensures that of the compatibility boundary conditions for both problems – see Remarks 3.1 and 4.1.

5.2. It is a further issue what form the strain boundary conditions have if for instance displacements are given in the tangent plane to the surface and force stress is prescribed perpendicularly to it and so on. Investigations to find an appropriate reply to the latter problem are in progress.

6. Appendix

6.1. Let b_π^σ and $b_{\eta\pi}$ be the mixed and covariant components of the tensor of curvature on S. Further let $\tilde{\varphi}^b$ and $\mathcal{H}_{\eta b}$ be differentiable vector and tensor fields defined on V and S. The covariant derivatives taken on the surface with respect to the surface coordinates and the surface covariant derivatives are denoted by $\tilde{\varphi}^\rho{}_{|\pi}$, $\mathcal{H}_{\eta b|\pi}$ and $\tilde{\varphi}^\rho{}_{||\pi}$, $\mathcal{H}_{\eta b||\eta}$, respectively. The following relations hold

$$\tilde{\varphi}^\rho{}_{;\pi} = \tilde{\varphi}^\rho{}_{|\pi} = \tilde{\varphi}^\rho{}_{||\pi} - b_\pi^\rho \tilde{\varphi}^3 \,, \tag{6.1}$$

$$\mathcal{H}_{\eta\beta;\pi} = \mathcal{H}_{\eta\beta|\pi} = \mathcal{H}_{\eta\beta||\pi} - b_{\eta\pi}\mathcal{H}_{3\beta} - b_{\beta\pi}\mathcal{H}_{\eta 3} \,, \tag{6.2}$$

$$\mathcal{H}_{\eta 3;\pi} = \mathcal{H}_{\eta 3|\pi} = \mathcal{H}_{\eta 3||\pi} + b_\pi^\sigma \delta\mathcal{H}_{\eta\sigma} - b_{\eta\pi}\delta\mathcal{H}_{33} \,. \tag{6.3}$$

6.2. Transformation of the volume integral I_1^V – see equation (3.2) – requires

– substitution of (3.4a,b) for the variations δt^{kl} and $\delta\mu^a{}_b$

– performance of integrations by parts making use of the Gauss theorem

and

– an appropriate rearrangement after utilizing the definitions given by (2.11) for $\mathcal{Y}^{xy}$ and $\mathcal{D}^s{}_t$.

In addition one should utilize the assumption in Remark 2.4. After performing the steps listed above we have

$$\begin{aligned} I_1^V &= I_2^V + I_1^S = \\ &= \int_V (\mathcal{Y}^{XY}\delta\mathcal{H}_{XY} + \mathcal{D}^S{}_T\delta\mathcal{F}_S{}^T)\,\mathrm{d}V - \int_S (\varepsilon^{3\chi\eta}\gamma_{\chi l}\delta\mathcal{F}_\eta{}^l + \varepsilon^{3\pi\eta}\kappa_\pi{}^b\delta\mathcal{H}_{\eta b})\,\mathrm{d}A \,. \end{aligned} \tag{6.4}$$

This transformation is valid both for the first problem and for the second one.

Integral $I_1^{S_{t\varphi}}$ of equation (3.2) can be manipulated into a more suitable form by applying the Stokes theorem:

$$I_1^{S_{t\varphi}} = \oint_g \tau^\eta \hat{\varphi}^b \delta\mathcal{H}_{\eta b}\,\mathrm{d}s + \int_{S_{t\varphi}} \varepsilon^{3\pi\eta}\hat{\varphi}^b{}_{;\eta}\delta\mathcal{H}_{\eta b}\mathrm{d}A - \int_{S_{t\varphi}} \varepsilon^{3\pi\eta}\varepsilon_{b\pi s}\delta\mathcal{F}_\eta{}^s\hat{\varphi}^b\,\mathrm{d}A \,.$$

Substituting (3.5a,b) into the sum $I_1^{S_{t\varphi}} + I_1^S$ and taking the relation $S = S_{t\varphi} \cup S_{t\mu}$ into account we have

$$I_1^{S_{t\varphi}} + I_1^S = I_2^{S_{t\varphi}} + I_3^{S_{t\varphi}} + I_1^{S_{t\mu}} + I_2^{S_{t\mu}} + I_2^S + I_1^G \tag{6.5}$$

where

$$\begin{aligned} I_2^{S_{t\varphi}} &= -\int_{S_{t\varphi}} \varepsilon^{3\pi\eta}\left(\kappa_\pi{}^b - \hat{\varphi}^b{}_{;\eta}\right)\delta\mathcal{H}_{\eta b}\,\mathrm{d}A \,, & I_3^{S_{t\varphi}} &= -\int_{S_{t\varphi}} \varepsilon^{3\pi\eta}\varepsilon_{b\pi s}\delta r^s{}_{;\eta}\hat{\varphi}^b\,\mathrm{d}A \,, \\ I_1^{S_{t\mu}} &= -\int_{S_{t\mu}} \varepsilon^{3\pi\eta}\kappa_\pi{}^b\delta w_{b;\eta}\,\mathrm{d}A \,, & I_2^{S_{t\mu}} &= -\int_{S_{t\mu}} \varepsilon^{3\pi\eta}\varepsilon_{b\pi l}\kappa_\pi{}^b\delta r^l\mathrm{d}A \,, \\ I_2^S &= -\int_S \varepsilon^{3\chi\eta}\gamma_{\chi l}\delta r^l{}_{;\eta}\,\mathrm{d}A \,, & I_1^G &= \oint_g \tau^\eta\hat{\varphi}^b\left(\delta w_{b;\eta} + \varepsilon_{b\pi l}\delta r^l\right)\,\mathrm{d}s \,. \end{aligned} \tag{6.6}$$

If we now integrate the right sides of $I_2^{S_{t\varphi}}$, $I_1^{S_{t\mu}}$ and I_3^S by parts – this transformation is based upon the Stokes theorem – then perform integrations by parts along the curve g, we obtain

$$I_3^{S_{t\varphi}} + I_1^{S_{t\mu}} + I_2^{S_{t\mu}} + I_2^S + I_1^G = -\int_{S_{t\varphi}} \varepsilon^{3\eta\chi} \left(\gamma_{\chi l;\eta} + \varepsilon_{\chi lb}\hat{\varphi}^b{}_{;\eta}\right) \delta r^l \, \mathrm{d}A$$
$$- \int_{S_{t\mu}} \left[n_3 \mathcal{Y}^{3b} \delta w_b + n_3 \mathcal{D}^3{}_l \delta r^l\right] \mathrm{d}A + \int_g \tau^\eta (\kappa_\eta{}^b - \hat{\varphi}^b{}_{;\eta}) \delta w_b \, \mathrm{d}s \,. \quad (6.7)$$

6.3. Substituting equation (3.3a) into the integral $I_1^{S_{u\mu}}$ and making use of the Stokes theorem we have:

$$I_1^{S_{u\mu}} = I_2^{S_{u\mu}} + I_2^G = \int_{S_{u\mu}} \varepsilon^{3\chi\eta} \hat{u}_{l;\chi} \delta \mathcal{F}_\eta{}^l \, \mathrm{d}A + \oint_g \tau^\eta \hat{u}_l \delta \mathcal{F}_\eta{}^l \, \mathrm{d}A \,. \quad (6.8)$$

Recalling the relation $S = S_{u\mu} \cup S_{t\mu}$ the integral taken over S in (6.4) can be resolved into two parts

$$I_1^S = I_3^{S_{t\mu}} + I_3^{S_{u\mu}} = \int_{S_{t\mu}} \ldots \mathrm{d}A + \int_{S_{u\mu}} \ldots \mathrm{d}A \,. \quad (6.9)$$

In view of (6.9) it is now our aim to transform the sum

$$I_2^{S_{u\mu}} + I_3^{S_{u\mu}} = -\int_{S_{u\mu}} \varepsilon^{3\pi\eta} \kappa_\pi{}^3 \delta \mathcal{H}_{\eta 3} \, \mathrm{d}A - \int_{S_{u\mu}} \varepsilon^{3\pi\eta} \kappa_\pi{}^\beta \delta \mathcal{H}_{\eta\beta} \, \mathrm{d}A$$
$$+ \int_{S_{u\mu}} (\hat{u}_{3;\chi} - \gamma_{\chi 3}) \, \varepsilon^{3\chi\rho} \delta \mathcal{F}_\rho{}^3 \, \mathrm{d}A + \int_{S_{u\mu}} (\hat{u}_{\lambda;\chi} - \gamma_{\chi\lambda}) \, \varepsilon^{3\chi\rho} \delta \mathcal{F}_\rho{}^\lambda \, \mathrm{d}A \quad (6.10)$$

into a more appropriate form. This aim can be achieved

– if we introduce the notations

$$\tilde{\varphi}^\rho = -\varepsilon^{3\chi\rho} \left(\hat{u}_{3;\chi} - \gamma_{\chi 3}\right) \qquad \xi \in S_{u\mu} \quad (6.11)$$

and

$$\tilde{\varphi}^3 = -\varepsilon^{132} \left(\hat{u}_{2;1} - \gamma_{12}\right) \,, \qquad \xi \in S_{u\mu} \quad (6.12)$$

– if we substitute the representation (as a matter of fact side condition) (4.6b) for $\delta \mathcal{F}_\rho{}^3$,
– if we write (4.6b) for $\delta \mathcal{F}_2{}^2$ in the last integral of equation (6.10),
– if we substitute the right sides of the equations

$$-\int_{S_{u\mu}} \tilde{\varphi}^\rho \varepsilon^{3\pi\eta} \delta \mathcal{H}_{\eta\rho||\pi} \, \mathrm{d}A = \int_{S_{u\mu}} \varepsilon^{3\pi\eta} \tilde{\varphi}^\rho{}_{||\pi} \delta \mathcal{H}_{\eta\rho} \, \mathrm{d}A + \oint_g \tau^\eta \tilde{\varphi}^\rho \delta \mathcal{H}_{\eta\rho} \, \mathrm{d}s$$
$$-\int_{S_{u\mu}} \tilde{\varphi}^3 \varepsilon^{3\pi\eta} \delta \mathcal{H}_{\eta 3||\pi} \, \mathrm{d}A = \int_{S_{u\mu}} \varepsilon^{3\pi\eta} \tilde{\varphi}^3{}_{||\pi} \delta \mathcal{H}_{\eta 3} \, \mathrm{d}A + \oint_g \tau^\eta \tilde{\varphi}^3 \delta \mathcal{H}_{\eta 3} \, \mathrm{d}s$$

each obtained by making use of the Stokes theorem

and

– if we make an appropriate rearrangement.

After performing the aforementioned steps we get

$$I_2^{S_{u\mu}} + I_3^{S_{u\mu}} = I_4^{S_{u\mu}} + I_3^G \tag{6.13}$$

where

$$\begin{aligned} I_4^{S_{u\mu}} = & \int_{S_{u\mu}} \left[\varepsilon^{312}\left(\hat{u}_{1;1} - \gamma_{11}\right)\delta\mathcal{F}_2{}^1 + \varepsilon^{312}\left(\hat{u}_{2;2} - \gamma_{22}\right)\delta\mathcal{F}_1{}^2\right] \mathrm{d}A \\ & - \int_{S_{u\mu}} \varepsilon^{312}\left[\hat{u}_{2;1} + \hat{u}_{1;2} - (\gamma_{12} + \gamma_{21})\right]\delta\mathcal{F}_1{}^1 \,\mathrm{d}A \\ & + \int_{S_{u\mu}} \varepsilon^{3\pi\eta}\left[\tilde{\varphi}^{\rho}_{||\pi} - b^{\rho}_{\pi}\tilde{\varphi}^3 - \kappa_{\pi}{}^{\beta}\right]\delta\mathcal{H}_{\eta\rho}\,\mathrm{d}A \\ & - \int_{S_{u\mu}} \varepsilon^{3\pi\eta}\left[\tilde{\varphi}^3_{||\pi} - b_{\rho\pi}\tilde{\varphi}^{\rho} - \kappa_{\pi}{}^3\right]\delta\mathcal{H}_{\eta 3}\,\mathrm{d}A \end{aligned} \tag{6.14a}$$

and

$$I_3^G = \oint_g \tau^{\eta}\tilde{\varphi}^{\rho}\delta\mathcal{H}_{\eta\rho}\,\mathrm{d}s + \oint_g \tau^{\eta}\tilde{\varphi}^3\delta\mathcal{H}_{\eta 3}\,\mathrm{d}s\,. \tag{6.14b}$$

6.4. The integral

$$I_3^{S_{t\mu}} = -\int_{S_{t\mu}} (\varepsilon^{3\chi\eta}\gamma_{\chi l}\delta\mathcal{F}_{\eta}{}^{l} + \varepsilon^{3\pi\eta}\kappa_{\pi}{}^{b}\delta\mathcal{H}_{\eta b})\,\mathrm{d}A$$

can be manipulated into the form

$$I_3^{S_{t\mu}} = I_4^{S_{t\mu}} + I_4^G \tag{6.15}$$

where

$$I_4^{S_{t\mu}} = -\int_{S_{t\mu}} \left[n_3\mathcal{Y}^{3b}\delta w_b + n_3\mathcal{D}^3{}_l\delta r^l\right]\mathrm{d}A \tag{6.16a}$$

and

$$I_4^G = \oint_g \tau^{\eta}\gamma_{\eta l}\delta r_b^l\,\mathrm{d}s + \oint_g \tau^{\eta}\kappa_{\eta}{}^{b}\delta w_b\,\mathrm{d}s \tag{6.16b}$$

if we substitute $(4.4)_{1,2}$ for $\delta\mathcal{F}_{\eta}{}^{l}$ and $\delta\mathcal{H}_{\eta b}$ and then perform integrations by parts – the latter step is based on the Stokes theorem.

The sum of the line integrals $I_3^G + I_4^G$ can be cast into the final form

$$I_2^G + I_3^G + I_4^G = -\oint_g \left(\frac{d\tilde{\varphi}^b}{ds} - \tau^{\eta}\kappa_{\eta}{}^{b}\right)\delta w_b\,\mathrm{d}s - \oint_g \left[\frac{d\tilde{u}_b}{ds} - \tau^{\eta}\left(\gamma_{\eta b} + \varepsilon_{\eta b 3}\tilde{\varphi}^3\right)\right]\delta r^{\lambda}\,\mathrm{d}s \tag{6.17}$$

if we substitute $(4.4)_{1,2}$ for $\delta\mathcal{F}_{\eta}{}^{l}$ and $\delta\mathcal{H}_{\eta b}$ and then perform integrations by parts in order to remove the covariant derivatives from the integrand obtained after the substitution.

Acknowledgement. The support provided by the Hungarian National Research Foundation (project No. T031998) is gratefully acknowledged.

REFERENCES

1. Kozák, I. and Szeidl, G.: *The field equations and boundary conditions with force stresses and couple stresses in the linearized theory of micropolar elastostatics*, Acta Technica Sci. Hung., 91(1-2), (1980), 57-80.
2. Kozák, I.: *Remarks and contributions to the variational principles of the linearized theory of elasticity in terms of the stress functions*, Acta Technica Sci. Hung., 92(1-2), (1981), 45-65.
3. Bertóti, E.: *Indeterminancy of first order stress functions and the stress and rotation based formulation of linear elasticity*, Computational Mechanics, 14, (1994), 249-256.
4. Bertóti, E.: *On mixed variational formulation of linear elasticity using nonsymmetric stresses and displacements*, International Journal for Numerical Methods in Engineering., 42, (1997), 561-578.
5. Szeidl, G.: *Dual variational principles for the first plane problem of micropolar theory of elasticity*, Publ. Techn. Univ. Heavy Industry, Miskolc, Ser. D. Natural Sciences, 35, (1982) 3-20. (in Russian).
6. Iván, I. and Szeidl, G.: *Macro conditions of compatibility and strain boundary conditions for some mixed plane boundary value problems of micropolar elatostatics*, Publ. Univ. of Miskolc, Series D. Natural Sciences, Mathematics, 36, (1996) 35-45.
7. Niordson, F. I.: *Shell Theory*, North Holland, 1985.
8. Nowacki, W.: *Theory of Micropolar Elasticity*, Springer Verlag, Wien, New-York, Udine, 1970.
9. Carlson D. E.: *On Günther's stress functions for couple stresses*, Quart. Appl. Math. 25, (1967), 139-146.
10. Schaefer, H.: *Die Spannungsfunktionen eines Kontinuums mit Momentenspannungen I. und II.*, Bulletin de l'Académie Polonaise des Sciences, Série des Sciences techniques, XV., (1967), 63-67, 69-73.

Journal of Computational and Applied Mechanics, Vol. 1., No. 2., (2000), pp. 205–222

BOUNDARY CONTOUR METHOD FOR PLANE PROBLEMS IN A DUAL FORMULATION WITH LINEAR ELEMENTS

Sándor Szirbik
Department of Mechanics, University of Miskolc
3515 Miskolc – Egyetemváros, Hungary
mechsany@gold.uni-miskolc.hu

[Received: May 2, 2000]

Abstract. The present paper is devoted to the boundary contour method for plane problems in the dual system of elasticity. It has been shown that the integrals on the right side of the corresponding boundary integral equations are divergence free in the dual system provided that the unknown functions satisfy the field equations. Consequently these integrals can be given in closed form if appropriate shape functions have been chosen to approximate the unknown functions on the contour. Numerical examples prove the efficiency of this technique.

1. Introduction

It has been proved in the article [1] by A. Nagarajan, E. Lutz and S. Mukherjee that the integrand of the direct boundary element method is divergence free in the primal system of the two and three-dimensional elasticity theory. The authors of [1] have come to the conclusion that the numerical solution of three-dimensional problems require the calculation of line integrals instead of surface integrals, while for planar problems evaluation of functions should be performed instead of calculating line integrals. Article [1] supposes linear approximation. The accuracy is greatly increased if one uses quadratic elements [2]. This method can also be employed for rewriting hypersingular integral equations into boundary contour equations. With this technique one can compute stresses and can solve shape optimization problems in two dimensions [3].

The boundary integral equations of the direct method in the dual system of elasticity and for plane problems can be found in a thesis [4]. In view of the formulation presented in [4] there arises the question if it is possible to repeat the line of thought leading to the boundary contour method in a dual formulation as well. The reply to this question is yes and the main result of the present paper is a dual formulation similar, as regard its main features, to that given in paper [1].

The paper is organized into seven sections. Section 2 is devoted to some preliminaries. It is proved in Section 3 that the integrand of the direct boundary element method is divergence free in the dual system of elasticity. In addition we have determined the corresponding shape functions provided that the approximation is linear. Discretized equations are set up in Section 4. The aim is to prepare an algorithm for

our computations. Section 5 is devoted to the question of how to compute stresses at internal points. Section 6 presents some simple numerical examples. The last Section is a summary of the conclusions. The paper is also supplemented with an Appendix in which the shape functions and some manipulations are presented.

2. Fundamental solutions and integral equations of the direct method

Cartesian coordinates and indicial notations are used throughout this paper. {Greek} [Latin] subscripts have the range $\{1,2\},[1,2,3]$, summation over repeated indices is implied. In accordance with the notations introduced $\delta_{\kappa\lambda}$ is the Kronecker symbol, ∂_κ stands for the derivatives with respect to x_κ and $\varepsilon_{3\kappa\lambda}$ is the permutation tensor. $\mathcal{F}_\lambda$ stands for the stress functions of order one. In plane components of stresses and strains are denoted by $t_{\kappa\lambda}$ and $e_{\kappa\lambda}$. If there are body forces, the particular solution of the equilibrium equations is $\overset{o}{t}_{\kappa\lambda}$. The shear modulus of elasticity and the Poisson number are denoted by μ and ν, respectively. The rigid body rotation is denoted by φ_3.

In the dual system of elasticity plane strain problems are governed by the dual kinematic equations

$$t_{\kappa\lambda} = \varepsilon_{\kappa\rho 3}\mathcal{F}_\lambda\ \partial_\rho + \overset{o}{t}_{\kappa\lambda}\,, \tag{2.1}$$

the inverse of Hook's law

$$e_{\kappa\lambda} = \frac{1}{2\mu}\left(t_{\kappa\lambda} - \nu t_{\psi\psi}\delta_{\kappa\lambda}\right)\,, \tag{2.2}$$

the dual balance equations

$$\epsilon_{\kappa\rho 3}e_{\lambda\kappa}\partial_\rho + \varphi_3\partial_\lambda = 0 \tag{2.3}$$

(equations of compatibility for a simply connected region) and the symmetry condition

$$\epsilon_{3\lambda\kappa}t_{\lambda\kappa} = 0\,. \tag{2.4}$$

For simplicity first we shall consider a simply connected inner region A_i. The contour $\mathcal{L}_o$ of the region A_i can be divided into two parts denoted by $\mathcal{L}_t$ and $\mathcal{L}_u$. We shall assume that $[\mathcal{L}_t]$ $\{\mathcal{L}_u\}$ is the union of those arcs on which [stress functions (loaded arcs)] {displacements} are imposed. These arcs are denoted by $\mathcal{L}_{t2}$, $\mathcal{L}_{t4}$ and $\mathcal{L}_{u1}$, $\mathcal{L}_{u3}$, respectively. The corresponding boundary conditions are of the form

$$F_\lambda(s) = \hat{F}_\lambda + C_\lambda(P_{ti}) \qquad s\in\mathcal{L}_{ti} \qquad i=2,4 \tag{2.5}$$

and

$$\frac{\mathrm{d}\hat{u}_\lambda}{\mathrm{d}s} = n_\rho\left[\epsilon_{\rho\kappa 3}e_{\kappa\lambda} - \varphi_3\delta_{\rho\lambda}\right] \qquad s\in\mathcal{L}_u\,, \tag{2.6}$$

where $\hat{F}_\lambda(s)$ and $\hat{u}_\lambda(s)$ are known functions, while C_λ is an integration constant, the number of which equals the number of loaded arcs. Here and in the sequel we shall

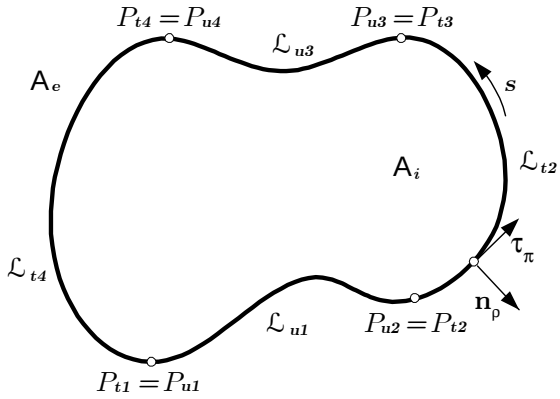

Figure 1.

assume that there are no body forces. In the absence of body forces

$$\hat{F}_\lambda(s) = \int \hat{t}_\lambda(s)\mathrm{d}s\,, \tag{2.7}$$

where $\hat{t}_\lambda(s)$ is the stress vector on $\mathcal{L}_t$.

Substituting the dual kinematic equation (2.1) into Hook's law (2.2) and the result into the compatibility equations (2.3) we get two scalar equations. These equations are associated with the symmetry condition, i.e., we have three equations for the unknowns $\mathcal{F}_1, \mathcal{F}_2$ and φ_3

$$\begin{bmatrix} a\Delta - b\partial_1\partial_1 & -b\partial_2\partial_1 & -\partial_1 \\ -b\partial_2\partial_1 & a\Delta - b\partial_2\partial_2 & -\partial_2 \\ -\partial_1 & -\partial_2 & 0 \end{bmatrix} \begin{bmatrix} \mathcal{F}_1 \\ \mathcal{F}_2 \\ -\varphi_3 \end{bmatrix} = \begin{bmatrix} 0 \\ 0 \\ 0 \end{bmatrix} \tag{2.8}$$

where

$$a = \frac{1}{2\mu}(1-\upsilon) \qquad b = \frac{1}{2\mu}(\frac{1}{2}-\upsilon)\,. \tag{2.9}$$

Let D_{ik} $(i,k = 1,2,3)$ be the differential operator in equation (2.8). Further let $\mathrm{u}_k = (\mathcal{F}_1 \mid \mathcal{F}_2 \mid -\varphi_3)$ be the vector of unknowns (or state vector). With these notations equation (2.8) can be rewritten as

$$D_{ik}\mathrm{u}_k = 0\,. \tag{2.10}$$

Let $Q(\eta_1, \eta_2)$ and $M(x_1, x_2)$ be the source point and the point of effect. The position vector of $M(x_1, x_2)$ relative to $Q(\eta_1, \eta_2)$ is $r_\lambda = x_\lambda - \eta_\lambda$. The distance between Q and M is $R = R\,(M, Q) = |\mathbf{r}|$. For a two point function $f(R)$ it holds that

$$\frac{\partial}{\partial x_\lambda} f(R) = -\frac{\partial}{\partial \eta_\lambda} f(R)\,. \tag{2.11}$$

Let $e_i(Q)$ be a unit vector at Q. Solution to the differential equation

$$\overset{M}{D}_{ik}\mathfrak{u}_k + \delta\,(M-Q)\,e_i(Q) = 0 \tag{2.12}$$

is referred to as fundamental solution. Here the letter M over D_{ik} denotes that the derivation is taken with respect to the point M. It can be shown that

$$\mathfrak{u}_k = \mathfrak{U}_{kl}(M,Q)e_l(Q)\,, \tag{2.13}$$

where

$$[\mathfrak{U}_{kl}(M,Q)] = \frac{\mu}{4\pi(1-\nu)} \times$$
$$\times \begin{bmatrix} -2\ln R - 3 - 2\dfrac{r_2 r_2}{R^2} & 2\dfrac{r_1 r_2}{R^2} & \dfrac{2}{\mu}(1-\nu)\dfrac{r_1}{R^2} \\ 2\dfrac{r_2 r_1}{R^2} & -2\ln R - 3 - 2\dfrac{r_1 r_1}{R^2} & \dfrac{2}{\mu}(1-\nu)\dfrac{r_2}{R^2} \\ \dfrac{2}{\mu}(1-\nu)\dfrac{r_1}{R^2} & \dfrac{2}{\mu}(1-\nu)\dfrac{r_2}{R^2} & 0 \end{bmatrix} \tag{2.14}$$

For our later considerations we shall introduce the notation

$$\mathfrak{t}_\lambda = -\frac{\mathrm{d}u_\lambda}{\mathrm{d}s}\,. \tag{2.15}$$

The vector $\mathfrak{t}_\lambda$ is opposite to the derivative of the displacement vector with respect to the arc coordinate s measured on the contour $\mathcal{L}_o$. Omitting the long formal transformations for the vector $\mathfrak{t}_\lambda$ calculated from the fundamental solution we get [4]

$$\mathfrak{t}_\lambda(\overset{o}{M}) = e_l(Q)\mathfrak{T}_{l\lambda}(\overset{o}{M},Q) \tag{2.16}$$

where

$$\mathfrak{T}_{l\lambda}(\overset{o}{M},Q) = \frac{1}{8\pi(1-\nu)R^2} \times$$
$$\times \begin{bmatrix} n_1 r_1\left(4\dfrac{r_2^2}{R^2} - 2(3-2v)\right) & -n_2 r_1\left(4\dfrac{r_2^2}{R^2} + 2(1-2v)\right) \\ +n_2 r_2\left(4\dfrac{r_2^2}{R^2} - 2(3-2v)\right) & -n_1 r_2\left(4\dfrac{r_1^2}{R^2} - 2(1-2v)\right) \\ -n_1 r_2\left(4\dfrac{r_1^2}{R^2} + 2(1-2v)\right) & n_2 r_2\left(4\dfrac{r_1^2}{R^2} - 2(3-2v)\right) \\ -n_2 r_1\left(4\dfrac{r_2^2}{R^2} - 2(1-2v)\right) & +n_1 r_1\left(4\dfrac{r_1^2}{R^2} - 2(3-2v)\right) \\ -n_1\dfrac{2}{\mu}(1-\nu)\dfrac{r_1^2 - r_2^2}{R^2} & -n_1\dfrac{4}{\mu}(1-\nu)\dfrac{r_1 r_2}{R^2} \\ -n_2\dfrac{4}{\mu}(1-\nu)\dfrac{r_1 r_2}{R^2} & +n_2\dfrac{2}{\mu}(1-\nu)\dfrac{r_1^2 - r_2^2}{R^2} \end{bmatrix} \tag{2.17}$$

Here and in the sequel the small circle over the letters Q and M shows that the corresponding point is located on the contour. The normal n_λ is taken at the point $\overset{o}{M}$.

If we take two elastic states of the region A_i – the second state is denoted by asterisk which is placed over the corresponding letters – then the so-called dual Somigliana identity can be written as

$$\int_{A_i} \left[\mathfrak{u}_k (D_{kl} \overset{*}{\mathfrak{u}}_l) - \overset{*}{\mathfrak{u}}_k (D_{kl} \mathfrak{u}_l) \right] \mathrm{d}A = \oint_{\mathcal{L}_o} [\mathfrak{u}_\lambda \overset{*}{\mathfrak{t}}_\lambda - \overset{*}{\mathfrak{u}}_\lambda \mathfrak{t}_\lambda] \, \mathrm{d}s \,. \tag{2.18}$$

If the quantities denoted by asterisks are from the fundamental solution and $Q \in A_i$, then exploiting the above, we have the first dual Somigliana formula

$$\mathfrak{u}_k(Q) = \oint_{\mathcal{L}_o} \mathfrak{U}_{k\lambda}(\overset{o}{M}, Q) \mathfrak{t}_\lambda(\overset{o}{M}) \, \mathrm{d}s_{\overset{o}{M}} - \oint_{\mathcal{L}_o} \mathfrak{T}_{k\lambda}(\overset{o}{M}, Q) \mathfrak{u}_\lambda(\overset{o}{M}) \, \mathrm{d}s_{\overset{o}{M}} \,. \tag{2.19}$$

If $Q = \overset{o}{Q} \in \partial A_i = \mathcal{L}_o$, then equation (2.18) yields the second dual Somigliana formula

$$c_{\kappa\lambda}(\overset{o}{Q}) \mathfrak{u}_\lambda(\overset{o}{Q}) = \oint_{\mathcal{L}_o} \mathfrak{U}_{k\lambda}(\overset{o}{M}, \overset{o}{Q}) \mathfrak{t}_\lambda(\overset{o}{M}) \, \mathrm{d}s_{\overset{o}{M}} - \oint_{\mathcal{L}_o} \mathfrak{T}_{k\lambda}(\overset{o}{M}, \overset{o}{Q}) \mathfrak{u}_\lambda(\overset{o}{M}) \, \mathrm{d}s_{\overset{o}{M}} \,, \tag{2.20}$$

where $c_{\kappa\lambda}(\overset{o}{Q})$ depends on the angle formed by the tangents to the contour at $\overset{o}{Q}$. The above integral equation is that of the direct method in the dual system of elasticity. Finally if $Q \notin (A_i \cup \mathcal{L}_o)$, then the left side of the identity (2.18) is identically equal to zero and the third dual Somigliana formula can immediately be set up

$$0 = \oint_{\mathcal{L}_o} \mathfrak{U}_{k\lambda}(\overset{o}{M}, Q) \mathfrak{t}_\lambda(\overset{o}{M}) \, \mathrm{d}s_{\overset{o}{M}} - \oint_{\mathcal{L}_o} \mathfrak{T}_{k\lambda}(\overset{o}{M}, Q) \mathfrak{u}_\lambda(\overset{o}{M}) \, \mathrm{d}s_{\overset{o}{M}} \,. \tag{2.21}$$

3. Fundamental relations for linear approximation

We shall assume that the stress functions $\mathfrak{u}_\lambda$ fulfill the basic equations and $\mathfrak{t}_\lambda$ is calculated from $\mathfrak{u}_\lambda$. Under this condition the opposite to the derivative of the displacement vector can be obtained from (2.6):

$$\mathfrak{t}_\lambda(\overset{o}{M}) = -n_\rho(\overset{o}{M}) \left(\epsilon_{\rho\pi 3} e_{\pi\lambda}(\overset{o}{M}) - \delta_{\rho\lambda} \varphi_3(\overset{o}{M}) \right) . \tag{3.1}$$

We denote again the quantities derived from the fundamental solution by asterisks.

Let $\overset{*}{e}_{k\pi\lambda}(\overset{o}{M}, Q)$ be the strain tensor that follows from the stress function vector $\overset{*}{\mathfrak{u}}_\lambda(\overset{o}{M}) = \mathfrak{U}_{k\lambda}(\overset{o}{M}, Q)$. It is also clear that the corresponding rotation $\overset{*}{\varphi}_3(\overset{o}{M})$ is $\mathfrak{U}_{k3}(\overset{o}{M}, Q)$. Making use of these notations and the relation (3.1) we can write

$$\overset{*}{\mathfrak{t}}_\lambda(\overset{o}{M}, Q) = \mathfrak{T}_{k\lambda}(\overset{o}{M}, Q) = -n_\rho(\overset{o}{M}) \left(\epsilon_{\rho\pi 3} \overset{*}{e}_{k\pi\lambda}(\overset{o}{M}, Q) - \delta_{\rho\lambda} \mathfrak{U}_{k3}(\overset{o}{M}, Q) \right) \tag{3.2}$$

for the derivative $-\mathrm{d}\overset{*}{u}_\lambda/\mathrm{d}s$. Upon substitution of $\overset{*}{\mathrm{u}}_\lambda(\overset{o}{M})$ for u_λ and $\overset{*}{\mathrm{t}}_\lambda(\overset{o}{M},Q)$ for t_λ in (2.19) we have, after renaming some dummy indices, that

$$I_\kappa(Q) = \oint_{\mathcal{L}_o} n_\rho(\overset{o}{M}) \left(-\mathfrak{U}_{\kappa\lambda}(\overset{o}{M},Q) \left(\epsilon_{\rho\pi 3} e_{\pi\lambda}(\overset{o}{M}) - \delta_{\rho\lambda}\varphi_3(\overset{o}{M}) \right) + \right.$$
$$\left. + \left(\epsilon_{\rho\pi 3} \overset{*}{e}_{\kappa\pi\lambda}(\overset{o}{M},Q) - \delta_{\rho\lambda}\mathfrak{U}_{\kappa 3}(\overset{o}{M},Q) \right) \mathrm{u}_\lambda(\overset{o}{M}) \right) \mathrm{d}s_{\overset{o}{M}} . \tag{3.3}$$

Since those terms for which $k = 3$ in (2.19) will play no role in the further transformation we have dropped them by writing κ for k.

Let $P_{\kappa\rho}$ be the coefficient of $n_\rho(\overset{o}{M})$ in (3.3):

$$P_{\kappa\rho}(\overset{o}{M}) = P_{\kappa\rho}(\overset{o}{M},Q) = -\mathfrak{U}_{\kappa\lambda}(\overset{o}{M},Q) \left(\epsilon_{\rho\pi 3} e_{\pi\lambda}(\overset{o}{M}) - \delta_{\rho\lambda}\varphi_3(\overset{o}{M}) \right) +$$
$$+ \left(\epsilon_{\rho\pi 3} \overset{*}{e}_{\kappa\pi\lambda}(\overset{o}{M},Q) - \delta_{\rho\lambda}\mathfrak{U}_{\kappa 3}(\overset{o}{M},Q) \right) \mathrm{u}_\lambda(\overset{o}{M}) . \tag{3.4}$$

By using Gauss's theorem the line integral $I_\kappa(Q)$ can be transformed into a surface integral:

$$I_\kappa(Q) = \oint_{\mathcal{L}_o} P_{\kappa\rho}(\overset{o}{M},Q) n_\rho(\overset{o}{M}) \mathrm{d}s_{\overset{o}{M}} = \int_{A_i} P_{\kappa\rho}(M,Q) \overset{M}{\partial}_\rho \mathrm{d}A_M , \tag{3.5}$$

where, as can be seen after some hand-made calculations – see the Appendix for details – it holds

$$P_{\kappa\rho}(M,Q) \overset{M}{\partial}_\rho = 0 , \tag{3.6}$$

that is, there exists a function $\phi_\kappa(M,Q)$ such that

$$P_{\kappa 1} = \frac{\partial \phi_\kappa(M,Q)}{\partial x_2} \qquad \text{and} \qquad P_{\kappa 2} = -\frac{\partial \phi_\kappa(M,Q)}{\partial x_1} . \tag{3.7}$$

This means that the integrand $P_{\kappa\rho}$ is divergence free.

Taking now the line integral between the contour points $\overset{o}{M}_1$ and $\overset{o}{M}_2$ and using the above results we get the desired solution

$$\int_{\overset{o}{M}_1}^{\overset{o}{M}_2} P_{\kappa\rho}(\overset{o}{M},Q) n_\rho(\overset{o}{M}) \mathrm{d}s_{\overset{o}{M}} = \int_{\overset{o}{M}_1}^{\overset{o}{M}_2} \tau_\pi(\overset{o}{M}) \phi_\kappa(\overset{o}{M},Q) \overset{M}{\partial}_\pi \mathrm{d}s_{\overset{o}{M}} = \phi_\kappa(\overset{o}{M}_2,Q) - \phi_\kappa(\overset{o}{M}_1,Q) . \tag{3.8}$$

When deriving the above relations we have not taken the position of Q relative to the region A_i into account. In other words the above results remain valid for the second and third dual Somigliana formulae as well.

Assume that the contour is divided into n_{be} boundary elements. The extremities of the elements are locally denoted by M_1 and M_2. (Here and in the sequel for simplicity

we have omitted the zero standing over the letter M.) Then integrating element by element we have

$$I_\kappa(Q) = \sum_{e=1}^{n_{be}} [\phi_\kappa^e(M_2, Q) - \phi_\kappa^e(M_1, Q)] \tag{3.9}$$

where the upper index e shows that ϕ_κ is taken on the e-th element.

Let K be the middle point of the element e. Over the element and its neighborhood we shall approximate the unknown vector $\mathfrak{u}_k$ by linear functions for the stress functions, and by a constant for the rigid body rotation, i.e.,

$$\begin{bmatrix} \mathcal{F}_1 \\ \mathcal{F}_2 \\ -\varphi_3 \end{bmatrix}^e = \begin{bmatrix} a_1 + a_2 x_1 + a_3 x_2 \\ a_4 + a_5 x_1 - a_2 x_2 \\ a_6 \end{bmatrix}. \tag{3.10}$$

The constants

$$(\mathbf{a}^e)^T = \begin{bmatrix} a_1 & a_2 & a_3 & a_4 & a_5 & a_6 \end{bmatrix} \tag{3.11}$$

in (3.10) are related to the six physical quantities

$$(\mathbf{p}^e)^T = \begin{bmatrix} \mathcal{F}_1^{M_1} & \mathcal{F}_2^{M_1} & \mathfrak{t}_1^K & \mathfrak{t}_2^K & \mathcal{F}_1^{M_2} & \mathcal{F}_2^{M_2} \end{bmatrix} \tag{3.12}$$

taken on the element e via the equation

$$\mathbf{T}^e \mathbf{a}^e = \mathbf{p}^e, \tag{3.13}$$

where the transformation matrix $\mathbf{T}^e$ depends only on the nodal coordinates and the outward unit normal at K. After some hand-made calculations we have

$$\mathbf{T}^e = \begin{bmatrix} 1 & x_1^{M_1} & x_2^{M_1} & 0 & 0 & 0 \\ 0 & -x_2^{M_1} & 0 & 1 & x_1^{M_1} & 0 \\ 0 & \dfrac{1}{2\mu} n_1^K & \dfrac{1}{2\mu}(1-\nu) n_2^K & 0 & \dfrac{1}{2\mu}\nu n_2^K & n_1^K \\ 0 & -\dfrac{1}{2\mu} n_2^K & \dfrac{1}{2\mu}\nu n_1^K & 0 & \dfrac{1}{2\mu}(1-\nu) n_1^K & n_2^K \\ 1 & x_1^{M_2} & x_2^{M_2} & 0 & 0 & 0 \\ 0 & -x_2^{M_2} & 0 & 1 & x_1^{M_2} & 0 \end{bmatrix}. \tag{3.14}$$

Since M_1, M_2 and K are different, the matrix $\mathbf{T}^e$ is invertible.

For our later considerations a new local coordinate system (η_1, η_2), centered at the point $M_1(x_1, x_2)$ is introduced. The axes η_1 and η_2 are parallel to the axes x_1 and x_2 of the global coordinate system. For the shape functions in the local system we get from (3.10) that

$$\begin{bmatrix} \mathcal{F}_1 \\ \mathcal{F}_2 \\ -\varphi_3 \end{bmatrix}^e = \begin{bmatrix} (a_1 + a_2 x_1 + a_3 x_2) + a_2 \eta_1 + a_3 \eta_2 \\ (a_4 + a_5 x_1 - a_2 x_2) + a_5 \eta_1 - a_2 \eta_2 \\ a_6 \end{bmatrix} = \begin{bmatrix} \hat{a}_1 + a_2 \eta_1 + a_3 \eta_2 \\ \hat{a}_4 + a_5 \eta_1 - a_2 \eta_2 \\ a_6 \end{bmatrix}. \tag{3.15}$$

The vector of constants in the local system is denoted by

$$(\hat{\mathbf{a}}^e)^T = \left[\begin{array}{cccccc} \hat{a}_1 & a_2 & a_3 & \hat{a}_4 & a_5 & a_6 \end{array} \right] . \tag{3.16}$$

It can be shown with ease that the following relation holds

$$\hat{\mathbf{a}}^e = \mathbf{B}\,\mathbf{a}^e , \tag{3.17}$$

where the transformation matrix $\mathbf{B}$ depends only on the coordinates x_1 and x_2 of the point M_1:

$$\mathbf{B} = \begin{bmatrix} 1 & x_1^{M_1} & x_2^{M_1} & 0 & 0 & 0 \\ 0 & 1 & 0 & 0 & 0 & 0 \\ 0 & 0 & 1 & 0 & 0 & 0 \\ 0 & -x_2^{M_1} & 0 & 1 & x_1^{M_1} & 0 \\ 0 & 0 & 0 & 0 & 1 & 0 \\ 0 & 0 & 0 & 0 & 0 & 1 \end{bmatrix} . \tag{3.18}$$

Relation (3.15) is a linear combination of those linearly independent state vectors which satisfy the fundamental equation:

$$\begin{aligned} \mathfrak{u}_1^T &= \left[\begin{array}{ccc} 1 & 0 & 0 \end{array} \right] , & \mathfrak{u}_2^T &= \left[\begin{array}{ccc} \eta_1 & -\eta_2 & 0 \end{array} \right] , \\ \mathfrak{u}_3^T &= \left[\begin{array}{ccc} \eta_2 & 0 & 0 \end{array} \right] , & \mathfrak{u}_4^T &= \left[\begin{array}{ccc} 0 & 1 & 0 \end{array} \right] , \\ \mathfrak{u}_5^T &= \left[\begin{array}{ccc} 0 & \eta_1 & 0 \end{array} \right] , & \mathfrak{u}_6^T &= \left[\begin{array}{ccc} 0 & 0 & 1 \end{array} \right] . \end{aligned} \tag{3.19}$$

The functions $\phi_{\kappa i}$ that follow from the vectors $\mathfrak{u}_i$ $(i = 1, \ldots, 6)$ have been calculated by making use of equation (3.7). These functions are given in the Appendix. In what follows we shall assume that the origin of the local coordinate system is located at the collocation point Q_j.

4. Discretized equations

The contour $\mathcal{L}_o$ of the region A_i is discretized into n_{be} boundary elements – see Figure 2. The boundary element method equations are enforced only at the end points M_1 and M_2 of the elements. Turning to global numbering we denote these points by Q_j where $j = 1, \ldots, n_{be}$. Let $\mathbf{u}_j^T = [u_1(Q_j) \mid u_2(Q_j)]$ be the matrix of stress functions. The matrix $\mathbf{C}$ is defined by the equation

$$\mathbf{C}(Q_j) = \left[\begin{array}{cc} c_{11}(Q_j) & c_{12}(Q_j) \\ c_{21}(Q_j) & c_{22}(Q_j) \end{array} \right] . \tag{4.1}$$

Exploiting equations (3.13) and (3.17) the boundary integral equation (2.19) can be manipulated into the form

$$\mathbf{C}(Q_j)\mathbf{u}_j = \sum_{e=1}^{n_{be}} \mathbf{\Phi}^{je}\,\mathbf{B}^j\,\left(\mathbf{T}^e\right)^{-1}\,\mathbf{p}^e \qquad j = 1, \ldots, n_{be} , \tag{4.2}$$

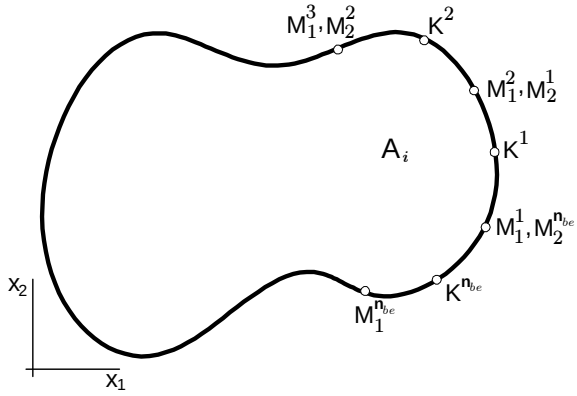

Figure 2.

where

$$\mathbf{\Phi}^{je} = \begin{bmatrix} \phi_{11}^{je}(M_2) - \phi_{11}^{je}(M_1) & \phi_{12}^{je}(M_2) - \phi_{12}^{je}(M_1) & \ldots & \phi_{16}^{je}(M_2) - \phi_{16}^{je}(M_1) \\ \phi_{21}^{je}(M_2) - \phi_{21}^{je}(M_1) & \phi_{22}^{je}(M_2) - \phi_{22}^{je}(M_1) & \ldots & \phi_{26}^{je}(M_2) - \phi_{26}^{je}(M_1) \end{bmatrix}. \tag{4.3}$$

With the notation

$$\mathbf{M}^{je} = \mathbf{\Phi}^{je}\,\mathbf{B}^{j}\,\left(\mathbf{T}^{e}\right)^{-1} \tag{4.4}$$

equation system (4.2) can be cast into the form

$$\underbrace{\begin{bmatrix} \mathbf{M}^{11} & \mathbf{M}^{12} & \ldots & \mathbf{M}^{1n_{be}} \\ \mathbf{M}^{21} & \mathbf{M}^{22} & \ldots & \mathbf{M}^{2n_{be}} \\ \ldots & \ldots & \ldots & \ldots \\ \mathbf{M}^{n_{be}1} & \mathbf{M}^{22} & \ldots & \mathbf{M}^{n_{be}n_{be}} \end{bmatrix}}_{2n_{be}\times 6n_{be}} \underbrace{\begin{bmatrix} \mathbf{p}^1 \\ \mathbf{p}^2 \\ \ldots \\ \mathbf{p}^{n_{be}} \end{bmatrix}}_{2n_{be}\times 1} = \underbrace{\begin{bmatrix} \mathbf{C}(Q_1)\,\mathbf{u}_1 \\ \mathbf{C}(Q_2)\,\mathbf{u}_2 \\ \ldots \\ \mathbf{C}(Q_{n_{be}})\,\mathbf{u}_{n_{be}} \end{bmatrix}}_{2n_{be}\times 1}, \tag{4.5}$$

where

$$\begin{aligned} \left(\mathbf{p}^1\right)^T &= \begin{bmatrix} \mathcal{F}_1^{1M_1} & \mathcal{F}_2^{1M_1} & \mathfrak{t}_1^{1K} & \mathfrak{t}_2^{1K} & \mathcal{F}_1^{1M_2} & \mathcal{F}_2^{1M_2} \end{bmatrix} \\ \left(\mathbf{p}^2\right)^T &= \begin{bmatrix} \mathcal{F}_1^{2M_1} & \mathcal{F}_2^{2M_1} & \mathfrak{t}_1^{2K} & \mathfrak{t}_2^{2K} & \mathcal{F}_1^{2M_2} & \mathcal{F}_2^{2M_2} \end{bmatrix} \end{aligned} \tag{4.6a}$$

and

$$\left(\mathbf{p}^{n_{be}}\right)^T = \begin{bmatrix} \mathcal{F}_1^{n_{be}M_1} & \mathcal{F}_2^{n_{be}M_1} & \mathfrak{t}_1^{n_{be}K} & \mathfrak{t}_2^{n_{be}K} & \mathcal{F}_1^{n_{be}M_2} & \mathcal{F}_2^{n_{be}M_2} \end{bmatrix}. \tag{4.6b}$$

With regard to the assumed continuity of the stress functions at the points Q_j we have

$$\mathcal{F}_\lambda^{n_{be}M_2} = \mathcal{F}_\lambda^{1M_1}, \quad \mathcal{F}_\lambda^{eM_2} = \mathcal{F}_\lambda^{(e+1)M_1} \qquad e = 1, \ldots, n_{be} - 1\,. \tag{4.7}$$

Introducing the notation

$$\mathbf{M}^e = \begin{bmatrix} \mathbf{M}^{1e} \\ \mathbf{M}^{2e} \\ \dots \\ \mathbf{M}^{n_{be}e} \end{bmatrix} \qquad e = 1, \dots, n_{be} \tag{4.8}$$

and taking equation (4.7) into account one can see that the last two columns of the matrix $\mathbf{M}^e$ and the first two columns of the next matrix $\mathbf{M}^{e+1}$ are multiplied, due to the continuity, by the same $\mathcal{F}_\lambda$. Accordingly, the corresponding columns can be added to each other. It is also obvious that the last two columns of the matrix $\mathbf{M}^{n_{be}}$ should be added to the first two columns of the matrix $\mathbf{M}^1$. After these transformations the size of the equation system (4.5) has been decreased. Finally we have

$$\mathbf{H}\,\mathbf{f} = \mathbf{q}\,, \tag{4.9}$$

where $\mathbf{H}$ is a matrix with size $(2n_{be} * 4n_{be})$,

$$\mathbf{f} = \begin{bmatrix} \mathcal{F}_1^{1M_1} & \mathcal{F}_2^{1M_1} & \mathfrak{t}_1^{1K1} & \mathfrak{t}_2^{1K1} & \mathcal{F}_1^{2M_2} & \mathcal{F}_2^{2M_2} & \dots & \mathcal{F}_1^{n_{be}M_{n_{be}}} & \mathcal{F}_1^{n_{be}M_{n_{be}}} \end{bmatrix} \tag{4.10}$$

is the vector of physical quantities and $\mathbf{q}$ is the right side of equation system (4.5).

It should be noted that the functions ϕ_{11}, ϕ_{21}, ϕ_{14} and ϕ_{24} which have been obtained from the constant shape functions, are singular when the point of effect M approaches the source point Q_j because the distance between the two points tends to zero. In order to avoid strongly singular integrals we should take into account that $\mathfrak{t}_\lambda(\overset{o}{M}) = 0$ if $\mathfrak{u}_\lambda(\overset{o}{Q}) = \mathfrak{u}_\lambda(\overset{o}{M}) = \text{constant}$. Under this condition equation (2.20) yields

$$c_{\kappa\lambda}(\overset{o}{Q})\mathfrak{u}_\lambda(\overset{o}{Q}) = \sum_{e=1}^{n_{be}} \int_{\mathfrak{L}_e} n_\rho(\overset{o}{M}) \left(\epsilon_{\rho\pi 3} \overset{*}{e}_{\kappa\pi\lambda}(\overset{o}{M}, \overset{o}{Q}) - \delta_{\rho\lambda} \overset{*}{\mathfrak{U}}_{\kappa 3}(\overset{o}{M}, \overset{o}{Q}) \right) \mathfrak{u}_\lambda(\overset{o}{Q})\, \mathrm{d}s_{\overset{o}{M}}\,. \tag{4.11}$$

Subtracting now equation (4.11) from (2.20) we obtain

$$\begin{aligned} 0 = \sum_{e=1}^{n_{be}} \int_{\mathfrak{L}_e} & -n_\rho(\overset{o}{M}) \mathfrak{U}_{\kappa\lambda}(\overset{o}{M}, \overset{o}{Q}) \left(\epsilon_{\rho\pi 3} e_{\pi\lambda}(\overset{o}{M}) - \delta_{\rho\lambda} \varphi_3(\overset{o}{M}) \right) + \\ & + n_\rho(\overset{o}{M}) \left(\epsilon_{\rho\pi 3} \overset{*}{e}_{\kappa\pi\lambda}(\overset{o}{M}, \overset{o}{Q}) - \delta_{\rho\lambda} \overset{*}{\mathfrak{U}}_{\kappa 3}(\overset{o}{M}, \overset{o}{Q}) \right) \left(\mathfrak{u}_\lambda(\overset{o}{M}) - \mathfrak{u}_\lambda(\overset{o}{Q}) \right) \mathrm{d}s_{\overset{o}{M}}\,. \end{aligned} \tag{4.12}$$

After this transformation $c_{\kappa\lambda}(\overset{o}{Q})$ has also been eliminated from the equation. Equation (4.12) differs from equation (2.20) in the extra term

$$n_\rho(\overset{o}{M}) \left(\epsilon_{\rho\pi 3} \overset{*}{e}_{\kappa\pi\lambda}(\overset{o}{M}, \overset{o}{Q}) - \delta_{\rho\lambda} \overset{*}{\mathfrak{U}}_{\kappa 3}(\overset{o}{M}, \overset{o}{Q}) \right) \mathfrak{u}_\lambda(\overset{o}{Q})\,. \tag{4.13}$$

This term is divergence free, therefore the new coefficient of $n_\rho(\overset{o}{M})$ on the right side is also divergence free. Thus, for this purpose, $\mathfrak{u}_\lambda(\overset{o}{Q})$ can be regarded as a constant.

If we consider the j-th element which involves the source point $\overset{o}{Q}$ at its first nodal point M_1, then these constants are denoted by $\mathfrak{u}_1(\overset{o}{Q}) = \hat{a}_1^j$ and $\mathfrak{u}_2(\overset{o}{Q}) = \hat{a}_4^j$ in the local coordinate system. With these notations for the e-th element we get

$$\left(\mathfrak{u}_\lambda(\overset{o}{M}) - \mathfrak{u}_\lambda(\overset{o}{Q})\right)^e = \mathbf{U}^e\left(\eta_1, \eta_2\right)\, \tilde{\mathbf{a}}^e \tag{4.14}$$

where the columns of $\mathbf{U}^e\left(\eta_1, \eta_2\right)$ are formed by the vectors $\mathfrak{u}_i \;\; (i = 1, \ldots, 6)$. The vector of constants $\tilde{\mathbf{a}}^e$ can now be rewritten as

$$\left(\tilde{\mathbf{a}}^e\right)^T = \left[\begin{array}{cccccc} \left(\hat{a}_1^e - \hat{a}_1^j\right) & a_2^e & a_3^e & \left(\hat{a}_4^e - \hat{a}_4^j\right) & a_5^e & a_6^e \end{array}\right]. \tag{4.15}$$

ϕ_{11}, ϕ_{21}, ϕ_{14} and ϕ_{24} are singular when the point of effect approaches the source point, but in this case $\hat{a}_1^e = \hat{a}_1^j$ and $\hat{a}_4^e = \hat{a}_4^j$, therefore we can avoid the evaluation of these potential functions. Consequently the line of thought presented in Section 3 can be repeated word by word and it turns out that the functions $\phi_{\kappa i}$ will remain unchanged. Finally the discretized equation corresponding to the equation (4.12) assumes the form

$$\mathbf{0} = \sum_{e=1}^{n_{be}} \mathbf{\Phi}^{je}\, \tilde{\mathbf{a}}^e \qquad j = 1, \ldots, n_{be} \tag{4.16}$$

where the elements of the matrix $\mathbf{\Phi}^{je}$ are those integrals obtained from the shape functions. The structure of the matrix $\mathbf{\Phi}^{je}$ has already been presented – see equation (4.3).

The next transformation becomes clearer, if the equation (4.16) is written out in full:

$$\underbrace{\left[\begin{array}{cccc} \mathbf{\Phi}^{11} & \mathbf{\Phi}^{12} & \ldots & \mathbf{\Phi}^{1n_{be}} \\ \mathbf{\Phi}^{21} & \mathbf{\Phi}^{22} & \ldots & \mathbf{\Phi}^{2n_{be}} \\ \ldots & \ldots & \ldots & \ldots \\ \mathbf{\Phi}^{n_{be}1} & \mathbf{\Phi}^{22} & \ldots & \mathbf{\Phi}^{n_{be}n_{be}} \end{array}\right]}_{\mathbf{\Phi}} \left[\begin{array}{c} \tilde{\mathbf{c}}^1 \\ \tilde{\mathbf{c}}^2 \\ \ldots \\ \tilde{\mathbf{c}}^{n_{be}} \end{array}\right] = \left[\begin{array}{c} 0 \\ 0 \\ \ldots \\ 0 \end{array}\right]. \tag{4.17}$$

Clearly, if the j-th element (j is the equation counter or, which is the same, the block row counter) coincides with the e-th element (e is the element counter or which is the same the block column counter), then we are in the main diagonal, i.e., the j-th element involves the source point, consequently $\hat{a}_1^e - \hat{a}_1^j = 0$ and $\hat{a}_4^e - \hat{a}_4^j = 0$. Thus the singular terms $\phi_{\kappa 1}^{jj}(M_1)$, $\phi_{\kappa 4}^{jj}(M_1)$ of the matrix $\phi_{\kappa i}^{jj}(M_1)$ drop out and the other terms in matrix $\phi_{\kappa i}^{jj}(M_1)$ have already been zero. With regard to the assumed continuity of the stress functions at the nodal points, the previous establishment is true for the matrix $\phi_{\kappa i}^{jj-1}(M_2)$.

Decompose $\tilde{\mathbf{a}}^e$ into two parts. The first part is the vector $\hat{\mathbf{a}}^e$, the part left is denoted by

$$\left(\mathbf{d}^e\right)^T = \left[\begin{array}{cccccc} -\hat{a}_1^j & 0 & 0 & -\hat{a}_4^j & 0 & 0 \end{array}\right]. \tag{4.18}$$

The point M_2 of the element e coincides with the point M_1 of the element $e+1$. Assuming continuity it follows that $\phi^e_{\kappa i}(M_2) = \phi^{e+1}_{\kappa i}(M_1)$, therefore we can write

$$\mathbf{0} = \sum_{e=1}^{n_{be}} \mathbf{\Phi}^{je}\, \mathbf{d}^e \qquad j = 1, \ldots, n_{be}\,. \tag{4.19}$$

With regard to equation (4.19), the following relations hold for the diagonal blocks of the matrix $\mathbf{\Phi}$:

$$\mathbf{\Phi}^{kk} = \begin{bmatrix} \phi^{kk}_{11}(M_2) & \phi^{kk}_{12}(M_2) & \ldots & \phi^{kk}_{16}(M_2) \\ \phi^{kk}_{21}(M_2) & \phi^{kk}_{22}(M_2) & \ldots & \phi^{kk}_{26}(M_2) \end{bmatrix} \qquad k = 1, \ldots, n_{be}\,. \tag{4.20a}$$

In the same way we have

$$\mathbf{\Phi}^{k,k-1} = \begin{bmatrix} -\phi^{k,k-1}_{11}(M_1) & -\phi^{k,k-1}_{12}(M_1) & \ldots & -\phi^{k,k-1}_{16}(M_1) \\ -\phi^{k,k-1}_{21}(M_1) & -\phi^{k,k-1}_{22}(M_1) & \ldots & -\phi^{k,k-1}_{26}(M_1) \end{bmatrix} \qquad k = 2, \ldots, n_{be} \tag{4.20b}$$

and

$$\mathbf{\Phi}^{1,n_{be}-1} = \begin{bmatrix} -\phi^{1,n_{be}-1}_{11}(M_1) & -\phi^{1,n_{be}-1}_{12}(M_1) & \ldots & -\phi^{1,n_{be}-1}_{16}(M_1) \\ -\phi^{1,n_{be}-1}_{21}(M_1) & -\phi^{1,n_{be}-1}_{22}(M_1) & \ldots & -\phi^{1,n_{be}-1}_{26}(M_1) \end{bmatrix}. \tag{4.20c}$$

Making use of equations (4.20a,b,c), (3.13) and (3.17), equation system (4.17) can be manipulated into the form

$$\mathbf{0} = \sum_{e=1}^{n_{be}} \mathbf{\Phi}^{je}\, \hat{\mathbf{a}}^e = \sum_{e=1}^{n_{be}} \mathbf{\Phi}^{je}\, \mathbf{B}^j\, \left(\mathbf{T}^{-1}\right)^e\, \mathbf{p}^e \qquad j = 1, \ldots, n_{be}\,. \tag{4.21}$$

We remark that this equation is originated from the second dual Somiglina formula (2.20). Introducing the notation

$$\mathbf{N}^{je} = \mathbf{\Phi}^{je}\, \mathbf{B}^j\, \left(\mathbf{T}^e\right)^{-1} \tag{4.22}$$

the equation system (4.21) can be written as

$$\sum_{e=1}^{n_{be}} \mathbf{N}^{je} \mathbf{p}^e = 0^e \qquad j = 1, \ldots, n_{be}\,. \tag{4.23}$$

It has not been taken into account so far that the matrices $\mathbf{p}^e$ should meet the continuity condition (4.7). Under this condition the line of thought leading to (4.9) can be repeated word by word. Finally we get

$$\mathbf{K}\,\mathbf{f} = \mathbf{0}\,, \tag{4.24}$$

where $\mathbf{K}$ is a matrix with size $(2n_{be} * 4n_{be})$ and $\mathbf{f}$ denotes the vector of physical quantities – see (4.10) for details.

5. Stresses at internal points

If the physical quantities at the nodal points are known, then for computing the vectors of constants we should apply the equation

$$\mathbf{a}^e = [\mathbf{T}^e]^{-1}\, \mathbf{p}^e\,. \tag{5.1}$$

With the knowledge of the vector $\mathbf{a}^e$ we can compute the stress functions at an arbitrary point. Making use of the equation (2.19) and applying the notations we have introduced, equation (2.19) can be manipulated into the form

$$\mathbf{u}(Q) = \sum_{e=1}^{n_{be}} \mathbf{\Phi}^{Qe}\, \mathbf{B}^Q\, \mathbf{a}^e \tag{5.2}$$

where $\mathbf{B}^Q$ is the transformation matrix corresponding to the internal source point Q. Recalling equation (2.1) for the stress components at Q we can write

$$\begin{aligned} \sigma_{11} &= \frac{\partial \mathbf{u}_1(Q)}{\partial x_2}\,, \qquad & \tau_{12} &= \frac{\partial \mathbf{u}_2(Q)}{\partial x_2}\,, \\ \tau_{21} &= -\frac{\partial \mathbf{u}_1(Q)}{\partial x_1}\,, \qquad & \sigma_{22} &= -\frac{\partial \mathbf{u}_2(Q)}{\partial x_1}\,. \end{aligned} \tag{5.3}$$

Derivatives of the stress functions are obtained from equation (5.2)

$$\mathbf{u}(Q)\partial x_\alpha = \sum_{e=1}^{n_{be}} \left[(\mathbf{\Phi}^{Qe}\partial x_\alpha)\, \mathbf{B}^Q + \mathbf{\Phi}^{Qe}\, (\mathbf{B}^Q \partial x_\alpha) \right]\, \mathbf{a}^e\,. \tag{5.4}$$

Using equation (2.11) the above equation (5.4) can be rewritten as

$$\mathbf{u}(Q)\partial x_\alpha = \sum_{e=1}^{n_{be}} \left[\mathbf{\Phi}^{Qe}\, (\mathbf{B}^Q \partial x_\alpha) - (\mathbf{\Phi}^{Qe}\partial \eta_\alpha)\, \mathbf{B}^Q \right]\, \mathbf{a}^e\,. \tag{5.5}$$

6. Examples

The main step of the numerical computations consists in solving the equation system (4.24). It is worthy of repeating that the matrix $\mathbf{K}$ is not a square one and the vector $\mathbf{f}$ involves the physical quantities. The total number of physical quantities is $4n_{be}$ on the contour $\mathfrak{L}_o$. Some of them are known from the boundary conditions. (Three physical quantities can be prescribed from the six possible physical quantities on each element. The total number of the physical quantities that can be prescribed is, however, less than $3 \times 2n_{be}$ since continuity must hold at the extremities.) The columns of the matrix $\mathbf{K}$ that are multiplied by the prescribed quantities should be grouped on the right side of the equation to get the right side of the equation system to be solved. We should know at least $2n_{be}$ physical quantities from the boundary conditions to get a solvable linear equation system.

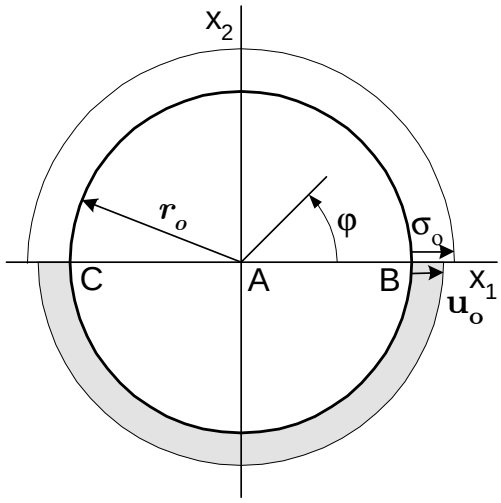

In case of mixed boundary value problems we have more equations than the number of unknowns. If we regard some of the prescribed quantities as unknowns, then we can obtain a solvable linear equation system.

Two simple numerical examples are presented. The material properties ($\mu = 8 \cdot 10^4$ MPa, $\nu = 0.3$) are the same for each example.

Problem 1. First we shall consider a circular region with radius $r_0 = 10$ mm. On the arc BC of the contour for which the polar angle $\varphi \in [0, \pi]$ the normal stress is $\sigma_o = 100$ MPa and there is no shear stress. On the arc CB of the contour $u_o = (1 - 2\nu)\sigma_o r_o / 2\mu$ is the radial displacement and there is no displacement in the circumferential direction – see Figure 3. In this case

$$\mathcal{F}_1 = \sigma_\mathrm{o} x_2 = \sigma_\mathrm{o} r \sin\varphi\,, \qquad \mathcal{F}_2 = -\sigma_\mathrm{o} x_1 = -\sigma_\mathrm{o} r \cos\varphi\,,$$

$$\sigma_{11} = \sigma_{22} = \sigma_\mathrm{o} = 100\,\mathrm{MPa}\,, \qquad \tau_{12} = 0\,,$$

$$u_1 = \frac{1-2\nu}{2\mu}\sigma_\mathrm{o} r \sin\varphi\,, \qquad u_2 = \frac{1-2\nu}{2\mu}\sigma_\mathrm{o} r \cos\varphi\,.$$

The exact solutions for this problem are given by the equations

$$\mathrm{u}_1 = \mathcal{F}_1 = \sigma_\mathrm{o} r_\mathrm{o} \sin\varphi\,, \qquad \mathrm{u}_2 = \mathcal{F}_2 = -\sigma_\mathrm{o} r_\mathrm{o} \cos\varphi\,,$$

$$\mathrm{t}_1 = \frac{1-2\nu}{2\mu}\sigma_\mathrm{o} \sin\varphi\,, \qquad \mathrm{t}_2 = -\frac{1-2\nu}{2\mu}\sigma_\mathrm{o} \cos\varphi\,.$$

where r and φ are polar coordinates. One can check with ease that these solutions determine a homogenous state of stress. At the internal points the exact solutions for

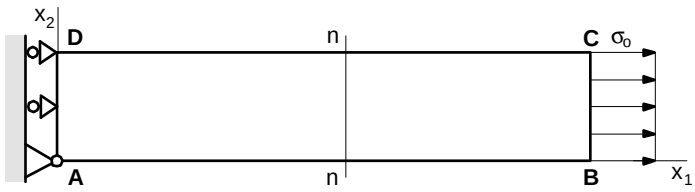

the stresses are as follows:

$$\sigma_{11} = \sigma_{22} = \sigma_{\mathrm{o}} = 100 \text{ [MPa]}, \qquad \tau_{12} = 0 \, .$$

Table 1 below represents numerical results at various internal points.

Table 1: Solutions for stress components

x_1 [mm]	x_2 [mm]	σ_{11} [MPa]	τ_{12} [MPa]	σ_{22} [MPa]
-8.00	0.00	100.00	$1.69{\cdot}10^{-15}$	100.00
-6.00	0.00	100.00	$7.61{\cdot}10^{-15}$	100.00
-4.00	0.00	100.00	$1.07{\cdot}10^{-14}$	100.00
-2.00	0.00	100.00	$1.12{\cdot}10^{-14}$	100.00
0.00	0.00	99.99	0.08	100.00
2.00	0.00	100.00	$1.69{\cdot}10^{-13}$	100.00
4.00	0.00	100.00	0	100.00
5.00	5.00	100.00	$5.73{\cdot}10^{-15}$	100.00
5.00	7.00	100.00	$1.73{\cdot}10^{-14}$	100.00

Problem 2. The width and length of the rectangle $ABCD$ in plane strain are 20 mm and 100 mm, respectively. The rectangle is subjected to a horizontal and uniform load $\sigma_o = 200$ MPa on the line BC. The upper and lower sides are, however, unloaded. The right end of the region is supported as shown in Figure 3. In this case the solutions computed are comparable with the solutions $\sigma_{11} = 200$ MPa, $\tau_{12} = 0$ and $\sigma_{22} = 0$ valid for a bar in tension. Table 2 below contains numerical results for the stresses at some internal points located on the line $n - n$ ($x_1 = 50$ mm).

Table 2: Solutions for stress components

x_1 [mm]	x_2 [mm]	σ_{11} [MPa]	τ_{12} [MPa]	σ_{22} [MPa]
50.00	2.00	200.00	$7.42{\cdot}10^{-17}$	$-3.46{\cdot}10^{-15}$
50.00	4.00	200.00	$-1.38{\cdot}10^{-17}$	$2.53{\cdot}10^{-15}$
50.00	6.00	200.00	$-7.63{\cdot}10^{-17}$	$-4.73{\cdot}10^{-15}$
50.00	8.00	199.99	$8.60{\cdot}10^{-16}$	$3.88{\cdot}10^{-16}$

7. Conclusion

The boundary contour method for plane problems of elasticity in a dual formulation (regarding the stress functions of order one and the rigid body rotation as unknowns) is presented in this paper. After having shown what form the Somigliana formulae have in the dual system of elasticity we proved that the integrand of the direct method is divergence free like the case of primal system [1,2]. Making use of this property an implementation is carried out with linear approximation and the idea that there are no stresses due to constant stress functions has also been taken into account. The corresponding shape functions ϕ_{ki} are also given. It is an advantage of the resulting system of linear equations that there is no need to perform numerical integration when one computes the coefficient matrix and the right side. It is a further advantage that computation of stresses on the boundary elements requires derivations, that is, on the contrary to conventional BEM, one can avoid computation of singular integrals. Two simple examples are given to illustrate the applicability of the method.

It is the aim of our further investigations to apply quadratic approximation and to clarify how to use the method for outer regions if there is a constant stress state at infinity. This work is in progress.

8. Appendix

The compatibility equation and the symmetry conditions for the elastic state $\overset{*}{\mathfrak{u}}_\lambda$ are of the form

$$\left[\epsilon_{\rho\pi 3}\overset{*}{e}_{\kappa\pi\lambda}(\overset{o}{M},Q)-\delta_{\rho\lambda}\mathfrak{U}_{\kappa 3}(\overset{o}{M},Q)\right]\overset{M}{\partial}_\rho=0 \tag{8.1}$$

and

$$\epsilon_{\lambda\pi 3}\overset{*}{\mathfrak{t}}_{\kappa\pi\lambda}=0 \tag{8.2}$$

Since $\overset{*}{\mathfrak{t}}_{\kappa\pi\lambda}$ and $e_{\kappa\lambda}$ are 'elastic states' we can write

$$\overset{*}{\mathfrak{t}}_{\kappa\pi\lambda}e_{\pi\lambda}=\mathfrak{t}_{\pi\lambda}\overset{*}{e}_{\kappa\pi\lambda} \tag{8.3}$$

With regard to (2.3), (2.4), (8.1), (8.2) and (8.3) it follows from (3.6) that

$$\begin{aligned}P_{\kappa\rho}(M,Q)\overset{M}{\partial}_\rho=&-\left(\mathfrak{U}_{\kappa\lambda}(\overset{o}{M},Q)\overset{M}{\partial}_\rho\right)\left(\epsilon_{\rho\pi 3}e_{\pi\lambda}(\overset{o}{M})-\delta_{\rho\lambda}\varphi_3(\overset{o}{M})\right)-\\&-\mathfrak{U}_{\kappa\lambda}(\overset{o}{M},Q)\left(\left[\epsilon_{\rho\pi 3}e_{\pi\lambda}(\overset{o}{M})-\delta_{\rho\lambda}\varphi_3(\overset{o}{M})\right]\overset{M}{\partial}_\rho\right)+\\&+\left(\left[\epsilon_{\rho\pi 3}\overset{*}{e}_{\kappa\pi\lambda}(\overset{o}{M},Q)-\delta_{\rho\lambda}\mathfrak{U}_{\kappa 3}(\overset{o}{M},Q)\right]\overset{M}{\partial}_\rho\right)\mathfrak{u}_\lambda(\overset{o}{M})+\\&+\left(\epsilon_{\rho\pi 3}\overset{*}{e}_{\kappa\pi\lambda}(\overset{o}{M},Q)-\delta_{\rho\lambda}\mathfrak{U}_{\kappa 3}(\overset{o}{M},Q)\right)\left(\mathfrak{u}_\lambda(\overset{o}{M})\overset{M}{\partial}_\rho\right)=\end{aligned}$$

$$= -\left(\mathfrak{U}_{\kappa\lambda}(\overset{o}{M},Q)\overset{M}{\partial}_{\rho}\right)\epsilon_{\rho\pi 3}e_{\pi\lambda}(\overset{o}{M}) + \epsilon_{\rho\pi 3}\overset{*}{e}_{\kappa\pi\lambda}(\overset{o}{M},Q)\left(\mathfrak{u}_{\lambda}(\overset{o}{M})\overset{M}{\partial}_{\rho}\right) +$$

$$+\left(\mathfrak{U}_{\kappa\lambda}(\overset{o}{M},Q)\overset{M}{\partial}_{\rho}\epsilon_{\rho\pi 3}\right)\epsilon_{\lambda\pi 3}\varphi_3(\overset{o}{M}) - \left(\mathfrak{u}_{\lambda}(\overset{o}{M})\overset{M}{\partial}_{\rho}\epsilon_{\rho\pi 3}\right)\epsilon_{\lambda\pi 3}\mathfrak{U}_{\kappa 3}(\overset{o}{M},Q) =$$

$$= -\overset{*}{\mathfrak{t}}_{\kappa\pi\lambda}e_{\pi\lambda} + \mathfrak{t}_{\pi\lambda}\overset{*}{e}_{\kappa\pi\lambda} + \epsilon_{\lambda\pi 3}\overset{*}{\mathfrak{t}}_{\kappa\pi\lambda}\varphi_3(\overset{o}{M}) - \epsilon_{\lambda\pi 3}\mathfrak{t}_{\kappa\pi}\overset{*}{\varphi}_3(\overset{o}{M}) = 0$$

In other words $P_{\kappa\rho}$ is divergence free.

Without entering into details, below we list the shape functions:

$$\phi_{11} = \frac{1}{2\pi}\arctan\frac{\eta_2}{\eta_1} + \frac{1}{4\pi(1-\nu)}\frac{\eta_1\eta_2}{\eta_1^2+\eta_2^2}$$

$$\phi_{12} = \frac{-1}{4\pi(1-\nu)}\eta_2\left(\ln\sqrt{\eta_1^2+\eta_2^2} + \frac{4\nu-3}{2} + \frac{2\eta_2^2}{\eta_1^2+\eta_2^2}\right)$$

$$\phi_{13} = \frac{1}{4\pi(1-\nu)}\eta_1\left((1-\nu)\ln\sqrt{\eta_1^2+\eta_2^2} + \frac{3-\nu}{2} - \frac{\eta_1^2}{\eta_1^2+\eta_2^2}\right)$$

$$\phi_{14} = \frac{-1}{4\pi(1-\nu)}\left((1-2\nu)\ln\sqrt{\eta_1^2+\eta_2^2} + \frac{\eta_1^2}{\eta_1^2+\eta_2^2}\right)$$

$$\phi_{15} = \frac{1}{4\pi(1-\nu)}\eta_1\left(\nu\ln\sqrt{\eta_1^2+\eta_2^2} + \frac{5\nu}{2} - \frac{\eta_1^2}{\eta_1^2+\eta_2^2}\right)$$

$$\phi_{16} = \frac{-\mu}{4\pi(1-\nu)}\eta_2\left(2\ln\sqrt{\eta_1^2+\eta_2^2} + 3\right)$$

$$\phi_{21} = \frac{1}{4\pi(1-\nu)}\left((1-2\nu)\ln\sqrt{\eta_1^2+\eta_2^2} + \frac{\eta_2^2}{\eta_1^2+\eta_2^2}\right)$$

$$\phi_{22} = \frac{-1}{4\pi(1-\nu)}\eta_1\left(\ln\sqrt{\eta_1^2+\eta_2^2} + \frac{4\nu-3}{2} + \frac{2\eta_1^2}{\eta_1^2+\eta_2^2}\right)$$

$$\phi_{23} = \frac{-1}{4\pi(1-\nu)}\eta_2\left(\nu\ln\sqrt{\eta_1^2+\eta_2^2} + \frac{5\nu}{2} - \frac{\eta_2^2}{\eta_1^2+\eta_2^2}\right)$$

$$\phi_{24} = -\frac{1}{2\pi}\arctan\frac{\eta_1}{\eta_2} - \frac{1}{4\pi(1-\nu)}\frac{\eta_1\eta_2}{\eta_1^2+\eta_2^2}$$

$$\phi_{25} = \frac{-1}{4\pi(1-\nu)}\eta_2\left((1-\nu)\ln\sqrt{\eta_1^2+\eta_2^2} + \tfrac{3-\nu}{2} - \frac{\eta_2^2}{\eta_1^2+\eta_2^2}\right)$$

$$\phi_{26} = \frac{\mu}{4\pi(1-\nu)}\eta_1\left(2\ln\sqrt{\eta_1^2+\eta_2^2} + 3\right)$$

Acknowledgement. The support provided by the Hungarian National Research Foundation (project No. T031998) is gratefully acknowledged.

REFERENCES

1. Nagarjan, A. Lutz, E. and Mukherjee, S.: *A novel boundary element method for linear elasticity with no numerical integration for two dimensional and line integrals for three-dimensional problems*, Journal of Applied Mechanics, **264** (61), (1994), 264-269.
2. Phan, A. V., Mukherjee, S. and Mayer, J. R. R.: *The boundary contour method for two-dimensional linear elasticity with quadratic boundary elements*, Computational Mechanics, **20**, (1997), 310-319.
3. Phan, A. V., Mukherjee, S. and Mayer, J. R. R.: *Stresses, stress sensitivities and shape optimization in two dimensional linear elasticity by the boundary contour method*, International Journal for Numerical Methods in Engineering, **42**, (1998), 1391-1407.
4. Szeidl, G.: *Dual problems in continuum mechanics (Derivation of the defining equations, Single valuedness of mixed boundary value problems, Boundary element method for plane problems)*, Habilitation Thesis of the University of Miskolc, Miskolc, 1997, i-vii, 1-65. (in Hungarian)

Journal of Computational and Applied Mechanics, Vol. 1., No. 2., (2000), pp. 223–233

CONTACT ANALYSIS OF COMPOSITE AND STEEL SURFACES IN SLIDING CONTACT

Károly Váradi, Zoltán Néder
Institute of Machine Design, Technical University of Budapest
Műegyetem rkp. 3., Budapest, Hungary, H-1111
varadik@eik.bme.hu

Klaus Friedrich
Institute for Composite Materials Ltd. (IVW), University of Kaiserslautern
Erwin-Schrödinger str. Geb. 58, Kaiserslautern, Germany, D-67663
friedrich@ivw.uni-kl.de

[Received: May 15, 2000]

Abstract. An anisotropic numerical contact algorithm has been developed for real composite-steel surfaces in sliding contact. The results were based on measured surface roughness data, under conditions of different fibre orientations relative to the sliding direction. The location of the real contact area at certain positions of sliding contact could be predicted. These results can be considered as input data for contact temperature calculations and wear predictions.

Keywords: Anisotropic numerical contact algorithm, sliding contact, real contact area

1. Introduction

Sliding contact of metal bodies having real engineering surfaces can usually be characterised as load transmission through isolated contact spots forming the real contact area. Over the real contact area the real contact pressure is much higher than the nominal contact pressure. The denominations are shown in Figure 1. Sliding contact

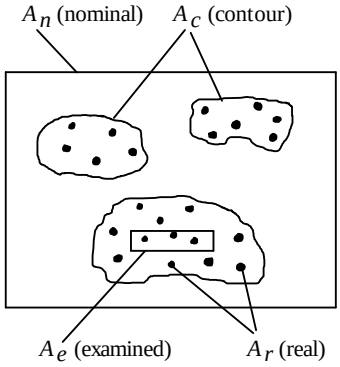

Figure 1. Definitons of different contact areas

of composite-steel bodies produces a slightly different behaviour due to the anisotropy of the composite material, the fibre-matrix structure, etc. At the starting moment of the wear process an asperity type contact may dominate the situation, but after a certain running-in period other conditions can be found, such as the formation of a flat layer of debris material due to matrix wear and worn fibre particles. In addition, in the case of unidirectional composites, the fibre orientation, relative to the sliding direction, also has a dominant effect on the wear mechanism.

To evaluate the contact parameters of rough surfaces different models were developed in the last two decades [1-6]. In the earlier analytical and numerical solutions elastic models were applied, later elastic-plastic or plastic models with different plastic limit pressure (p^*) conditions [2, 6] were introduced. In these considerations p^* was equal to (1.6,...,3.0)σ_Y, where σ_Y is the yield strength of the material.

Anisotropic contact problems were studied in [7-9]. In these works the plane of isotropy was oriented normal to the plane of contact. Váradi et al. extended their isotropic contact algorithm [5] to solve anisotropic contact problems [10] by using the influence matrix approach where the elements of the anisotropic influence matrix were obtained by coupled FE models. The approximate coupling technique considered only the displacements along the coupled surfaces. Their numerical algorithm took into consideration the non-linear material behaviour of a composite structure, based on plastic limit pressure condition, using an approximate approach. Ovaert and Ramachandra [11] used a 2D contact model to estimate the mean asperity contact pressure and the real area of contact of the worn polymer specimens after sliding against hardened steel disks.

Table 1. Mechanical and thermal properties of the materials in sliding contact E, G and ν are the anisotropic elastic material properties, σ_Y is the yield strength of the isotropic materials)

$V_f = 0.6$	Steel [13]	CF[14]	PEEK [14]	CF/PEEK Composite (calculated)
E_{11} [MPa]	210000	235000	3600	142440
E_{22} [MPa]		15000		6618
E_{33} [MPa]		15000		6618
G_{12} [MPa]	80769	6432	1286	2932
G_{13} [MPa]		6432		2932
G_{23} [MPa]		5357		2196
ν_{12}	0.3	0.166	0.4	0.26
ν_{13}		0.166		0.26
ν_{13}		0.4		0.507
σ_Y		1000		119

The present paper aims to study the real contact area formation between composite-steel surfaces in sliding contact at the very beginning of the wear process assuming asperity contact. The evaluation of the real contact area is the first step to obtain reliable contact temperature results and therefore data for realistic wear prediction at

a later state of the study. The contact analysis of rough surfaces requires measured surface roughness data obtained by laser profilometry.

The composite material is a unidirectional continuous carbon fibre-polyetheretherketone (PEEK) system, having a fibre volume fraction of =0.6 (XC-2, ICI Fiberite, USA). The material properties of the composite, together with the properties of the steel, the carbon fibres and the PEEK, respectively, are collected in Table 1, for further numerical evaluations. Anisotropic material properties are calculated by rule-of-mixture type equations.

2. The measured surface pairs

To study the real contact area formation between sliding composite-steel surfaces, pin-on-disk experiments were carried out using CF/PEEK pins prepared and located in normal (N), parallel (P) and anti-parallel (AP) fibre orientations relative to the sliding direction. The disk was made of 100Cr6 steel.

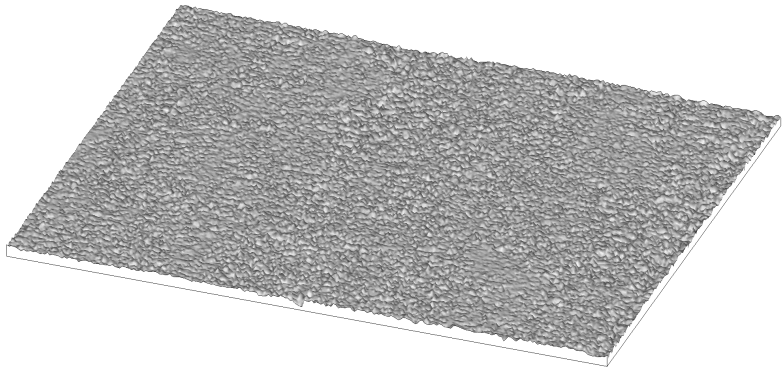

Figure 2. Surface roughness measurement for worn pin surface in the case of N-fibre orientation

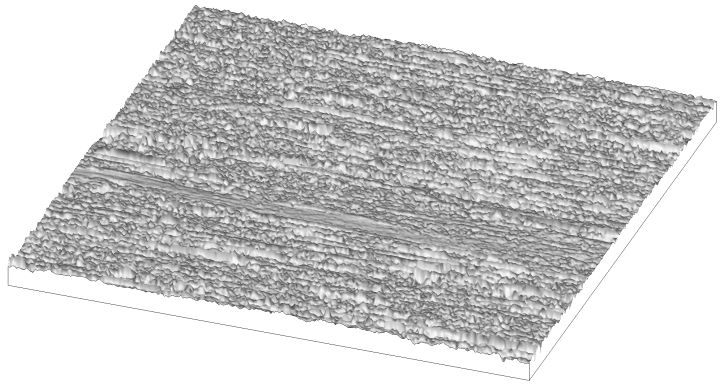

Figure 3. Surface roughness measurement for worn pin surface in the case of P-fibre orientation

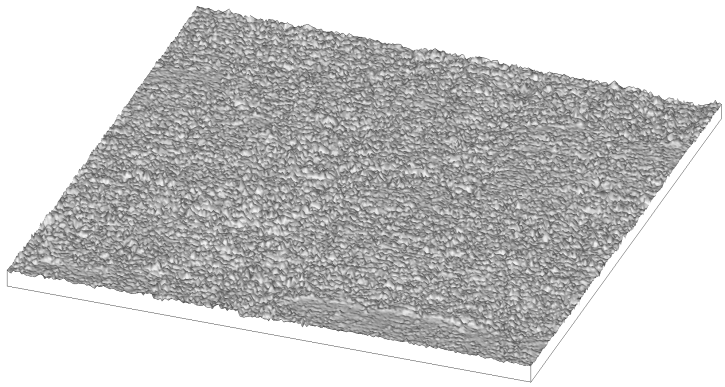

Figure 4. Surface roughness measurement for worn pin surface in the case of AP-fibre orientation

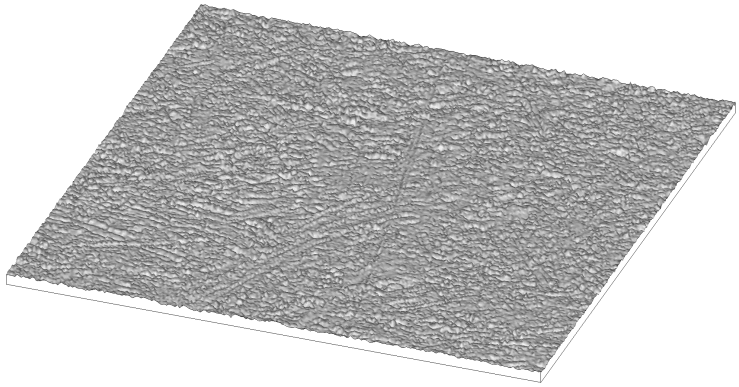

Figure 5. Surface roughness measurement for the steel disk

For the different fibre orientations worn surface pairs were measured by laser profilometry. The wear test run 10 seconds with a nominal pressure of $\bar{p} = 1$ MPa and a sliding speed of $v = 1$ m/s. The reason of the short running time was to keep the asperity contact situation before the transfer film layer of the matrix material started to form.

In each case the measured area was 0.5×0.5 mm^2 and the resolution was 500 points/mm. Figures 2 to 5 show the measured surface segments for some representing surface types.

3. Contact analysis of real surfaces

3.1. Measured surfaces Using the measured surface roughness data, a surface segment of 0.1×0.1 from the measured pin surface and a segment of 0.1×0.2 from the measured steel disk surface were selected for sliding contact evaluations. The arrangement is shown in Figure 6.

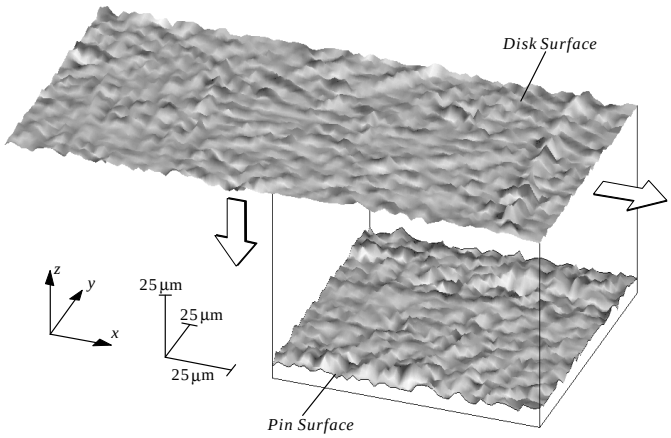

Figure 6. The measured surfaces of pin and disk for simulation of the real contact areas in sliding

3.2. 3D anisotropic numerical contact algorithm. The present algorithm is based on an elastic contact solution for rough surfaces described in [5]. This algorithm has an approximate elastic-plastic version using the plastic limit pressure condition of $p^* = 3.0\sigma_Y$, presented also in [5]. This approximate technique gives results in the range of larger plastic deformations, which are in good agreement with the elastic-plastic finite element (FE) evaluation of the same problem. In the range of the limited plastic deformation, however, the accuracy of the numerical contact algorithm is reduced. To improve the accuracy a new version of this algorithm has been developed and verified by a non-linear FE solution.

Compared to the original version of the contact algorithm [5], the displacement and stress type contact conditions are the same, whereas the plastic limit pressure condition will not be constant. Referring to [2], in the case of isotropic materials the first plastic deformation starts at $p^* = 1.6\sigma_Y$ and its maximum is $p^* = 3\sigma_Y$ in the range of larger plastic deformations. In the case of limited plastic deformation let's consider $p^* = 2\sigma_Y$ as a good "starting value" (see comments on FE results at the end of this Section).

Considering a single asperity at first, F is the total force transferred in this vicinity. F_0 is the limiting load, at which the maximum contact pressure, in the "middle" of the contact area reaches the value of $p^*_{\min} = 2\sigma_Y$. This results in the beginning of local plastic deformation. If F is much higher than F_0 a high amount ("large") plastic deformation will represent this case. Based on the results in [2] and the present FE elastic-plastic verification, about $25F_0$ is the load level that represents the beginning of large plastic deformation where $p^* = 3\sigma_Y$. Between these two limit pressure values linear interpolation is assumed, i.e. the actual limit pressure conditions are as follows:

$$p^* = \begin{cases} p^*_{\min} + \dfrac{p^*_{\max} - p^*_{\min}}{25F_0 - F_0}(F - F_0) & \text{if } F_0 \le F \le 25F_0 \\ p^*_{\min} & \text{if } F > 25F_0 \end{cases} \tag{3.1}$$

To be able to evaluate (within an acceptable accuracy) the limiting load F_0 for each asperity in contact, the approximate elastic-plastic contact algorithm solves the contact problem by using increasing loads during the subsequent calculations. The evaluated F_0 values are assigned to each asperity in contact, and at higher loads the actual plastic limit pressure value can be calculated by (3.1) for each asperity. This iteration is part of the numerical contact analysis, so it does not require extra CPU time, but the complete solution itself is time consuming because it needs a series of solutions while the load is increased until its required value.

The algorithm was verified by an axisymmetric elastic-plastic FE evaluation for a rigid asperity compressed into a flat PEEK surface under the following data:

- asperity radius: $R = 100$ μm,
- asperity load: $F = 0.3$ N,
- material properties listed in Table 1.

The FE model (Figure 7) contains 3672 2D elements and 40 contact elements, similar to [12].

Results are plotted in Figure 8 for each contact parameter. Comparing the results obtained by the numerical and FE techniques, it can be concluded that the results are in good agreement both in the range of limited and large plastic deformations. Considering the contact pressure distributions (Figure 9), the $p^* = 2\sigma_Y$ condition and the assumed linear limit pressure condition (3.1) improved the accuracy of the numerical contact technique.

Therefore, the technique developed can better evaluate the location of the "contact spots" forming the real contact area, the contact pressure distribution and the normal approach for a given load specified as an average pressure, acting over the nominal contact area (see Figure 1). In the case of sliding friction this contact technique can also be used. The friction force as a distributed traction would not change the contact results basically because the normal displacement component due to the traction is much smaller than the displacement due to the normal contact pressure that is involved in the contact equations [5]. At the same time the contact pressure value, that produces plastic deformation, is lower because the distributed traction has also effect on the stress state.

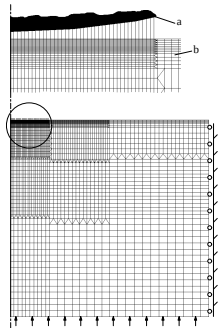

Figure 7. Axisymmetric FE model for the PEEK body (b) indented by a rigid asperity (a) (the upper figure is an enlargement of the details in the circular area)

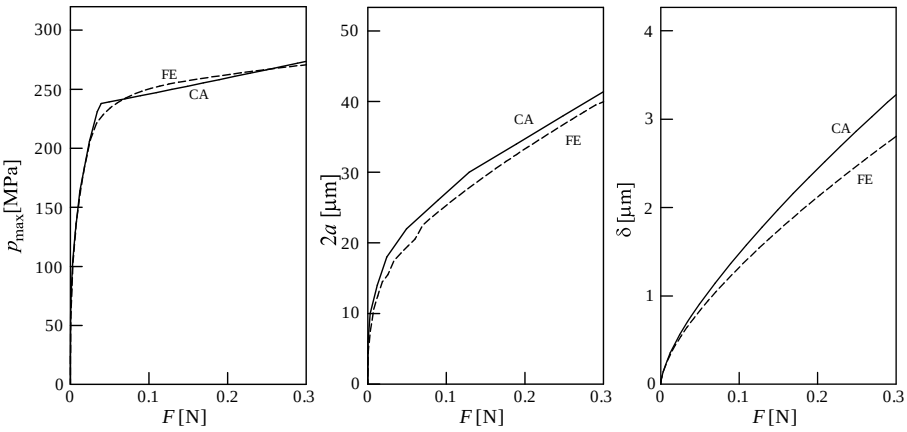

Figure 8. Contact parameters obtained by the numerical contact algorithm (CA) and FE technique

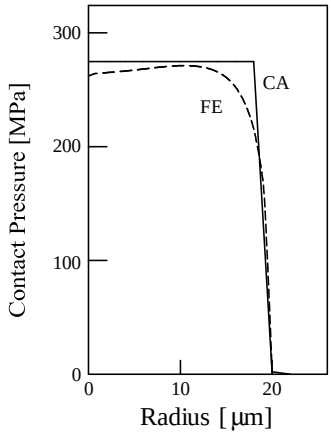

Figure 9. Contact pressure distributions

If anisotropic bodies are considered, the described algorithm is applicable if the influence matrix represents the anisotropic body. It requires a FE solution for a segment of the anisotropic half space following the multiple coupling technique described [10]. Material properties were taken from Table 1.

3.2. Contact Failure Criteria Contact failure criteria for a unidirectional continuous fibre matrix system under static conditions were studied in [10] and verified by ball indentation tests. Assuming a steel counterpart sliding over composite structures the following statements, as first ideas, can be specified for N-, P- and AP-fibre orientations:

1. If the fibres are arranged under N-orientation, failure of the composite due to sliding steel asperities can occur by plastic deformation and rupture of the matrix, fibre/matrix shear and compressive damage including fracture of the fibres.

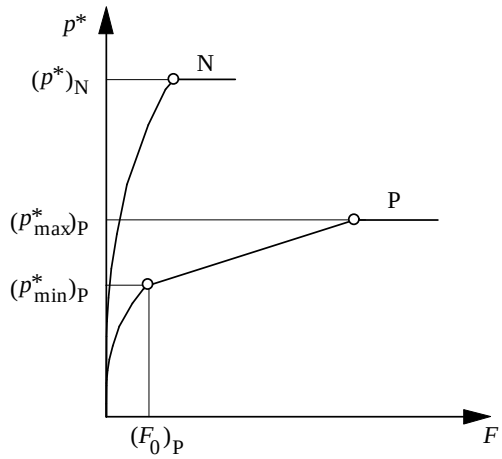

Figure 10. Contact failure criteria for composites

To specify a pressure limit at which shear strains at the fibre/matrix interface exceed a critical value requires further analysis of the behaviour of the composite structure. According to [11] initiation of failure starts below the surface followed by subsequent crack propagation to the surface.

To control the compression damage of the composite structure studied, the longitudinal compressive strength $\sigma_{||C}$ should be considered. ($\sigma_{||C}$ is an average value representing the failure of the matrix, the interface and the fibers.) This approach is an approximation, because the overall compression of a body and the local contact behaviour are not the same problem.

The condition of the longitudinal compressive strength may be considered as an upper limit for the vertical stresses inside the contact area. This condition does not allow any further plastic type deformation (Figure 10). The contact failure type criterion is therefore assumed to be:

$$p^* = \sigma_{||C} \tag{3.2}$$

2. If the fibers are arranged under P-orientation, failure of the composite, due to sliding steel asperities, relates primarily to plastic deformation of the matrix and flexural fracture of the fibres (Figure 10).

As a first order approach, the transverse compressive strength of the composite structure $\sigma_{\perp C}$ may be considered as a yield strength type criterion. The matrix can accumulate certain plastic deformation without any fracture type failure. To approximate this type of behaviour, the plastic limit pressure conditions, in equation $(3.1)_1$ are as follows:

$$\begin{array}{ll} p^*_{\min} = 2\sigma_{\perp C} & (\text{"starting" plastic deformation}) \\ p^*_{\min} = 2\sigma_{\perp C} & (\text{in the range of larger plastic deformation}) \end{array} \tag{3.3}$$

For the composite material studied here, the limiting strength values were chosen as follows: $\sigma^*_{||C} = 1200$ MPa and $\sigma^*_{\perp C} = 220$ MPa [14].

3.3. The Real Contact Area and the Contact Pressure Distribution in Sliding Contact Applying the described contact algorithm and the contact failure

criteria, different surface pairs were brought into contact to evaluate the locations of the real contact areas and the contact pressure distributions. The nominal pressure was $\bar{p} = 10MPa$ for each fibre orientation. Contact results are presented in Figure 11 representing two arbitrary positions of the sliding motion shown in Figure 6. It becomes obvious that different tendencies for the N-, P- and AP-fibre orientation exist. In the case of N-fibre orientation, due to the contact failure criterion used, smaller contact areas and higher pressure maxima than in the other two cases appear.

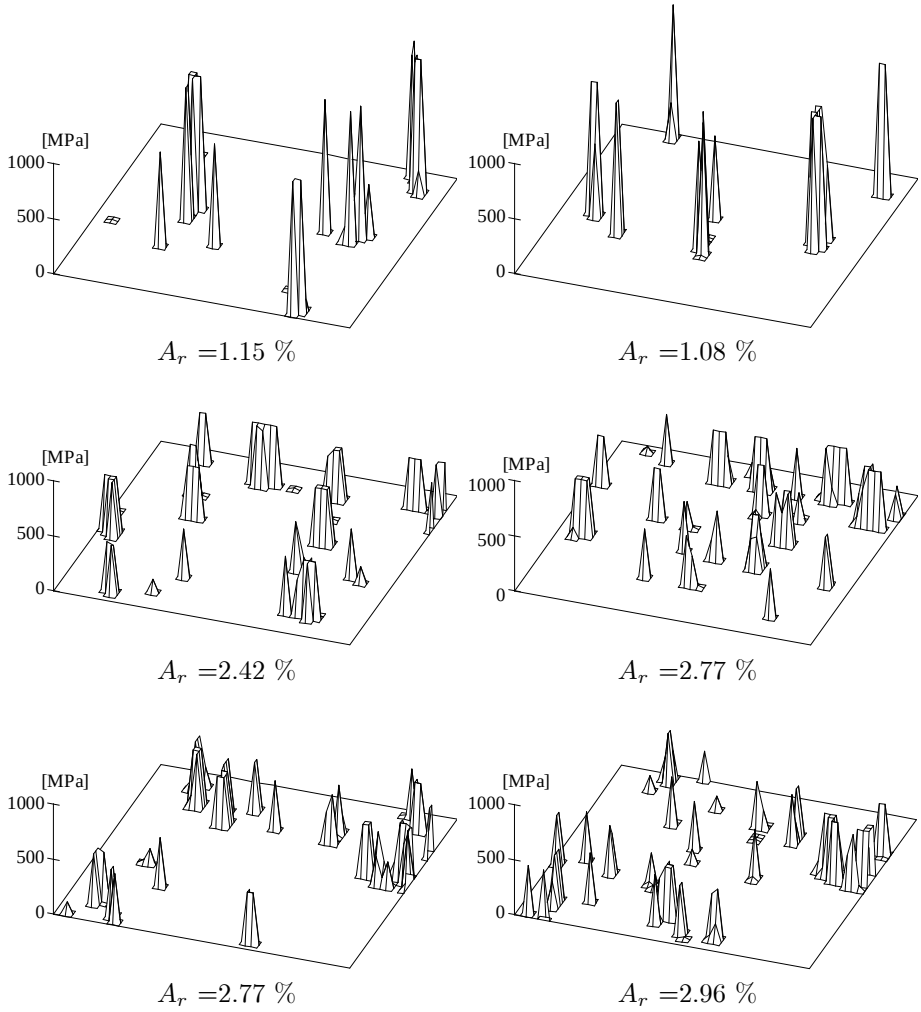

Figure 11. The real contact area and contact pressure distribution between composite and steel real surfaces in the case of N- (a), P- (b) and AP-fibre (c) orientations

Comparing the new version of the numerical contact algorithm with the previous one, the contact pressure maxima follow the pressure distribution given by equation (3.1), however, due to this change the real contact area becomes larger in the related calculations.

4. Concluding remarks

The new version of a numerical contact algorithm, applied for composite steel surfaces, produced more accurate contact simulation results, especially in the range of limited plastic deformation. Furthermore it can evaluate the location of the real contact area and the contact pressure distribution assuming different failure criteria.

When analysing the contact conditions under a compressive loading situation, the real contact area obtained by both the contact algorithm and the experimental techniques [15] show the same tendencies, i.e. asperity-type contact, verifying that in the case of composite-steel contact we have (at least at the beginning of the test) asperity-type contact, similarly to that known for metal-metal contact.

Acknowledgement. The presented research was supported by the Deutsche Forschungsgemeinschaft (DFG FR675/19-2) and by the Hungarian National Scientific Research Foundation (T 023351). Zoltán Néder is greatful to the Bolyai János Fellowship Foundation for support of his research activities.

REFERENCES

1. Kragelsky, I.V.: *Friction and Wear*, Pergamon Press, Oxford, 1982.
2. Johnson, K.L.: *Contact Mechanics*, Cambridge University Press, Cambridge, 1985.
3. Webster, M. N. and Sayles, R.S.: *A numerical model for the elastic frictionless contact of real rough surfaces*, Journal of Tribology, **108**, (1986) 314-320.
4. Yu Yonging and Zheng Linqing: *A full numerical solution for elastic contact of three-dimensional real rough surfaces*, Wear, **157**, (1992) 151-161.
5. Váradi, K., Néder, Z. and Friedrich, K.: *Evaluation of the real contact areas, pressure distribution and contact temperatures during sliding contact between real metal surfaces*, Wear, **200**, (1996), 52-62.
6. Wang, S. and Komvopoulos, K.: *A fractal theory of the interfacial temperature distribution in the slow sliding regime: Part I. - Elastic contact and heat transfer analysis, Part II. - multiple domains, Elastoplastic contacts and applications*, Journal of Tribology, **116**, (1994) 812-823 and 824-832.
7. Gladwell, G.M.L.: *Contact Problems in the Classical Theory of Elasticity*, Alpen ann den Rijn: Sitjthoff and Noordhoff, 1980, 575-631.
8. Svelko, V. A.: *The action of a stamp on an elastic anisotropic half-space*, Journal of Applied Mathematics and Mechanics, **34**(1), (1970), 172-178.
9. Ovaert, T. C.: *On the indentation of a transversely isotropic half-space with application to thin solid lubricant films*, Journal of Tribology, **115**, (1993), 650-657.
10. Váradi, K., Néder, Z., Flöck, J. and Friedrich, K.: *Numerical and experimental contact analysis of a steel ball indented into a fibre reinforced polymer composite material*, Journal of Materials Science, **33**, (1998), 841-851.
11. Ovaert, T.C. and Ramachandra, S.: *Wear particle formation of polymer against smooth hardened steel counterfaces*, Tribology Transaction, **40**, (1997), 445-452.
12. Friedrich, K., Flöck, J., Váradi, K. and Néder, Z.: *Real contact area, con-*

tact temperature rise and transfer film formation between original and worn surfaces of cf/peek composites sliding against steel, 25th Leeds-Lyon Symposium on Tribology, Lyon, France, 8-11 September 1998 (in press)

13. *VDI Wärmeatlas*, 3. Auflage 1997.
14. Cogswell, F. N.: *Thermoplastic Aromatic Polymer Composites*, Butterworth-Heinemann Ltd., Oxford, 1992
15. Friedrich, K., Flöck, J., Váradi, K. and Néder, Z.: *Numerical and finite element contact and thermal analysis of real composite-steel surfaces in sliding contact*, Wear, **225-229**, Part I, (1999), 368-379.

Journal of Computational and Applied Mechanics, Vol. 1., No. 2., (2000), pp. 235–258

NUMERICAL TREATMENT OF ELASTOPLASTIC PROBLEMS BY THE p-VERSION OF THE FINITE ELEMENT METHOD

István Páczelt, Frigyes Nándori
Department of Mechanics, University of Miskolc
3515 Miskolc – Egyetemváros, Hungary
mechpacz@gold.uni-miskolc.hu, mechnf@gold.uni-miskolc.hu

Tamás Szabó
Computational Mechanics Research Group, Hungarian Academy of Sciences
3515 Miskolc – Egyetemváros, Hungary
mechsza@gold.uni-miskolc.hu

[Received: September 19, 2000]

Abstract. The constitutive equations are formulated in the unrotated reference frame. Kinematic and isotropic hardening rules are assumed and the radial return mapping algorithm is applied to find the actual yield surface. By assuming large and incompressible plastic deformations, the total Lagrangian formulation of the finite element method is applied with p-extension elements making use of the truncated space and the product space.

Keywords: Elastoplastic problems, large strains, finite elements with p-extension

1. Introduction

Workstations and the latest PC-s make the numerical solution of plastic problems with large strains possible. A great number of conferences have been devoted to the problems arising during the simulation of plastic processes [1]-[9]. More and more papers are published with the aim of developing effective procedures for the solution of plastic problems. Finite rotations of material axes make the treatment of strain-stress rates and their numerical integration over a load step difficult. As is well known, there are various objective stress rates, the rules for their systematic constructions and a couple of new ones are presented in the paper [10] by Kozák.

The Jauman stress rate has been used in large strain plastic problems over the past ten years. However, stress oscillations were experienced for large rotations and during the treatment of a complex material behavior (e.g., viscoplasticity, kinematic hardening, isotropic hardening).

The oscillatory response can be removed if the Cauchy stress measure and its objective rate are defined in an unrotated orthogonal reference frame established by means of the polar decomposition of the deformation gradient at each material point. Using this concept, it can be shown that the stress response will increase monotonically in simple shear for incremental linear-elasticity. The same idea was used by Hallquist

[5,6] to work out implicit dynamic codes and by Flangan and Taylor [4] to develop codes for a transient dynamic analysis with explicit time integration. With the strains, stresses and their objective rates, each defined in the unrotated frame, the structure of small-strain plasticity is fully retained, which is advantageous to develop a finite element code. This concept firstly used by Hallquist was further developed by Healy and Dodds [7].

In this paper first we will summarize the kinematics of finite deformations, then present the strain-stress rates and the elastoplastic constitutive equations by assuming that the kinematic and isotropic hardening rules are valid. Finally, we will apply the finite element method to axisymmetric problem with p-extension elements. The approximation of the p-extension elements can be constructed either by the truncated space or the product space [18]. The two approaches are different in the number of the bubble functions. The approximations of the displacement field and the volumetric change will also be investigated. Numerical examples demonstrate the effectiveness of the applied elastoplastic theory.

2. State variables

A number of textbooks are devoted to the formulation of nonlinear solid mechanics – see for instance [2, 12]. Here we summarize the most important basic relations that are required for a finite element formulation.

In our analysis we consider the motion of a body in a fixed Cartesian coordinate system $(X_1,\ X_2,\ X_3)$. The position vector of a generic material point is denoted by $\mathbf{X}$ at time 0 (in the reference or undeformed configuration), and by $\mathbf{x}$ at time t (in the deformed or current configuration). The reference and deformed configurations are denoted by B_0 and B, respectively.

The displacement vector is given by

$$\mathbf{u} = \mathbf{x} - \mathbf{X} \,. \tag{2.1}$$

The fundamental measure of deformation is the deformation gradient

$$\mathbf{F} = \frac{\partial \mathbf{x}}{\partial \mathbf{X}} \,. \tag{2.2}$$

If the mapping $\mathbf{X} = \mathbf{x}(\mathbf{X}, t)$ is one-to-one, then

$$J = \det \mathbf{F} > 0 \,. \tag{2.3}$$

As is well known, the deformation gradient $\mathbf{F}$ can be decomposed into a product of two matrices

$$\mathbf{F} = \mathbf{V} \cdot \mathbf{R} = \mathbf{R} \cdot \mathbf{U} \tag{2.4}$$

where $\mathbf{R}$ is the orthogonal rotation tensor, while $\mathbf{V}$ and $\mathbf{U}$ are the symmetric left and right stretch tensors. The principal values λ_i of $\mathbf{V}$ and $\mathbf{U}$ are equal.

The velocity field, which is the material time derivative of the displacements, is written as

$$\mathbf{v} = \frac{\partial \mathbf{x}}{\partial t} = \dot{\mathbf{x}}\,. \tag{2.5}$$

The velocity gradient $\mathbf{L}$ (velocity strain tensor) is defined as the gradient of the velocity field with respect to the current configuration. Making use of the chain rule and (2.2), we can write

$$\mathbf{L} = \frac{\partial \mathbf{v}}{\partial \mathbf{x}} = \frac{\partial \mathbf{v}}{\partial \mathbf{X}} \frac{\partial \mathbf{X}}{\partial \mathbf{x}} = \dot{\mathbf{F}} \cdot \mathbf{F}^{-1}\,. \tag{2.6}$$

We denote the symmetric and skew parts of the velocity gradient by $\mathbf{D}$ (the rate of the deformation tensor) and $\mathbf{W}$ (the spin rate of the velocity gradient). According to the decomposition theorem

$$\mathbf{L} = \mathbf{D} + \mathbf{W} \qquad \text{where} \qquad \mathbf{D} = \frac{1}{2}\left(\mathbf{L} + \mathbf{L}^T\right) \qquad \text{and} \qquad \mathbf{W} = \frac{1}{2}\left(\mathbf{L} - \mathbf{L}^T\right)\,. \tag{2.7}$$

The tensors $\mathbf{D}$ and $\mathbf{W}$ are both instantaneous rates, i.e., are not associated with the load history. When integrated over the load history, the principal values of $\mathbf{D}$ are the logarithmic strains of the line elements oriented in the principal directions if the principal directions do not rotate.

Applying the polar decomposition theorem to $\mathbf{F}$, we have

$$\mathbf{L} = (\mathbf{R}\cdot\mathbf{U})^{\cdot}\cdot\mathbf{F}^{-1} = \dot{\mathbf{R}}\cdot\mathbf{U}\cdot\mathbf{F}^{-1} + \mathbf{R}\cdot\dot{\mathbf{U}}\cdot\mathbf{F}^{-1} = \\ = \dot{\mathbf{R}}\cdot\mathbf{U}\cdot\mathbf{U}^{-1}\cdot\mathbf{R}^{-1} + \mathbf{R}\cdot\dot{\mathbf{U}}\cdot\mathbf{U}^{-1}\cdot\mathbf{R}^{-1}\,,$$

since

$$(\mathbf{R}\cdot\mathbf{U})^{-1} = \mathbf{U}^{-1}\cdot\mathbf{R}^{-1} = \mathbf{U}^{-1}\mathbf{R}^T, \qquad \text{and} \qquad \boldsymbol{\Omega} = \dot{\mathbf{R}}\cdot\mathbf{R}^T\,.$$

In view of the fact that $\mathbf{R}$ is an orthogonal tensor ($\mathbf{R}^T = \mathbf{R}^{-1}$) we obtain

$$\mathbf{L} = \dot{\mathbf{R}}\mathbf{R}^T + \mathbf{R}\cdot\dot{\mathbf{U}}\cdot\mathbf{U}^{-1}\cdot\mathbf{R}^T = \boldsymbol{\Omega} + \mathbf{R}\cdot\dot{\mathbf{U}}\cdot\mathbf{U}^{-1}\cdot\mathbf{R}^T\,. \tag{2.8}$$

Furthermore, we have

$$\mathbf{R}^T\cdot\mathbf{R} = \mathbf{1} \qquad \text{and} \qquad \frac{d\left(\mathbf{R}^T\mathbf{R}\right)}{dt} = \mathbf{0}$$

in which $\mathbf{1}$ is the unit tensor. It is obvious that

$$\dot{\mathbf{R}}^T\cdot\mathbf{R} = -\mathbf{R}^T\cdot\dot{\mathbf{R}}\,. \tag{2.9}$$

With (2.8), $(2.7)_2$ yields

$$\mathbf{D} = \mathbf{R}\cdot\frac{1}{2}\left(\dot{\mathbf{U}}\cdot\mathbf{U}^{-1} + \mathbf{U}^{-1}\cdot\dot{\mathbf{U}}\right)\cdot\mathbf{R}^T \equiv \mathbf{R}\cdot\mathbf{d}\cdot\mathbf{R}^T \tag{2.10a}$$

where $\mathbf{d}$ is the unrotated deformation rate:

$$\mathbf{d} = \frac{1}{2}\left(\dot{\mathbf{U}}\cdot\mathbf{U}^{-1} + \mathbf{U}^{-1}\cdot\dot{\mathbf{U}}\right) = \mathbf{R}^T\mathbf{D}\mathbf{R}\,. \tag{2.10b}$$

The double scalar product of the Cauchy stress tensor $\mathbf{T}$ and the rate of deformation tensor $\mathbf{D}$ gives the stress power per unit volume

$$\mathbf{T} : \mathbf{D} . \tag{2.11}$$

Introducing the unrotated Cauchy stress tensor

$$\mathbf{t} = \mathbf{R}^T \cdot \mathbf{T} \cdot \mathbf{R} , \tag{2.12}$$

the double scalar product (2.11) can be written as

$$\mathbf{T} : \mathbf{D} = \mathbf{R}^T \cdot \mathbf{T} \cdot \mathbf{R} : \mathbf{R}^T \cdot \mathbf{D} \cdot \mathbf{R} = \mathbf{t} : \mathbf{d} . \tag{2.13}$$

The right and left Cauchy-Green tensors $\mathbf{C}$ and $\mathbf{D}$ are defined by

$$\mathbf{C} = \mathbf{F}^T \cdot \mathbf{F} = \mathbf{U}^2 \qquad \text{and} \qquad \mathbf{B} = \mathbf{F} \cdot \mathbf{F}^T = \mathbf{V}^2 , \tag{2.14}$$

respectively. We remark that the eigenvalues of the two tensors are identical but the eigenvectors are different.

We adopt the total Lagrangian formulation of the problem. This means that all quantities are taken in the reference configuration. As is well known, the deformation measure, i.e., the Green-Lagrange strain tensor is defined by

$$\mathbf{E} = \frac{1}{2} \left(\mathbf{U}^2 - \mathbf{1} \right) = \frac{1}{2} \left(\mathbf{F}^T \cdot \mathbf{F} - \mathbf{1} \right) . \tag{2.15}$$

Furthermore, we have

$$\dot{\mathbf{E}} = \frac{1}{2} \left(\dot{\mathbf{F}}^T \cdot \mathbf{F} + \mathbf{F}^T \cdot \dot{\mathbf{F}} \right) = \mathbf{F}^T \cdot \mathbf{D} \cdot \mathbf{F} , \tag{2.16}$$

which, as can be seen by using (2.6) and (2.7), includes the velocity gradient

$$\mathbf{D} = \frac{1}{2} \left(\dot{\mathbf{F}} \cdot \mathbf{F}^{-1} + \left(\mathbf{F}^{-1} \right)^T \cdot \dot{\mathbf{F}}^T \right) .$$

Substituting the polar decomposition $\mathbf{F} = \mathbf{R} \cdot \mathbf{U}$ into equation (2.16), we obtain

$$\dot{\mathbf{E}} = \mathbf{U}^T \cdot \mathbf{R}^T \cdot \mathbf{D} \cdot \mathbf{R} \cdot \mathbf{U} \tag{2.17}$$

from which, with regard to equation (2.10b), it follows

$$\dot{\mathbf{E}} = \mathbf{U}^T \cdot \mathbf{d} \cdot \mathbf{U} . \tag{2.18}$$

Since $\mathbf{U} = \mathbf{U}^T$ is a symmetric tensor, the unrotated deformation rate $\mathbf{d}$ can be expressed from (2.18):

$$\mathbf{d} = \mathbf{U}^{-1} \cdot \dot{\mathbf{E}} \cdot \mathbf{U}^{-1} . \tag{2.19}$$

The work-conjugate of the Green-Lagrange strain tensor $\mathbf{E}$ is the second Piola-Kirchhoff stress tensor $\mathbf{P}^{II}$, which can be given in terms of the Cauchy stress tensor $\mathbf{T}$ as follows

$$\mathbf{P}^{II} = J \, \mathbf{F}^{-1} \cdot \mathbf{T} \cdot \mathbf{F}^{-T} . \tag{2.20}$$

Substituting the polar decomposition $\mathbf{F} = \mathbf{R} \cdot \mathbf{U}$ into (2.20) and using (2.12), we have

$$\mathbf{P}^{II} = J\,\mathbf{U}^{-1} \cdot \mathbf{t} \cdot \mathbf{U}^{-1}\,. \tag{2.21}$$

Deriving this equation with respect to time t, we obtain a formula for the rate of the stress tensor

$$\dot{\mathbf{P}}^{II} = \dot{J}\,\mathbf{U}^{-1} \cdot \mathbf{t} \cdot \mathbf{U}^{-1} + J\,\left(\mathbf{U}^{-1}\right)^{\cdot} \cdot \mathbf{t} \cdot \mathbf{U}^{-1} + J\,\mathbf{U}^{-1} \cdot \dot{\mathbf{t}} \cdot \mathbf{U}^{-1} + J\,\mathbf{U}^{-1} \cdot \mathbf{t} \cdot \left(\mathbf{U}^{-1}\right)^{\cdot} \tag{2.22}$$

where

$$\dot{J} = J\,\mathrm{tr}\,(\mathbf{D}) \tag{2.23}$$

in which $\mathrm{tr}\,(\mathbf{D})$ is the trace of the tensor $\mathbf{D}$. In order to determine $(\mathbf{U}^{-1})^{\cdot}$ we consider the equation

$$\mathbf{U}^{-1} \cdot \mathbf{U} = \mathbf{1} \tag{2.24}$$

as our point of departure. Taking its derivative with respect to time t, we have

$$(\mathbf{U}^{-1})^{\cdot} \cdot \mathbf{U} + \mathbf{U}^{-1} \cdot \dot{\mathbf{U}} = \mathbf{0} \tag{2.25}$$

from which

$$(\mathbf{U}^{-1})^{\cdot} = -\mathbf{U}^{-1} \cdot \dot{\mathbf{U}} \cdot \mathbf{U}^{-1}\,. \tag{2.26}$$

Substituting (2.23) and (2.26) into (2.22) and making use of (2.21), we obtain the relation

$$\dot{\mathbf{P}}^{II} = J\,\mathbf{U}^{-1} \cdot \dot{\mathbf{t}} \cdot \mathbf{U}^{-1} + tr\,(\mathbf{D})\,\mathbf{P}^{II} - \mathbf{U}^{-1} \cdot \dot{\mathbf{U}} \cdot \mathbf{P}^{II} - \mathbf{P}^{II} \cdot \dot{\mathbf{U}} \cdot \mathbf{U}^{-1} \tag{2.27}$$

for the stress rate.

3. Large strain elastoplasticity

3.1. An objective time derivative of the Cauchy stress tensor. The constitutive law for an elastoplastic material determines the relation between a materially objective stress rate and a work conjugate deformation rate.

Let us consider the equation relating the unrotated stress tensor $\mathbf{t}$ to the Cauchy stress tensor $\mathbf{T}$:

$$\mathbf{t} = \mathbf{R}^{T} \cdot \mathbf{T} \cdot \mathbf{R}\,. \tag{3.1}$$

After taking the time derivative of the above equation, we get

$$\dot{\mathbf{t}} = \dot{\mathbf{R}}^{T} \cdot \mathbf{T} \cdot \mathbf{R} + \mathbf{R}^{T} \cdot \dot{\mathbf{T}} \cdot \mathbf{R} + \mathbf{R}^{T} \cdot \mathbf{T} \cdot \dot{\mathbf{R}}\,. \tag{3.2}$$

Utilizing the expression $\boldsymbol{\Omega} = \dot{\mathbf{R}} \cdot \mathbf{R}^{T}$ in (2.8), we can express the rate of the orthogonal rotation tensor and its transpose:

$$\dot{\mathbf{R}} = \boldsymbol{\Omega} \cdot \mathbf{R}\,, \qquad \dot{\mathbf{R}}^{T} = \mathbf{R}^{\mathbf{T}} \cdot \boldsymbol{\Omega}^{T} = -\mathbf{R}^{T} \cdot \boldsymbol{\Omega} \tag{3.3}$$

by which equation (3.2) gives

$$\dot{\mathbf{t}} = \mathbf{R}^T \cdot \mathbf{T}^{\nabla} \cdot \mathbf{R}\,, \qquad \mathbf{T}^{\nabla} = \dot{\mathbf{T}} - \boldsymbol{\Omega} \cdot \mathbf{T} + \mathbf{T} \cdot \boldsymbol{\Omega} \tag{3.4}$$

where $\mathbf{T}^{\nabla}$ is the Green-Naghdi objective stress rate tensor [2, 10].

With the tensor of material constants $\mathbf{C}^{ep}$ the constitutive equation takes the form

$$\mathbf{T}^{\nabla} = \mathbf{C}^{ep} \colon \mathbf{D}\,. \tag{3.5}$$

Let us reformulate the constitutive law in the unrotated but deformed configuration. Making use of equations (3.4), (3.5) and (2.10b), we have

$$\dot{\mathbf{t}} = \mathbf{R}^T \cdot (\mathbf{C}^{ep} : \mathbf{D}) \cdot \mathbf{R} = \mathbf{C}^{ep} : (\mathbf{R}^T \cdot \mathbf{D} \cdot \mathbf{R}) = \mathbf{C}^{ep} : \mathbf{d}\,. \tag{3.6}$$

One can see from equation (3.6) that the integration of the rate of the rotation tensor over the load history is avoided. However, all quantities should be transformed into the unrotated deformed configuration. Constitutive law (3.6) was first used by Hallquist [5]. When this method is chosen it is essential to perform the polar decomposition of the deformation gradient as accurately as possible.

3.2. Determination of the elastoplastic state. We shall assume that the material is isotropic and the undeformed configuration is stress free. The Mises yield surface is applied together with the associated flow rule. The hardening rule, which specifies how the yield function is modified during a plastic flow, can be kinematic, isotropic or a combination of the previous two. The yield surface is given as

$$f\ (\boldsymbol{\xi}, \overline{e}^p) = \|\boldsymbol{\xi}\| - \sqrt{\frac{2}{3}}\kappa\,(\overline{e}^p) \leq 0 \tag{3.7}$$

where

- $\kappa\,(\overline{e}^p)$ is the hardening rule,
- $\boldsymbol{\xi} = \mathbf{s} - \boldsymbol{\alpha}$, in which the deviatoric stress $\mathbf{s} = \operatorname{dev}\mathbf{t} = \mathbf{t} - \frac{1}{3}tr\,(\mathbf{t})\,\mathbf{1}$, $\boldsymbol{\alpha}$ is the centre of the yield surface (called back stress),
- $\|\boldsymbol{\xi}\| = \sqrt{\boldsymbol{\xi} : \boldsymbol{\xi}}$,
- $\overline{e}^p$ is the equivalent plastic strain $\overline{e}^p = \int\limits_0^t \sqrt{\frac{2}{3}}\,\|\mathbf{d}^p\,(\tau)\|\,d\tau$,
- $\mathbf{d} = \mathbf{d}^e + \mathbf{d}^p$ is the strain rate decomposed into elastic and plastic parts.

The decomposition of $\mathbf{d}$ is based on the decomposition of the deformation gradient proposed by Lee [11] for ductile metals

$$\mathbf{F} = \mathbf{F}^e \cdot \mathbf{F}^p \tag{3.8}$$

where $\mathbf{F}^e$ represents the elastic deformation, i.e., the distortion of the lattice, while $\mathbf{F}^p$ represents the plastic deformation. Substituting (3.8) into (2.6), we have

$$\mathbf{L} = \dot{\mathbf{F}} \cdot \mathbf{F}^{-1} = \dot{\mathbf{F}}^e \cdot \mathbf{F}^p \cdot \left(\mathbf{F}^{-p} \cdot \mathbf{F}^{-e}\right) + \mathbf{F}^e \cdot \dot{\mathbf{F}}^p \cdot \left(\mathbf{F}^{-p} \cdot \mathbf{F}^{-e}\right) =$$
$$= \dot{\mathbf{F}}^e \cdot \mathbf{F}^{-e} + \mathbf{F}^e \cdot \dot{\mathbf{F}}^p \cdot \mathbf{F}^{-p} \cdot \mathbf{F}^{-e} \equiv \mathbf{L}^e + \mathbf{F}^e \cdot \mathbf{L}^p \cdot \mathbf{F}^{-e} \tag{3.9}$$

We shall assume in the course of elastoplastic deformations that the elastic strains are vanishingly smaller than the plastic strains. Furthermore, we shall also assume for the elastic deformation that $\mathbf{F}^e = \mathbf{V}^e$ in (3.9), i.e., the rigid rotation is added to plastic term. Hence, we can rewrite the decomposition

$$\mathbf{F} = \mathbf{F}^e \cdot \mathbf{F}^p = \mathbf{V}^e \cdot \mathbf{V}^p \cdot \mathbf{R}. \tag{3.10}$$

Assuming small elastic strains $\boldsymbol{\varepsilon}^e$, it holds

$$\mathbf{F}^e = \mathbf{1} + \boldsymbol{\varepsilon}^e \approx \mathbf{1}\,. \tag{3.11}$$

Consequently, we can decompose the approximation of the velocity strain tensor and its symmetric part into the forms

$$\mathbf{L} \approx \mathbf{L}^e + \mathbf{L}^p, \qquad \text{and} \qquad \mathbf{D} \approx \mathbf{D}^e + \mathbf{D}^p. \tag{3.12}$$

Substituting $(3.12)_2$ into (2.10b) the unrotated deformation rate can also be decomposed into elastic and plastic parts

$$\mathbf{d} = \mathbf{R}^T \cdot (\mathbf{D}^e + \mathbf{D}^p) \cdot \mathbf{R} = \mathbf{d}^e + \mathbf{d}^p \tag{3.13}$$

as is the case for small strain plasticity.

3.3. Determination of the stresses in the unrotated configuration. The integration of the plastic equations is performed over finite time increments. A good review can be found in the works of Simo and Taylor [16,17]. The radial return mapping procedure seems to be very effective for integrating the elastoplastic problem numerically.

Imposing kinematic and isotropic hardening rules, the yield surface will be both translated and inflated. The translation is associated with the plastic modulus $H_\alpha^{'}(\overline{e}^p)$, and the inflation with the hardening rule $\kappa(\overline{e}^p)$, where e is the equivalent strain.

Points inside the yield surface (3.7) ($f \leq 0$) refer to elastic states, and points on the yield surface ($f = 0$) refer to plastic states.

As is known from the Prandtl-Reuss equations

$$\mathbf{s} = 2G(\dot{\mathbf{e}} - \dot{\mathbf{e}}^p)\,, \tag{3.14}$$

where $\mathbf{s}$ is the deviatoric stress rate, $\dot{\mathbf{e}}$ is the deviatoric strain rate, $\dot{\mathbf{e}}^p$ is the plastic part of the deviatoric strain rate, G is the elastic shear modulus and

$$\mathbf{e} = \boldsymbol{\varepsilon} - \frac{1}{3}\mathrm{tr}\,(\boldsymbol{\varepsilon})\,\mathbf{1} \tag{3.15}$$

where $\boldsymbol{\varepsilon}$ is the strain tensor. According to the associative rule

$$\mathbf{d}^p = \dot{\mathbf{e}}^p = \gamma \frac{\partial f}{\partial \boldsymbol{\xi}} = \gamma \hat{\mathbf{n}} \tag{3.16a}$$

where γ is the plastic coefficient:

$$\gamma \equiv \|\dot{\mathbf{e}}^p\| = \left\| \gamma \frac{\partial f}{\partial \boldsymbol{\xi}} \right\| = \|\gamma \hat{\mathbf{n}}\| = \frac{1}{1 + \frac{\kappa' + H'_\alpha}{3G}}\,. \tag{3.16b}$$

Here $H_{\alpha}^{'}(\overline{e}^{p})$ and $\kappa'(\overline{e}^{p})$ are obtained by derivation with respect to $\overline{e}^{p}$ and $\hat{\mathbf{n}}$ is the unit normal of the yield surface:

$$\hat{\mathbf{n}} = \frac{\boldsymbol{\xi}}{\|\boldsymbol{\xi}\|} \,. \tag{3.16c}$$

The translation rate of the centre of the yield surface is given by

$$\dot{\boldsymbol{\alpha}} = \frac{2}{3} H_{\alpha}^{'}(\overline{e}^{p})\, \dot{\mathbf{e}}^{p} \tag{3.17}$$

where $H_{\alpha}^{'}(\overline{e}^{p})$ is the plastic modulus.

The pressure rate due to the elastic volume change is calculated as

$$\dot{p} = \frac{1}{2}\mathrm{tr}\,\left(\dot{\mathbf{t}}\right) = K\,\mathrm{tr}\,(\dot{\boldsymbol{\varepsilon}}) \tag{3.18}$$

where K is the bulk modulus: $K = E/(3-6\nu)$, E is the Young's modulus, ν is the Poisson's ratio.

Regarding equation (3.14) as our point of departure, a standard transformation leads to the following equation

$$\dot{\mathbf{s}} = 2G[\mathbf{I} - \gamma\hat{\mathbf{n}} \otimes \hat{\mathbf{n}}] : \dot{\mathbf{e}} \tag{3.19}$$

in which $\mathbf{I}$ is a fourth order unit tensor, $\otimes$ denotes the tensor product, the element $ijkl$ of the tensor $[\hat{\mathbf{n}} \otimes \hat{\mathbf{n}}]$ is evaluated from the relation $\hat{n}_{ij}\hat{n}_{kl}$, and $\hat{n}_{ij}$ is the element of the tensor $\hat{\mathbf{n}}$.

In view of the representation

$$\mathbf{t} = \mathbf{s} + \frac{1}{3}\mathrm{tr}\,(\mathbf{t})\,\mathbf{1}\,, \tag{3.20}$$

a rate constitutive equation can be obtained by using (3.15), (3.18) and (3.19):

$$\dot{\mathbf{t}} = \mathbf{C}^{ep}(\mathbf{t}) : \dot{\boldsymbol{\varepsilon}} \tag{3.21}$$

where $\mathbf{C}^{ep}$ is the fourth order tensor of the tangent moduli

$$\mathbf{C}^{ep}(\mathbf{t}) = K\,\mathbf{1} \otimes \mathbf{1} + 2G\left[\mathbf{I} - \frac{1}{3}\mathbf{1} \otimes \mathbf{1}\right] - 2G\gamma\hat{\mathbf{n}} \otimes \hat{\mathbf{n}} \quad . \tag{3.22}$$

Integration of the nonlinear equation (3.19) with respect to time t is not simple since the elastoplastic problem depends on the load history. A great number of return mapping algorithms are available. The radial return mapping seems to be the most efficient procedure (see Appendix 1).

4. Consistent tangential stiffness matrix

With the knowledge of $\boldsymbol{\sigma}_n$, $\overline{e}_n^{p}$ and $\boldsymbol{\varepsilon}_n$ at time t^n, the vector of the strain increments

$$\Delta\boldsymbol{\varepsilon} = \boldsymbol{\varepsilon} - \boldsymbol{\varepsilon}_n \tag{4.1}$$

can be determined by using the nonlinear constitutive law and satisfying the yield surface as well:

$$\Delta\boldsymbol{\varepsilon} \to \tilde{\boldsymbol{\sigma}}(\mathbf{t}, \bar{e}_n^p, \boldsymbol{\varepsilon}_n, \Delta\boldsymbol{\varepsilon})\,. \tag{4.2}$$

The principle of the virtual work can be applied to find a unique value for $\Delta\boldsymbol{\varepsilon}$. The principle itself assumes the form

$$G(\mathbf{u}, \delta\mathbf{u}) = \int_V \rho\ddot{\mathbf{u}} \cdot \delta\mathbf{u}\,\mathrm{d}V + \int_V \tilde{\boldsymbol{\sigma}}\left(\mathbf{t}_n, \boldsymbol{\varepsilon}_n, \bar{e}_n^p, \nabla\mathbf{u} - \boldsymbol{\varepsilon}_n\right) : \nabla\delta\mathbf{u}\,\mathrm{d}V - \\ - \int_V \rho\mathbf{k} \cdot \delta\mathbf{u}\,\mathrm{d}V - \int_{A_p} \overline{\mathbf{p}} \cdot \delta\mathbf{u}\,\mathrm{d}A = 0 \tag{4.3}$$

where $\delta\mathbf{u}$ is the variation of $\mathbf{u}$ ($\delta\mathbf{u} = \mathbf{0}$ if $\mathbf{r} \in A_u$), $\rho\mathbf{k}$ stands for the body forces and $\ddot{\mathbf{u}}$ is the acceleration.

Equation (4.3) can be written in linearized form and can be solved with the Newton iteration. This means that one should solve a sequence of linearized problems given by

$$DG(\mathbf{u}_{n+1}^{(i)}, \delta\mathbf{u}) \cdot \Delta\mathbf{u}_{n+1}^{(i)} \equiv \int_V \nabla\delta\mathbf{u} : \left[\mathbf{C}_{n+1}^{(i)} : \nabla\left(\Delta\mathbf{u}_{n+1}^{(i)}\right)\right]\,\mathrm{d}V = -G(\mathbf{u}_{n+1}^{(i)}, \delta\mathbf{u}) \tag{4.4}$$

until the residual $G(\mathbf{u}_{n+1}^{(i)}, \delta\mathbf{u})$ vanishes.

In order to achieve fast convergency during the numerical computations we need a constitutive tensor $\mathbf{C}_{n+1}^{(i)}$ in a consistent form. Simo and Taylor [16] gave this tensor in the following form

$$\mathbf{C}_{n+1}^{(i)} = \mathbf{C}_{n+1}^{ep} = K\,\mathbf{1}\otimes\mathbf{1} + 2G\beta\left[\mathbf{I} - \frac{1}{3}\mathbf{1}\otimes\mathbf{1}\right] - 2G\,\bar{\gamma}\,\hat{\mathbf{n}}\otimes\hat{\mathbf{n}} \tag{4.5}$$

where

$$\beta = \sqrt{\frac{2}{3}}\frac{[\kappa_{n+1} + \Delta H_\alpha]}{\left\|\boldsymbol{\xi}_{n+1}^*\right\|} \qquad \text{and} \qquad \bar{\gamma} = \frac{1}{1 + \frac{[\kappa' + \Delta H'_\alpha]_{n+1}}{3G}} - (1-\beta)\,.$$

The matrix version of (4.5), which is applied in the finite element applications, was given by Dodds [3]. This matrix relates the increments of the unrotated stresses and strains

$$\Delta\mathbf{t} = \mathbf{C}^{*ep}\Delta\mathbf{d} \tag{4.6}$$

where

$$\mathbf{C}^{*ep} = \tilde{\mathbf{C}} - 2G\gamma\,\mathbf{n}\,\mathbf{n}^T$$

($\Delta\mathbf{t}$, $\Delta\mathbf{d}, \mathbf{n}$ are vectors with six components). The components of the tensor $\tilde{\mathbf{C}}$ are as follows

$$\tilde{C}_{11} = \tilde{C}_{22} = \tilde{C}_{33} = K + \frac{4}{3}G\,\tilde{\beta}\,, \qquad \tilde{C}_{21} = \tilde{C}_{31} = \tilde{C}_{32} = K - \frac{2}{3}G\,\tilde{\beta}$$
$$\tilde{C}_{44} = \tilde{C}_{55} = \tilde{C}_{66} = G\,\tilde{\beta}\,.$$

Here

$$\tilde{\beta} = \begin{bmatrix} \dfrac{\mathbf{s}_{n+1}^{(i)} \colon \mathbf{s}_{n+1}^{(i)}}{\mathbf{s}_{n+1}^{*(i)} \colon \mathbf{s}_{n+1}^{*(i)}} \end{bmatrix}, \qquad \mathbf{n} = \frac{\mathbf{s}_{n+1}^{(i)}(\text{vector})}{R_{n+1}^{(i)}} \qquad \text{and} \qquad R_{n+1}^{(i)} = \sqrt{\frac{2}{3}}\kappa\left(\overline{e}_{n+1}^{p(i)}\right).$$

For the numerical treatment of large plastic deformations we shall apply the total Lagrangian formulation. The increment of the stress tensor is measured by the second Piola-Kirchhoff stress tensor $\mathbf{P}^{II}$. Using the components of stress tensor $\mathbf{P}^{II}$ we construct the vector of stresses $\mathbf{S}$ which is related to the vector of the Green-Lagrange strains $\boldsymbol{\varepsilon}_G$ through the matrix of tangent moduli. For the vectors of stresses and strain increments, we assume that

$$\mathbf{P}^{II} \quad \rightarrow \quad \Delta\mathbf{S} = \mathbf{C}^{ep}\Delta\boldsymbol{\varepsilon}_G. \tag{4.7}$$

Integrating equation (2.27) in a finite time interval, we have

$$\Delta\mathbf{P}^{II} = J\,\mathbf{U}^{-1}\cdot\Delta\mathbf{t}\cdot\mathbf{U}^{-1} + \operatorname{tr}(\Delta\mathbf{D})\,\mathbf{P}^{II} - \mathbf{U}^{-1}\cdot\Delta\mathbf{U}\cdot\mathbf{P}^{II} - \mathbf{P}^{II}\cdot\Delta\mathbf{U}\cdot\mathbf{U}^{-1}. \tag{4.8}$$

The integration of equation (2.19) gives the increment in terms of the unrotated deformation rate

$$\Delta\mathbf{d} = \mathbf{U}^{-1}\cdot\Delta\mathbf{E}\cdot\mathbf{U}^{-1}. \tag{4.9}$$

In order to obtain a symmetric matrix $\mathbf{C}^{ep}$ for the tangent moduli from the combination of (4.8), (4.9) and (4.6), we shall assume the followings:

1. Since the plastic deformation is incompressible the larger deformations are the more negligible the value of $\operatorname{tr}(\Delta\mathbf{D})$ is.
2. The term $\Delta\mathbf{U}$ is negligible comparing to $\mathbf{U}^{-1}$ and $\mathbf{P}^{II}$. This assumption will slow down the convergency to some extent.

Based on the preceding assumptions, we can write

$$\Delta\mathbf{P}^{II} = J\,\mathbf{U}^{-1}\cdot\Delta\mathbf{t}\cdot\mathbf{U}^{-1} \quad \Longrightarrow \quad \Delta\mathbf{S} = \mathbf{C}^{ep}\Delta\boldsymbol{\varepsilon}_G \tag{4.10}$$

where

$$\mathbf{C}^{ep} = J\mathbf{Q}\mathbf{C}^{*ep}\mathbf{Q}^T. \tag{4.11}$$

Making use of the notations

$$u_1 = U_{11}^{-1}, \quad u_2 = U_{21}^{-1}, \quad u_3 = U_{22}^{-1}, \quad u_4 = U_{31}^{-1}, \quad u_5 = U_{32}^{-1}, \quad u_6 = U_{33}^{-1},$$

the matrix $\mathbf{Q}$ can be given in the form

$$\mathbf{Q} = \begin{bmatrix} u_1^2 & u_2^2 & u_4^2 & 2u_1u_2 & 2u_2u_4 & 2u_1u_4 \\ u_2^2 & u_3^2 & u_5^2 & 2u_2u_3 & 2u_3u_5 & 2u_2u_5 \\ u_4^2 & u_5^2 & u_6^2 & 2u_4u_5 & 2u_5u_6 & 2u_4u_6 \\ u_1u_2 & u_2u_3 & u_4u_5 & u_1u_3+u_2^2 & u_4u_3+u_2u_5 & u_1u_5+u_2u_4 \\ u_2u_4 & u_3u_5 & u_5u_6 & u_2u_5+u_4u_3 & u_3u_6+u_5^2 & u_2u_6+u_4u_5 \\ u_1u_4 & u_2u_5 & u_4u_6 & u_1u_5+u_2u_4 & u_2u_6+u_4u_5 & u_1u_6+u_4^2 \end{bmatrix}. \tag{4.12}$$

For axially symmetric and $2D$ problems, the matrix $\mathbf{Q}$ is tailored by deleting the appropriate rows and columns. The rows and columns of $\mathbf{Q}$ are ordered as follows: x, y, z, xy, yz, xz.

The fast convergence of the Newton iteration with the tangential matrix $\mathbf{C}^{*ep}$ proves its efficiency in spite of the two preceding assumptions we made in connection with the transformation.

5. Solution of the nonlinear elastoplastic problem

5.1. The total Lagrangian formulation. In the course of elastoplastic deformations, the points of the body assume different elastoplastic states. Some points are in elastic state and the rest are in plastic state. We treat the elastoplastic problem by means of the principle of the virtual work. Referring to the book by Bathe [2] but not entering into details, we write the variational equation

$$\int\limits_{{}^oV} \left[\delta\left(\Delta\tilde{\mathbf{E}}_L^{(i)}\right) : \mathbf{C}^{ep} : \Delta\tilde{\mathbf{E}}_L^{(i)} + \delta\left(\Delta\tilde{\mathbf{E}}_{NL}^{(i)}\right) : \mathbf{P}_n^{II}\right] \mathrm{d}^oV = \\ = \delta W_{n+1} - \int\limits_{{}^oV} \delta\left(\Delta\tilde{\mathbf{E}}_L^{(i)}\right) : \mathbf{P}_n^{II}\, \mathrm{d}^oV\,, \quad (5.1)$$

which expresses the equilibrium and compatibility requirements over the time period from t_n to t_{n+1}. The Green-Lagrange strain tensor at the time t_{n+1} is given by

$$\mathbf{E} = \frac{1}{2}\left[\mathbf{F}_{n+1}^T \cdot \mathbf{F}_{n+1} - \mathbf{1}\right] \quad (5.2)$$

where

$$\mathbf{F}_{n+1} = \frac{\partial\,(\mathbf{X} + \mathbf{u}_{n+1})}{\partial\,\mathbf{X}} = \mathbf{1} + \frac{\partial\,\mathbf{u}_{n+1}}{\partial\,\mathbf{X}} = \mathbf{1} + (\nabla\mathbf{u})_{n+1} \equiv 1 + grad\,(\mathbf{u}_{n+1})\,. \quad (5.3)$$

$\mathbf{E}_{n+1}$ can be expressed in terms of the displacement vector as well:

$$\mathbf{E}_{n+1} = \frac{1}{2}\left[(\nabla\mathbf{u})^T + (\nabla\mathbf{u}) + (\nabla\mathbf{u})^T \cdot (\nabla\mathbf{u})\right]_{n+1}\,. \quad (5.4)$$

If convergency is achieved in the i^{th} iteration step by performing a load step from time t_n to t_{n+1}, then it is expedient to decompose the displacement as follows

$$\mathbf{u}_{n+1}^{(i)} = \mathbf{u}_n + \tilde{\mathbf{u}}^{(i)} = \mathbf{u}_n + \tilde{\mathbf{u}}^{(i-1)} + \tilde{\tilde{\mathbf{u}}}^{(i)} \equiv \mathbf{u}_{n+1}^{(i-1)} + \tilde{\tilde{\mathbf{u}}}^{(\mathbf{i})}\,, \quad (5.5)$$

where $\tilde{\mathbf{u}}^{(i)}$ denotes the displacement increment corresponding to $\Delta\mathbf{u}^{(i)}$. Consequently, equation (5.4) can be rewritten:

$$\mathbf{E}_{n+1}^{(i)} = \mathbf{E}_n + \Delta\tilde{\mathbf{E}}_L^{(i)} + \Delta\tilde{\mathbf{E}}_{NL}^{(i)}\,, \quad (5.6)$$

where

$$\Delta\tilde{\mathbf{E}}_L^{(i)} = \frac{1}{2}\left[\left(\nabla\tilde{\mathbf{u}}^{(i)}\right)^T + \left(\nabla\tilde{\mathbf{u}}^{(i)}\right) + (\nabla\mathbf{u}_n)^T \cdot \left(\nabla\tilde{\mathbf{u}}^{(i)}\right) + \left(\nabla\tilde{\mathbf{u}}^{(i)}\right)^T \cdot (\nabla\mathbf{u}_n)\right] \quad (5.7)$$

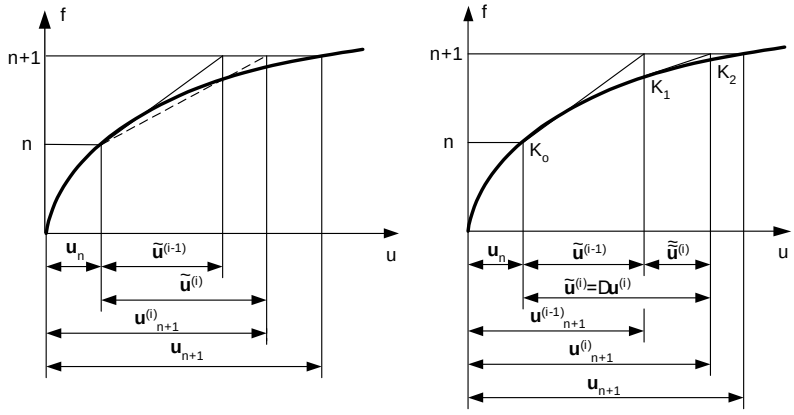

Figure 1. Iteration schemes for one load step

and

$$\Delta\tilde{\mathbf{E}}_{NL}^{(i)} = \frac{1}{2}\left[\left(\nabla\tilde{\mathbf{u}}^{(i)}\right)^T \cdot \left(\nabla\tilde{\mathbf{u}}^{(i)}\right)\right]. \tag{5.8}$$

It is more favorable to recalculate the constitutive matrix $\mathbf{C}^{ep}$ in each iteration step (see Figure 6.1b) than to follow the iteration scheme shown in Figure 6.1a. Therefore equation (5.1) is modified as

$$\int_{{}^oV}\left[\delta\left(\Delta\overset{\approx}{\mathbf{E}}_L^{(i)}\right) : \mathbf{C}_{(i-1)}^{ep} : \Delta\overset{\approx}{\mathbf{E}}_L^{(i)} + \delta\left(\Delta\overset{\approx}{\mathbf{E}}_{NL}^{(i)}\right) : \mathbf{P}_n^{II}\right] \mathrm{d}^oV =$$

$$= \delta W_{n+1} - \int_{{}^oV}\delta\left(\Delta\overset{\approx}{\mathbf{E}}_L^{(i)}\right) : \mathbf{P}_{n+1}^{II(i-1)}\,\mathrm{d}^oV, \tag{5.9}$$

where

$$\mathbf{E}_{n+1}^{(i)} = \mathbf{E}_{n+1}^{(i-1)} + \Delta\overset{\approx}{\mathbf{E}}_L^{(i)} + \Delta\overset{\approx}{\mathbf{E}}_{NL}^{(i)}. \tag{5.10}$$

$$\Delta\overset{\approx}{\mathbf{E}}_L^{(i)} = \frac{1}{2}\left[\left(\nabla\overset{\approx}{\mathbf{u}}^{(i)}\right)^T + \left(\nabla\overset{\approx}{\mathbf{u}}^{(i)}\right) + \left(\nabla\mathbf{u}_{n+1}^{(i-1)}\right)^T \cdot \left(\nabla\overset{\approx}{\mathbf{u}}^{(i)}\right) + \left(\nabla\overset{\approx}{\mathbf{u}}^{(i)}\right)^T \cdot \left(\nabla\mathbf{u}_{n+1}^{(i-1)}\right)\right] \tag{5.11}$$

$$\Delta\overset{\approx}{\mathbf{E}}_{NL}^{(i)} = \frac{1}{2}\left[\left(\nabla\overset{\approx}{\mathbf{u}}^{(i)}\right)^T \cdot \left(\nabla\overset{\approx}{\mathbf{u}}^{(i)}\right)\right] \tag{5.12}$$

$$\mathbf{P}_{n+1}^{II(i-1)} = J_{n+1}^{(i-1)}\left(\mathbf{U}_{n+1}^{(i-1)}\right) \cdot \mathbf{t}_{n+1}^{(i-1)} \cdot \left(\mathbf{U}_{n+1}^{(i-1)}\right)^{-1} \tag{5.13}$$

5.2. Finite element discretization. For the numerical treatment of (5.9), we perform the discretization by the finite element method. The increment in displacement is approximated as

$$\overset{\approx}{\mathbf{u}}^{(i)} \quad \Longrightarrow \quad \mathbf{N}(\mathbf{X})\,\overset{\approx}{\mathbf{q}}^{(i)} \tag{5.14}$$

where $\mathbf{N}(\mathbf{X})$ is the matrix of shape functions, $\overset{\approx}{\mathbf{q}}^{(i)}$ is the vector of displacement parameters. The matrix of shape functions can be constructed by using either the product space or the truncated space [18].

Using the approximation (5.14), we can give the vector of the strain increments corresponding to the Green-Lagrange strain tensor

$$\Delta\overset{\approx}{\mathbf{E}}^{(i)} \Longrightarrow \overset{\approx}{\boldsymbol{\varepsilon}}_L^{(i)} + \overset{\approx}{\boldsymbol{\varepsilon}}_{NL}^{(i)} = \mathbf{B}_L^{(i-1)}(\mathbf{X})\,\overset{\approx}{\mathbf{q}}^{(i)} + \mathbf{B}_{NL}^{(i-1)}(\mathbf{X})\,\overset{\approx}{\mathbf{q}}^{(i)} \tag{5.15}$$

where $\overset{\approx}{\boldsymbol{\varepsilon}}_L^{(i)}$ and $\overset{\approx}{\boldsymbol{\varepsilon}}_{NL}^{(i)}$ are the so-called linear and nonlinear strain increments, respectively.

Making use of equations (5.14) and (5.15), we can discretize the integrals below:

$$\int_{{}^oV} \delta\left(\Delta\overset{\approx}{\mathbf{E}}_L^{(i)}\right) : \mathbf{C}_{(i-1)}^{ep} : \Delta\overset{\approx}{\mathbf{E}}_L^{(i)}\,\mathrm{d}^oV \Longrightarrow \delta\overset{\approx}{\mathbf{q}}^{(i)T} \underbrace{\int_{{}^oV} \mathbf{B}_L^{(i-1)T}\mathbf{C}_{(i-1)}^{ep}\mathbf{B}_L^{(i-1)}\mathrm{d}^oV}_{\mathbf{K}_L^{(i-1)}} \overset{\approx}{\mathbf{q}}^{(i)}\,, \tag{5.16}$$

$$\int_{{}^oV} \delta\left(\Delta\overset{\approx}{\mathbf{E}}_{NL}^{(i)}\right) : \mathbf{P}_n^{II}\,\mathrm{d}^oV \Longrightarrow \delta\overset{\approx}{\mathbf{q}}^{(i)T} \underbrace{\int_{{}^oV} \mathbf{B}_{NL}^{(i-1)T}\boldsymbol{\sigma}_n\mathbf{B}_{NL}^{(i-1)}\mathrm{d}^oV}_{\mathbf{K}_{NL}^{(i-1)}} \overset{\approx}{\mathbf{q}}^{(i)}\,, \tag{5.17}$$

$$\int_{{}^oV} \delta\left(\Delta\overset{\approx}{\mathbf{E}}_L^{(i)}\right) : \mathbf{P}_{n+1}^{II(i-1)}\,\mathrm{d}^oV \Longrightarrow \delta\overset{\approx}{\mathbf{q}}^{(i)T} \underbrace{\int_{{}^oV} \mathbf{B}_L^{(i-1)T}\hat{\boldsymbol{\sigma}}_n^{(i-1)}\,\mathrm{d}^oV}_{\mathbf{f}_\sigma^{(i-1)}}\,, \tag{5.18}$$

$$\delta W_{n+1} = \delta\overset{\approx}{\mathbf{q}}^{(i)T}\left[\int_{{}^oV} \mathbf{N}^{To}(\rho\mathbf{k})_{n+1}\,\mathrm{d}^oV - \int_{{}^oA_p} \mathbf{N}^{To}\overline{\mathbf{p}}_{n+1}\,\mathrm{d}^oA\right] = \delta\overset{\approx}{\mathbf{q}}^{(i)T}\mathbf{f}_{n+1}\,. \tag{5.19}$$

The load vectors evaluated over the volume ${}^oV$ and the surface ${}^oA_p$ correspond to the reference configuration. Consequently, the traction $\bar{\mathbf{p}}_{n+1}$ exerted at time t_{n+1} can be transformed into the reference configuration

$${}^o\bar{\mathbf{p}}_{n+1} = \mathbf{F}_{n+1}^{-1}\cdot\bar{\mathbf{p}}_{n+1}\,. \tag{5.20}$$

However, the body force follows the transformation rule

$${}^o(\rho\mathbf{k})_{n+1} = (\det\mathbf{J})^{-1}(\rho\mathbf{k})_{n+1}\,. \tag{5.21}$$

With the integrals (5.16)-(5.19) and the transformations (5.20), (5.21), the incremental form of the virtual work is discretized as

$$\delta\overset{\approx}{\mathbf{q}}^{(i)T}\left\{[\mathbf{K}_L^{(i-1)}+\mathbf{K}_{NL}^{(i-1)}]\overset{\approx}{\mathbf{q}}^{(i)} - \left(\mathbf{f}_{n+1}-\mathbf{f}_\sigma^{(i-1)}\right)\right\} = 0 \qquad i = 1,2,\ldots \tag{5.22}$$

where $\delta\overset{\approx}{\mathbf{q}}^{(i)T}$ is arbitrary, consequently the following equation holds

$$[\mathbf{K}_L^{(i-1)}+\mathbf{K}_{NL}^{(i-1)}]\overset{\approx}{\mathbf{q}}^{(i)} = \mathbf{f}_{n+1}-\mathbf{f}_{\sigma}^{(i-1)} \equiv \mathbf{r}^{(i-1)} \tag{5.23}$$

in which the sum in brackets is the tangential stiffness matrix:

$$\mathbf{K}_L^{(i-1)}+\mathbf{K}_{NL}^{(i-1)} = \mathbf{K}_T^{(i-1)} \tag{5.24}$$

At the beginning of the iteration ($i = 1$) we use the elastoplastic state obtained at time t_n to initialize the iteration. The iteration is terminated if the unbalanced load vector $\mathbf{r}^{(i)}$ vanishes, i.e., if

$$\left\|\mathbf{r}^{(i)}\right\| = \sqrt{\mathbf{r}^{(i)T}\mathbf{r}^{(i)}} \leq TOL\,\|\mathbf{f}_{n+1}\| \tag{5.25}$$

where $TOL = 0.001 - 0.0001$.

5.3. Updating the stress state. The solution of equation (5.23) in the i^{th} iteration gives the vector of displacements $\overset{\approx}{\mathbf{q}}^{(i)}$, in this way we can calculate $\overset{\approx}{\mathbf{u}}^{(i)}$ from (5.14) and $\mathbf{u}_{n+1}^{(i)}$ from (5.5). Then we obtain the actual stress state as given subsequently.

The time integration of the velocity is performed by the method proposed by Pinsky, Ortiz and Pister [13]. This is a mid-increment scheme, second order accurate and unconditionally stable. The procedure determines the displacement at the middle of the time interval

$$\mathbf{u}_{n+1/2}^{(i)} = \frac{1}{2}\left(\mathbf{u}_n + \mathbf{u}_{n+1}^{(i)}\right) \tag{5.26}$$

The steps of the algorithm:

Step 1. Determination of the deformation gradient for the states $n + 1/2$ and $n + 1$

$$\mathbf{F}_{n+1}^{(i)} = \frac{\partial\left(\mathbf{X}+\mathbf{u}_{n+1}^{(i)}\right)}{\partial\mathbf{X}}, \quad J_{n+1}^{(i)} = \det\left(\mathbf{F}_{n+1}^{(i)}\right), \quad \mathbf{F}_{n+1/2}^{(i)} = \frac{\partial\left(\mathbf{X}+\mathbf{u}_{n+1/2}^{(i)}\right)}{\partial\mathbf{X}}. \tag{5.27}$$

Step 2. Polar decomposition with the method described in Appendix II:

$$\mathbf{F}_{n+1}^{(i)} = \mathbf{R}_{n+1}^{(i)}\cdot\mathbf{U}_{n+1}^{(i)}, \qquad \mathbf{F}_{n+1/2}^{(i)} = \mathbf{R}_{n+1/2}^{(i)}\cdot\mathbf{U}_{n+1/2}^{(i)}. \tag{5.28}$$

Step 3. Integration of the tensor $\mathbf{L} = \dot{\mathbf{F}}\cdot\mathbf{F}^{-1}$:

Since

$$\mathbf{L} = \frac{\partial\mathbf{v}}{\partial\mathbf{x}} = \frac{\partial\mathbf{v}}{\partial\mathbf{X}}\cdot\mathbf{F}^{-1},$$

we can write

$$\frac{\partial}{\partial\mathbf{x}}\frac{\partial\mathbf{u}}{\partial t} = \frac{\partial}{\partial\mathbf{X}}\frac{\partial\mathbf{u}}{\partial t}\cdot\mathbf{F}^{-1},$$

from which it follows by an integration with respect to time t that

$$\int\frac{\partial}{\partial\mathbf{x}}\frac{\partial\mathbf{u}}{\partial t}\,\mathrm{d}t = \int\frac{\partial}{\partial\mathbf{X}}\frac{\partial\mathbf{u}}{\partial t}\cdot\mathbf{F}^{-1}\,\mathrm{d}t.$$

If the deformation gradient is taken at the middle of the time step we get

$$\int \frac{\partial}{\partial \mathbf{x}} \, \mathrm{d}\mathbf{u} = \int \frac{\partial}{\partial \mathbf{X}} \, \mathrm{d}\mathbf{u} \cdot \mathbf{F}_{n+1/2}^{-1} \, .$$

The deformation gradient is then calculated as follows

$$\frac{\partial \left(\Delta \mathbf{u}^{(i)}\right)}{\partial \mathbf{x}} = \frac{\partial \left(\Delta \mathbf{u}^{(i)}\right)}{\partial \mathbf{X}} \cdot \mathbf{F}_{n+1/2}^{-1} \, ,$$

where $\Delta \mathbf{u}^{(i)}$ is the displacement increment

$$\Delta \mathbf{u}^{(i)} = \tilde{\mathbf{u}}^{(i)} = \mathbf{u}_{n+1}^{(i)} - \mathbf{u}_n \, .$$

For the increment of $\mathbf{L}$ we now can write

$$\Delta \mathbf{L}^{(i)} = \Delta \mathbf{F}^{(i)} \cdot \mathbf{F}_{n+1/2}^{-1} \, , \tag{5.29}$$

where the increment of the deformation gradient $\mathbf{F}$ is

$$\Delta \mathbf{F}^{(i)} = \frac{\partial \left(\Delta \mathbf{u}^{(i)}\right)}{\partial \mathbf{X}} \, . \tag{5.30}$$

Step 4. Computation of the symmetric part of $\Delta \mathbf{L}^{(i)}$:

$$\Delta \mathbf{D}^{(i)} = \frac{1}{2} \left[\Delta \mathbf{L}^{(i)} + \Delta \mathbf{L}^{(i)T} \right] \quad . \tag{5.31}$$

Step 5. Transformation of the increment in the rate of deformation tensor to an increment of the unrotated deformation rate tensor:

$$\Delta \mathbf{d}^{(i)} = \mathbf{R}_{n+1/2}^{(i)T} \cdot \Delta \mathbf{D}^{(i)} \cdot \mathbf{R}_{n+1/2}^{(i)} \quad . \tag{5.32}$$

Step 6. With the knowledge of $\Delta \mathbf{d}^{(i)}$ we can perform the calculations detailed in Appendix I in order to determine the elastoplastic state together with the yield surface and the Cauchy stress tensor. Using a symbolic notation

$$\mathbf{t}_{n+1}^{(i)} \Longleftarrow RRA(\mathbf{t}_{n+1}^{(i-1)}, \bar{e}_{n+1}^{p(i-1)}, \boldsymbol{\alpha}_{n+1}^{(i-1)}, \Delta \mathbf{d}^{(i)}) \, , \tag{5.33}$$

where *RRA* denotes the radial return mapping algorithm.

In the course of the time integration we obtain the following quantities:

the equivalent plastic strain

$$\bar{e}_{n+1}^{p(i)} \, , \tag{5.34}$$

the deviatoric stress at the centre of the yielding surface

$$\boldsymbol{\alpha}_{n+1}^{(i)} \, , \tag{5.35}$$

the deviatoric stress tensor

$$\mathbf{s}_{n+1}^{(i)} \, , \tag{5.36}$$

the total stress tensor

$$\mathbf{t}_{n+1}^{(i)} ,$$

and the elastoplastic consistent matrix $\mathbf{C}_{(i)}^{ep}$ (see (4.11) for details).

Applying the p-version of the finite element method the hydrostatic stress field is smoothed by a low order approximation $(p/2)$.

Step 7. Let us transform the Cauchy stress $\mathbf{t}_{n+1}^{(i)}$ obtained in the unrotated configuration to the reference coordinate system

$$\mathbf{P} = J_{n+1}^{(i)} (\mathbf{U}_{n+1}^{(i)})^{-1} \cdot \mathbf{t}_{\mathbf{n+1}}^{(\mathbf{i})} \cdot (\mathbf{U}_{n+1}^{(i)})^{-1} . \tag{5.37}$$

5.4. The global algorithm of the nonlinear problem. As is given in the previous subsection, we perform the seven steps in each Gauss integration point, and we obtain the point K_1 starting from point K_0 in iteration $i = 1$, then point K_2 from point K_1 in iteration $i = 2$, and so on (see Figure 6.1b). That is, in each iteration i we determine the stiffness matrices $\mathbf{K}_L^{(i-1)}$, $\mathbf{K}_{NL}^{(i-1)}$ and the vector of internal forces $\mathbf{f}_\sigma^{(i-1)}$ with the quantities calculated in the seven steps.

The external forces are applied gradually in a sequence of load steps, and in the course of the equilibrium iteration (i) the elastoplastic condition is always checked.

The scheme of the algorithm:
Loop for the load steps $(n = 1, 2, ..., nload)$.

α. Equilibrium iteration $(i = 1, 2, ...)$.

A/ Generate the system matrices and vectors:

$$\mathbf{K}_L^{(i-1)}, \mathbf{K}_{NL}^{(i-1)}, \mathbf{f}_\sigma^{(i-1)}, \mathbf{f}_\sigma^{(0)} = \mathbf{0} .$$

B/ Solve for $\approx\!\!\!\!\!\!\sim\!\!\!\!\!\!\sim^{(i)}$

$$[\mathbf{K}_L^{(i-1)} + \mathbf{K}_{NL}^{(i-1)}] \approx\!\!\!\!\!\!\sim\!\!\!\!\!\!\sim^{(i)} = \mathbf{f}_{n+1} - \mathbf{f}_\sigma^{(i-1)} \equiv \mathbf{r}^{(i-1)} .$$

C/ Update the vector of displacement parameters

$$\mathbf{q}_{n+1}^{(i)} = \mathbf{q}_{n+1}^{(i-1)} + \approx\!\!\!\!\!\!\sim\!\!\!\!\!\!\sim^{(i)} .$$

D/ Loop for the finite elements $(e = 1, ..., n_e)$:
a/ Loop for the Gauss integration points:
I/ Determination of the displacement field

$$\mathbf{u}_{n+1}^{(i)} = \mathbf{N}(\mathbf{X})\, \mathbf{q}_{n+1}^{(i)} .$$

II/ Calculate the displacement of the half step

$$\mathbf{u}_{n+1/2}^{(i)} = \frac{1}{2} \left(\mathbf{u}_n^{(i)} + \mathbf{u}_{n+1}^{(i)} \right) .$$

III/ Update the stresses (Step 1-7) in accordance with Section 5.3.

b/ Generate the element stiffness matrices and the vector of internal forces

$$\left(\mathbf{K}_L^{(i)}\right)_e, \left(\mathbf{K}_{NL}^{(i)}\right)_e, \left(\mathbf{f}_\sigma^{(i)}\right)_e .$$

E/ Check for convergence
if $\left\|\mathbf{r}^{(i)}\right\| \leq TOL \left\|\mathbf{f}_{n+1}\right\|$ then go to (β) else $i = i + 1$ and go to (A) .

β. Prepare the next load step $n = n + 1$

$$\mathbf{q}_n \Longleftarrow \mathbf{q}_{n+1}, \qquad \mathbf{f}_n \Longleftarrow \mathbf{P}_n^{II} .$$

If $n \leq nload$ then go to (α) else STOP.

6. Numerical example

An axisymmetric cylinder with a height of 40 mm and a diameter of 35 mm is compressed between two rough rigid plates (see Figure 2). The material is elastoplastic with the following hardening rule

$$\kappa\left(\overline{e}^p\right) = \sigma_\infty - \left(\sigma_\infty - \sigma_Y\right) \exp\left(-\gamma \overline{e}^p\right) + \sigma^o \overline{e}^p$$

where $\sigma_\infty = 0.343$ MPa, $\sigma_Y = 0.243$ MPa, $\sigma^o = 0.15$ MPa, $\gamma = 0.1$. The elastic properties of the material are characterized by Young's modulus and Poisson's ratio: $E = 70$ MPa, $\nu = 0.2$.

Two meshes were used for the discretization of the quarter of the domain. In the first mesh denoted by (2×2) there are 4 axsisymmetric p-extension elements [18], the

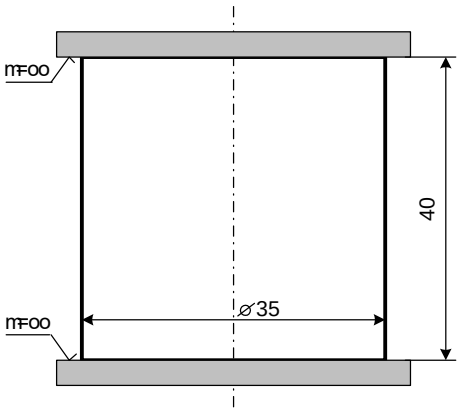

Figure 2.

mesh has two elements in the radial direction and two elements in axial direction. The second mesh denoted by (4×4) has a double density compared to the first one, i.e., it has direction and four elements in the axial direction. First we will use the product space for the approximation of the displacement fields. We note that the number of bubble functions of the truncated space is equal to 15 for $p = 8$, however we have 49 bubble functions in the product space for $p = 8$. This gives a possibility to investigate different ways in which the approximation of the volumetric change. Symmetry conditions are specified on the axis and in the middle plane of the cylinder. Sticking conditions and a prescribed compressive displacement are specified at the tool-workpiece interface.

The total height reduction of 20% is obtained in 10 increments. The polynomial degree of the approximation is $p = 8$, the numerical integration is performed on 9×9 Gauss points. The volumetric change is evaluated directly from the displacement fields.

The deformed shapes and the distributions of the plastic strains $\overline{\epsilon}^p$ are displayed for the two meshes in Figures 3 and 4. In the gray scale of plastic strains black corresponds to the maximum value (1.137) and white corresponds to the minimum value (0). The maximum value (1.137) has been computed at the upper right corner of the domain. The corresponding von Mises stresses have also been evaluated as shown in Figures 5 and 6. In the gray scale of the von Mises stresses black corresponds to the maximum value ($0.4015\, MPa$) and white corresponds to the minimum value (0). The results for the different meshes show good agreement. Here we see the effectiveness of the p-extension as the results are reliable also for a coarse mesh.

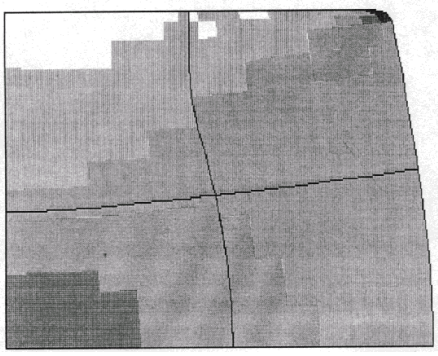

Figure 3.

Distribution of plastic strains for the mesh (2×2)

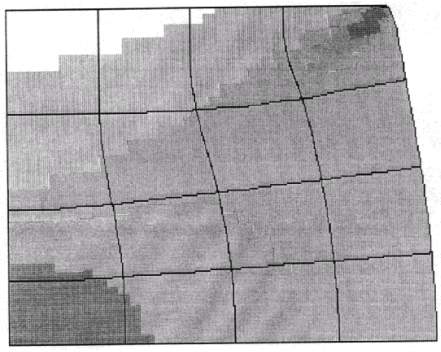

Figure 4.

Distribution of plastic strains for the mesh (4×4)

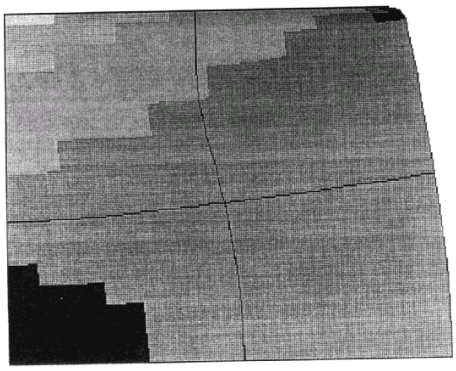

Figure 5.

Distribution of the von Mises stress for the mesh (2×2)

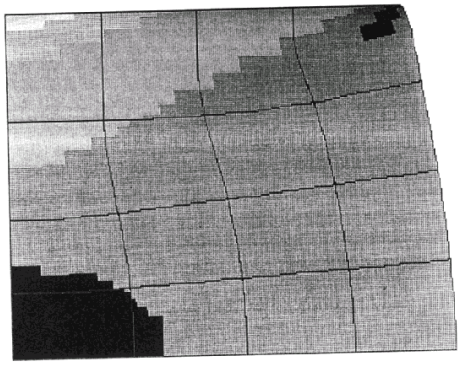

Figure 6.

Distribution of the von Mises stress for the mesh (2×2)

The weakening of the volumetric change is not needed for the product space if $p = 8$ and the order of integration is 9×9. In this case, the number of integration points for one element (81) is smaller than the number of bubble functions (98), therefore the element has extra degrees of freedom to satisfy the elastoplastic equations.

The truncated space [18] can also be used for the solution of the elastoplastic problem. We experienced that the volumetric change should be weakened. Therefore we applied the least square method with a polynomial degree of $p/2$ to smooth the volumetric change field. The same layout of the problem has been analyzed with the following material parameters: $\sigma_\infty = 30\,\mathrm{MPa}$, $\sigma_Y = 20\,\mathrm{MPa}$, $\sigma^o = 2\,\mathrm{MPa}$, $\gamma = 0.1$. The elastic properties are given by the Young's modulus $E = 2700\,\mathrm{MPa}$, and the Poisson's ratio $\nu = 0.35$. The total height reduction, which is 10%, is obtained in 5 increments.

For the second mesh (4×4) we performed the computations for different degrees of approximation by using the truncated space. The computed characteristic stress components are shown in Table 1. As can be seen, we obtained similar results for $p = 6$ and $p = 8$, i.e., convergence has been achieved by the p-version of the finite element method for a large strain elastoplastic problem.

Table 1. Characteristic stress values

p	min/max	σ_r	σ_φ	σ_z	τ_{rz}
2	min	$-0.2745 \cdot 10^2$	$-0.2797 \cdot 10^2$	$-0.4076 \cdot 10^2$	$-0.1042 \cdot 10^2$
2	max	$+0.1604 \cdot 10^2$	$+0.1155 \cdot 10^2$	$-0.3289 \cdot 10^1$	$+0.5686 \cdot 10^1$
4	min	$-0.4093 \cdot 10^2$	$-0.4094 \cdot 10^2$	$-0.6099 \cdot 10^2$	$-0.9211 \cdot 10^1$
4	max	$+0.1123 \cdot 10^2$	$+0.1121 \cdot 10^2$	$-0.8859 \cdot 10^1$	$+0.6156 \cdot 10^1$
6	min	$-0.2970 \cdot 10^2$	$-0.3262 \cdot 10^2$	$-04746 \cdot 10^2$	$-0.8916 \cdot 10^1$
6	max	$+0.6110 \cdot 10^1$	$+0.9757 \cdot 10^1$	$-0.1119 \cdot 10^2$	$+0.5541 \cdot 10^1$
8	min	$-0.3086 \cdot 10^1$	$-0.3204 \cdot 10^2$	$-0.4609 \cdot 10^2$	$-0.8887 \cdot 10^1$
8	max	$+0.6110 \cdot 10^1$	$+0.9766 \cdot 10^2$	$-0.1118 \cdot 10^2$	$0.6324 \cdot 10^1$

We note that when the height reduction was increased over 20%, the element in the upper right corner of the mesh became distorted so the convexity of the element was destroyed.

7. Conclusion

A finite element code has been developed to solve large strain elastoplastic problems using p-extension elements. The total Lagrangian formulation of the finite element method has been implemented. Large and incompressible plastic deformations were assumed. The constitutive computations have been performed in the unrotated frame. The radial return mapping algorithm was used for the treatment of the yield surface. Kinematic and isotropic hardening rules were adopted.

From the numerical experiments we concluded that p-extension of the finite elements can be applied for the analysis of large strain elastoplastic problems. The

approximation of the displacement fields has been investigated by means of two different polinomial spaces: the product space and the trunceted space.

Making use of the product space and integrating numerically with a (9×9) integration order, we obtained smooth solutions for the case when p was equal to 8 both for the displacement fields and for the volumetric change. The advantageous behavior of the product space follows from the fact that the number of bubble functions is greater than the number of integration points.

Applying the truncated space with polynomial degree p for the approximation of the displacement fields, we obtained smooth solutions if the volumetric change was weakened. We experienced that smoothing the volumetric change by the least square method with polynomials of degree $p/2$ provides a proper choice for the different values of p (for $p = 2, 4, 6, 8$).

Since the p-extension of the finite elements are sensitive for stress concentrations, the deformed elements may be distorted at the vicinity of the singular points. Therefore remeshing of the domain is required even for relatively small displacements.

8. Appendix I: Radial return mapping

We shall assume that all quantities are known at time t_n. Increasing the load gradually we determine all quantities with an elastic prediction. Therefore the point representing the elastic state we have predicted will be, in all probability, outside the yield surface. Then due to an orthogonal mapping the point will be placed on the surface. The elastic prediction gives the stress deviatoric tensor:

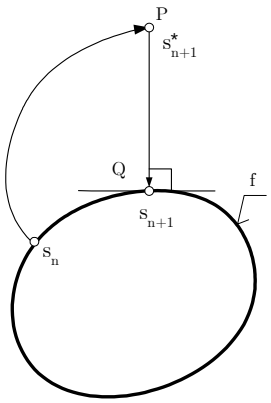

Figure 7.

$$\mathbf{s}^*_{n+1} = \mathbf{s}_n + 2G\Delta\mathbf{e}_{n+1}\,. \tag{8.1}$$

The treatment of the plastic problem is practically an optimization problem. Let f be an arbitrary but convex yield surface. We have to find the point of f with the smallest distance from a point elastically predicted and located outside f. The unit normal to the yield surface at the end of the time interval $[t_n, t_{n+1}]$ is denoted by $\mathbf{n}$. It is obvious that

$$\hat{\mathbf{n}} = \left.\frac{\partial f}{\partial \boldsymbol{\xi}}\right|_{n+1} \cdot \frac{1}{\left\|\frac{\partial f}{\partial \boldsymbol{\xi}}\right\|_{n+1}} = \frac{\boldsymbol{\xi}_{n+1}}{\left\|\frac{\partial f}{\partial \boldsymbol{\xi}}\right\|_{n+1}}\,. \tag{8.2}$$

Making use of equation (3.7) we can write

$$\frac{\partial f}{\partial \boldsymbol{\xi}} = \frac{\partial}{\partial \boldsymbol{\xi}}\sqrt{\boldsymbol{\xi} : \boldsymbol{\xi}} = \frac{\boldsymbol{\xi}}{\|\boldsymbol{\xi}\|}\,,$$

where

$$\boldsymbol{\xi} = \mathbf{s}_{n+1} - \boldsymbol{\alpha}_{n+1} \quad . \tag{8.3}$$

Starting from the elastoplastic state corresponding to t_n one can obtain the state at t_{n+1} through the following integral

$$\int_{t_n}^{t_{n+1}} 2G\dot{\mathbf{e}}^p d\tau = \int_{t_n}^{t_{n+1}} 2G\gamma\hat{\mathbf{n}}\, d\tau,$$

which is calculated approximately as

$$2G\left(\gamma\Delta t\right)\,\hat{\mathbf{n}}\ ,$$

where Δt is the time step ($\Delta t = t_{n+1} - t_n$). Therefore

$$\mathbf{s}_{n+1} = \mathbf{s}^*_{n+1} - 2G\left(\gamma\Delta t\right)\,\hat{\mathbf{n}}\,. \tag{8.4}$$

Since the yield surface is modified due to hardening, we need to calculate the equivalent strain as well

$$\bar{e}^p_{n+1} = \bar{e}^p_n + \int_{t_n}^{t_{n+1}} \sqrt{\frac{2}{3}}\left\|\dot{\mathbf{e}}^p\right\|\, d\tau = \bar{e}^p_n + \sqrt{\frac{2}{3}}\left(\gamma\Delta t\right) \quad . \tag{8.5}$$

Making use of equation (3.17), we can write

$$\begin{aligned}\boldsymbol{\alpha}_{n+1} &= \boldsymbol{\alpha}_n + \int_{t_n}^{t_{n+1}} \frac{2}{3}H'_\alpha\left(\bar{e}^p\right)\,\gamma\hat{\mathbf{n}}\, d\tau = \boldsymbol{\alpha}_n + \tfrac{2}{3}H'_\alpha\left(\bar{e}^p_{n+1/2}\right)\left(\gamma\Delta t\right)\,\hat{\mathbf{n}} \\ &= \boldsymbol{\alpha}_n + \frac{2}{3}\frac{H_\alpha\left(\bar{e}^p_{n+1}\right) - H_\alpha\left(\bar{e}^p_n\right)}{\bar{e}^p_{n+1} - \bar{e}^p_n}\left(\gamma\Delta t\right)\,\hat{\mathbf{n}}\end{aligned}$$

for the translation of the centre of the yield surface. Taking (8.5) into account and introducing the notation

$$\Delta H_\alpha = H_\alpha\left(\bar{e}^p_{n+1}\right) - H_\alpha\left(\bar{e}^p_n\right)$$

we have

$$\boldsymbol{\alpha}_{n+1} = \boldsymbol{\alpha}_n + \sqrt{\frac{2}{3}}\Delta H_\alpha\,\hat{\mathbf{n}}\,. \tag{8.6}$$

From (8.3), (8.4) and (8.6) the value of $\boldsymbol{\xi}$ at time t_{n+1} is written as

$$\boldsymbol{\xi}_{n+1} = \mathbf{s}_{n+1} - \boldsymbol{\alpha}_{n+1} = \mathbf{s}^*_{n+1} - \boldsymbol{\alpha}_n - \left[2G\left(\gamma\Delta t\right) + \sqrt{\frac{2}{3}}\Delta H_\alpha\right]\,\hat{\mathbf{n}} \quad . \tag{8.7}$$

Substituting the tensor

$$\boldsymbol{\xi}^*_{n+1} = \mathbf{s}^*_{n+1} - \boldsymbol{\alpha}_n\,, \tag{8.8}$$

we can determine the normal vector $\hat{\mathbf{n}}$

$$\hat{\mathbf{n}} = \frac{\boldsymbol{\xi}^*_{n+1}}{\left\|\boldsymbol{\xi}^*_{n+1}\right\|}\,. \tag{8.9}$$

From (3.7), (8.7) and (8.9) a nonlinear equation is obtained

$$f = f(\gamma\Delta t) = -\sqrt{\tfrac{2}{3}}\kappa\left(\bar{e}^p_{n+1}\right) + \left\|\boldsymbol{\xi}^*_{n+1} - \left[2G\left(\gamma\Delta t\right) + \sqrt{\tfrac{2}{3}}\Delta H_\alpha\right]\frac{\boldsymbol{\xi}^*_{n+1}}{\left\|\boldsymbol{\xi}^*_{n+1}\right\|}\right\| \\ = -\sqrt{\tfrac{2}{3}}\kappa\left(\bar{e}^p_{n+1}\right) + \left\|\boldsymbol{\xi}^*_{n+1}\right\| - \left[2G\left(\gamma\Delta t\right) + \sqrt{\tfrac{2}{3}}\Delta H_\alpha\right] = 0\,, \tag{8.10}$$

where

$$\bar{e}^p_{n+1} = \bar{e}^p_n + \sqrt{\frac{2}{3}}\left(\gamma\Delta t\right) \quad ,$$

and the functions $\kappa\left(\bar{e}^p\right), H_\alpha\left(\bar{e}^p\right)$ are also nonlinear. Since all the quantities are known at time t_n, we can determine $(\gamma\Delta t)$. Introducing the notation $\lambda = \gamma\Delta t$, the steps of the Newton iteration are as follows:

I $$\bar{e}^{p(k)}_{n+1} = \bar{e}^p_n + \sqrt{\frac{2}{3}}\lambda^{(k)}\,,$$

II $$D\,f\left(\lambda^{(k)}\right) \equiv \frac{\partial f}{\partial \bar{e}^p_{n+1}}\frac{\partial \bar{e}^p_{n+1}}{\partial \lambda} = -2G\left[1 + \frac{\kappa' + H'_\alpha}{3G}\right]^{(k)}\,,$$

III $$\lambda^{(k+1)} = \lambda^{(k)} - \frac{f\left(\lambda^{(k)}\right)}{D\,f\left(\lambda^{(k)}\right)}\,,$$

IV If $\left|f\left(\lambda^{(k)}\right)\right| \geq \mathrm{TOL}$ then $k \longleftarrow k+1$ and goto(I) else STOP.

Solving the nonlinear equation (8.10), we can calculate $\bar{e}^p_{n+1}$ from (8.5) and $\boldsymbol{\alpha}_{n+1}$ from (8.6). The deviatoric stress tensor $\mathbf{s}_{n+1}$ is determined in such a way that we measure the radius of the yield surface, that is the value

$$\mathbf{s}_{n+1} = \boldsymbol{\alpha}_{n+1} + \sqrt{\frac{2}{3}}\kappa\left(\bar{e}^p_{n+1}\right)\,\hat{\mathbf{n}} \tag{8.11}$$

from the centre of the yield surface in the direction $\hat{\mathbf{n}}$. The elastic part of the stress tensor is calculated from the volume change:

$$\mathbf{t}_{n+1} = \mathbf{s}_{n+1} + K\,\mathrm{tr}(\Delta\boldsymbol{\varepsilon})\,\mathbf{1} = \mathbf{s}_{n+1} + K\,\left(\det\mathbf{F}_{n+1} - 1\right)\,\mathbf{1} \tag{8.12}$$

where

$$\Delta\boldsymbol{\varepsilon} = \boldsymbol{\varepsilon} - \boldsymbol{\varepsilon}_n\,. \tag{8.13}$$

The iteration over the interval $[t_n, t_{n+1}]$ leads to the elastoplastic state to be sought. The quantities in the iteration step i are denoted by $()^{(i)}_{n+1}$.

9. Appendix II: The polar decomposition of F

The steps of the procedure detailed below were proposed by Hager and Carlson [9], Healy and Dodds [7]:

Step 1: Calculate the right Cauchy-Green strain tensor and its second power

$$\mathbf{C} = \mathbf{F}^T \cdot \mathbf{F}, \qquad \mathbf{C}^2 = \mathbf{C}^T \cdot \mathbf{C}\,. \tag{9.1}$$

Step 2: Determine the eigenvalues

$$\lambda_1^2, \lambda_2^2, \lambda_3^2 \tag{9.2}$$

of $\mathbf{C}$ using the Jacobi method [2].

Step 3: Determine the scalar invariants of the tensor $\mathbf{U}$

$$I_U = \lambda_1+\lambda_2+\lambda_3, \quad II_U = \lambda_1\lambda_2+\lambda_2\lambda_3+\lambda_3\lambda_1, \quad III_U = \lambda_1\lambda_2\lambda_3 = \det\mathbf{F} = J\,. \tag{9.3}$$

Step 4: Determine $\mathbf{U}$ and $\mathbf{U}^{-1}$ in terms of the invariants of $\mathbf{C}$, $\mathbf{C}^2$

$$\mathbf{U} = \beta_1 \left(\beta_2 \mathbf{1} + \beta_3 \mathbf{C} - \mathbf{C}^2\right)\,, \tag{9.4}$$

where

$$\beta_1 = \frac{1}{(I_U II_U - III_U)}, \quad \beta_2 = I_U III_U, \quad \beta_3 = I_U^2 - II_U$$

and

$$\mathbf{U}^{-1} = \gamma_1 \left(\gamma_2 \mathbf{1} + \gamma_3 \mathbf{C} + \gamma_4 \mathbf{C}^2\right) \tag{9.5}$$

where

$$\gamma_1 = \frac{1}{III_U\,(I_U II_U - III_U)}, \qquad \gamma_2 = I_U II_U^2 - III_U\left(I_U^2 + II_U\right)$$
$$\gamma_3 = -III_U - I_U\left(I_U^2 + 2II_U\right), \quad \gamma_4 = I_U\,.$$

Step 5: Calculation of the tensor $\mathbf{R}$ in the knowledge of $\mathbf{F}$ and $\mathbf{U}^{-1}$

$$\mathbf{R} = \mathbf{F} \cdot \mathbf{U}^{-1} \tag{9.6}$$

Acknowledgement. The support provided by the Hungarian National Research Foundation (project No. T025172) is gratefully acknowledged.

REFERENCES

1. Adkins, J.E., and Rivlin,R.S.: *Large Elastic Deformations of Isotropic Materials*, Part IX. Pl.Trans. 1952.
2. Bathe, K.J.: *Finite Element Procedures*, Prentice-Hall, 1996.
3. Doods, R.H.: *Numerical techniques for plasticity computations in finite-element analysis.* Computer & Structures, **26**, (1987), 767-779.
4. Flanagan, D.P. and Taylor, L.M.: *An accurate numerical algorithm for stress integration with finite rotations*, Comp. Math. Appl. Mech. Eng. **62**, (1987), 305-320.
5. Hallquist, J.O.: *NIKE 2D-A Vectorized, Implicit Finite Deformation, Finite-Element Code for Analysing the Static and Dynamic Response of 2D Solids*, Lawrence Livermore Laboratory Internal Report, UCID-19677, 1983.

6. Hallquist, J.O.: *NIKE 3D-A Vectorized, Implicit Finite Deformation, Finite-Element Code for Analysing the Static and Dynamic Response of 3D Solids*, Lawrence Livermore Laboratory Internal Report, UCID-18822, 1983.
7. Healy,B.E. and Dodds, R.H.: *A large strain plasticity model for implicit finite element analyses*, Computational Mechanics, **9**, (1992), 95-112.
8. Hill, R.: *Aspects of invariance in solid mechanics*, Adv. In Appl. Mech. **18**, (1978), 1-75.
9. Hoger, A. and Carlson, D.E.: *Determination of the strech and rotation in the polar decomposition of the deformation gradient*, Quart. Appl. Math. **10**. (1984), 113-117.
10. Kozák, I.: *Relative Motion of Continua and Time Derivatives of Tensors*, Department of Mechanics, University of Miskolc, Miskolc, 1995.
11. Lee, E.H.: *Elastic-plastic deformation at finite strain,* J. Appl. Mech. **36**, (1969), 1-6.
12. Ogden, R.W.: *Non-linear Elastic Deformations*, Ellis Horwood, Chichester, 1984.
13. Pinsky, P.M., Ortiz, M. and Pister, K.S.: *Numerical integration of rate constitutive equations in finite deformation analysis*, Comp. Math. Appl. Mech. Eng. **40**, (1983), 137-158.
14. Reed, K.W. and Atluri, S.N.: *Constitutive modeling and computational implementation for finite strain plasticity*, Int. J. Plasticity, **1**, (1985), 63-87.
15. Simo, J.C. and Ortiz,M.: *A unified approach to finite deformation elasto-plastic analysis based on the use of hyper-elastic constitutive equations,* Comp. Math. Appl. Mech. Eng. **49**, (1985), 221-245.
16. Simo, J.C. and Taylor, R.S.: *Consistent tangent operations for rate-independent elastoplasticity*, Comp. Math. Appl. Mech. Eng. **48**, (1985), 101-118.
17. Simo, J.C. and Taylor, R.S.: *A return mapping algorithm for plane stress elastoplasticity.* Int. J. Num. Meth. Engng. **22**, (1986), 649-670.
18. Szabó, B.A. and Babuska, I.: *Finite Element Analysis*, Wiley-Interscience Publications, 1991.

Notes for Contributors

to the Journal of Computational and Applied Mechanics

Aims and scope. The aim of the journal is to publish research papers on theoretical and applied mechanics. Special emphasis is given to articles on computational mechanics, continuum mechanics (mechanics of solid bodies, fluid mechanics, heat and mass transfer) and dynamics. Review papers on a research field and materials effective for teaching can also be accepted and are published as review papers or classroom notes. Papers devoted to mathematical problems relevant to mechanics will also be considered.

Frequency of the journal. Two issues a year (approximately 80 pages per issue).

Submission of Manuscripts. Submission of a manuscript implies that the paper has not been published, nor is being considered for publication elsewhere. Papers should be written in standard grammatical English. Two copies of the manuscript should be submitted on pages of A4 size. The text is to be 130 mm wide and 190 mm long and the main text should be typeset in 10pt CMR fonts. Though the length of a paper is not prescribed, authors are encouraged to write concisely. However, short communications or discussions on papers published in the journal must not be longer than 2 pages. Each manuscript should be provided with an English Abstract of about 50–70 words, reporting concisely on the objective and results of the paper. The Abstract is followed by the Mathematical Subject Classification – in case the author (or authors) give the classification codes – then the keywords (no more than five). References should be grouped at the end of the paper in numerical order of appearance. Author's name(s) and initials, paper titles, journal name, volume, issue, year and page numbers should be given for all journals referenced.

The journal prefers the submission of manuscripts in LaTeX. Authors should prefer the standard LaTeX article style and are not recommended to define their own LaTeX commands. Visit our home page for further details concerning the issue how to edit your paper.

For the purpose of refereeing, two copies of the manuscripts should initially be submitted in hardcopy to an editor of the journal. The eventual supply of an accepted-for-publication paper in its final camera-ready form (together with the corresponding files on an MS–DOS diskette) will ensure more rapid publication. Format requirements are provided by the home page of the journal from which sample LaTeX files can be downloaded:

`http://www.uni-miskolc.hu/home/web/pumns/mechanics`

These sample files can also be obtained directly (via e-mail) from a member of the Editorial Board, Gy. Szeidl (mechszgy@gold.uni–miskolc.hu), upon request.

Twenty offprints of each paper will be provided free of charge and mailed to the correspondent author.

The Journal of Computational and Applied Mechanics is abstracted in Zentralblatt für Mathematik and in the Russian Referativnij Zhurnal.

Responsible for publication: Rector of the Miskolc University
Published by the Miskolc University Press under the leadership of Dr. József PÉTER
Responsible for duplication: works manager Mária KOVÁCS
Number of copies printed: 200
Put to the Press on December 15, 2000
Number of permission: TU 00-20-ME **HU ISSN 1586–2070**

A Short History of the Publications of the University of Miskolc

The University of Miskolc (Hungary) is an important center of research in Central Europe. Its parent university was founded by the Empress Maria Teresia in Selmecbánya (today Banska Štiavnica, Slovakia) in 1735. After the first World War the legal predecessor of the University of Miskolc moved to Sopron (Hungary) where, in 1929, it started the series of university publications with the title *Publications of the Mining and Metallurgical Division of the Hungarian Academy of Mining and Forestry Engineering* (Volumes I.-VI.). From 1934 to 1947 the Institution had the name Faculty of Mining, Metallurgical and Forestry Engineering of the József Nádor University of Technology and Economical Sciences at Sopron. Accordingly, the publications were given the title *Publications of the Mining and Metallurgical Engineering Division* (Volumes VII.-XVI.). For the last volume before 1950 – due to a further change in the name of the Institution – *Technical University, Faculties of Mining, Metallurgical and Forestry Engineering, Publications of the Mining and Metallurgical Divisions* was the title.

For some years after 1950 the Publications were temporarily suspended.

After the foundation of the Mechanical Engineering Faculty in Miskolc in 1949 and the movement of the Sopron Mining and Metallurgical Faculties to Miskolc, the Publications restarted with the general title *Publications of the Technical University of Heavy Industry* in 1955. Four new series - Series A (Mining), Series B (Metallurgy), Series C (Machinery) and Series D (Natural Sciences) - were founded in 1976. These came out both in foreign languages (English, German and Russian) and in Hungarian.

In 1990, right after the foundation of some new faculties, the university was renamed to University of Miskolc. At the same time the structure of the Publications was reorganized so that it could follow the faculty structure. Accordingly three new series were established: Series E (Legal Sciences), Series F (Economic Sciences) and Series G (Humanities and Social Sciences). The seven series are formed by some periodicals and such publications which come out with various frequencies.

Papers on computational and applied mechanics were published in the

Publications of the University of Miskolc, Series D, Natural Sciences.

This series was given the name Natural Sciences, Mathematics in 1995. The name change reflects the fact that most of the papers published in the journal are of mathematical nature though papers on mechanics also come out.

The series

Publications of the University of Miskolc, Series C, Fundamental Engineering Sciences

founded in 1995 also published papers on mechanical issues. The present journal, which is published with the support of the Faculty of Mechanical Engineering as a member of the Series C (Machinery), is the legal successor of the above journal.

Journal of Computational and Applied Mechanics

Volume 1, Number 2 (2000)

Contents